EPA/600/R-99/049
June 1999

Three Dimensional Hydrodynamic Model for Stratified Flows in Lakes and Estuaries (HYDRO3D): Theory, User Guidance, and Applications for Superfund and Ecological Risk Assessments

by

Y. Peter Sheng, Ph.D.[1], Mansour Zakikhani, Ph.D.[2], Steven C. McCutcheon, Ph.D., P.E.[3]

with contributions by

Edward Z. Hosseinipour, Ph.D.[2] and Pei-Fang Wang, Ph.D.[2]

Donald Eliason, Ph.D.[1]

Douglas S. Henn[4] and Stephen F. Parker, Ph.D.[4]

Earl Hayter, Ph.D.[3] and Phyllis Kohl[5]

[1]University of Florida
Gainesville, Florida 32611

[2]ASci Corporation
Athens, Georgia 30613

[3]Ecosystems Research Division
Athens, Georgia 30605

[4]Aeronautical Research Associates of Princeton, Inc.
Princeton, New Jersey 08540

[5]Clemson University
Clemson, South Carolina 29634

ECOSYSTEMS RESEARCH DIVISION
NATIONAL EXPOSURE RESEARCH LABORATORY
OFFICE OF RESEARCH AND DEVELOPMENT
U.S. ENVIRONMENTAL PROTECTION AGENCY
ATHENS, GEORGIA 30605

DISCLAIMER

The information in this document has been funded wholly or in part by the U.S. Environmental Protection Agency under Cooperative Agreement Number CR-814345-01-0 with the University of Florida. It has been subject to the Agency's peer and administrative review, and it has been approved for publication as an EPA document. Mention of trade names or commercial products does not constitute endorsement or recommendation for use by the U.S. Environmental Protection Agency.

FOREWORD

As environmental controls become more costly to implement and the penalties of judgment errors become more severe, environmental quality management requires more efficient analytical tools based on greater knowledge of the phenomena to be managed. As part of this Division's research on the occurrence, movement, transformation, impact, and control of environmental contaminants, the Processes and Modeling Branch develops management or engineering tools to help pollution control officials address environmental problems.

In assessing ecological risk, models are needed to simulate the effects of complex reversing flows in lakes, harbors, coastal areas, and estuaries and to determine where chemicals are transported to in surface waters and where contaminated sediments accumulate. HYDRO3D is a dynamic modeling system that can be used to simulate currents in water bodies as they respond to tides, winds, density gradients, river flows, and basin geometry and bathymetry.

Rosemarie C. Russo, Ph.D.
Director
Ecosystems Research Division
Athens, Georgia

ABSTRACT

Increasing demands for maintaining the quality of stratified surface waters at reasonable levels have required the development of three-dimensional hydrodynamic models. To meet these needs, the HYDRO3D program has been documented to aid in the simulation of lakes, harbors, coastal areas, and estuaries.

HYDRO3D is a dynamic modeling system that can be used to simulate currents in water bodies as they respond to tides, winds, density gradients, river flows, and basin geometry and bathymetry. The code is a three-dimensional, time-dependent, σ-stretched coordinate, free surface model that can be run in fully three-dimensional (3-D) mode, two-dimensional vertically-averaged (x-y), and two-dimensional laterally-averaged x-z mode.

The prognostic variables are the three components (x-y-z) of the velocity field, temperature, and salinity. The governing equations together with their initial and boundary conditions are solved by finite difference techniques. A horizontally and vertically staggered lattice of grid points is used for computation. The code solves for steady-state or the time-dependent water surface displacement, vertically-integrated velocities, 3-D velocities, temperature, salinity, and dissolved species concentrations. The vertical turbulence parameterization schemes include constant eddy viscosity, variable eddy viscosities (Munk-Anderson type), and a simplified version of a second-order closure model.

The applications provided here demonstrated that the model is capable of realistic simulation of flow and salinity transport in complex and dynamic water bodies. These applications include simulations of tidal circulation and salinity transport in Suisun Bay, California and, Charlotte Harbor, Florida and; wind-forced circulation in Green Bay, Lake Michigan. Tidal circulation in Prince William Sound, Alaska was investigated to determine the feasibility of applying the model under emergency conditions. Finally, the calibration of the model for the Mississippi Sound is illustrated.

HYDRO3D is a far-field model that like any other computer code, has limitations. The present version does not contain a flooding and drying scheme. Near field effects of cooling water discharges, diffusers, other jets, and reservoir withdrawal cannot be adequately simulated. In addition, short-period waves are not included in the model.

The information provided in this manual, along with the complete program listing which will be provided separately, should be sufficient for the user to operate the code. However, a successful model simulation of HYDRO3D requires sufficient data and familiarity with the code. The documentation

provides a brief review of the theory and structure of the program. Data requirements are noted and example applications demonstrates uses of the program.

Page Intentionally Blank

CONTENTS

CONTENTS - continued

CONTENTS - continued

Page Intentionally Blank

LIST OF FIGURES

Page Intentionally Blank

ACKNOWLEDGEMENTS

The development of a complex hydrodynamics model is an effort that extends over a number of years and involves the cooperative efforts of many individuals and groups. However, these models are not developed to a practical level without the long-term commitment and intensive effort of at least one person dedicated to the creation of a useful simulation tool. In the case of the HYDRO3D (or EHSM3D) model described in this report, that individual is Dr. Peter Sheng. Dr. Sheng began the development of state-of-the-art studies at Case Western Reserve University between 1969 and 1975. A precursor of the HYDRO3D model was developed for the simulation of lake, estuarine and coastal circulation (Sheng et al. 1978, Sheng and Lick, 1980). During his post-doctoral research Dr. Sheng developed a sediment transport model (Sheng and Lick 1979, Sheng 1980) which was driven by the precursor of EHSM3D to provide current information and a wave model to provide wave information. These earlier works are still widely cited as the appropriate framework for analyzing hydrodynamic and sediment transport problems in lakes. During these landmark studies, Dr. Sheng recognized the need to develop better hydrodynamic models which can resolve turbulent mixing and the effects of complex geometry and bathymetry in a more rigorous fashion. During his employment with Aeronautical Research Associates of Princeton, Dr. Sheng was able to significantly improve the hydrodynamic and sediment transport models through several research projects.

Among the important projects were those with the U.S. Army Engineer Coastal Engineering Research Center (CERC) and the Hydraulics Laboratory (HL) at the Waterways Experiment Station (WES). Dr. Sheng developed an updated version of the original hydrodynamic and sediment transport models (Sheng, 1983; Sheng and Butler, 1982), with the cooperation of Lee Butler and others at WES. This version was used in several studies in coastal and estuarine waters, e.g., the Mississippi Sound and the adjacent shelf in Gulf of Mexico, Humboldt Bay, and Los Angeles-Long Beach Harbor. The Mississippi Sound study (Sheng, 1983) was particularly interesting because it included the modeling of tidal and wind-driven circulation, modeling of waves, modeling of sediment transport, and field and laboratory sediment measurements. The model resulting from this study was notable for the use of a simplified second order turbulence closure technique and a variable grid. Cooperative efforts between Peter Sheng and the engineers at WES eventually produced a curvilinear grid model (Sheng 1986a; Sheng 1987) that is similar to HYDRO3D. Since 1986, Peter Sheng and his group at the University of Florida continued to further enhance the hydrodynamic and sediment transport models through studies on the James River (Sheng et al. 1989a), Chesapeake Bay (Sheng et al. 1989b) and Lake Okeechobee (Sheng et al. 1989c). The work with similar models and enhanced versions have contributed to the improvement of the HYDRO3D code. At the same time, the earlier modeling studies done in cooperation with WES generated

several in-house projects through which the original hydrodynamics model was further improved. Particularly noteworthy was the Chesapeake Bay project. As a result of the Chesapeake Bay Study, a new version of the basic (Sheng 1983) model was developed. The new version has improved the capability to maintain channel stratification during year-long simulations and uses a z-grid or cartesian coordinate in the vertical dimension. Additional improvements include a new representation of the momentum-convection terms and the addition of a spatial third-order scheme called QUICKEST, in the transport equations for salt and heat (Johnson et al. 1989). This work has been performed primarily by Dr. Billy Johnson of the WES Hydraulics Laboratory, and Dr. Kim and Mr. David Marks with the Coastal Engineering Research Center. Mr. Mark Dortch and others with the Environmental Laboratory at WES have made significant contributions in developing linkage to larger scale water quality models. These efforts are valuable in ensuring that this hydrodynamics model and others are fully useful in routine water quality simulation. As noted, the recent advances by the WES have resulted in different versions of the model from that being documented here, but these studies have provided a number of improvements, some of which have been incorporated into the version of the code being documented herein. As a result, we find it very appropriate to acknowledge the contribution of the WES to the development of this type of hydrodynamics model for stratified flows.

The support of the U.S. Geological Survey has also been important in the development and documentation of the EHSM3D model. Dr. Ralph Cheng of the Water Resources Division National Research Program was the project officer of the effort that among other things, funded the development of the salt balance equations and testing of the model. Mr. Carl Goodwin of the Florida District Office provided data to test the model. A draft of this manual (Sheng et al. 1986) was submitted for those studies and that manual was used as a guide for this document. We therefore wish to acknowledge the original contributions of Mr. Douglas Henn and Dr. Stephen Parker to elements of this document and we have added them contributors to this document on that basis. The original document (Sheng et al. 1986) was edited by Mr. Peter Smith of the U.S. Geological Survey California District and Mr. Smith has made a significant contribution to the testing and correction of an early version of the EHSM3D model. Mr. Smith and Dr. Cheng have also recently published a satisfactory validation of the EHSM3D model in San Pablo Bay of the San Francisco Bay system (Smith and Cheng 1989). In addition, we wish to acknowledge the recent review of this report by Mr. Smith. He noted, in his formal review comments and has relayed in previous conversations with Dr. Steve McCutcheon and Ms. Sandra Bird of the U.S. EPA Environmental Research Laboratory at Athens, Georgia, several areas where the users manual was inadequate for general use and several areas where the documentation does not seem to fully correspond with or explain the equations in the code. Mr. Smith has also noted several areas where the model could be improved, based on his tests for adapting the code for different purposes and including getting the code to run faster on a supercomputer. The contribution of Mr. Smith and the Geological Survey is appreciated.

At the U.S. EPA Environmental Research Laboratory in Athens (ERL-Athens), Georgia, Dr. Steve McCutcheon has been responsible for the development of hydrodynamics and sediment transport models and headed the

competitive selection process that selected Dr. Peter Sheng and the University of Florida to develop a more comprehensive sediment transport model. As part of this effort, a three dimensional hydrodynamics model has been delivered by Dr. Sheng. This model (HYDRO3D or EHSM3D) provides information about fluid velocities and shear stress for the sediment transport algorithms under development. The hydrodynamic model has been tested in a study of Green Bay by Ms. Sandra Bird (ERL-Athens, formerly with AScI Corp.), Dr. Mansour Zakikhani (AScI Corp.), Dr. Pei-Fang Wang (AScI Corp.), Dr. Steve McCutcheon (ERL-Athens), Dr. James Martin (AScI Corp.), and Dr. Edward Hosseinipour (AScI Corp.). Ms. Bird did much of the initial testing and implementation of the model at ERL-Athens and she developed the original linkage to larger scale models being used in the study. Dr. Zakikhani has continued the testing and calibration of the model and made a number of changes to achieve some improvements in it's use (Zakikhani et al. 1989). He has developed and written the user guidance contained in this manual with other authors listed. More recently, Dr. Wang has continued the testing of the model and has developed the Green Bay Case study originally begun by Ms. Bird and Dr. Zakikhani. Dr. Wang also developed the comparison with the analytical solution and resoulved a number of questions about how to described the model and input data. Drs. Wang and Zakikhani summarized the case study on the Mississippi Sound. Dr. Hosseinipour has coordinated the efforts producing the manual and the Green Bay Study used as an example.

The implementation and testing of the model in Green Bay has been supported by Mr. William Richardson of the Large Lakes Research Station attached to the U.S. EPA Environmental Research Laboratory at Duluth, Minnesota. Data collection to complete the testing in the future has been undertaken by the U.S. EPA Great Lakes National Program Office in cooperation with NOAA, Sea Grant, State of Wisconsin and several other institutions. Developed of the sediment transport and hydrodynamics models at the University of Florida has been supported by the U.S. EPA Ecological Risk Assessment Research Program coordinated at ERL-Athens by Dr. Harvey Holm (now with the U.S. EPA Newport Field Station) and Dr. Craig Barber.

The development of this documentation has also been supported by the Center for Exposure Assessment Modeling (CEAM) at ERL-Athens managed by Mr. Robert B. Ambrose, Jr. The CEAM supports general purpose models that can be used for Superfund site investigations, including those where complex hydrodynamic circulation has an effect on the spread of contamination in harbors, lakes and estuaries. Such sites include those located in Eagle Rock Harbor of Puget Sound, New Bedford Harbor in Massachusetts, and Sheboygan Harbor in the Great Lakes.

Support of the Civil Engineering Department of Clemson University for Ms. Phyllis Kohl and Dr. Earl Hayter is also gratefully acknowledged. This hydrodynamics model was selected for preliminary testing in Prince William Sound to aid in tracking the long-term effects of the March 24, 1989 oil spill from the EXXON Valdez. Dr. Hayter and Ms. Kohl tested the feasibility of using the model to simulate circulation in the Sound and continued the study as a Masters Thesis at Clemson. The continued testing and preliminary report on the results contained herein is appreciated.

Ms. Donna Hinson (AScI Corp.), Ms. Tawnya Robinson (AScI Corp.), Mr. Tim Register (ERL-Athens), and other support staff at ERL-Athens have assisted in in retyping, proofreading, scanning the original drafts, retyping equations, and redoing graphics. These efforts are very much appreciated. We especially appreciated the efforts of Ms. Robinson and Ms. Hinson in resolving last minute software glitches in getting the document in the final format. Mr. Robert Ryans (ERL-Athens) edited the document and assisted with revisions of the format. As always, we appreciate his diligence and dedication to improving the editorial quality of these manuals.

This document has been significantly improved by the reviews of a number of colleagues. These include Dr. Raymond Walton (EBASCO Environmental, Seattle), Dr. Alan Blumberg (HydroQual, New Jersey), Dr. Tien-Shuen Wu (Northwest Florida Management District), Dr. Michael Amein (North Carolina State University, Raleigh), Dr. Frederick Morris (Saint John's River Water Management District, Palatka, Florida), and Mr. Peter Smith (U.S. Geological Survey). The reviews of Dr. Walton, Dr. Morris, and Mr. Smith were especially helpful in improving the usefulness of this documentation. We have mentioned Mr. Smith's assistance above. We appreciate the various reminders from Drs. Walton and Morris and the other reviewers about the elements that make a documentation report useful.

Dr. McCutcheon wrote the Preface, Acknowledgements, and Introduction of this report. He edited the report for consistency and supplemented various sections to fully describe the work. Dr. Sheng, Mr. Henn, and Dr. Parker wrote the original draft of Section 2. Dr. Sheng, Dr. Eliason, Dr. Zakikhani, Dr. Hosseinipour, and Dr. McCutcheon enhanced and revised the section. Dr. Zakikhani and Dr. Sheng wrote the User's Manual, Section 3 using Sheng et al. (1986) as a guide. Dr. Wang performed the calculations and wrote about the comparison of the model simulations with an analytical solution suggested by Dr. Hosseinipour. Dr. Sheng performed the calculations and wrote about the studies for Suisun Bay and Charlotte Harbor and Dr.s Zakikhani, McCutcheon, and Hosseinipour revised the sections to answer reviewer comments. Dr. Wang and Dr. Zakikhani performed the calculations and wrote about the studies for Green Bay using simulations initially began by Ms. Bird. Dr. Hayter and Ms. Kohl performed the calculations and wrote about the feasibility studies for Prince William Sound. Dr. Zakikhani revised the section to address review comments. Dr. Wang and Dr. Zakikhani excerpted a summary of the study of the Mississippi Sound from Sheng (1983). Dr. Zakikhani and Dr. Hosseinipour wrote the Programmers Guide for material available from the original draft by Sheng et al. (1986). Dr. Zakikhani and Dr. McCutcheon wrote the Conclusions and Recommendations, and the Abstract.

Dr. McCutcheon, Dr. Hosseinipour, and Dr. Zakikhani are responsible for the editorial and technical accuracy of this document. Dr. Sheng is responsible for the technical accuracy of the theoretical basis of the model as described in Section 2, for the calculations and conclusions described in the sections on Suisun Bay and Charlotte Harbor, and for the original code, EHSM3D. Dr. McCutcheon, Dr. Wang, Dr. Zakikhani, and Dr. Hosseinipour are responsible for changes in the code as part of the Green Bay study and for the slightly revised code now referred to as HYDRO3D.

Steve C. McCutcheon (Athens, Georgia)

PREFACE

The HYDRO3D computer program is one of several codes under development at the U.S. EPA Environmental Research Laboratory in Athens, Georgia (ERL-Athens). The development of hydrodynamic and sediment transport codes at ERL-Athens is proceeding as follows:

Name	Dimen-sion-ality	Type	Status	Existing and Anticipated Level of Support as of April 1990
HYDRO3D	3D	Dynamic circulation model for far-field transport in lakes, estuaries, and coastal areas. Employs approximate second-order closure scheme.	Documented in this report. The code is expected to be ready for release by July 1, 1990. A beta test version is ready now for preliminary implementation at Superfund sites and other critical study areas. Updates to the code are anticipated in September 1990 when the final hydrodynamic and sediment transport model is delivered by the University of Florida.	Level II - Code, documentation, and start-up instructions available from CEAM. Implementation, debugging, and interpretation assistance not fully available, except on a limited basis.
HYDRO2D-V	2D	Vertically averaged finite element hydrodynamic model coupled with a cohesive sediment transport code described as SED2D-V below.	Documentation has not been published and is not readily available except in draft for beta test users. CEAM may be able to assist select EPA projects, especially those involving Superfund sites. Documentation and code will be available by summer 1990.	Level II (anticipated) - Code, documentation, and start-up instructions will be available from CEAM. Implementation, debugging, error correction, and interpretation assistance is available from Dr. Earl Hayter, Clemson University on a negotiated basis.
HYDRO1D-DYNHYD	1D	Branched version of Dynamic Estuary Model involving Manning roughness coefficient and wind stress.	Documented as part of the WASP4 code. Fully operational and applied in a number of studies, but the basic equations have some limitations that must be understood. Case studies include use in moderately dynamic flows in estuaries and rivers.	Level I - Code, documentation, and start-up instructions available from CEAM. Implementation, debugging, error correction, and interpretation assistance fully available for most studies.

List of Hydrodynamic and Sediment Transport Models Available At ERL-Athens, continued

Name	Dimen-sion-ality	Type	Status	Existing and Anticipated Level of Support as of April 1990
HYDRO1D-RIVMOD	1D	Dynamic routing model for single channels.	Preliminary documentation will be available July 1990. The code has not been formally released but is available for use in select CEAM projects and by beta testing.	Limited support is available in the early stages of development. Users with limited experience are referred to models of the Corps of Engineers and U.S. Geological Survey if HYDRO1D-DYNHYD and kinematic wave routing in HSPF are not adequate for the problem to be solved. Level II support is anticipated after the summer of 1990.
HSPF (kinematic wave routing)	1D	Kinematic wave (stage-discharge) and simple sediment routing for dendritic branched channels.	Documentation and code are fully available and operational. Limitations are well described in documentation.	Level I - Code, and start-up instructions available from CEAM. Documentation available from NTIS. Implementation debugging, error correction, and interpretation assistance fully available for most studies from CEAM and U.S. Geological Survey.
SED3D	3D	Dynamic sediment dispersion, resuspension, and deposition model based on the most recent understanding of the important processes. Model integrated into an updated version of the HYDRO3D code described above.	Documentation and code expected in FY91. Beta test versions may be available by late summer 1990 for selected projects, especially those involving Superfund sites.	Not available but Level II support is anticipated.
SED2D-V	2D	Finite element cohesive sediment transport for vertically averaged estuaries, rivers and other unstratified water bodies. Linked with HYDRO2D-V to calculate average shear stress levels.	Documentation has not been published and is not readily available except in draft for beta test users. CEAM may be able to assist select EPA projects, especially those involving Superfund sites. Documentation and code will be available by summer 1990.	Level II (anticipated) - Code, documentation, and start-up instructions will be available from CEAM. Implementation, debugging, error correction, and interpretation assistance is available from Dr. Earl Hayter, Clemson University on a negotiated basis.

WASP4	1D, 2D, & 3D	Simple sediment mass balance with advection, deposition, and resuspension velocities, and eddy diffusivity mixing. Precise sediment transport calculations require input from other algorithms or codes.	Documented, fully operational and applied in a number of studies of lakes, estuaries, and rivers.	Level I - Code, documentation, and start-up instructions available from CEAM. Implementation, debugging, error correction, and interpretation assistance fully available for most studies.

Note: CEAM is the Center for Exposure Assessment Modeling located at U.S. EPA Environmental Research Laboratory, College Station Road, Athens, GA 30605, (404) 546-3130, Bulletin Board Phone: (404) 546-3402.

The HYDRO3D code is essentially the same code as EHSM3D (Estuarine Hydrodynamic Software Model) developed by Peter Sheng in conjunction with the U.S. Army Engineer Waterways Experiment Station (Sheng 1983) and the U.S. Geological Survey (Sheng et al. 1986). The recent applications have concentrated on investigations in estuaries as the title EHSM3D indicates. However, the HYDRO3D code is a general purpose computer program designed to simulate complex dynamic currents in lakes, estuaries, harbors, and coastal waters. The original code was developed in the Canadian-American Great Lakes (Sheng et al. 1978, Sheng and Lick 1980). Prior to documenting the code with this report, ERL-Athens investigated the feasibility of using the code in lake settings (Zakikhani et al. 1989) and made a few minor changes to improve the usefulness of the program. However, these recent changes by ERL-Athens are not significant enough to warrant changing the model name except that the name EHSM3D is misleading regarding the applicability to lakes and other waters.

SECTION 1

INTRODUCTION

1.1 PROGRAMATIC NEEDS FOR MODELS TO SIMULATE STRATIFIED FLOWS

There is increasing emphasis being placed on the simulation of stratified flows in lakes and estuaries by a number U.S. Environmental Protection Agency (EPA) Programs. The emphasis arises from the need to prevent and mitigate pollution in lakes, estuaries, and other stratified surface waters. For example, the *Superfund Program* is beginning to investigate more sites where human and ecological health is affected by contaminant transport in stratified surface water flows. In addition, the *Ecological Risk Assessment Research Program* of the EPA Office of Research and Development (ORD) is developing, in conjunction with the *Office of Pesticides and Toxic Substances*, exposure assessment tools to determine the exposure of biota in lakes and estuaries. These exposure assessments involve determining how chemical concentrations are controlled by flows that are normally stratified. Also, stratified flows and other complex flows control the transport of chemicals attached to sediments. Other EPA programs that will require some understanding of the hydrodynamic transport of sediment include, the EPA *Great Lakes National Program Office ARCS (Assessment and Remediation of Contaminated Sediments) Program* for the cleanup of contaminated sediments from the Great Lakes toxic hotspots; the EPA *Office of Water Programs* and the *ORD Sediment Quality Initiative* aimed at developing waste load allocation methods for sedimentary contaminants; the ORD initiatives to investigate eutrophication and toxic chemical fate in large lakes and marine waters; the *ORD Global Climate Program* on the affects on contaminants and biogeochemical cycles in stratified coastal waters, estuaries, and lakes; the *ORD Oil Spill Response Initiative*; the development of response and cleanup plans for the *ORD Alternative Fuels Initiative; the EPA National Estuary Studies* guided by the *Office of Marine and Estuarine Protection*; the EPA *Region IV Gulf of Mexico Initiative*, and the EPA *Office of Radiation Safety* programs to determine the fate of marine sediments contaminated with radioactive elements. To support these programs, hydrodynamics models are required to simulate the effects of complex reversing flows at harbor entrances into lakes and estuaries, to determine where chemicals are transported to, and where contaminated sediments accumulate. Other programs involving sediment transport will also require methods to determine the hydrodynamic effects on the transport and dispersion of fine sediments enriched with nutrients, metals, radioactive elements, and pesticides and other toxic organic chemicals. The resuspension and deposition of fine sediment is best simulated using a hydrodynamic model to map out levels of fluid shear stress at the bottom and throughout the water column.

A list of the Programs and areas of research that this work will support include:

- Superfund site assessment and remediation,
- Determining transport of nutrients and contaminants for bioremediation of hazardous waste sites,
- Ecological and human health risk assessments in the Great Lakes and other critical stratified surface waters,
- Contaminated sediment resuspension, deposition, and transport studies,
- Waste load allocation for sedimentary contaminants (EPA Office of Water Sediment Quality Criteria Programs and ORD Sediment Quality Initiative),
- Waste load allocation for conventional and toxic substances (pesticides, organic chemicals, and metals) in estuaries (see Ambrose et al. 1990) and lakes,
- Effects of global climate change on circulation in lakes, estuaries, and coastal waters,
- ORD Oil Spill Response Plan,
- Development of emergency response and cleanup plans for the ORD Alternative Fuels Initiative,
- Determining Circulation and Sediment Transport for EPA National Estuaries Studies and Regional Estuaries Programs, and
- Tracing the fate of radioactively contaminated marine sediments.

The primary reasons that simulations of three-dimensional stratified flows are of added importance is the need to describe shear stress in greater detail to fully simulate sediment resuspension and deposition, and to predict the effects of complex flows on contaminant transport. Scientists and engineers have long recognized that sediment resuspension is episodic and highly variable in spatial extent. A number of methods have been developed to measure resuspension in the field and laboratory [sea flume devices, sediment profile measurements (Sheng et al. 1989b), core shaking methods, and laboratory flumes]. Experience has shown, however, that these measurements can not be made frequently enough or at enough locations to adequately represent a mapped history of shear stresses that cause resuspension and control deposition. As a result, hydrodynamic models calibrated with select measurements at a few locations are the only practical approach the determining the flux of contaminated sediments between the water column and benthos at the moment.

Until recently, the state of the art in contaminant transport simulation in lakes and estuaries involved calibrating a transport model (see Ambrose et al. 1987 for example) with measurements in the water body of interest (see Ambrose et al. 1990 for the general procedures and other examples). Measurements of chlorides, total salt, total dissolved solids, major ions or cations, other conservative substances, and even some non-conservative parameters such as water temperature are collected and used to surmise what combination of advective circulation or flow, and dispersive mixing caused the observed concentration distributions. Unfortunately, it has been virtually impossible to determine if these types of model calibrations were unique and thus representative of a wider range of conditions. In effect, modelers have been able to describe the effects of advection (or circulation) and mixing in

a black box fashion (an input-output model calibrated to describe a system without regard to determining important mechanisms or processes that define the cause and effect relationships for water quality). However, the approach rarely leads to valid predictions.

There is now more evidence that hydrodynamic simulations are required so that water quality can be predicted and not just described as has been done in the past. The effects of circulation and mixing must be predicted for a number of very dangerous chemicals proposed for wide-scale manufacture or use. These chemicals can not be released to the environment simply to calibrate a model. Hydrodynamic transport (and effects on sediment if the chemical sorbs to particles) must be predicted beforehand. Likewise, spills of large amounts of oil and other materials can not be introduced simply to learn the affect of currents, wind, and tides on its fate and to determine its effects on the environment.

Also, it is difficult to measure circulation and mixing in all flows. Thus it is more cost effective to calibrate a model with a few selected measurements and use the model to extrapolate to conditions of interest.

Finally, most contamination problems in simpler river and stream flows have been cleaned up or controlled. What remain are sedimentary contaminants contributed by diffuse, unmeasurable sources. These sedimentary contaminants are controlled by hydrodynamics and sediment transport from the sources, and dispersion of in-place contaminated sediments. Effective cleanup requires investigation of leaving the contaminated sediment in place (the "no action alternative") and investigation of various remedial alternatives. In most cases, hydrodynamics and sediment transport must be predicted to adequately assess the risks to human health and ecological viability. It is therefore clear that complex stratified flows in lakes, harbors, estuaries, and coastal areas must be understood if:

- Superfund and hazardous waste sites are to assessed and cleaned up,
- If existing point and nonpoint sources are to be adequately controlled,
- If future sources are to regulated on a rational basis, and
- If spills are to be prevented from causing extensive damage.

To address these needs, the engineers and model developers at the U.S. EPA Environmental Research Laboratory at Athens (ERL-Athens), Georgia have begun development of computer programs to simulate sediment transport and hydrodynamics. In addition, ERL-Athens has begun the development of hydrodynamic programs to address the complex transport of dissolved contaminants in stratified lakes and estuaries. This involves the initial testing and application of a hydrodynamics code originally developed by Sheng & Lick (1979) and significantly enhanced by Sheng (1983) and Sheng et al. (1986). This code was selected because of its use in the development of three dimensional sediment transport and dispersion models by Dr. Peter Sheng (University of Florida) for ERL-Athens. This computer code and documentation (represented by this report) are being developed as an interim tool that will be improved and expanded upon after the sediment transport model has been developed in September 1990 if necessary.

ERL-Athens intends to distribute and maintain this computer code for a limited group of engineers and scientists who investigate the effects of complex circulation in lakes and estuaries. As this constituency of hydrodynamics and water quality modelers grows, ERL-Athens expects to expand the support for these types of investigations by rigorously evaluating alternative codes and methods, streamlining application procedures, and publishing updated codes and supporting documentation as warranted.

1.2 USE OF HYDRODYNAMIC MODELS BY TECHNICAL EXPERTS AND MANAGERS AND HOW THIS MANUAL MAY BE OF ASSISTANCE

As hydrodynamics models continue to be developed, there will be some debate about how these computer codes are best employed to avoid misuse and misapplication. Misuse is a more important issue for complex models like hydrodynamic and sediment transport models, contrasted with the simpler models that are already widely used in assessing environmental problems. It is difficult to fully document and provide comprehensive guidance for complex codes that will assist in preventing incorrect interpretations. Complex codes generally require greater experience and more in-depth training that is not readily available from many graduate study programs in environmental engineering and science. Also, these codes are being rapidly developed and it is difficult to maintain up-to-date documentation in such cases.

To assist in the use of hydrodynamic simulation programs, this documentation will provide several types of information useful to technical experts and managers of projects. First, this introductory section will review screening level studies and the potential information available. Second, this section will briefly review procedures for calibrating and validating models. Third, this introductory section will briefly review data requirements.

Section 2 of this documentation will review the theoretical basis of this code and review the structure of the program to aid in matching the development of the theory with sections of code implementing those equations. This section is intended for applications experts with experience in fluid mechanics and who need a more precise definition of the limitations and uses of the code. The practical implications of the theoretical basis of the computer program are discussed in the Introduction of Section 2 and in Section 2.5, Turbulence Closure. These sections should be of interest to all readers. Most important is the discussion of modeling limitations indicating that the model can not be properly applied to:

- Waterbodies where wetting and drying occurs over larger areas (i.e., tidal flats and shallow reservoir embayments),
- Power plant cooling water discharges, sewage diffusers, and other jets with excess momentum (near-field effects),
- Withdrawals from reservoirs, and
- Flows in which short-periods waves are important causes of mixing.

Section 2 includes several important components that establish the theoretical validity of the code for certain hydrodynamic conditions. Section

2.2 on the program formulation involves a review of the governing equations, how the model domain is described with a grid system, how the equations are nondimensionalized, what dimensionless variables and parameters are used, how the governing equations are rewritten in stretched coordinates, how the equations are vertically averaged for two-dimensional applications, and how vertical velocities are computed. Section 2.3 describes the boundary and initial conditions that must be specified. Section 2.4 describes the external and internal modes for numerically solving the equations. Section 2.5 describes the three means of simulating turbulence in this program. The final two sections give more information about the grid system used to describe the water body of interest and provide program flow charts.

Section 3 is an abbreviated user's manual intended for the applications expert. This section is not as comprehensive as might be desired but it does cover data requirements to initiate and operate the code, and data requirements for calibrating and validating the model for a specific site. In the latter part of this valuable section, input data and their formats are described. Unfortunately, it is not yet possible to tabulate typical ranges of all the parameters but reference to those documents that provide some of this useful information is cite here and elsewhere in the report. In addition, assistance to less experienced modelers in selecting model parameters and interpreting the results is available from the ERL-Athens Center for Exposure Assessment Modeling (CEAM). Project managers may wish to review the introduction to Section 3 that describes the general data requirements. To best understand critical data requirements for a specific study, it is recommended that the applications expert setup the program to make preliminary simulations with estimates of the input data. This will provide the best indication of the frequency and spatial coverage required for a data collection study.

Section 4 lists several case studies using the model, HYDRO3D, and EHSM3D and CELC3D (codes that preceded HYDRO3D and for which the simulations are essentially the same). This section should be useful for program managers and applications experts. Program managers may wish to note the diverse nature of the affects on circulation simulated by the program for lakes, estuaries, and coastal areas. The case studies show that the model has been adequately setup for the deep waters and complex bathymetry and geometry in Prince William Sound where tidal amplitudes are typically 4 to 5 meters (13 to 16 feet), in the extremely deep waters of the Gulf of Mexico, for the complex bathymetry and swift currents in Suisun Bay of San Francisco Bay, for the shallower partially mixed Charlotte Harbor estuary where the tides from the Gulf of Mexico are on the order of 1 meter (2 to 3 feet), and in wind dominated Green Bay attached to Lake Michigan. Finally, a detailed calibration and testing case study from Sheng (1983) is included. This was a study of the Mississippi Sound and the adjacent deep waters of the Gulf of Mexico. In the final case study illustrating calibration of the model, a second, older version of the code documented in Sheng (1983) was used to perform the simulations. As with, EHSM3D the hydrodynamics results from this code should be essentially the same as those that could be obtained with HYDRO3D for this site.

The case studies, including a comparison to an analytical solution, are intended to demonstrate the usefulness and validity of the program. While minor coding inconsistencies and errors may remain in any code, the extensive use of this code and its predecessors indicate that all major problems have been resolved and that it is ready for application.

There are other notable applications as well and these are referenced in the report at appropriate points. For example, Smith and Cheng (1989) have just recently examined the use of this model in a study of San Pablo Bay in the San Francisco Bay.

The case study of Green Bay indicates the usefulness of the model in a large lake setting where inflows, wind driven circulation, and seiche from Lake Michigan may be important at various times. Other studies of Lake Okeechobee due to be published in 1990 or 1991 (also see Sheng et al. 1989c), and older studies in other parts of the Great Lakes indicate that the model is potentially useful throughout the Great Lakes and in large shallow lakes. A review of the theoretical basis of the model indicates that it should be useful in smaller lakes as well. Applications in reservoirs have not been attempted as far as we are aware. At this time, the hydrostatic approximation seems to preclude adequate simulation of the vertical accelerations of flow that may be important in reservoir outflows.

Other limitations are that the model does not simulate near-field cooling water inflows, diffuser flows, and other jet discharges. Also, the equations do not take all short-period wave effects into account.

The section on case studies should also give a project manager some understanding of the intensity of the calculations involved and the overall data requirements. However, only the case study for the Mississippi Sound involves a rigorous calibration of the model and thus Section 4 only gives some indication of overall data requirements. This is primarily because study objectives must be integrated into such a determination.

Section 5 is the Programmer's Guide. This is intended to give limited assistance the applications expert to install and run the program. At this time (May 1990), the code has a few VAX specific FORTRAN Statements that users must modify when working on other processors. We believe this will take about one-man week of effort and expect to resolve these problems before the final release of the code by July 1, 1990.

1.3 SCREENING LEVEL SIMULATIONS

One of the more important debates among hydrodynamics modeling experts is whether or not these complex models can be applied in a screening mode with available data. In the case studies, we illustrate how a model can be setup for illustrative purposes by using examples from Suisun Bay and Charlotte Harbor first used in a workshop by Sheng et al. (1986). We also investigated the use of the model in the recent oil spill emergency in Prince William Sound and these preliminary results are reported herein. For Prince William Sound, we found that the code could be setup in a matter of days and made ready for

follow-up studies to calibrate the model for longer-term assessments and management of the cleanup. However, it is noted in the studies and highlighted by the reviewers of this report that simulations based on limited data can be misleading and highly suspect if not properly interpreted. Nevertheless, it is clear that some useful information is to be gained and we now include it as a useful means to obtain limited information or screen out some alternatives. Primarily, we recommend screening level simulations using existing data to design data collection programs for model calibration, for extrapolation of tide and current measurements to areas not covered by existing data, and for preliminary investigations of effects on circulation and transport in place guesswork and approximate means even if adequate calibration data are not available.

1.4 CALIBRATION AND VALIDATION

Calibration and validation of a computer code applied to a specific site results in a simulation model of the site. The ability of the model to describe or predict conditions at a site depends on how well the code is calibrated. Calibration is the process of selecting model parameters and configuring the computational domain to be simulated. Model simulations based on alternative selections of parameters are compared with measured data. The coefficients used in the simulations that best match the measurements are chosen as the calibrated parameters. Validation is used to determine how uncertain the results of the model are for limited ranges of conditions in the water body of interest (lake, estuary, or coastal waters). For additional information on calibration and validation see McCutcheon et al. (1990) for estuary modeling, and Chapra and Rechow (1983) and Henderson-Sellers (1984) for lake modeling.

The general procedure for calibrating and testing the adequacy of a model is as follows:

- Determine study objectives,
- Define the subset of objectives to be addressed by model studies,
- Collect historical data from monitoring or previous studies,
- Attempt a preliminary calibration of the model,
- Design a calibration data collection study based on the preliminary calibration,
- Simulate conditions during the calibration period and compare to determine if the preliminary calibration is sufficient (if it is not, calibrate the model),
- If the model is calibrated, collect a second independent set of data for validation,
- Validate the model for the limited range of conditions defined by the calibration and validation data sets (if the model can not be validated repeat the calibration step and collect more validation data for a second attempt), and
- Determine uncertainty in the calibrated model simulations by sensitivity analysis.

See Ambrose et al. (1990) and Ambrose and Martin (1990) for guidance on these

procedures.

1.5 DATA REQUIREMENTS

In general, data requirements for calibrating a hydrodynamics model are extensive but not overwhelming. Typically, the following data are necessary:

- Navigation charts and maps or soundings to define bathymetry and geometry,
- Measurements of current speed, salinity, and water temperature at two or more levels at each of important boundaries of the water body (mouth of estuary, lake outlet, fresh water inflows, rivers, etc.),
- Measurements of current speed, salinity, and water temperature at two or more levels at a number of stations throughout the water body (for calibration and validation),
- Some measurements of the initial condition of the current, salinity, and temperature fields at the beginning of the simulation, and
- Long term monitoring stations for water level to identify critical episodes or seasonal changes.

Multiple stations may be necessary to define some open boundaries. Five to ten stations in the domain should be sampled to calibrate and validate a model. Long term monitoring at one or two stations in the study area is desirable. Sampling frequencies depend on study objectives (as do sampling location to some extent). Calibration for episodic events requires data collection at the boundaries and internally over a period that at least exceeds the occurrence of the event and hopefully defines conditions beforehand and after. Simulation of seasonal changes requires multiple deployments of current meters and water quality sampling equipment over longer periods.

See Section 3 for more details on data requirements.

SECTION 2

MODELING SYSTEM

Section 2 presents the basic model theory and describes how the modeling system is formulated. The section is intended to assist engineers and scientists charged with the application of the model, but some of the introductory material may interest project managers. Unfortunately, this document can not cover many of the basic elements of hydromechanics that are generally needed to fully grasp the limitations a complex hydrodynamics model, and the reader should look elsewhere for this information. See for example, White (1977), Monin and Yaglom (1971), Reynolds (1974), Rodi (1980), Hinze (1959), Schlichting (1979), Goldstein (1960), Turner (1973), and Tennekes and Lumley (1972) among the few good references that can provide useful background information. Sheng (1983) provides additional discussion ofthe theoretical basis of the model not covered here.

HYDRO3D is a FORTRAN code designed to simulate two-dimensional (2-D) and three-dimensional (3-D) stratified (or non-stratified) flows in lakes, estuaries, coastal waters, and harbors. In solving for the effects of density stratification on circulation, the model also simulates the distributions of dissolved solids (salt) and temperature. These flows and the associated mass and heat transport are simulated dynamically. Important forces taken into account in the simulations are those caused by tides, winds, density gradients caused by salt (dissolved solids) and heat, and forces due to the resistance of flow over irregular bathymetry and around irregular geometry in the water body of interest. The grid system that users set-up for model simulations is rectilinear in the plan view but uses a sigma stretched grid in the vertical direction. A sigma stretched grid divides the depth into vertical layers of equal thickness and maintains those equal thicknesses even as the total depth of flow changes during the simulations.

The governing equations solved by this model are an approximation that are designed to simulate some water flows but not all possible conditions that arise in the natural environment. The important approximations in the equations are related to the manner in which turbulence in the flow is simulated, and the treatment of vertical velocity accelerations.

The original principles from which the governing equations for any mechanistic hydrodynamics model are derived include:

- Newton's second law that force is equal to mass times acceleration,
- Conservation of water in a defined volume,
- Conservation of heat, and
- Conservation of dissolved solids or salt.

Application of these principles results in a set of equations for the sum of the forces acting on a fluid element in all three directions of three-dimensional space, plus the conservation equations for water, salt, and heat. Fluid density is calculated from dissolved solids and heat using an equation of state.

If it is noted that Newton's law of viscosity (Streeter and Wylie 1975) adequately relates fluid viscosity to shear stress in the fluid (viscous drag force caused by fluid moving over the bottom or other layers of fluid), then the original force balance equations (derived from Newton's second law) can be expressed in an mathematically exact form known as the Navier-Stokes equations (White 1974, Schlichting 1979, Monin and Yaglom 1971). Newton's law of viscosity is essentially an empirical formulation but it is based on extensive observation and can also be explained by several mechanistic and conceptual premises. As a result of the extensive and comprehensive observations, one can confidently treat all water flows as Newtonian, i.e., there is a linear dependence between water viscosity and shear stress of the flow (Streeter and Wylie 1975, Bird et al. 1977).

Unfortunately, the Navier-Stokes equations can not be solved exactly for most turbulent flows because there is insufficient computer memory and speed available from present day processors (including supercomputers). See Rodi (1980) for a discussion of computing needs to solve a typical environmental fluid mechanics problem using the Navier-Stokes equations. To derive a practical means of solving the equations, an averaging technique dating back to the 1894 work of Sir Osborne Reynolds (for whom the Reynolds number in fluid mechanics is named), is typically employed (see Monin and Yaglom 1971). This technique resolves the turbulent velocity and mass transport into two components; a mean velocity or concentration (or temperature for the conservation of heat equation), and a fluctuating component typically written for the three coordinate directions, i, j, and k, as $U_i = u_i + u_i'$, $U_j = u_j + u_j'$, and $U_k = u_k + u_k'$ and for concentration or heat as $C = c + c'$ or $H = h + h'$. The fluctuating component about the mean velocity or constituent property of the flow (temperature or concentration) is determine by the period of time over which the properties are averaged. When the mean and fluctuating components are substituted into the Navier-Stokes equations to achieve what is known as Reynolds averaging of the equations, the resulting Reynolds equations (White 1977) can be readily solved for many types of environmental fluid flows with several numerical methods (Rodi 1980).

Reynolds averaging is a powerful technique that makes a number of numerical and analytical solutions possible (Schlichting 1979). Unfortunately, averaging introduces two severe disadvantages to overcome in solving the resulting equations. First, the Reynolds equations are no longer time-continuous (or, exact dynamic) expressions. Second, the substitution of two variables (the mean and fluctuating components) for one variable, results in a mathematical closure problem, i.e., there are no longer enough equations to solve for all the unknown variables.

The averaged equations represent fluid motion as a series of averages and fluctuating components that change from average values of both components in one discrete interval to other average values in the next discrete

interval. This change in behavior can be handled by a number of finite difference (used in this model) and finite element numerical schemes, as well as by other numerical schemes such as the method of characteristics (Lai 1965). In fact, these schemes can be used to solve the equations over short enough time intervals that the solution describes most of the important dynamic behavior (or turbulence) of the fluid flow. As a result, the solution is finely resolved enough in most cases to refer to the simulations as being dynamic (as is done for this model). This is normally the cases for flows in estuaries, lakes, harbors, and coastal waters. However, the optimum averaging interval (model time step) can not be theoretically derived and thus must be arbitrarily selected using judgement and experience.

In addition, the time interval for averaging effects the value of eddy coefficients through a direct effect on the fluctuating component that will be further described below. In effect, this introduces another correlated parameter to the selection process that includes time intervals, spatial segmentation (how the grid is set-up), and eddy coefficients for momentum, mass (contaminants or salt), and heat. In certain ranges, these parameters are not highly correlated (i.e., one is not very sensitive to values of the others); but in general one can not select a grid to represent a water body, a time step for the solution, and eddy coefficients independently without understanding the mutual effects. As a result, the time averaging is necessary to solve the equations but introduces a need for some experience and guidance in applications.

The second drawback in the averaged equations is the addition of new variables, making it impossible to achieve mathematical closure of the set of equations. This becomes the problem known as turbulence closure (Rodi 1980, Sheng 1983) that has been studied extensively (Hinze 1959, Rodi 1980, Monin and Yaglom 1971, Reynolds 1974, Tennekes and Lumley 1972).

Turbulence closure is effectively achieved by deriving additional equations for momentum, mass, and heat transport (see McCutcheon et al. 1990). The equations that can be derived, range from simple expression for mixing lengths (Prandtl 1925) and eddy coefficients (Streeter and Wylie 1975) related to various mean flow properties. Mixing length and eddy coefficient methods have been classified as zero-order turbeulence closure schemes (Rodi 1980). Higher-order closure schemes can be derived from conservation of kinetic energy, expressions for turbulence length scales, and other approaches (see Rodi 1980 and ASCE 1988 for comprehensive reviews). Regardless of the approach, each equation has at least one or more empirical constants that must be determined from observations. The highest order schemes have only one or two constants that may be widely applicable to most environmental flows (Rodi 1980, 1984, ASCE 1988) but these will never be universal constants because of the closure problem. The more approximate schemes, i.e., eddy coefficients, remain much more empirical (McCutcheon et al. 1990). Equation coefficients and parameters are quite variable from one flow to another, and vary within a flow at different locations and at different times. As a result is it is difficult to forecast eddy coefficients. Therefore, calibration with field measurements is necessary for precise studies. There is less uncertainty in the parameters of the higher order schemes but these schemes are not fully practical. Therefore, the state of the art is to use eddy coefficient methods

(McCutcheon et al. 1990), but there are some cases where higher schemes are useful and this model has one option involving a simplified second order scheme that will be described later in this section. In general, practitioners should recognize that higher order closure schemes are expected to attain recognition as state-of-the-art in a few years and should begin using the methods forthwith.

The basic approach used in this model to achieve turbulence closure is to use the eddy coefficient approach. The three options available include:

- Constant eddy coefficients,
- Munk and Anderson type vertical eddy coefficients, and
- Simplified second-order scheme expressed in terms of eddy coefficients.

The eddy coefficients are derived in the terms of the Reynolds equations where the fluctuating components describing the turbulent momentum, mass, and heat flux terms (Rodi 1980, ASCE 1988). These turbulent fluxes are assumed to be proportional to the vertical gradients of mean velocity, concentration, and temperature. The proportionality constants in these expressions, are the eddy coefficients (see Rodi 1980) used in this model.

2.1 OVERVIEW OF THE MODELING SYSTEM

Development and implementation of a complex mathematical model such as HYDRO3D requires that the fundamental concepts be formulated in a clear and concise fashion. To facilitate the interpretation, maintenance, and upkeep of the computer code it is necessary to use structured and modular programming techniques. In accordance with these criteria the HYDRO3D modeling system consists of 65 subroutines, 2 INCLUDE files and post-processor files for graphical presentation of results.

The governing equations of the model are incorporated in a discrete form using a finite difference numerical method coded in VAX, FORTRAN 77. In solving the equations the program can be run with either a fixed time step or a variable time step.

HYDRO3D is a dynamic model that allows the specification of a variable wind field and a variable river inflow or outflow. It also allows tidal forcing boundary conditions at multiple sites. The vertical turbulence closure parameterization schemes of HYDRO3D include: 1) constant eddy viscosity, 2) variable (Munk-Anderson) type eddy viscosity, 3) and a simplified version of a second-order closure model.

Although every effort has been made to develop a general purpose hydrodynamic modeling package, HYDRO3D has its limitations like any other computer code. In spite of the many special features contained in the code, HYDRO3D does not have the full capability to allow universal application of the model to all water bodies under all physical conditions with arbitrarily chosen grid patterns and time steps. To understand the limitations of this program, those planning to apply the model are advised to read this manual and

a previous report (Sheng 1983). Experience has clearly shown that the user must thoroughly understand the capabilities and limitations of HYDRO3D before attempting to solve a site-specific problem.

Specific limitations of the modeling system that are obvious from the governing equations and that have been noted from applications of the program include:

- Use of hydrostatic pressure distribution that precludes detailed simulation of the effect of jets and other near-field mixing phenomena from cooling water discharges, sewage diffusers and pipes, and other high momentum discharges. It also precludes simulation of reservoir withdrawals where vertical accelerations are significant.
- Exclusion from governing equations of the effects of short period gravity waves that describe near-shore circulation.
- Lack of flooding and drying features to simulate tidal flats and deltas in lakes where tidal amplitudes or water surface elevation changes are large and the near shore bottom slopes are small.
- Effects of grid resolution, especially near boundaries, that may slow the speed of the calculations or cause erratic results if rapidly changing bathymetry is not adequately resolved.

In addition, there are other less general limitations related to turbulence modeling and other features that may cause problems in a few applications for inexperienced users. These will be introduced in the following material as the need becomes obvious. Since the range of experience of users is not clear in the initial stages of development, however, these experience-related disadvantages of the modeling system can not be fully complied in this first edition of the documentation. These will be compiled in future documents as feedback is received from users of the model and documentation. Therefore, present users should have an adequate understanding of the physics of water circulation, numerical methods, and computer programming to understand and use the model.

2.2 MODEL FORMULATION

The governing equations used in this program and the assumptions aon which the equations are based are described in the following subsections.

2.2.1 Governing Equations

The governing partial differential equations are based on the following assumptions:

- The hydrostatic pressure distribution adequately describes the vertical distribution of fluid pressure,
- The Boussinesq approximation is useful (small density differences in stratified flows are assumed to have a negligible effect on fluid inertia), and
- The eddy viscosity approach adequately describes turbulent mixing in the flow.

Use of the hydrostatic pressure distribution means that vertical accelerations of the fluid are ignored. This generally limits the model to simulations of far-field conditions. Significant deviations of simulations with actual flow conditions may occur in near-field flows involving jets into receiving waters. This is especially true if the high momentum effects more that 5 to 10 percent of grid points. For more information on the hydrostatic pressure distribution, see White (1974) and Sheng (1983).

As a result of the use of the hydrostatic pressure distribution, it is not readily feasible to use HYDRO3D to simulate the detailed behavior of cooling water inflows (from coal-fired or nuclear plants), sewage inflows from diffusers, outfalls, pipes, and other jet-like discharges into lakes, estuaries, coastal waters, and harbors that involve high velocities and flow rates. However, the existence of intense near-field mixing in limited areas does not preclude use of this model. For example, the existence of a diffuser or high velocity jet from a pipe or channel into the vicinity of one or two grid points (a few at most) of the computational domain can be simulated.

Simulations that compensate for the effects of near-field mixing usually involve:

- Specification of elevated values of the eddy coefficients at the affected grid points, or
- Design of the computational domain to exclude the high momemtum areas from the simulation.

Near field mixing is usually computed according to the approaches in EPA (1985), Fischer et al. (1979), Jira and Donecker (1988), Roberts (1979), Wright (1977), and Jirka (1982). These calculations could be used to estimate elevated eddy coefficients or calculate the expected mixing for boundary conditions to the hydrodynamics model when the hydrodynamics model domain excludes the near-field effect. These procedures must be worked out on a case by case basis, but these approaches represent to state-of-the-art at the moment (1990).

Model users should note that neither the selection of elevated eddy coefficients nor the selection of an ideal model domain can be accomplished easily. Normally, users should expect to calibrate the model and collect extra data in the vicinity of the jet(s). There are no reliable means of relating eddy coefficients to jet mixing averaged over large scale distances. Extra data will be required if boundary conditions are quite variable and if the effect of the jet extends into the model domain. To reduce extra data collection, selection of boundaries to isolate the effects of jets is recommended. For example, moving model domain boundaries to the mouth of embayments or arms of an estuary or lake will avoid the complications. Of course, selection of a different model (one that solves the vertical momemtum equation) should also be considered as well.

The use of the Boussinesq approximation does not seem to severely limit the application of the model. The approximation is normally valid for most water flows in the natural environment (see Monin and Yaglom 1971).

The use of the eddy-viscosity concept indicates significant limitations of the governing equations, as implied in the introduction of this section. In general, a simple eddy viscosity scheme does not keep track of the generation and dissipation of turbulence (Rodi 1980). The eddy viscosity scheme is based on the assumption that the flow is uniform and that the turbulence is dissipated under the same conditions under which it is generated. Unfortunately, these are conditions that do not exist in complex flows (multi-directional at different levels, reversing with time, etc.), and especially in stratified flows (see McCutcheon et al. 1990 for more discussion of these limitations). In general, turbulence is generated by complex interactions from wind shear, fluid shear on the bottom, flow around islands and obstructions, and internal density currents, as well as by other mechanisms not included in HYDRO3D (i.e., turbulence due to waves). This turbulence is transported throughout the water bodies of interest and can be dissipated under very different conditions. For example, bottom generated turbulence from tidal flats can be swept into deeper channels where the turbulence is of different scales and intensity. Also, salt stratified flows are nonuniform (the vertical salinity gradient varies downstream as the density differences decay due to mixing across the interface) and bottom generated turbulence is dissipated under different salinity gradients downstream. In many cases, the generation and dissipation conditions are not radically different and the eddy coefficients are useful. But in general, the transport of turbulence must be taken into account, especially if the model is used in forecasting. This is one reason why the simplified second order closure scheme employed by this code is important.

From the assumptions outlined above, the basic flow equations for an incompressible fluid (i.e., water) can be expressed using the right hand Cartesian coordinate system (with x,y,z) shown in Figure 1. These equations are written as:

Continuity Equation:

$$\frac{\partial u}{\partial x} + \frac{\partial v}{\partial y} + \frac{\partial w}{\partial z} = 0 \tag{1}$$

Momentum Equations:

$$\frac{\partial u}{\partial t} + \frac{\partial u^2}{\partial x} + \frac{\partial uv}{\partial y} + \frac{\partial uw}{\partial z} = fv - \frac{1}{\rho_o}\frac{\partial p}{\partial x} + \frac{\partial}{\partial x}\left[A_H \frac{\partial u}{\partial x}\right] + \frac{\partial}{\partial y}\left[A_H \frac{\partial u}{\partial y}\right] + \frac{\partial}{\partial z}\left[A_V \frac{\partial u}{\partial z}\right] \tag{2}$$

$$\frac{\partial v}{\partial t} + \frac{\partial uv}{\partial x} + \frac{\partial v^2}{\partial y} + \frac{\partial vw}{\partial z} = - fu - \frac{1}{\rho_o}\frac{\partial p}{\partial y} + \frac{\partial}{\partial x}\left[A_H \frac{\partial v}{\partial x}\right] + \frac{\partial}{\partial y}\left[A_H \frac{\partial v}{\partial y}\right] + \frac{\partial}{\partial z}\left[A_V \frac{\partial v}{\partial z}\right] \tag{3}$$

$$\frac{\partial p}{\partial z} = - \rho g \tag{4}$$

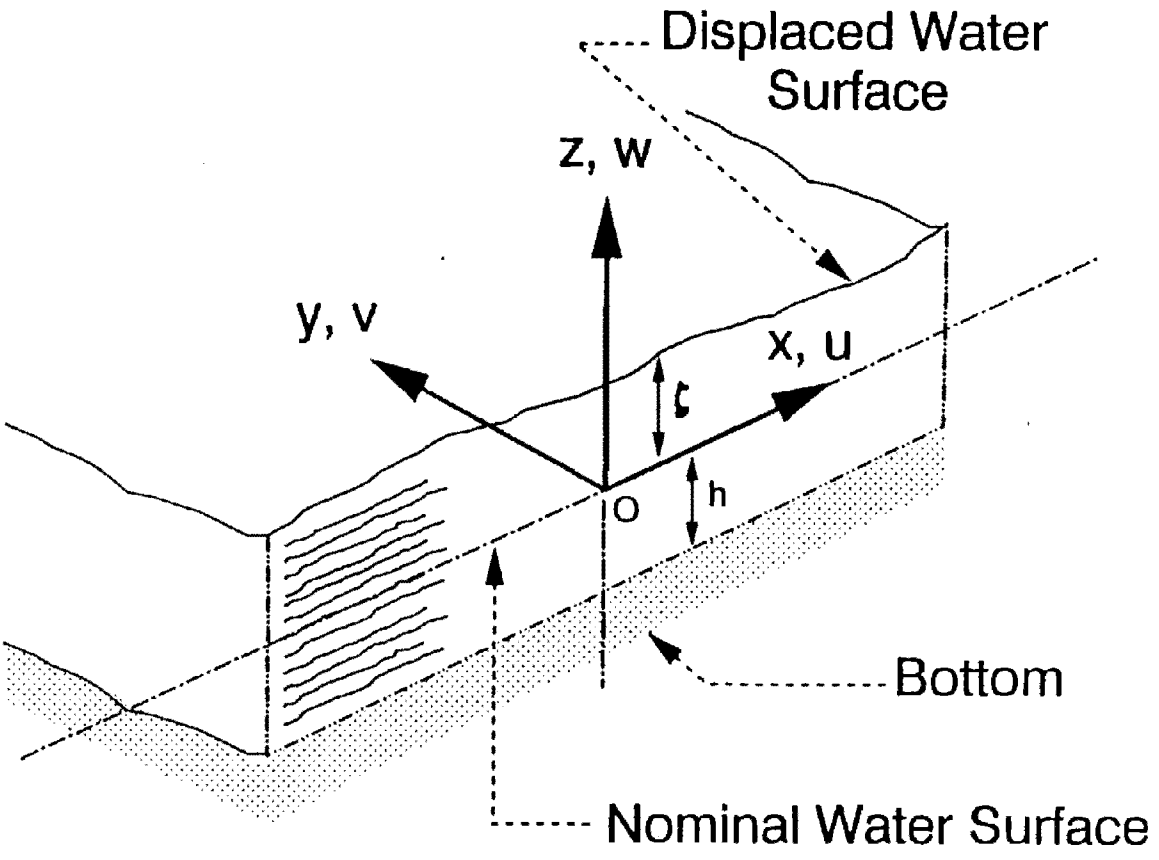

Figure 1. Cartesian coordinates at the nominal water surface.

Temperature and Salinity Equations:

$$\frac{\partial T}{\partial t} + \frac{\partial uT}{\partial x} + \frac{\partial vT}{\partial y} + \frac{\partial wT}{\partial z} = \frac{\partial}{\partial x}\left[K_H \frac{\partial T}{\partial x}\right] + \frac{\partial}{\partial y}\left[K_H \frac{\partial T}{\partial y}\right] + \frac{\partial}{\partial z}\left[K_V \frac{\partial T}{\partial z}\right] \quad (5)$$

$$\frac{\partial S}{\partial t} + \frac{\partial uS}{\partial x} + \frac{\partial vS}{\partial y} + \frac{\partial wS}{\partial z} = \frac{\partial}{\partial x}\left[D_H \frac{\partial S}{\partial x}\right] + \frac{\partial}{\partial y}\left[D_H \frac{\partial S}{\partial y}\right] + \frac{\partial}{\partial z}\left[D_V \frac{\partial S}{\partial z}\right] \quad (6)$$

Equation of State:

$$\rho = \frac{P}{(\alpha + 0.698P)}$$

where

$$\rho = P/(\alpha + 0.698P)$$

$$P = 5890 + 38T - 0.375T^2 + 3S$$

$$\alpha = 1779.5 + 11.25T - 0.0745T^2 - (3.8 + 0.01T)\ S \quad (7)$$

Equation 7 is based on the equation of state by Eckert (1958), where temperature, T, is in degrees centigrade, salinity, S, is in ppt (part per thousand) and density, ρ, is in g/cm^3.

In Equations 1 through 6, (u,v,w) are velocities in (x,y,z) directions (see Figure 1), f is the Coriolis parameter defined as $2\Omega \sin\phi$ (where Ω is the rotational speed of the earth, and ϕ is the latitude), ρ_o is a reference fluid density, ρ is the variable density, p is pressure, T is temperature, S is salinity, (A_H, K_H, D_H) are horizontal turbulent eddy coefficients, and (A_V, K_V, D_V) are vertical turbulent eddy coefficients for momentum, mass, and heat, respectively. In addition to the above equations, HYDRO3D includes an equation for dissolved species concentration written similar to Equation 6.

2.2.2 Grid System

HYDRO3D uses a vertically stretched grid, i.e., the so-called "σ-stretching", which leads to a smoother representation of the topography and the same order of vertical resolution for the shallow and deeper parts of the water body as shown in Figure 2. The transformation is done using the following equation.

$$\sigma = \frac{z - \zeta\ (x,y,t)}{h(x,y) + \zeta(x,y,t)} \quad (8)$$

σ-stretching offers some advantages over z-grid configurations, but there are some problems that can arise in setting up the grid for steep bottom slopes. The σ-stretching 3-D model allows the smoother resolution of bathymetry that the stair-step configuration of z-grids (Leendertse and Liu 1975). It is necessary, however, to have sufficient resolution in the horizontal and lateral directions of the σ-grid to avoid erratic results. In addition, Sheng et al. (1989b) and Johnson et al. (1989) report that the z-grid is better that the σ-grid in the presence of steep bottom slopes. It was

$$\sigma = \frac{z-\zeta}{\zeta+h} \approx \frac{z}{h}$$

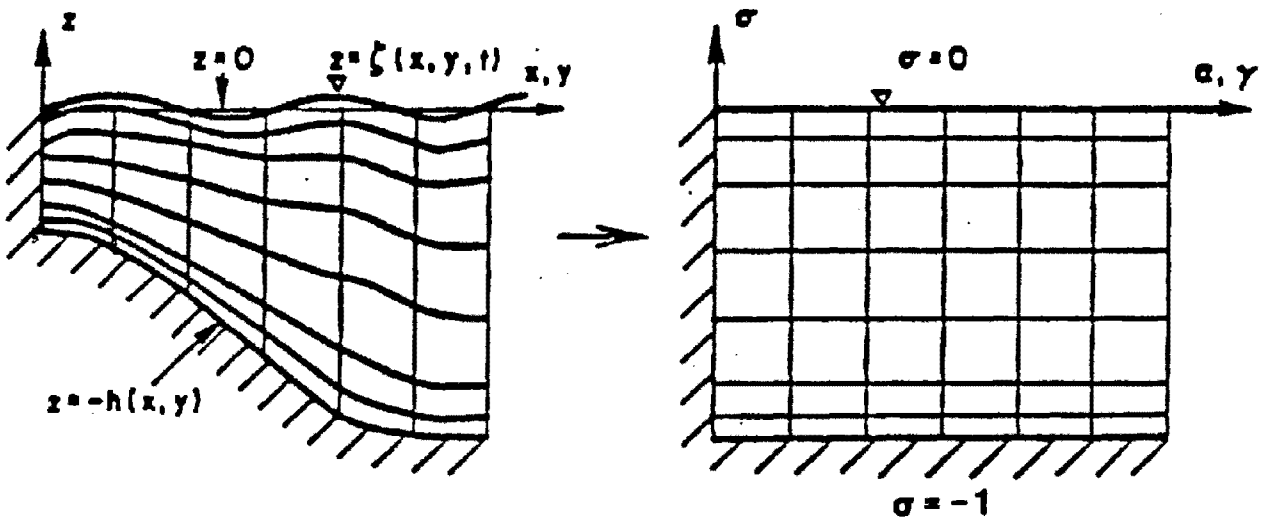

Figure 2. Vertical stretching of the coordinates.

found that it is advisable to evaluate the baroclinic gradient along the constant z-plane (horizontal plane) and that higher order advection schemes should be avoided.

The σ-stretching introduces extra terms into the original Cartesian equations of motion. However, most of these extra terms appear in the horizontal diffusion terms, which are generally less significant.

In the horizontal direction, HYDRO3D allows the use of either a uniform or a non-uniform Cartesian grid. For non-uniform grids, there are two options. The HYDRO3D program will accept either an arbitrary, non-uniform grid or a smoothly varying stretched grid (see Figure 3) which satisfies the following equations:

$$x = a_x + b_x \alpha^{C_x} \tag{9}$$

$$y = a_y + b_y \gamma^{C_y} \tag{10}$$

where (α,γ) represent the uniformly-spaced computational grid and (a_x, b_x, C_x, a_y, b_y, C_y) are stretching constants. A uniform grid can be obtained by setting: $a_x = 0$, $b_x = 1$, $C_x = 1$, $a_y = 0$, $b_y = 1$, and $C_y = 1$. To generate a non-uniform grid according to the transformation Equations 9 and 10, the example in Sheng and Butler (1980) can be followed. The detailed procedure for deriving the σ-stretched grid can be found in Sheng and Lick (1980) and Sheng (1983).

The lateral stretching introduces stretching coefficients, $\mu_x = dx/d\alpha$ and $\mu_y = dy/d\gamma$ into the spatial derivative terms in the transformed equations of motion. When a non-stretched grid is used, then $\mu_x = \mu_y = 1$.

2.2.3 Non-Dimensionalization of the Governing Equations

Dimensionless governing equations make it easy for a user to compare the relative importance of various terms and to minimize numerical errors. When properly non-dimensionalized, the part of each term contained within a parenthesis or bracket of Equations 13 through 17 that follow should be of unity order and the part of the term containing the dimensionless number(s) will indicate the order of the term.

The governing equations are nondimensionalized using the following dimensionless variables:

$$(u^*, v^*, w^*) = \left(\frac{u,}{U_r}, \frac{v,}{U_r}, \frac{wX_r}{Z_r U_r} \right)$$

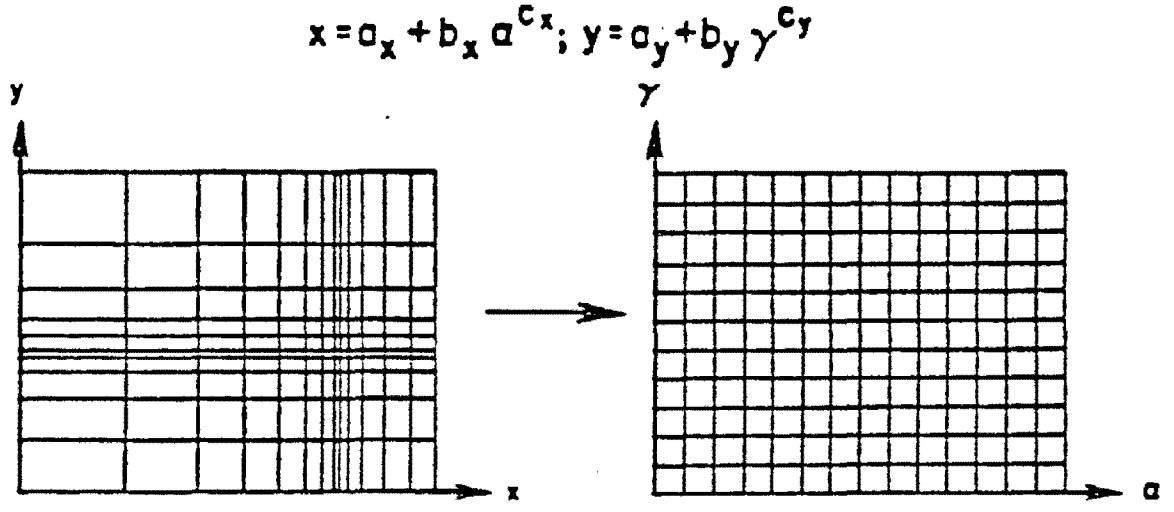

Figure 3. Lateral stretching of the coordinates.

$$(x^*,\ y^*,\ z^*) = \left(\frac{x}{X_r},\ \frac{y}{X_r},\ \frac{zX_r}{Z_rX_r} \right)$$

$$(\tau_x^*,\ \tau_y^*) = \left(\frac{\tau_x^W,}{\rho_o f Z_r U_r} \quad \frac{\tau_y^W}{\rho_o f Z_r U_r} \right)$$

$$t^* = tf$$

$$q_s^* = \frac{T_o}{(T_r - T_o)} \quad \frac{q}{\rho_o C_p f Z_r T_o}$$

$$\zeta^* = \frac{g\zeta}{FU_rX_r} = \frac{\zeta}{S_r}$$

$$\rho^* = \frac{\rho - \rho_o}{\rho_r - \rho_o}$$

$$T^* = \frac{T - T_o}{T_r - T_o}$$

$$A_H^* = \frac{A_H}{A_{Hr}}$$

$$A_V^* = \frac{A_v}{A_{vr}}$$

$$K_H^* = \frac{K_H}{K_{Hr}}$$

$$K_V^* = \frac{K_v}{K_{vr}}$$

$$D_H^* = \frac{D_H}{D_{Hr}}$$

$$D_V^* = \frac{D_v}{D_{vr}}$$

$$\omega^* = \frac{\omega X_r}{U_r} \qquad (11)$$

Where X_r is the reference length in lateral direction, usually the maximum dimension of the basin or water body, Z_r in the reference depth, usually the average depth of the basin, the U_r is the reference velocity, ω is the vertical velocity in the σ-direction, t is time, f is the Coriolis parameter, q is the heat flux at the surface, C_p is the specific heat of water, $S_r = fU_rX_r/g$, ζ is the displacement of the water surface at any time as defined in Figure 1, ρ_o is a base fluid density usually taken as the minimum density in the water body being simulated, ρ is the variable density, ρ_r is another reference density usually taken as the maximum density, T is water temperature, T_0 is a base water temperature usually taken as the minimum, T_r is a reference water temperature usually taken as the maximum, A_H, K_H, D_H are horizontal turbulent eddy coefficients, and A_V, K_V, D_V are vertical turbulent eddy coefficients for momentum, mass, and heat, respectively. Some of these parameters are defined in Appendix A for future reference.

The following dimensionless parameters are derived when the equations are nondimensionalized:

Vertical Ekman Number: $$E_v = \frac{A_{vr}}{fZ_r^2} = \frac{t_i}{t_{vdm}}$$

Lateral Ekman Number: $$E_H = \frac{A_{Hr}}{fX_r^2} = \frac{t_i}{t_{\ell dm}}$$

Vertical Prandtl Number: $$Pr_v = \frac{A_{vr}}{K_{vr}} = \frac{t_{vdh}}{t_{vdm}}$$

Lateral Prandtl Number: $$Pr_H = \frac{A_{Hr}}{K_{Hr}} = \frac{t_{\ell dh}}{t_{\ell dm}}$$

Vertical Schmidt Number: $$Sc_v = \frac{A_{vr}}{D_{vr}} = \frac{t_{vds}}{t_{vdm}}$$

Lateral Schmidt Number: $$Sc_H = \frac{A_{Hr}}{D_{Hr}} = \frac{t_{\ell ds}}{t_{\ell dm}}$$

Froude Number: $$Fr = \frac{U_r}{(gZ_r)^{1/2}} = \frac{t_{ge}}{t_c}$$

Rossby Number: $$Ro = \frac{U_r}{fX_r} = \frac{t_i}{t_c}$$

$$\beta = \frac{gZ_r}{f^2 X_r^2} = \frac{(Ro)}{(Fr)^2} = \frac{(t_i)}{(t_{ge})^2}$$

$$S_z = \frac{S_r}{Z_r}$$

$$\varepsilon = \frac{(\rho_r - \rho_o)}{\rho_o}$$

Densimetric Froude Number: $$Fr_D = \frac{Fr}{\sqrt{\varepsilon}} = \frac{t_{gi}}{t_c} \qquad (12)$$

where the various t variables appearing in the above expressions represent the characteristic time scales associated with various physical processes. The inertia oscillation time scale is t_i, vertical turbulent diffusion time scales are t_{vdm}, t_{vdh}, t_{vds}, the lateral turbulent diffusion time scales are $t_{\ell dm}$, $t_{\ell dh}$, $t_{\ell ds}$, the convection time scale is t_c, the gravity wave time scale is t_{ge}, and the internal gravity wave is t_{gi}. These are better defined in Appendix C.

2.2.4 Dimensionless Equations in Stretched Coordinates

Using the dimensionless variables and parameters in Sections 2.2.3 and dropping the asterisks for clarity, the following dimensionless equations can be derived:

$$\frac{\partial \zeta}{\partial t} + \frac{\beta}{\mu_x}\frac{\partial Hu}{\partial x} + \frac{\beta}{\mu_y}\frac{\partial Hv}{\partial y} + \beta H\frac{\partial \omega}{\partial \sigma} = 0 \qquad (13)$$

$$\frac{1}{H}\frac{\partial Hu}{\partial t} = -\frac{1}{\mu_x}\frac{\partial \zeta}{\partial x} + \frac{E_v}{H^2}\frac{\partial}{\partial \sigma}\left(A_v \frac{\partial u}{\partial \sigma}\right) + v - \frac{Ro}{H}\left(\frac{1}{\mu_x}\frac{\partial Huu}{\partial x} + \frac{1}{\mu_x}\frac{\partial Huv}{\partial y} + \frac{\partial Hu\omega}{\partial \sigma}\right)$$

$$+ E_H\left[\frac{\partial}{\mu_x \partial x}\left(A_H \frac{\partial u}{\mu_x \partial x}\right) + \frac{\partial}{\mu_y \partial y}\left(A_H \frac{\partial u}{\mu_y \partial y}\right) + H.O.T.\right]$$

$$- \frac{Ro}{Fr_D^2}\left[H\int_\sigma^0 \frac{\partial \rho}{\mu_x \partial x}\, d\sigma + \frac{\partial H}{\mu_x \partial x}\left(\int_\sigma^0 \rho d\sigma + \sigma\rho\right)\right] = -\frac{\partial \zeta}{\mu_x \partial x} + \frac{E_v}{H^2}\frac{\partial}{\partial \sigma}\left(A_v \frac{\partial u}{\partial \sigma}\right) + B_x \tag{14}$$

$$\frac{1}{H}\frac{\partial Hv}{\partial t} = -\frac{1}{\mu y}\frac{\partial \zeta}{\partial y} + \frac{E_v}{H^2}\frac{\partial}{\partial \sigma}\left(A_v \frac{\partial v}{\partial \sigma}\right) - u - \frac{Ro}{H}\left(\frac{1}{\mu_x}\frac{\partial Huv}{\partial x} + \frac{1}{\mu_y}\frac{\partial Hvv}{\partial y} + \frac{\partial Hv\omega}{\partial \sigma}\right)$$

$$+ E_H\left[\frac{\partial}{\mu_x \partial x}\left(A_H \frac{\partial v}{\mu_x \partial x}\right) + \frac{\partial}{\mu_y \partial y}\left(A_H \frac{\partial v}{\mu_y \partial y}\right) + H.O.T.\right]$$

$$- \frac{Ro}{Fr_D^2}\left[H\int_\sigma^0 \frac{\partial \rho}{\mu_y \partial y}\, d\sigma + \frac{\partial H}{\mu_y \partial y}\left(\int_\sigma^0 \rho d\sigma + \sigma\rho\right)\right] = -\frac{\partial \zeta}{\mu_y \partial y} + \frac{E_v}{H^2}\frac{\partial}{\partial \sigma}\left(A_v \frac{\partial v}{\partial \sigma}\right) + B_y \tag{15}$$

$$\frac{1}{H}\frac{\partial HT}{\partial t} = \frac{E_v}{Pr_v}\frac{\partial}{H^2 \partial \sigma}\left(K_v \frac{\partial T}{\partial \sigma}\right) - \frac{Ro}{H}\left(\frac{\partial HuT}{\mu_x \partial x} + \frac{\partial HvT}{\mu_y \partial y} + \frac{\partial H\omega T}{\partial \sigma}\right)$$

$$+ \frac{E_H}{Pr_H}\left[\frac{\partial}{\mu_x \partial x}\left(K_H \frac{\partial T}{\mu_x \partial x}\right) + \frac{\partial}{\mu_y \partial y}\left(K_H \frac{\partial T}{\mu_y \partial y}\right) + H.O.T.\right] \tag{16}$$

$$\frac{1}{H}\frac{\partial HS}{\partial t} = \frac{E_v}{Sc_v}\frac{\partial}{H^2 \partial \sigma}\left(D_v \frac{\partial S}{\partial \sigma}\right) - \frac{Ro}{H}\left(\frac{\partial HuS}{\mu_x \partial x} + \frac{\partial HvS}{\mu_y \partial y} + \frac{\partial H\omega S}{\partial \sigma}\right)$$

$$+ \frac{E_H}{Sc_H}\left[\frac{\partial}{\mu_x \partial x}\left(D_H \frac{\partial S}{\mu_x \partial x}\right) + \frac{\partial}{\mu_y \partial y}\left(D_H \frac{\partial S}{\mu_y \partial y}\right) + H.O.T.\right] \tag{17}$$

$$\rho = \rho(T, S) \tag{18}$$

where H.O.T represents higher order terms, and the equation of state (in Equation 1*) has been shown before in Equation 7.

2.2.5 Vertically Integrated Equations

For vertically mixed estuaries, the governing equations can be integrated over the depth. The resulting a non-dimensional form is given as:

$$\frac{\partial \zeta}{\partial t} + \beta \left[\frac{\partial U}{\mu_x \partial x} + \frac{\partial V}{\mu_y \partial y} \right] = 0 \tag{19}$$

$$\frac{\partial U}{\partial t} = - \frac{H}{\mu_x} \frac{\partial \zeta}{\partial x} + \tau_{sx} - \tau_{bx} + V - Ro \left[\frac{\partial}{\mu_x \partial x} \left(\frac{UU}{H} \right) + \frac{\partial}{\mu_y \partial y} \left(\frac{UV}{H} \right) \right]$$

$$+ E_H \left[\frac{\partial}{\mu_x \partial x} \left(A_H \frac{\partial U}{\mu_x \partial x} \right) + \frac{\partial}{\mu_y \partial y} \left(A_H \frac{\partial U}{\mu_y \partial y} \right) \right] - \frac{Ro}{Fr_D^2} \frac{H^2}{2} \frac{\partial \rho}{\mu_x \partial x} = - \frac{H}{\mu_x} \frac{\partial \zeta}{\partial x} + D_x \tag{20}$$

$$\frac{\partial V}{\partial t} = - \frac{H}{\mu_y} \frac{\partial \zeta}{\partial y} + \tau_{sy} - \tau_{by} - U - Ro \left[\frac{\partial}{\mu_x \partial x} \left(\frac{UV}{H} \right) + \frac{\partial}{\mu_y \partial y} \left(\frac{VV}{H} \right) \right]$$

$$+ E_H \left[\frac{\partial}{\mu_x \partial x} \left(A_H \frac{\partial V}{\mu_x \partial x} \right) + \frac{\partial}{\mu_y \partial y} \left(A_H \frac{\partial V}{\mu_y \partial y} \right) \right] - \frac{Ro}{Fr_D^2} \frac{H^2}{2} \frac{\partial \rho}{\mu_y \partial y} = - \frac{H}{\mu_y} \frac{\partial \zeta}{\partial y} + D_y \tag{21}$$

where the variables are defined in Appendices A and C.

The nonlinear inertia, lateral diffusion, and baroclinic pressure gradient terms in Equations 20 and 21 are obtained by vertically integrating the corresponding terms in Equations 14 and 15, respectively. However, these terms are obtained by assuming that horizontal velocity and density are uniform in the vertical direction, an assumption which is not always valid. In addition, the vertically integrated equations ignore the baroclinic terms. Thus, the above forms of vertically integrated equations are not recommended for all flows, especially those involving baroclinic circulation. When barolclinic circulation is important, the fully 3-D version of HYDRO3D should be used. Details of the vertically integrated equations are briefly discussed later in this section.

2.2.6 Vertical Velocities

Equations describing the vertical velocity in the transformed coordinates are:

$$\omega = -\frac{1+\sigma}{\beta H}\frac{\partial \zeta}{\partial t} - \frac{1}{H}\int_{-1}^{\sigma}\left(\frac{\partial Hu}{\mu_x \partial x} + \frac{\partial Hv}{\mu_y \partial y}\right) d\sigma \tag{22}$$

$$w = H\omega + \frac{(1+\sigma)}{\beta}\frac{d\zeta}{dt} + \sigma\left[u\frac{\partial h}{\mu_x \partial x} + v\frac{\partial h}{\mu_y \partial y}\right] \tag{23}$$

where ω is the vertical velocity in σ-stretched coordinate system, and w is the vertical velocity in the original Cartesian coordinate system, respectively.

2.3 BOUNDARY AND INITIAL CONDITIONS

The HYDRO3D program can be applied to problems with a variety of initial and boundary conditions as given below.

2.3.1 Vertical Boundary Conditions

The boundary conditions at the free surface (σ = o) are:

$$A_v\left(\frac{\partial u}{\partial \sigma}, \frac{\partial v}{\partial \sigma}\right) = \frac{H}{E_v}(\tau_{sx}, \tau_{sy})$$

$$\frac{\partial T}{\partial \sigma} = \frac{HPr_v}{E_v} q_s$$

$$\frac{\partial S}{\partial \sigma} = 0 \tag{24}$$

where q_s is the heat flux at the surface, τ_{bx} is bottom shear stress in the x direction, τ_{by} is the bottom shear stress in the y-direction, and $\partial u/\partial\sigma$ and $\partial v/\partial\sigma$ are the partial derivatives of longitudinal and lateral velocities with respect to the σ coordinate defined earlier.

(τ_{sx}, τ_{sy}) and $\left(\frac{\partial u}{\partial \sigma} , \frac{\partial v}{\partial \sigma} \right)$ are in tensor form notation. The other parameters were defined earlier.

The boundary conditions at the bottom (σ = -1) are:

$$A_v \left(\frac{\partial u}{\partial \sigma} , \frac{\partial v}{\partial \sigma} \right) - \frac{H}{E_v} (\tau_{bx} , \tau_{by}) = \frac{u_r}{A_{vr}} H Z_r C_d (u_1^2 + v_1^2)^{1/2} (u_1 , v_1)$$

$$\frac{\partial T}{\partial \sigma} = 0$$

$$\frac{\partial S}{\partial \sigma} = 0 \qquad (25)$$

where C_d is the drag coefficient applied to the bottom surface, and (u_1, v_1) represents the velocity vector components at the first grid point above the bottom. The drag coefficient is related to the Manning roughness coefficient for bottom roughness as shown by McCutcheon et al. (1990). Also see Sheng (1983). McCutcheon et al. (1990) compiles representative values of the Manning for estuaries.

2.3.2 Lateral Boundary Conditions

Along the shoreline where river inflow or outflow may occur, the boundary conditions are:

$$u = u(x,y,\sigma,t)$$

$$v = v(x,y,\sigma,t)$$

$$\omega = 0$$

$$T = T(x,y,\sigma,t)$$

$$S = S(x,y,\sigma,t) \qquad (26)$$

where u, v, T, and S are velocity in the x-direction, velocity int he y-direction, water temperature, and salinity, respectively varying dynamically with time t and spatially in the (x, y, σ) coordinate system. ω is the vertical velocity, assumed to be zero.

At the solid boundary, both the normal and tangential velocity components are equal to zero. In addition, the normal derivatives of temperature and salinity are also set equal to zero.

Along an open boundary, either ζ or the velocity can be specified. For the water surface elevation ζ, there are currently three options:

$$\zeta = \zeta(x,y,t) = \sum_{n=1}^{n_{max}} A_n \cos\left(\frac{2\pi t}{T_n} + \phi_n\right) \tag{27}$$

or

$$\frac{\partial \zeta}{\partial x} = 0 \quad \text{and} \quad \frac{\partial \zeta}{\partial y} = 0 \tag{28}$$

or

$$\frac{\partial \zeta}{\partial t} \pm c \frac{\partial \zeta}{\partial x} = 0 \quad \text{and} \quad \frac{\partial \zeta}{\partial t} \pm c \frac{\partial \zeta}{\partial y} = 0 \tag{29}$$

where A_n, T_n, ϕ_n are the amplitude, period, and phase angle of the tabular tidal constituents, respectively; n_{max} is the maximum number of these tidal constituents; and c is the dimensionless phase speed of surface gravity wave at the open boundary. See the Case Studies for Suisun Bay and Charlotte Harboer (Equation 62) in Section 4 for an illustration of the application of Equation 27.

When open boundary conditions are given in terms of ζ, the normal velocity component is assumed to be of zero slope. The tangential velocity component may be either zero, or of zero slope, or computed from the momentum equations.

The salinity or total solids along an open boundary or river entrance is computed from a 1-D advection equation during the outflow. For example, along an open boundary perpendicular to the x-direction.

$$\frac{\partial HS}{\partial t} + Ro \frac{\partial HuS}{\mu_x \partial x} = 0 \tag{30}$$

where the spatial salinity flux is evaluated from the salinity values at the boundary and the interior grid point via a one-sided differencing scheme.

During the inflow, however, the salinity value at the open boundary can either take on a prescribed value or be determined from the 1-D advection equation while using the boundary salinity value and the prescribed salinity value to evaluate the spatial flux term. Section 4.3 on the Charlotte Harbor case study regarding the application of Equation 30 and other options.

2.3.3 Initial Conditions

To start a simulation, the initial spatial distributions of ζ, u, v, ω, T, and S must be specified. However, when initial data are completely unknown, there is usually little choice but to start with zero initial fields. This is a process referred to as spin-up. It invilved starting at resta nd running the model until reason conditions are attained. These attained conditions become the initial conditions of the next simulation if the simulation is stopped and restarted. If the simulation is continued, this point in time defines the beginning of the results that will be used to investigate circulation and mass transport. See Case Study 4.3 on Charlotte Harbor for a brief review of the procedure. When initial data are known at a limited number of locations an initial field can be generated by an appropriate interpolation scheme. In principle, the interpolated field must satisfy the conservation law governing that field variable.

For practical simulations of barotropic flow in the absence of salinity and temperature variation, the HYDRO3D code usually assumes zero initial flow if few initial data are known. This is reasonable because the spin-up time of a barotropic flow field is relatively short due to the use of a variable time-stepping scheme. In case of a baroclinic simulation where salinity and temperature varies with space and time, the spin-up time is longer and an interpolation routine is provided to produce a reasonable initial field from limited data points.

2.4 NUMERICAL SOLUTION ALGORITHM

2.4.1 External Mode

In the external solution mode the model solves for the surface displacement ζ and the vertically integrated velocities U and V in Equations 19 through 21. To speed up the model simulation, all the terms in Equations 19 through 21 related to the propagation of surface gravity wave are treated implicitly. The time derivatives and surface slopes in the momentum equations are generally treated implicitly, whereas the bottom stresses are computed explicitly from the latest vertical profiles of horizontal velocities.

The dimensionless finite-difference equations needed to obtain the external mode solution given in matrix notation as:

$$[A]\ \{F\}^{n+1} = [I]\ \{F\}^{n} + \Delta t\ \{D\}^{n} \qquad (31)$$

where:

$$[A] = \begin{bmatrix} 1 & \frac{\beta\Delta t}{\mu_x \Delta x}\gamma_x & \frac{\beta\Delta t}{\mu_y \Delta y}\delta_y \\ \frac{H\Delta t}{\mu_x \Delta x}\delta_x & 1 & 0 \\ \frac{H\Delta t}{\mu_y \Delta y}\delta_y & 0 & 1 \end{bmatrix}$$

$$[I] = \begin{bmatrix} 1 & 0 & 0 \\ 0 & 1 & 0 \\ 0 & 0 & 1 \end{bmatrix} \qquad (32)$$

$$\{F\} = \begin{Bmatrix} \zeta \\ U \\ V \end{Bmatrix}$$

$$\{D\} = \begin{Bmatrix} 0 \\ D_x \\ D_y \end{Bmatrix}$$

where Δx, Δz, Δt, δ_x, and δ_y are space intervals in the x-and y-directions, the time interval, and delta notations in x, y directions, respectively.

It is convenient to express the matrix [A] as the sum of three matrices. These are the identity matrix [I], a matrix $[A_x]$ and a matrix $[A_y]$. The matrices $[A_x]$ and $[A_y]$ are written as:

$$[A_x] = \begin{bmatrix} 0 & \frac{\beta\Delta t}{\mu_x \Delta x}\,\delta_x & 0 \\ \frac{H\Delta t}{\mu_x \Delta x}\,\delta_x & 0 & 0 \\ 0 & 0 & 0 \end{bmatrix}$$

$$[A_y] = \begin{bmatrix} 0 & 0 & \frac{\beta\Delta t}{\mu_y \Delta y}\,\delta_y \\ 0 & 0 & 0 \\ \frac{H\Delta t}{\mu_y \Delta y}\,\delta_y & 0 & 0 \end{bmatrix} \qquad (33)$$

The factorization of Equation 31 and neglecting of terms of order Δt^2 yields the following x-sweep and y-sweep expressions:

x-sweep:

$$([I] + [A_x])\,\{F\}^* = ([B] - [A_y])\,\{F\}^N + \Delta t\,\{D\}^N \qquad (34)$$

y-sweep:

$$([I] + [A_y])\,\{F\}^{N+1} = \{F\}^* + [A_y]\{F\}^N \qquad (35)$$

where N, and N+1 are the successive time step counters; $[F]^{N+1}$, $[F]^{N}$ and $[F]^{*}$ are the solution vectors at time steps N+1, N, and the intermediate between the x-sweep and y-sweep, respectively. $(D)^{N}$ is the residual(or forcing) matrix at time step N.

Alternatively, the x sweep and y sweep are also listed here can be written as:

x-sweep:

$$\zeta^{*} + \frac{\beta\Delta t}{\mu_x \Delta x}\,\delta_x\, U^{*} = \zeta^{n} - \frac{\beta\Delta t}{\mu_y \Delta y}\,\delta_y\, V^{n} \tag{36}$$

and

$$U^{*} + \frac{H\Delta t}{\mu_x \Delta x}\,\delta_x \zeta^{*} = U^{n} + D_x^{n}\,\Delta t \tag{37}$$

y-sweep:

$$\zeta^{n+1} + \frac{\beta\Delta t}{\mu_y \Delta y}\,\delta_y\, V^{n+1} = \zeta^{*} + \frac{\beta\Delta t}{\mu_y \Delta y}\,\delta_y\, V^{n} \tag{38}$$

and

$$V^{n+1} + \frac{H\Delta t}{\mu_y \Delta y}\,\delta_y\, \zeta^{n+1} = V^{n} + D_y^{n}\,\Delta t \tag{39}$$

where U^{n}, V^{n} are velocity matrices at time step N; and D_x^{n}, and D_y^{y} are the forcing or residual matrix in the x and y-sweep at time step n, respectively.

2.4.2 Internal Mode

The internal mode solution is obtained by defining deficit velocities as $\tilde{u} \equiv u - \bar{u}$ and $\tilde{v} \equiv v - \bar{v}$, where $\bar{u}$ and $\bar{v}$ are vertically averaged by subtracting the vertically averaged momentum equations from the three-dimensional momentum equations multiplied by H. The resulting differential equations are:

$$\frac{1}{H}\frac{\partial H\tilde{u}}{\partial t} = B_x - \frac{D_x}{H} + \frac{E_v}{H^2}\frac{\partial}{\partial \sigma}\left[A_v \frac{\partial}{\partial z}\,(\bar{u} + \tilde{u}) \right] \tag{40}$$

$$\frac{1}{H}\frac{\partial H\tilde{v}}{\partial t} = B_y - \frac{D_y}{H} + \frac{E_v}{H^2}\frac{\partial}{\partial \sigma}\left[A_v \frac{\partial}{\partial z}\,(\bar{v} + \tilde{v}) \right] \tag{41}$$

which can be written in a finite difference form as:

$$(H\tilde{u})^{n+1} = (H\tilde{u})^{n} + \Delta t\ (HB_x - D_x)^n + H^n\ \Delta t\ \frac{E_v^n}{(H^n)^2}\ \frac{\partial}{\partial r}\left[A_v\ \frac{\partial}{\partial z}\ (\bar{u} + \tilde{u})^{n+1}\right] \tag{42}$$

$$(H\tilde{v})^{n+1} = (H\tilde{v})^{n} + \Delta t\ (HB_y - D_y)^n + H^n\ \Delta t\ \frac{E_v^n}{(H^n)^2}\ \frac{\partial}{\partial r}\left[A_v\ \frac{\partial}{\partial z}\ (\bar{v} + \tilde{v})^{n+1}\right] \tag{43}$$

The vertical diffusion terms in the momentum equations are treated implicitly to ensure numerical stability in shallow water. It also is important to ensure that the vertically integrated deficit velocities always equal zero or:

$$\sum_{k=1}^{k_{max}} \tilde{u}_{i,j,k} = 0 \tag{44}$$

$$\sum_{k=1}^{k_{max}} \tilde{v}_{i,j,k} = 0 \tag{45}$$

where K_{max} is the maximum number of the vertical layers. To ensure that Equations 44 and 45 are satisfied, the nonlinear inertia, baroclinic, and horizontal turbulent diffusion terms in the vertically integrated Equations 20 and 21 must be evaluated by summing the corresponding terms in the 3-D equations at all vertical levels.

Once $\tilde{u}^{n+1}$ and $\tilde{v}^{n+1}$ are obtained, u and v can be obtained from:

$$u^{n+1} = \tilde{u}^{n+1} + \frac{U^{n+1}}{H^{n+1}} \tag{46}$$

$$v^{n+1} = \tilde{v}^{n+1} + \frac{V^{n+1}}{H^{n+1}} \tag{47}$$

Following these, the vertical velocities ω^{n+1} and w^{n+1} can be computed from:

$$\omega_k^{n+1} = \omega_{k-1}^{n+1} - \frac{\Delta\sigma}{\beta H}\left(\frac{\partial\zeta}{\partial t}\right)^{n+1} - \frac{\Delta\sigma}{H}\left[\left(\frac{\partial Hu}{\mu_x\partial x}\right)_k^{n+1} + \left(\frac{\partial Hv}{\mu_y\partial y}\right)_k^{n+1}\right] \tag{48}$$

$$w_k^{n+1} = H^{n+1}\,\omega_{k-1}^{n+1} + \frac{1+\sigma}{\beta}\left(\frac{d\zeta}{t}\right)^{n+1} + \sigma\left(u\frac{\partial h}{\mu_x\partial x} + v\frac{\partial h}{\mu_y\partial y}\right)_k^{n+1} \tag{49}$$

where the vertical velocity ω should be almost zero at the free surface.

2.5 TURBULENCE CLOSURE

Turbulence parameterization is necessary because of the averaged nature of the governing equations, as was discussed in the introductory part of this section. As noted, there is some art to selecting turbulence parameters. This selection process is therefore aided if there are several methods available to give the user some flexibility to chose a method tailored to his experience and the conditions at the site of interest. This code offers relatively good flexibility ranging from a simple constant eddy coefficient to a simplified second-order closure approach. In all, three methods are available to determine the vertical eddy coefficients. These are:

- Specification of constant eddy coefficients,
- Calculation by the Munk-Anderson formulation, and
- Calculation using a simplified second-order closure scheme.

There are a number of other closure schemes, but all have various theoretical and practical disadvantages, as do these options. See Sheng (1983), Blumberg (1986), Rodi (1980) and ASCE (1988) for more detailed information on these methods and other alternative methods. At the moment, we can not offer the users comprehensive guidance on turbulence modeling in this document. However, when simulations are sensitive to turbulence parameters and assistance is need, users should contact the Center for Exposure Assessment Modeling (CEAM), U.S. EPA ERL-Athens (see Preface). The CEAM can assist in calibrating a model or refer users to experts in the field to handle difficult problems. In addition, users may wish to consult any readme files associated with the distribution of this code or any information that may be available on the CEAM bulletin board to learn of supplements to this manual on turbulence parameterization. Several reviewers have noted the need to supplement the information available in this report and the CEAM will attempt to do this as time permits.

2.5.1 Constant Eddy Coefficients

For this option, constant eddy coefficients are specified in the vertical direction. These constant values are equal for momentum, mass, and

heat transfer (Peter Smith, in review) despite the knowledge that this is not precisely correct. (Monin and Yaglom 1971, Turner 1973). Given the approximate nature of the eddy viscosity approach however, this can be a practical means of making reasonable calculations.

The use of constant eddy coefficients is not normally recommended for precise calibrations of a hydrodynamic model (e.g., see McCutcheon et al. 1990 for guidance). Such an application, will only crudely approximate circulation, transport, and mixing in a stratified flow or a complex flow. In some screening analyses, however, approximate descriptions may be adequate for a preliminary investigation of circulation patterns. In addition, it may be useful to begin calibration of a model with this option to determine if a reasonable and stable solution is possible. As a result, the ability to specify a constant eddy coefficient is occasionally useful, but results can be inaccurate and misleading.

Because the use of constant eddy coefficients results in very approximate results, it is difficult to estimate the coefficients for various types of flows in different water bodies. Furthermore, published values can not be adequately assessed without knowledge of the sensitivity of model results to eddy coefficients. Unfortunately, this is rarely investigated or discussed in the available published reports. As a result all guidance on ranges of values must be used with care.

To assist in selecting eddy coefficients, see McCutcheon et al. (1990) for values obtained in estuaries, harbors, and coastal areas. Bowie et al. (1985) offers guidance for the relative order of magnitude of eddy coefficients that may be useful for selecting tentative values. Chapra and Reckhow (1983) and Henderson-Sellers (1984) discuss eddy coefficients for lakes and reservoirs. Typical values for North American large lakes are (Lynch 1986, Cheng et al. 1976, Csanady 1975):

$A_H = 10^3$ to 10^5 cm^2 s^{-1}	(horizontal eddy viscosity)
$A_V = 1$ to 100 cm^2 s^{-1}	(vertical eddy viscosity)
$U = 10$ cm s^{-1}	(horizontal velocity)
$L = 10^6$ to 10^7 cm	(horizontal length scale)
$H = 10^3$ to 10^4 cm	(vertical length scale)
$\Delta\rho/\rho = 10^{-3}$	(relative density difference over the depth)

Also see Sheng (1986b) for additional guidance on values of eddy coefficients that may be appropriate when studying lakes.

2.5.2 Munk-Anderson Type Eddy Coefficients

There are a number of different formulas for the vertical eddy coefficients for momentum, mass, and heat transfer (see McCutcheon et al. 1990 Henderson-Sellers 1982, Blumberg 1986, and Sheng 1983 for a review). Unfortunately, there is no clear guidance on which of these divergent formulations are best adapted to certain water bodies. McCutcheon et al. (1990) indicates that a Munk-Anderson type formulation among others may be useful for studies of estuaries when calibration may not be possible. Similar

guidance for lakes, coastal areas, and harbors is not readily available. When calibration is possible, McCutcheon et al. notes that there may be several alternative forms that are useful, but there has not been sufficient study to show that any form is significantly better that the Munk-Anderson form used in this and a number of other hydrodynamics codes (McCutcheon, 1983). As a result, the Munk-Anderson formulation offers useful flexibility and consistency with other models.

The Munk-Anderson formulation is based on the observation that eddy coefficients for stratified flows are a fraction of the eddy coefficients for non-stratified flows under the same conditions. The ratio of the stratified to non-stratified coefficients are equal to stability functions [ϕ_1(Ri) and ϕ_2(Ri)] of the gradient Richardson number (Richardson 1921, Turner 1973), expressed as:

$$A_v = A_{vo}\,\phi_1\,(Ri);\quad K_v = K_{vo}\,\phi_2(Ri);\ \text{and}\quad D_v = D_{vo}\,\phi_2(Ri) \tag{50}$$

where:

$$R_i = \frac{-gHZ_r\varepsilon}{U^2_r(1+\varepsilon\rho)}\frac{\partial\rho}{\partial\sigma}\left[\left(\frac{\partial u}{\partial\sigma}\right)^2+\left(\frac{\partial v}{\partial\sigma}\right)^2\right]^{-1} \tag{51}$$

ϵ is the dimensionless density and the other terms in the gradient Richardson number are also as have been described beforehand. The variables A_{vo}, K_{vo}, and D_{vo} are the eddy coefficients for momentum, mass, and heat transport under non-stratified conditions, respectively. For this code, it is assumed that the eddy coefficients for mass and heat transport are equivalent. This is not exactly the case and some small discrepancies may arise in the calculations of salinity and temperature. Also the usual practice is to assume that $A_{vo} = K_{vo} = D_{vo}$ (e.g., see McCutcheon 1983) as is done in this code. These variables are computed from the vertical transport of momentum as:

$$A_{vo} = \frac{Z_r U_r \Lambda^2_o}{H}\left[\left(\frac{\partial u}{\partial\sigma}\right)^2+\left(\frac{\partial v}{\partial\sigma}\right)^2\right]^{0.5} \tag{52}$$

where Λ_o is the length scale assumed to be a linear function of σ that increases with distance above the bottom and below the water surface, with a peak value at mid-depth, but not exceeding a certain defined fraction of the local depth.

Equation (52) is limited to describing the generation and dissipation of turbulence in boundary-layer like shear flows over the bottom. Among other effects, it does not include the transport of turbulence from different flow conditions, nor does it include the effects of surface waves. Waves can cause more intense mixing in the upper layers of deeper flows. In these cases where the flow is not a boundary-layer type, Equation (52) may be of limited validity. When flows are not boundary-layer types, it is typically assumed that the eddy coefficients are constant in the upper layers of flow, especially down to the thermocline in lakes (see Sheng et al. 1986a, Henderson-Sellers 1984) or constant below the thermocline (McCormick and Scavia 1981, McCutcheon 1983) depending on relative depths. For limited

additional information about the effects of wind mixing on the mixing coefficients see Kent and Pritchard (1959).

As noted above, the stability functions are of diverse forms but the Munk-Anderson formulations seems to be the best available for use. The general form of the Munk-Anderson (1948) formula is generally written as (McCutcheon et al. 1990).

$$\phi_1 = (1+\sigma_1 Ri)^{a1} \quad \text{and} \quad \phi_2 = (1+\sigma_2 Ri)^{a2} \tag{53}$$

where σ_1, a1, σ_2, a2 are empirical coefficients that vary from one water body to the next (McCutcheon et al. 1990), and seem to be spatially and temporally variable in a given body of water. See McCutcheon et al. (1990) for a tabulation of the coefficients that have been used in past studies of selected estuaries and coastal waters. Henderson-Sellers (1982) and Blumberg (1986) tabulate a few more values related to studies in lakes. Munk and Anderson (1948) found for the thermocline in the ocean that Equation 53 was best written as:

$$\phi_1 = (1+10Ri)^{-1/2} \quad \text{and} \quad \phi_2 = (1+3.33Ri)^{-3/2} \tag{54}$$

Not only the form of the stability function may vary from site to site,, but different Richardson numbers may also be used for different types of flow conditions. For example, the formation and deepening of the thermocline in a relatively shallow basin depends strongly on the relative importance of wind stress and heat flux at the free surface. In such a case, the following Richardson number could be used:

$$R_i = \frac{\kappa^2 g H Z_r \sigma^2 \varepsilon \quad \partial\rho}{U^2_r u^2_* (1+\varepsilon\rho) \; \partial\sigma} \tag{55}$$

where κ is the von Karman constant and u_* is the dimensionless friction (or shear) velocity at the free surface. McCutcheon et al (1990) review a number of other stability functions as well. These include gross Richardson numbers, Froude number, the Monin-Obukhov scaling length, the Nyquist Buoyancy frequency, and Richardson numbers based on shear velocity and average velocity along with various definitions of linear and nonlinear density gradients.

2.5.3 A Simplified Second-Order Closure Model

The simplified second-order closure model is derived from a complete Reynolds stress turbulent transport model by assuming a local equilibrium condition (Sheng 1982, 1983, 1984, 1986a). In addition to the mean flow equations, a set of algebraic equations are solved for the second-order correlations are solved to obtain the stability functions ϕ_1 and ϕ_2 in terms of the mean flow variables. These Cartesiaon coordinate equations, when written in dimensional and tensor forms, are:

$$\overline{-u_i'u_k'}\,\frac{\partial u_j}{\partial x_k} - \overline{u_j'u_k'}\,\frac{\partial u_i}{\partial x_k} - g_i\,\frac{\overline{u_j'\rho'}}{\rho_o} - g_j\,\frac{\overline{u_i'\rho}}{\rho_o}$$

$$- 2\,\varepsilon_{ik\ell}\,\Omega_k\,\overline{u_\ell'u_j'} - \varepsilon_{j\ell k}\,\Omega_\ell\,\overline{u_k'u_i'} - \frac{q}{\Lambda}\,\overline{u_i'u_j'} - \delta_{ij}\,\frac{q^2}{3} - \delta_{ij}\,\frac{q^3}{12\Lambda} = 0 \tag{56}$$

$$- \overline{u_i'u_j'}\,\frac{\partial \rho}{\partial x_j} - \overline{u_j'\rho'}\,\frac{\partial u_i}{\partial x_j} - \frac{\overline{g_i\rho'\rho'}}{\rho_o} - 2\,\varepsilon_{ijk}\Omega_j\,\overline{u_k'\rho'} - 0.75\,q - \frac{\overline{u_i'\rho'}}{\Lambda} = 0 \tag{57}$$

$$2\,\overline{u_j'\rho'}\,\frac{\partial \rho}{\partial x_j} + \frac{0.45\,q\,\overline{\rho'\rho'}}{\Lambda} = 0 \tag{58}$$

The subscripts i, j, and k correspond to the coordinate directions (x_i, x_j, x_k), usually numbered 1, 2, and 3. Therefore, u_i', u_j', and u_k' are velocity fluctuations about the mean velocities u_i, u_j, and u_k, respectively. Hence Equation 56 represents six separate formulas and Equation 57 represents three separate formulas. Also, ρ and ρ' are the mean density and density fluctuation, respectively; ρ_o is a reference density, usually taken as the minimum density; g is the gravitational vector; Ω is the vector for the rotational speed of the earth; ε is the pernutation tensor; q is the total turbulent micro-length velocity; and Λ is a turbulent length scale.

The detailed derivation of Equations 56 through 58 can be found in Sheng et al. (1989b). Also see Sheng (1983). A graphical comparison of this formulation versus some of the semi-empirical forms discussed in the last section is shown in Figure 4.

The length scale, Λ_o, is assumed to be a linear function of the vertical distance above the bottom or below the free surface. In addition, stratification is assumed to modify the length scale through the following empirical relationship:

$$\Lambda = \Lambda_o\,(\,1 + S_1\,Ri)S_2 \tag{59}$$

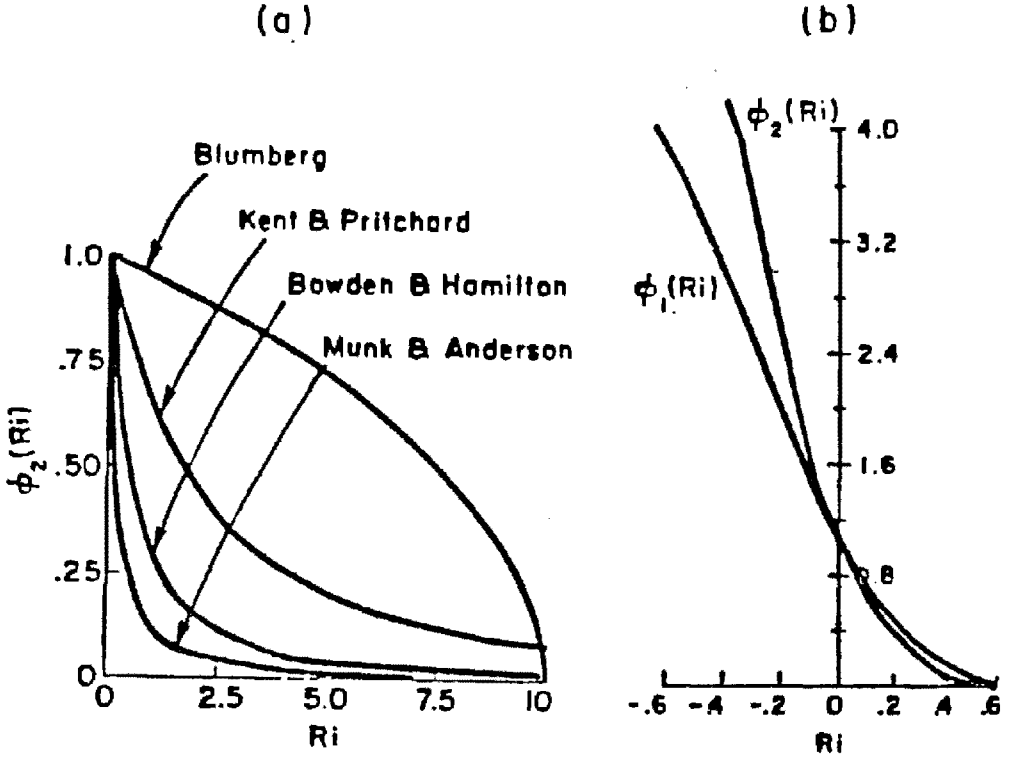

Figure 4. (a) Empirical stability functions of vertical turbulent eddy coefficients from Blumber (1975. (b) Stability functions determined from a second-order closure model of turbulent transport.

where S_1 and S_2 are arbitrary coefficients.

The length scale Λ is then adjusted such that the following relationships are satisfied (Sheng and Chin 1986):

$$\left|\frac{d\Lambda}{dZ}\right| \leq 0.65 \tag{60}$$

$$\Lambda \leq C_\Lambda H \tag{61}$$

$$\Lambda \leq C_\Lambda H_p \tag{62}$$

where C_Λ is usually on the order of 0.1 to 0.2, H is the total depth, and H_p is the depth of the pycnocline.

The simplified second-order closure model presented above is strictly valid when the turbulence time scale (Λ/q) is much less than the mean flow time scale and when turbulence does not change rapidly over Λ. It has been found, however, to be quite useful in simulating vertical flow structures in estuarine and coastal waters.

Figure 4 illustrates the behavior of the resulting stability functions as a function of the gradient Richardson number (see Equation 51). This response is similar to that obtained from the Munk-Anderson type vertical eddy coefficient functions of the gradient Richardson shown in Figure 4a. Figure 4 was not designed for an exact comparsion, but clearly the trend for the Munk-Anderson formulation [and similar forms by Kent and Pritchard 1959 and Bowden Hamilton (1975)] and the simplified second order closure formulation are the same for Ri>o (stable stratfication; if water is stratified, it is almost always stably stratified). The curve in Figure 4a by Blumberg, (1975) is from an alternative closure secheme.

2.6 GRID LAYOUT

The grid system used to describe any computational domain is explained below.

2.6.1 Staggered Grid

A staggered grid is used in both the horizontal and vertical directions of the computational domain (see Figure 5). This grid is often referred to as the "C-grid". In the horizontal directions, a unit cell consists of a ζ-point at the center ($\zeta_{j,i}$), a U-point to its right ($U_{j,i}$) and a V-point at its top ($V_{j,i}$). In the vertical direction, the vertical velocities are computed at the "full" grid points including the free surface ($k=k_{max}$).

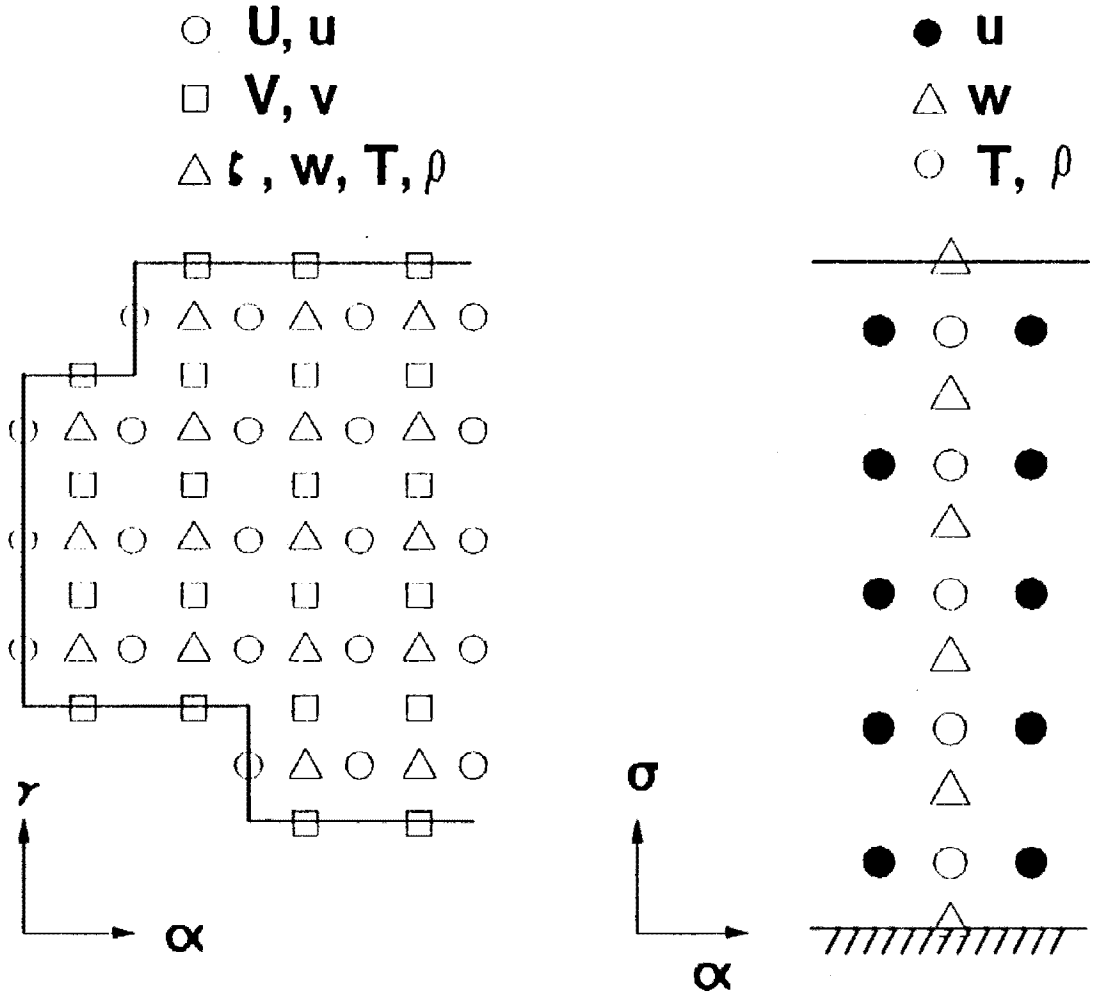

Figure 5. Staggered numerical grid.

Horizontal velocities, temperature, salinity and density are computed at the "half" grid points (half grid spacing below the full points).

2.6.2 Grid Index

Two arrays, each of dimension (J_{max}, I_{max}), are used to index the grid cells. The array NS indicates the condition of the left and right cell boundaries, whereas the array MS denotes the condition of the top and bottom cell boundaries (see Figure 6). JU1(I) and JU2(I) indicate the first and the last water points for computing U along the I-th column. JV1(I) and JV2(I) denote the second and the second to last water points for V. IU1(I) and IU2(I) indicate the second and the second to last water points for U along the I-th row. IV1(J) and IV2(J) denote the first and the last water points for V.

2.7 FLOW CHARTS

Flow charts of the major programs EHSMML, EHSMHC, EHSMEX, EHSMB3, and EHSMB4 are shown in Figures 7 through 11. The names of the major variables are listed in Appendix A.

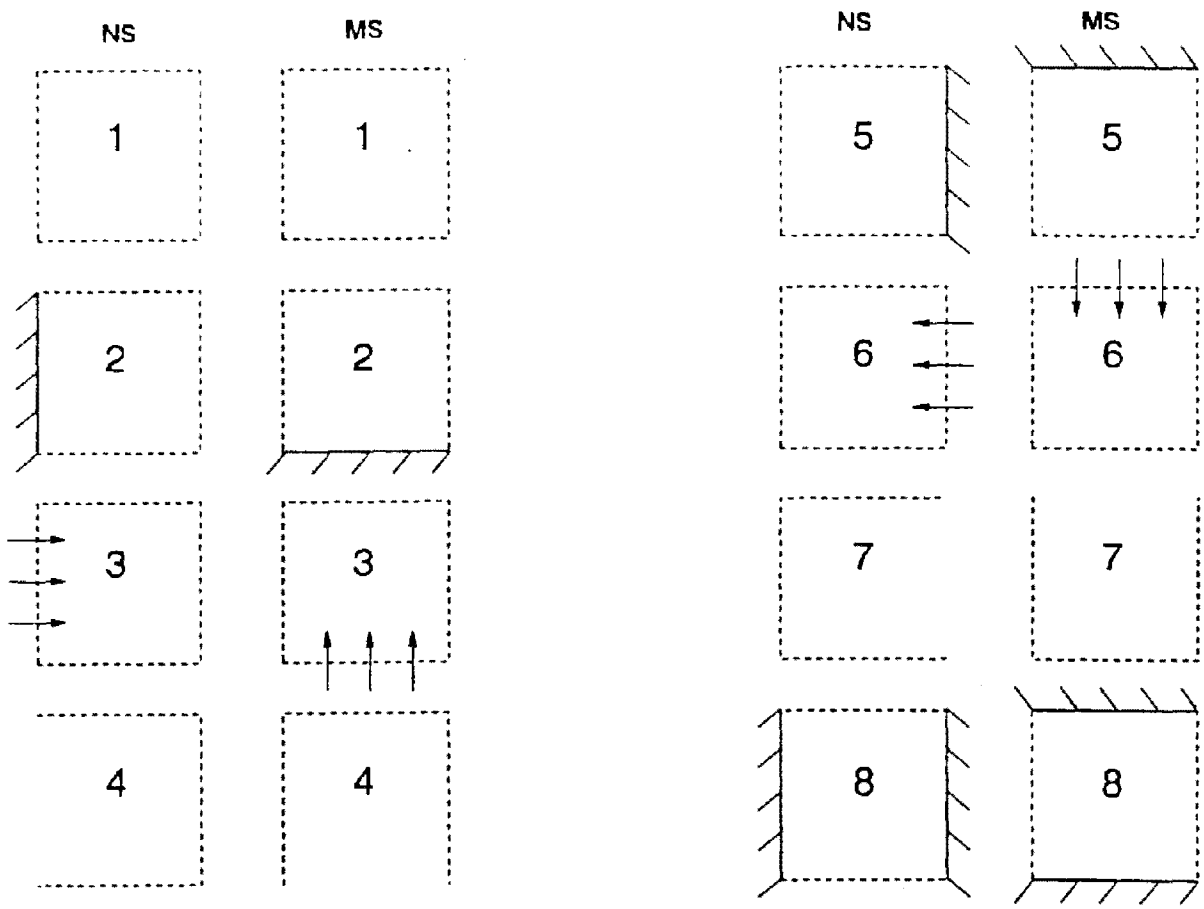

Figure 6. Grid indices NS and MS

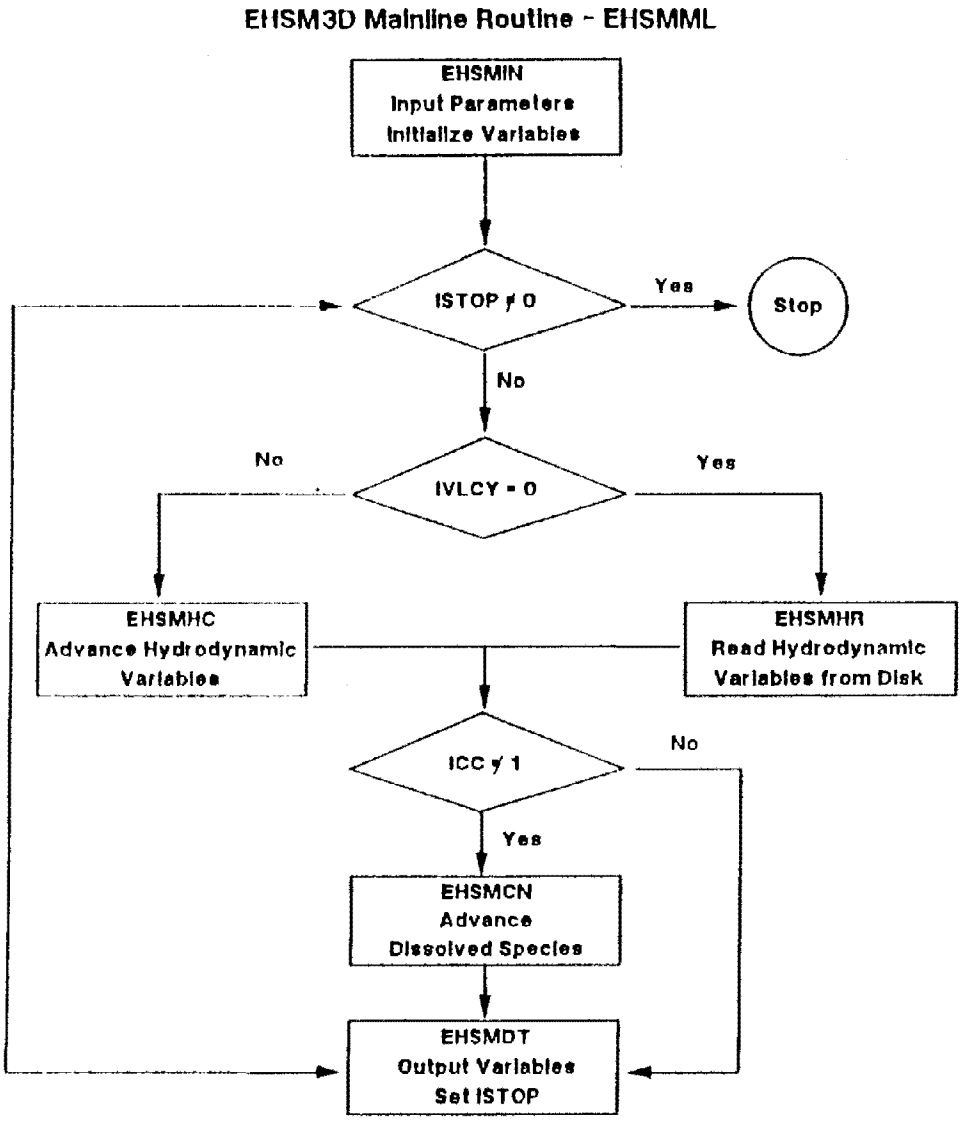

Figure 7. Flow chart of the Main Program EHSMML

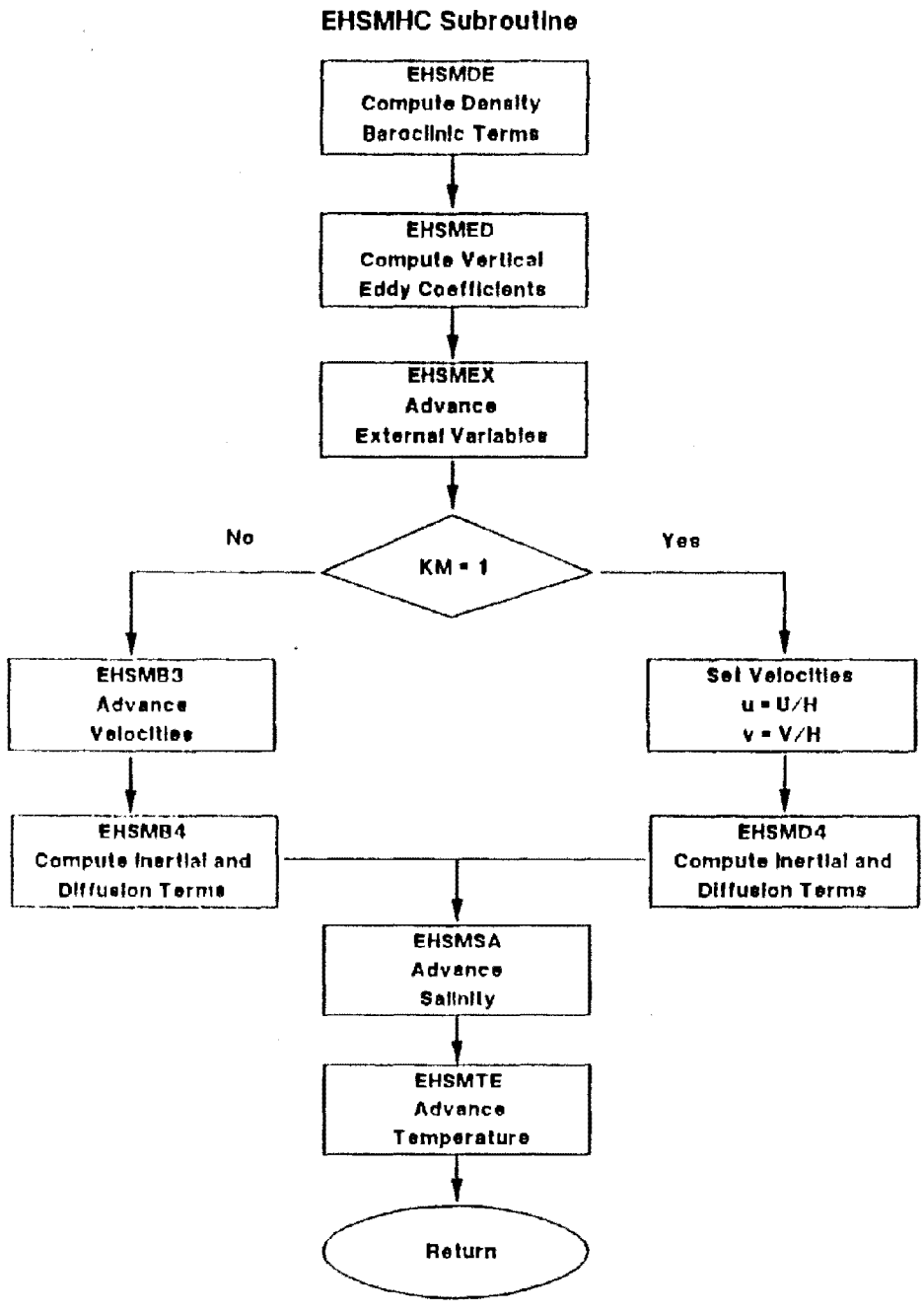

Figure 8. Flow chart of the Hydrodynamic Subroutine EHSMHC

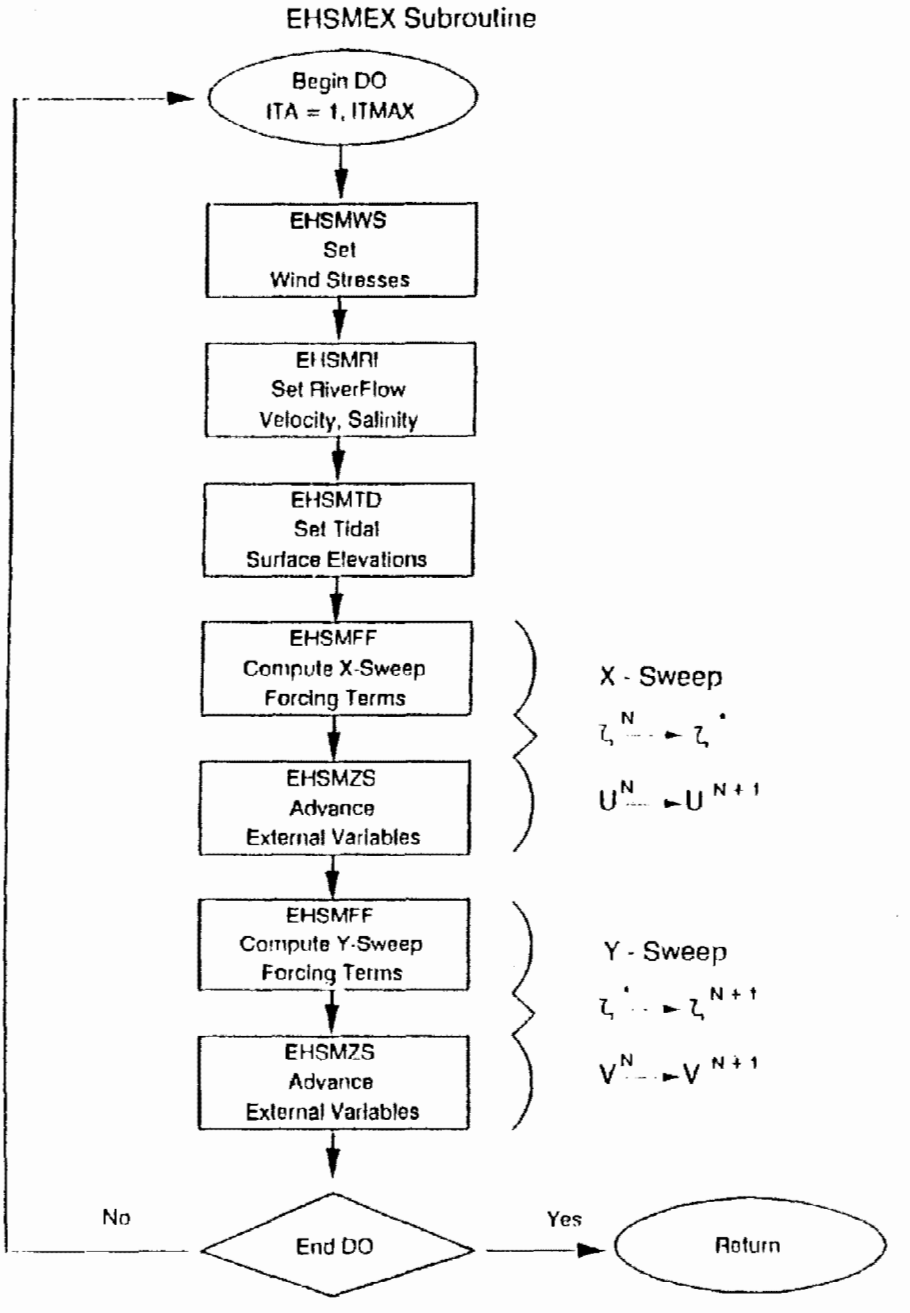

Figure 9. Flow chart of the External Mode Subroutine EHSMEX

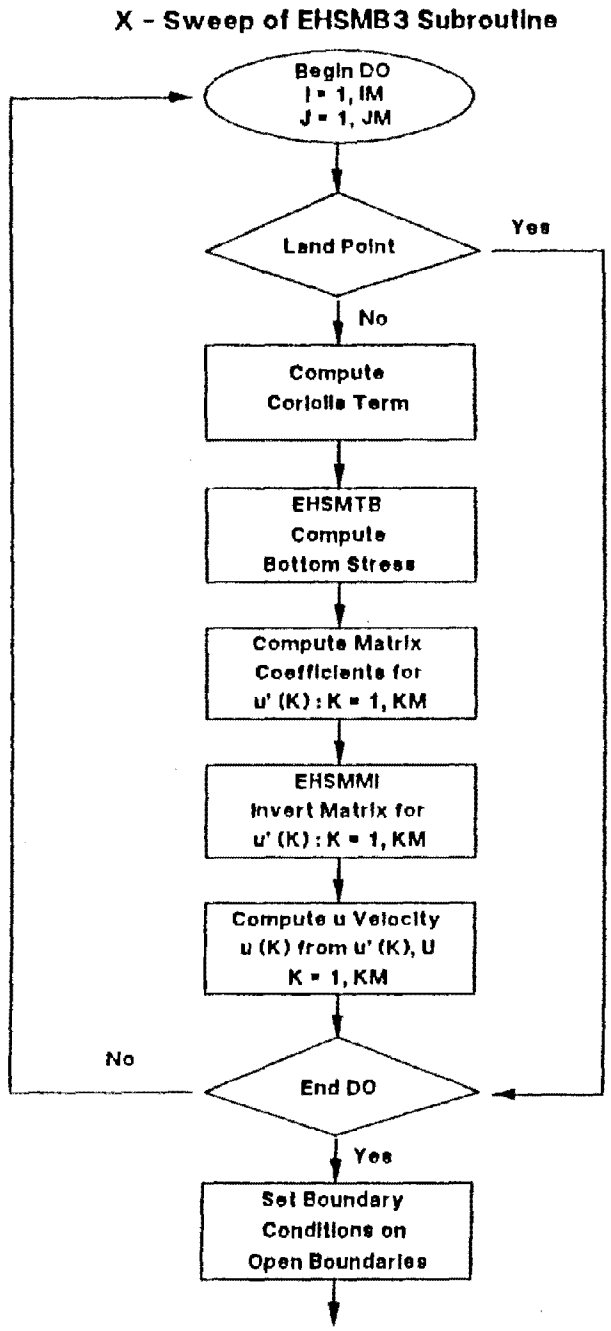

Figure 10. Flow chart of the Internal Mode Subroutine EHSMB3

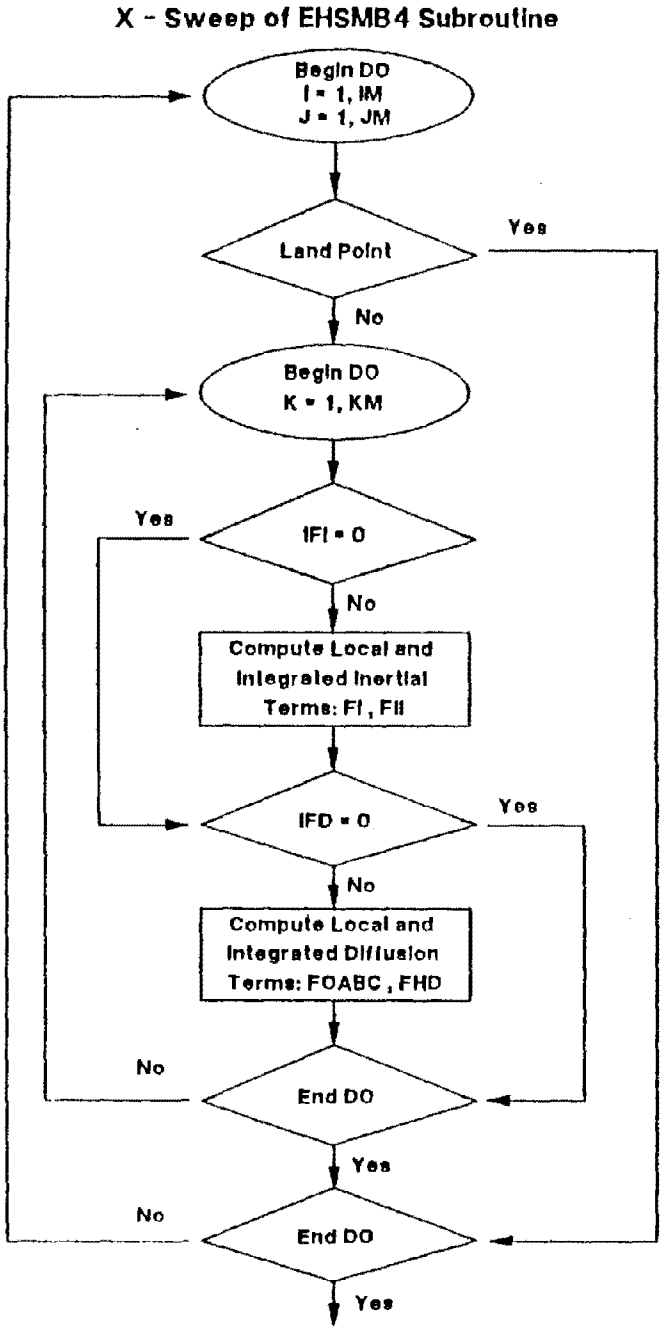

Figure 11. Flow chart of the Internal Mode Subroutine EHSMB4

SECTION 3

USER'S MANUAL

3.1 INTRODUCTION

This section briefly describes the operation of the program, data requirements, and the form of the output. There are several operational modes for 3-D and 2-D simulations discussed below. The input data requirements are briefly reviewed in general terms in Section 3.2 for project managers and applications experts. Specific data formats are reviewed in detail for applications experts in Section 3.3. Output information can be printed or recorded in dimensionless or dimensional forms and a number of different alternative output data files can be produced that are reviewed in Section 3.4 for applications experts.

As discussed in previous sections, the HYDRO3D program can simulate time-dependent currents in coastal, estuarine, harbor, and lake waters. Parameters simulated by the program include surface displacement (ζ), vertically integrated velocities (U,V), 3-D velocities (u,v,w), temperature (T), salinity (S), density (ρ), and dissolved species concentration (C). The code can be run as a fully 3-D model, or as a 2-D vertically integrated (x-y) model. In addition, the code has been designed to simulate 2-D laterally integrated flows as an x-z model. However, this option has not been fully tested and it is not presently recommended for use (if such calculations are necessary, users should contact the CEAM for guidance).

Changing from 3-D mode to 2-D mode or vice versa, requires changing three parameter statements in the include file, HYDRO3D.INC, and a few input parameters in the input file (*.INP, where * is an arbitrary file name assigned by the user). The file, HYDRO3D.INC, is included with the source code and has sufficient comments to explain to the user what parameters must be changed. See Section 3.3 for the parameters that should be specified in the input file (*.INP).

3.2 Data Requirements of the Program

- Data required to initiate the simulation:

  1) Grid information that defines the horizontal boundaries and bottom topography of the computational domain. The spatial scales of physical processes that the model can properly resolve depend on the

grid information as well as the governing equations.

2) Time step information. The temporal scales of physical processes that the model can properly resolve depending on the time step information as well as the governing equations.
3) Initial values of state variables at the beginning of the simulation. These include the flow variables as well as the water quality parameters (salinity, temperature, and concentration of a dissolved species).

- Data required to operate the program:

1) Vertical boundary conditions. These include the specification of fluxes of momentum, heat, and dissolved species at the air-sea interface as well as the bottom. Alternatively, these conditions could be given in terms of the state variables instead of their fluxes.
2) Lateral boundary conditions. These include the specification of solid boundaries, river flows, and open boundary conditions. To run a successful simulation, valid boundary conditions must be provided at all times throughout during the simulation.

With these data, the model can be used in a screening mode to develop an idea about the important processes that control circulation at a site. This is useful to aid in preliminary investigations and for designing calibration data collection studies. The simulations, however, must be interpreted with care until the model is tested with calibration and validation data.

The general procedure for calibrating and testing the adequacy of a model is as follows:

- Determine study objectives,
- Define the subset of objectives to be addressed by model studies,
- Collect historical data from monitoring or previous studies,
- Attempt a preliminary calibration of the model,
- Design a calibration data collection study based on the preliminary calibration,
- Simulate conditions during the calibration period and compare to determine if the preliminary calibration is sufficient (if it is not, calibrate the model),
- If the model is calibrated, collect a second independent set of data for validation,
- Validate the model for the limited range of conditions defined by the calibration and validation data sets (if the model can not be validated repeat the calibration step and collect more validation data for a second attempt), and
- Determine uncertainty in the calibrated model simulations by sensitivity analysis.

See Ambrose et al. (1990) and Ambrose and Martin (1990) for guidance on these procedures.

Calibration is the process of changing model parameters until the

simulations match measured data. Calibration is necessary because several critical model parameters such as the Manning roughness coefficient and eddy coefficients can not be adequately related to conditions at a site or forecast without simulating the site and changing the parameters as need to match selected conditions in the modeled domain. This is especially necessary if precise calculations are required, or if cause and effect relationships must be defined with some care (and these relationships are sensitive to hydrodynamics and transport).

Calibration and validation consists of collecting two independent data sets that define the distribution of currents, salinity, and temperature in the study domain to be modeled. Data must be collected at enough important locations and with sufficient frequency to adequately define the phenomena of interest. Data collection procedures are essentially the same for collecting calibration and validation data but the data sets must be collected independently. Occasionally, collection of only one data set for validation may be possible if there is sufficient data available for a preliminary calibration of the model.

In practice, some studies only collect one set of data for model calibration because of resource limitations. These studies are useful but care must be exercised if model results directly influence resource decisions. Without validation testing, it is not possible to accurately report uncertainty in the model simulations (see Chapra and Reckhow 1983).

When calibrating and validating a model, some care is necessary to compare model results and data. Both the simulations and data collected should describe the flow phenomena of interest at the same temporal and spatial scales. Field data should be collected over long enough periods at a number of stations and properly averaged. If necessary, simulations should be averaged for consistent comparisons. Field data collection sites should be representative of selected parts of the water body being simulated or data from several sites averaged to provide representative data. In addition to comparing averages, variances should be compared as well to evaluate the dynamic response of the model. See McCutcheon et al. (1990) for limited guidance on statistical testing methods and criteria for simpler models.

At this time, there is only limited guidance on the data necessary to calibrate a hydrodynamics model. Ambrose and Martin (1990) and Ambrose et al. (1990) provide guidance on data collection for hydrodynamic model calibration and validation for estuaries and that information is useful for lakes as well. For this specific model, Sheng (1983) provides a detailed study of the Mississippi Sound that should be reviewed to determine the frequency and spatial locations for calibration and validation sampling. Each site will be different, however. As a result, it is not possible to foresee all contingencies and recommend comprehensive data collection procedures.

In practice, the amount of data that should be collected for a specific study depends on many factors. The primary factors include the resources available, objectives of the study, flow conditions under study, uncertainties in the data, and limitations of the model. Generally, data should be collected over sufficiently long periods of time to define the phenomena that

control the water body hydrodynamics. If wind driven episodic events are of interest, these should be documented with measurements from start to finish. If spring tides, or other tidal conditions are important, sampling should take place during these occurrences. If long-term simulations are of interest, several cruises or data collection studies over important seasons or periods may be required.

The best practice, is to spend one to two weeks recording and reviewingstudy objectives, developing a subset of objectives to be addressed by modeling, and then design a modeling plan. From the modeling plan, it becomes clearly how much and what kinds of data are necessary to calibrate and validate the model. Also, the planning clarifies how much time will be necessary. Tentative sampling plans can be formulated and costs estimated at this point. The first component of the modeling plan should include a preliminary calibration with historic data. Following this the sampling plans and cost estimates should be revised. This is the optimine time to estimate resource requirements. After some experience is gained, this process can be streamlined somewhat. However, it does not seem possible to fully estimate data requirements and costs using a manual like this without knowledge of specific study objectives and a modeling plan.

3.3 Input Data Description

Most of the data are in a free format and this is denote by (*). Other data formats are as noted.

At this time, this manual does not provide sufficient guidance on the ranges of data that parameters can be selected from. For guidance, users are referred to McCutcheon et al. (1990), Grey (1986), Sheng (1983) and a number of studies using the model and earlier version of the code (Sheng et al. 1978, 1986, 1989a, 1989b, 1989c; Sheng and Lick 1979, 1980; Sheng 1975, 1980, 1982, 1984, 1986, 1987; Johnson et al. 1989; Smith and Cheng 1989). In addition, other 2-D and 3-D modeling studies should be consulted as well. Finally, users may wish to consult with the Center for Exposure Assessment Modeling, U.S EPA Environmental Research Laboratory, Athens, GA 30506 [(404) 546-3130, bulletin board (404) 546-3402].

Following are the data formats for each record line:

#1 TITLE CARD: ISTART(I4), TITLE(A64)

START: Start up flag.

- = 0 New start, initial flow variables read from input device (file).
- = 1 Restart, initial flow variables and salinity values read from discfile IR.
- = 2 Special restart, initial flow variables read from discfile IR but initial salinity values evaluated by interpolation from data at several stations.

TITLE: A brief description of the run, e.g., Circulation in Green Bay.

#2 PHYSICAL CONSTANTS: XREF, ZREF, UREF, COR, GR, ROO, ROR, TO, TR (*)

XREF: Reference length in lateral direction, usually the maximum

dimension of the basin (cm).

ZREF: Reference depth, usually the average depth of the basin (cm).

UREF: Reference velocity (usually 10 cm/sec for estuaries).

COR: Coriolis acceleration ($f = 2\Omega \sin \phi$; Ω = angular velocity of the earth; ϕ is the latitude).

GR: Gravitational acceleration (usually 981 cm/sec^2).

ROO: Base water density or minimal density in the model domain (g/cm^3).

ROR: Reference water density, e.g., density at 20°C and 30 ppt or maximum density in the model domain (g/cm^3).

TO: Base water temperature, e.g., 1°C or minimum temperature (°C) in the model domain.

TR: Reference water temperature, e.g., maximum temperature (°C) in the model domain.

#3 EQUATION FLAGS: IVLCY, ITEMP, ISALT, ICC, IFI, IFA, IFB, IFC, IFD (*)

IVLCY: Velocity flag.

- = 0 Does not compute velocities and other hydrodynamic-variables.
- = 1 Computes velocities and other hydrodynamic variables.

ITEMP: Temperature flag.

- = 0 Does not compute temperature distribution.
- = 1 Computes temperature distribution.

ISALT: Salinity flag.

- = 0 Does not compute salinity.
- = 1 Computes salinity.

ICC: Concentration flag

- = 0 Does not compute dissolved species concentration.
- = 1 Computes dissolved species concentration.

IFI: Nonlinear inertia flag for the momentum equations.

- = 0 Does not compute nonlinear inertia terms in the equations.
- = 1 Computes nonlinear inertia terms in conservative form with central differencing scheme.
- = 3 Computes nonlinear inertia terms in conservative form with second upwind differencing scheme.
- = 4 Computes nonlinear inertia terms in conservative form with combined central and upwind scheme.

IFA: Coefficient for group A of the higher-order lateral diffusion terms.

- = 0 Does not include one group A of the higher-order lateral diffusion terms.
- = 1 Includes one group A of the higher-order lateral diffusion terms.

IFB : Coefficient for group B of the higher-order lateral diffusion terms.

IFC : Coefficient for group B of the higher-order lateral diffusion terms.

IFD : Coefficient for the leading-order lateral diffusion terms

- = 0 Does not include lateral turbulent diffusion.
- = 1 Include the leading-order lateral diffusion terms.

#4 TEMPERATURE PARAMETERS: BVR, S1, S2, PR, PRV, TWE, TWH, FKB, TQO (*)

BVR: Reference turbulent thermal eddy diffusivity (cm^2/sec).

S1,S2: Empirical constants used in the simple variable vertical eddy coefficients.

PR: Turbulent Prandtl Number (typically assigned a value of 1).
PRV: Vertical turbulent Prandtl Number (typically assigned a value of 1).
TWE: Initial temperature in the epilimnion or upper layer(°C).
TWH: Initial temperature in the hypolimnion or upper layer(°C).
FKB: Vertical grid index of the initial thermocline location (not in use at this time)
TQO: Initial surface heat flux (cal/cm/cm/sec).

#5 CONCENTRATION PARAMETERS: IVER, ICON, IUBO, IBL, IBR, JBM, JBP, CREF, CMAX, CO, IC1, IC2, JC1, JC2, ID1, ID2, JD1, JD2 (*)

IVER: Vertical diffusion flag.
= 1 Explicit vertical diffusion term for water quality equations.
= 2 Implicit vertical diffusion term for water quality equations.
ICON: Advection flag for water quality equations (similar to IFI).
= 0 Does not compute advection terms in the equations.
= 1 Computes advection terms in conservative form with central differencing.
= 3 Computes advection terms in conservative form with second upwind differencing scheme.
= 4 Computes advection terms in conservative form with combined central and upwind differencing scheme.
IUBO: Bottom orbital velocity flag (enter value of 0; not used at this time 0).
IBL : Concentration computation does not have to be performed
IBR : for the entire computational domain. Instead, it can be
JBM : done for a window that covers an area from I=IBL to
JBP : I=IBR and from J=JBM to J=JBT, initially.
CREF: Reference species concentration (units determined by user).
CMAX: Maximum concentration allowed by the code (The run stops if Cmax is exceeded)
CO: Initial concentration (in units determined by user).
IC1: Initial concentration field may be specified to
IC2: be zero everywhere in the computational domain except
JC1: within two windows: the first one covers an area
JC2: from I=IC1 to I=IC2 and from J=JC1 to J=JC2.
ID1: the second one from I=ID1 to I=ID2 and J=JD1 to J=JD2.
ID2:
JD1:
JD2:

#6 TURBULENCE PARAMETERS: IEXP, IAV, AVR, AV1, AV2, AVM, AMR(*)

IEXP: Vertical eddy coefficient flag (see EHSMED.FOR and EHSMEZ.FOR for details).
= 0 Constant eddy coefficient. Must also set ISPAC(9) = 0.

The following options are used with variable eddy coefficients, i.e., when ISPAC(9) is nonzero. See record #12 following.

= -1 Richardson-number dependent on eddy coefficients with length scale linearly increasing from the bottom and surface.
= 2 Richardson-number dependent eddy coefficients with length scale linearly increasing from the bottom.
= -3 Eddy coefficients determined from simplified second-order

turbulence closure model.

IAV: Reference vertical eddy viscosity flag.
- = 0 Input parameter AVR is used as reference eddy viscosity.
- = 1 Reference eddy viscosity is computed form AV1+TXY*AV2, where TXY is the total wind stress and AV1 and AV2 are input parameters.

AVR: Reference vertical eddy viscosity (cm^2/sec).

AV1: Background vertical eddy viscosity when wind is zero (cm^2/sec).

AV2: If IAV = 1, unstratified vertical eddy viscosity is computed from AV1+TXY*AV2.

AVM: Minimum allowable vertical eddy coefficient (cm^2/sec).

AHR: Reference lateral turbulent eddy viscosity (cm^2/sec).

#6A MORE TURBULENCE PARAMETERS: FM1, FM2, ZTOP, SLMIN, QQMIN (*)

FM1: Empirical constant used in Richardson-number dependent eddy-coefficient formula.

FM2: Empirical constant used in Richardson-number-dependent eddy-coefficient formula.

ZTOP: Distance between the top of the computational domain and the free surface (cm).

SLMIN: Minimum scale length (cm).

QQMIN: Minimum total turbulent velocity (cm/sec)).

#6B MORE TURBULENCE PARAMETERS: QCUT, ICUT, GAMAX, GBMAX, FZS, KSMALL (*)

QCUT: (Not used for now).

ICUT: Eddy coefficient parameter.
- = 0 Cutoff not operating.
- = 1 Eddy coefficients below a sharp density gradient are not allowed to exceed that at the sharp gradient.

GAMAX: Maximum vertical eddy viscosity (for u, v variables),(cm^2/sec).

GBMAX: Maximum vertical eddy diffusivity (for s, t variables), (cm^2/sec).

FZS: The turbulence length scale is not allowed to exceed the product of FZS and the depth.

KSMALL: A non-zero value of KSMALL implements a routine to the vertical eddy coefficients (a value of 1 is recommended).

#7 WIND PARAMETERS: IWIND, TAUX, TAUY (*)

IWIND : Wind stress flag.
- = 0 Uniform wind stress specified by TAUX and TUAY.
- = 1 Variable wind stress read from file unit IR4.

TAUX: Wind stress at the air-sea interface in the x-direction.

TAUY: Wind stress at the air-sea interface in the y-direction.

#8 VERTICAL BOUNDARY CONDITION PARAMETERS: ISMALL, ISF, ISIE, IBTM, ITB, HADD, HMIN, ZREFBN, CTB, BZ1, H1, H2 (*)

ISMALL: Small amplitude flag.
- = 0 Small amplitude assumption is invoked. Surface elevation is not added to the depth to obtain the total depth.
- = 1 Small amplitude assumption is not invoked. Surface elevation is included in the total depth.

IBTM: Bottom topography flag.
- = 0 Depth changes linearly from H1 along the western boundary to H2

along the eastern boundary.
- = 1 Depth changes linearly from H1 along the southern boundary to H2 along the northern boundary.
- = 2 Depth deck (series of records) is read in at the end of this input stream.
- = 3 Components of depth (HU,HV,HS) are read from discfile (unit 11).

ITB : Bottom friction flag.
- = 1 Linear stress law with no slip condition is employed.
- > 3 Quadratic stress law is employed.

HADD: Constant datum added to the depth at all locations.

HMIN: Minimum depth.
- = 0. No adjustment on the depth data.
- > 0. Depth cannot be less than HMIN.

ZREFBN: Reference height above the bottom (ZREFB = ZREFN * BZ1/ZREF).

CTB: Constant bottom friction coefficient (.004 to 0.4). Also see JSPAC(2) on record #12. CTB is only used if a constant friction or drag coefficient is requested by setting JSPAC(2) = 0.

BZ1 : Constant bottom roughness height (0.1 cm to 0.5 cm).

H1: Depth along one boundary (cm).

H2: Depth along the opposing boundary (cm).

#8A ZREFTN, TZ1, SSS0 (*)

ZREFTN: Reference height at the top (cm).

TZ1 : Constant surface roughness height (cm).

SSS0: Initial uniform surface elevation (dimensionless divided by S_r = fU). $S_r = fU_rX_r/g$.

#9 LATERAL BOUNDARY CONDITION FLAGS: ITIDE, IOPEN, JWIND, IJLINE (*)

ITIDE : Tidal forcing flag.
- = 0 No tidal forcing.
- = 1 With tidal forcing and constituent tide boundary condition (This option is currently inactive).
- = 2 With tidal forcing and tabular tide boundary condition.
- = 3 Surface water elevations are prescribed.

IOPEN : Open boundary flag. A 4-digit number that indicates whether there are open boundaries along the west-south-east-north sides of the computational domain. Zero indicates no open boundary and 1 indicates open boundary. For example, 1010 means open boundaries on west and east.

JWIND : Open boundary flag in case of wind forcing only.

IJLINE: Number of open boundary lines along which tidal forcing information is to be specified.

#10 FOR EACH IJLINE, IF IJLINE.GT.0, READ:IJGAGE, IJDIR, IJROW, IJSTRT, IJEND (*)

IJGAGE: Gage number. Not important.

IJDIR: Direction of the line segments along which tidal data are prescribed. In case of constituent tides, IJDIR = 1 indicates the x-direction while IJDIR = 2 indicates the y-direction. In case of tabular tides, IJDIR = (1,2,3,4) indicates (west,south,east,north).

IJROW : Row/column index of the line segment.

IJSTRT: Grid index of the starting point on IJROW.

IJEND : Grid index of the ending point on IJROW.

#11 (ISPAC(I),I=1,10) (*)

(1) : Disk output flag.
- = 0 No output to diskfile (unit IW).
- > 0 Every ISPAC(1)-th time-step, output are written to diskfile.

(2) : Smoothing flag.
- = 0 No smoothing is applied.
- > 0 Every ISPAC(2)-th time-step, apply smoothing to salinity.

(3) : Open Boundary flag for elevation.
- = 0 Prescribed surface elevation on open boundary.
- > 0 Surface elevation has zero slope on open boundary.
- < 0 Surface elevation satisfies radiation condition on open boundary.

(4) : Open Boundary flag for mass flux.
- = 0 Compute tangential mass flux from equations of motion.
- < 0 Tangential mass flux = 0.
- > 0 Tangential mass flux has zero slope in normal direction.

(5) : Open Boundary flag for advection/diffusion terms.
- = 0 Computes advection/diffusion terms on open boundary.
- > 0 Set advection/diffusion terms to zero on open boundary.

(6) : 2-D flag.
- = 0 Performs the x-sweep and the y-sweep.
- > 0 Performs the x-sweep only.
- < 0 Performs the y-sweep only.

(7) : Basin geometry flag.
- = 0 Grid indices NS, MS, JU1, JU2, JV1, JV2, IU1, IU2, IV1, IV2, are determined from the depth arrays in EHSMI*.FOR routines.
- = 1 Previously determined grid indices are read from discfile (unit 12).

(8) : Smoother flag.
- = 0 No smoother is applied.
- > 0 Every ISPAC(8)-th step, smoothing is applied to the velocity field.

(9) : Vertical eddy coefficient flag.
- = 0 Constant vertical eddy coefficients.
- = 1 Variable vertical eddy coefficients computed from EHSMED and EHSMEZ routines.

(10): Residual current flag.
- = 0 Does not compute Eulerian residual currents.
- = 1 Computes Eulerian residual currents. See subroutine EHSMRS.

#12 (JSPAC(I), I=1, 10) (*)

(1) : Dimensionality flag.
- = 0 All output in dimensionless units.
- = 1 All output in c.g.s. unit.(Does not work at this time).

(2) : Bottom friction coefficient flag.
- = 0 Constant bottom friction coefficient is specified by CTB. See Record #8.
- = 1 Variable bottom friction coefficient is computed in EHSMEX and EHSMBC routines based on the law of the wall.

(3) : Coriolis acceleration terms.
- = -1 No Coriolis flag.

= 0 Coriolis acceleration terms are evaluated.

(4) : Dummy flag used to check steady state termination.

(5) : Open boundary salinity flag.

= 0 Prescribed salinity is used along open boundary during inflow.

= 1 Prescribed salinity is used in a 1-D advection equation to obtain the salinity along open boundary during inflow.

(6) : Dummy flag.

(7) : Dummy flag.

(8) : Bottom friction flag for the 2-D vertically-integrated version (KM=1).

= 0 Explicit bottom friction.

= 1 Implicit bottom friction.

(9): Open boundary flag for salinity and temperature (To be used later for thermally stratified flow. ≥ 1 will include salinity time varying data; = 2 Freeze open boundary salinity to initial values).

(10): Include initial values for salinity at interior nodes (stations).

#13 (RSPAC(I), I=1, 10) (*)

(1): Manning's n in association with other parameters in c.g.s. units.

(2): Dummy parameter.

(3): An small number used in checking the convergence to steady-state (0.0001 is recommended).

(4) : An small number used in checking the convergence to steady-state (0.0001 is recommended).

(5) : Dummy parameter.

(6) : Dummy parameter.

(7): Depth below which the bottom friction coefficient follows a ramp function (see EHSMTB.FOR).

(8): When depth falls below RSPAC(7), the bottom friction coefficient is
linearly interpolated between the one computed in EMSMTB and RSPAC(8).

(9): Coefficient for the spatial smoother (0.25 is recommended).

(10): Coefficient for the curvature check of the spatial smoother (4 is recommended, See Sheng (1983)), p. 258.

#14 TIME-STEPPING PARAMETERS: ISTEP, IT1, IT2, ITS, DELT, DELTMIN, DELTMAX, EPSILON, BUFAC, WTS, WTU, WTV (*)

ISTEP: Time-stepping flag.

= 0 Constant time-step is used in the time-integration of the finite-difference equations.

= 1 Dynamic time-stepping is used. At the end of each time-step, the total weighted maximum rate of change of the major variables is compared with EPSILON. If the rate of change is less than EPSILON, the time-step is allowed to increase by 10% to 20%. Otherwise, the time-step is cut back proportional to the ratio of EPSILON and the rate of change.

IT1: Initial time index. NOTE IT1 = 1 when beginning a simulation (ISTART = 0). If a simulation is being restarted (ISTART = 1 or 2), IT1 should be set equal to the value IT2 in the previous run plus 1.

IT2: Final time index.
ITS: Ratio of the internal time-step to the external time- step.

DELT: Initial time-step (seconds). For constant time stepping this is the time step used.
DELTMIN: Minimum allowable time-step when dynamic time-stepping is used.
DELTMAX: Maximum allowable time-step when dynamic time-stepping i s used.
EPSILON: Maximum allowable rate of change of major variables (5% or 0.05 is recommended).
BUFAC: When rate of change exceeds BUFAC*EPSILON, the run stops.
WTS: Weighting factor for surface elevation when computing EPSILON (0.1 is recommended)
WTU: Weighting factor for surface u-velocity when computing EPSILON (1. is recommended).
WTV: Weighting factor for surface v-velocity when computing EPSILON (1. is recommended).

#15 PRINTOUT PARAMETERS: ITEST, IP1, IP2, IP3, IPU, IPW, IPA, IPB, ID, JPA, JPB, JD, KPA, KPB, KD (*)
ITEST : Testing/debugging flag.
= 0 Operational run with minimal output information to printer.
= 1 Test run with extra output to the printer.
= 3 Creates time history file (*.SUV) that contains major variables at selecting stations and vertical levels. See Cards #20 and #21.
IP1 : Time index interval for brief printout.
IP2 : Time index interval for total printout.
IP3 : Time index interval for printout within each internal step (unused).
IPU : Horizontal velocity printout flag. IPU = 0 turns off printing and IPU = 1 activates printing.
IPW : Vertical velocity printout flag. IPW = 0 turns off printing and IPU = 1 activates printing.
IPA : First index for x-direction printout.
IPB : First index for y-direction printout.
ID: The printout does not have to cover the entire computational domain.
JPA : Instead, the printout goes from I=IPA to I=IPB, every ID-th
JPB: spacing in the x-direction, print information in y-direction
JD: from J=JPA to J=JPB, every JD-th spacing in the y-direction.
KPA : First index for z-direction printout.
KPB : Last index for z-direction printout.
KD: Time index interval for z-direction printout.

#16 PRINTOUT FORMAT FLAGS: IGI, IGH, IGT, IGS, IGU, IGW, IGC, IGQ, IGL, IGR, IGRI, IGTB (*)
IGI : Printout format flag for initial data.
= 0 Procedures digital printout (via EHSMWR routine) of initial data.
= 1 Procedures simple contour plot (via EHSMGR routine) of initial data.
IGH : Printout flag for depth arrays.
=-1 Does not print depth arrays.
= 0 Procedures digital printout of depth arrays.

= 1 Procedures graphical printout of depth arrays.

IGT : Printout format flag for temperature variables (Same as IGI).

IGS : Printout format flag for surface elevation (Same as IGI).

IGU : Printout format flag for mass flux and velocity and integrated velocity in the horizontal direction (Same as IGI).

IGW : Printout format flag for and velocity and integrated velocity in the vertical direction (Same as IGI).

IGC : Printout format flag for concentration variables (Same as IGI).

IGQ : Printout format flag for turbulent velocity. Set to <0 or >1 to turn off printing.

IGL : Printout format flag for turbulent scale. Same as IGQ.

IGR : Printout format flag for density field.

IGRI: Printout format flag for Richardson number.

IGTB: Printout format flag for bottom stress.

#17 DISKFILE INFO: IRD, IW, IWR, ICI, IWC, ICONC, IWS, IREAD, IR4 (*)

IRD: Unit number of input diskfile for storing arrays of major flow variables.

IW: Unit number of output diskfile for storing arrays of major flow variables.

IWR : Output flag for arrays of minor flow variables.

= 0 Does not writes to diskfile unit IW.

= 1 Writes to diskfile unit IW every ISPAC(1)-th steps. In case of dynamic time-stepping, writes to diskfile every time break specified by TBRK on data set (record) #19.

ICI : Concentration input flag.

= 0 Does not read concentration field from diskfile unit ICONC.

= 1 Reads concentration field from diskfile (unit ICONC).

IWC : Concentration output flag.

= 0 Does not write concentration field to the output diskfile (unit ICONC).

= 1 Writes concentration field to output diskfile unit ICONC.

ICONC : Unit number of diskfile for storing concentration variables.

IWS : Unit number of diskfile for storing Eulerian residual variables.

IREAD : If IVLCY = 0 and ICC > 0, reads flow variables from unit IR diskfile every IREAD-th steps.

IR4 : Unit number of the wind stress file.

#18 3 MAJOR I/O FILENAME: FNAME (6A4)

FNAME : A six-element vector specifying the names of (1) the input diskfile for flow variables, (2) the output diskfile for flow variables, and (3) the diskfile for concentration variables.

#19 TIME BREAKS FOR STORING MAJOR OUTPUT ARRAYS: (TBRK(I),I=1,10) (*)

TBRK: Time breaks (in hours) at which major flow output will be stored on file unit IW. Only used when ISTEP = 1.

> 0. Hours at which flow data are written to file unit IW.

< 0. Run is stopped after flow data at ABS(TBRK) hour are dumped to file unit IW.

#20 TIMEFILE (UNIT 18) GAGE STATIONS: NSTA, NRANGE, NFREQ (*)

NSTA: Number of stations (not to exceed NSTATS in HYDRO3D.INC) where

major flow variables are stored on a timefile (*.SUV). No data stored on timefile if NSTA = 0.

NRANGE: Dummy flag.

NFREQ : Flow data are stored on timefile every NFREQ steps.

#21 IF(NSTA.GT.0) READ : IST(K), JST(K), KST(K), STATID(K)(3I4, A48)

IST : x-Grid index of the timefile gage stations. Proceeds to read river info cards (records) when a zero IST is detected.

JST : y-Grid index of the timefile stations.

KST : z-Grid index of the timefile stations.

STATID: A 48-character title for each of the timefile stations.

#22 RIVER INFO: NRIVER (*)

NRIVER: Total number of river stations in the computational domain, not to exceed NRIVRS specified in HYDRO3D.INC.

#22A FOR EACH NRIVER.GT.0, READ: IRIVER, JRIVER, LRIVER, URIVER, VRIVER (*)

IRIVER: Grid index (of a river station) in the x-direction.

JRIVER: Grid index (of a river station) in the y-direction.

LRIVER: Alignment index of a river station.

= 1 River flows in the x-direction.

= 2 River flows in the y-direction.

< 0 Read time-varying river flow rate from a disc file.

URIVER: Volumetric flow rates in ft^3/sec for rivers with LRIVER=1.

VRIVER: Volumetric flow rates in ft^3/sec for rivers with LRIVER=2.

#23 INITIAL VERTICAL PROFILES OF SALINITY, TEMPERATURE, AND CONCENTRATION ALONG THE OPEN (WEST-SOUTH-EAST-NORTH) BOUNDARIES:
IF (ISALT.NE.0) READ (SABW(K),SABS(K),SABE(K),SABN(K),K=1,KM) (*)
(Note that ISALT is defined in Record # previously)

#23A,B,C IF ISALT.NE.0, READ NUMBER OF INITIAL SALINITY STATIONS: NISS
IF (NISS.GT.0) READ THE FOLLOWING CARDS FOR N=1,NISS
ISS(N), JSS(N), NDEPTH(N), TDEPTH(N)
(ZDEPTH,(K,N), K=1, NDEPTH(N))
(ZSAL(K,N), K=1, NDEPTH(N))

ZSEDI: Concentration data at each depth level of a station

ISS : I-grid index of the salinity station.

JSS : J-grid index of the salinity station.

NDEPTH: Number of depth levels at which salinity data are to be specified.

TDEPTH: Total water depth at the salinity station.

ZDEPTH: Depth measured from the water surface at each depth level of a station. The units of TDEPTH and ZDEPTH must be the same (c.g.s. or f.p.s.).

ZSAL: Salinity data at each depth level of a station.#24INITIAL VERTICAL PROFILES OF TEMPERATURE ALONG THE OPEN (WEST-SOUTH-EAST-NORTH) BOUNDARIES:
IF (ITEMP.NE.0) READ (TBW(K), TBS(K), TBE(K), TBN(K), K=1,KM

#24A,B,C IF ITEMP.NE.0, READ NUMBER OF INITIAL TEMPERATURE: NITT
IF (NITT.GT.0) READ THE FOLLOWING CARDS FOR N=1, NITT
ISST(N), JSST(N), NDEPTT(N), TDEPTT(N)
(ZDEPTT(K,N), K=1, NDEPTT(N))

(ZTEM(K,N), K=1, NDEPTT(N))

ISST: I-Grid index of the temperature station.

JSST: J-grid index of the temperature station.

NDEPTT: Number of depth levels at which temperature data are to be specified.

TDEPTT: Total water depth at the temperature station.

ZDEPTT: Depth measured from the water surface at each depth level of a station. The units of TDEPTT and ZDEPTT must be the same (c.g.s. or f.p.s.)

ZTEM: Temperature data at each depth level of a station.

#25 INITIAL VERTICAL PROFILES OF CONCENTRATION ALONG THE OPEN (WEST-SOUTH-EAST-NORTH) BOUNDARIES
IF (ICONC.NE.0) READ (CBW(k), CBS(k), CBE(k), CBN(k), K=1, KM)

#25A,B,C IF ICONC.NE.0, READ NUMBER OF INITIAL CONCENTRATIONS; NISSS
IF (NISSS.GT.0) READ THE FOLLOWING CARDS FOR N=1, NISSS
ISSS(N), JSSS(N), NDEPTS(N), TDEPTS(N),
(ZDEPTHS(K,N), K=1, NDEPTHS(N))
(ZSEDI(K,N), K=1, NDEPTHS(N))

ISSS: I-grid index of the concentration station

JSSS: J-grid index of the concentration station

NDEPTHS: Number of depth levels at which concentration data are to be specified

TDEPTHS: Total water depth at the concentration stations

ZDEPTHS: Depth measured from the water surface at each depth level of a station. The units of TDEPTHS and ZDEPTHS must be the same (c.g.s. or f.p.s.)

ZSAL: Salinity data at each depth level of a station.

#26 TIDAL BOUNDARY CONDITION PARAMETERS: NCG, NCONST, XYEAR, XMONTH, XDAY, XHOUR (*)

NCG : When ITIDE = 1, total number of tidal gages (not to exceed NTIDE specified in HYDRO3D.INC) where constituent tide information are to be specified. Since the constituent tide option does not work, there is no need to specify the following 4 groups of cards (#25 through #28). If ITIDE = 2, tabular tide information are to be read (#29 through #31).

NCONST: Total number of tidal constituents to be used (not to exceed NCNST in HYDRO3D.INC).

XYEAR : The year at the beginning of the constituent tidal record.

XMONTH: The month at the beginning of the constituent tidal record.

XDAY: The day at the beginning of the constituent tidal record.

XHOUR : The hour at the beginning of the constituent tidal record.

#26A INDEX NUMBER OF TIDAL CONSTITUENTS: (NCST(NCI),I=1,NCONST) (*)

NCST: Index number of tidal constituents.
FOR EACH (J=1,NCG), READ #26B,27,28:

#26B KNGAGE(J),HO(J),XLONG(J) (*)

#27 TIDAL AMPLITUDES: (AMP(I,KNGAGE(J)),I=1,NCONST) (*)

#28 TIDAL PHASES: (XKAPPA(I,KNGAGE(J)),I=1,NCONST) (*)
KNGAGE: Tidal gage number.
HO: Gage datum or mean sea level relative to depth datum.
XLONG : Longitude of tidal gage.
AMP : Constituent tidal amplitudes, in the same order as chosen by NCST.

XKAPPA: Constituent local epochs. Set XLONG = 0 if Greenwich epochs are used.

#29 TABULAR TIDE DATA (PERIOD): (TP(I),I=1,NCONST) (*)
TP: Tabular tidal periods along four boundaries (in seconds).
#30 (AMP, PHASE)ON(WEST AND EAST): J, NC, AMPW, PHW, CAW, AMPE, PHE, CAE
#31 (AMP, PHASE)ON(SOUTH AND NORTH): I, NC, AMPS, PHS, CAS, AMPN, PHN, CAN (*)
J: y-grid along the western and eastern boundaries. If J < 0, exit the read loop.
NC: Tidal constituent index. Must be less or equal to NCONST.
AMPW: Tidal amplitude at certain J along the western boundary.
PHW : Tidal phase at certain J along the western boundary.
CAW : Constant tidal amplitude added to AMPW.
AMPE: Tidal amplitude at certain J along the eastern boundary.
PHE : Tidal phase at certain J along the eastern boundary.
CAE : Constant tidal amplitude added to AMPE.
I: X-grid index along the southern and northern boundaries. If I<0, exit the read loop.
NC: Tidal constituent index. Must be less than or equal to NCONST.
AMPS: Tidal amplitude at certain I along the southern boundary.
PHS : Tidal phase at certain I along the southern boundary.
CAS : Constant tidal amplitude added to AMPS.
AMPN: Tidal amplitude at certain I along the northern boundary.
PHN : Tidal phase at certain I along the northern boundary.
CAN : Constant tidal amplitude added to AMPN.
#32 NUMBER OF THIN-WALL BARRIER: NBAR (*)
NBAR: Total number of thin-wall barriers.
#32A FOR EACH NBAR.GT.0. READ: IJBDIR(I), IJBROW(I), IJBSTR(I), IJBEND(I) (*)
IJBDIR: Direction of the thin-wall barrier
= 1 The thin-wall barrier is along the x-direction
= 2 The thin-wall barrier is along the y-direction
IJBROW: Grid index of the row/column where the thin wall barrier is located.
IJBSTR: Starting grid index of the barrier along IJBROW
IJBEND: Ending grid index of the barrier along IJBROW

#33 LATERAL GRID MAPPING: IGRID, XMAP, ALREF, ALYREF (*).
IGRID : Horizontal grid index.
= 0 Uniform horizontal grid. Skips cards (records) #34 through #36.
= 1 User-specific non-uniform horizontal grid. Grid information read from unit 14 file.
= 2 Exponentially stretched horizontal grid.
XMAP: Mapping ratio of the physical domain and the computational domain.

ALREF : Reference length in the x-direction of the computational domain.
ALYREF: Reference length in the y-direction of the computational domain.

#34 VARIABLE GRID MAPPING IN X DIRECTION: NGR, ALPHA1 (*)
NRG : Total number of mapping regions in the x-direction.
ALPHA1: Counter index of the first cell (usually 1).

#34A FOR EACH NRG, READ VARIABLE GRID MAPPING IN X DIRECTION: LPR, A, B, C (*)
LPR : Total number of cells in a grid region.
A: Coefficient of the coordinate-stretching equation:
X = A + B (ALPHA) ** C
B: Coefficient of the coordinate-stretching equation.
C: Exponent of the coordinate-stretching equation.

#35 VARIABLE GRID MAPPING Y DIRECTION: NRG, ALPHA1 (*)
NRG : Total number of mapping regions in the y-direction.
ALPHA1: Counter index of the first cell (usually 1).

#36 FOR EACH NRG,READ VARIABLE GRID MAPPING IN Y DIRECTION: LPR, A, B, C (*)
LPR : Total number of cells in a grid region.
A: Coefficient of the coordinate-stretching equation :
Y = A + B* (ALPHA) ** C
B: Coefficient of the coordinate-stretching equation.
C: Exponent of the coordinate-stretching equation.

#37 IF IBTM=2, READ BATHYMETRY DECK: ((HS(J, I), I=2, IM), J=2, JM) (*)

3.4 MODEL OUTPUT

This section discusses the creation of output files and the form of information available to the user. During the simulation, certain files will be used as input, some files will be created as temporary scratch files, and there will be some output files created. Manipulation of unit numbers and the names of these files are controlled in the input file (*.INP, reviewed in the last section) and/or the run file (RUN.COM). There are options to control the dimensions of the output data and these are also covered in the previous section. For some additional detail, the reader should also refer to Section 3.3 and Section 5.

In the HYDRO3D code, there are two options to control the dimensions of the output data. One option records the output in dimensionless form and the other records the information in a dimensional form (i.e, with physical units of measurement). The option to record the output in dimensional units involves a separate program that reads the standard output in dimensionless units, and converts to the final dimensional form. The conversion is controlled by flags in the input data file.

The HYDRO3D program reads the input files and produce several output files. These output files are controlled and produced by flags defined in the input file (*.INP) and by the proper files assigned in the run file (RUN.COM). To aid in bookkeeping and cataloging of results from different simulations, the output files created by the model use the name of the input data set with a unique extension as follows:

File name	Created for all Runs	Purpose
*.OUT	yes	Contains an "echo" of the input data including initial and boundary conditions, some computed results, and any error messages. Values are either in graphic or numeric form depending on flags assigned in the input file (*.INP, see Section 3.3).
*.SUV	yes	Contains time-dependent information calculated at assigned stations where the outputs are desired.
*.DAT		Needed when ISTART = 1 or 2 and contains initial computations that can be used in subsequent simulation runs.
GRID.PAR	yes	Contains bathymetry information needed for graphic presentation.
CONC.OUT		Contains output of dissolved species concentration and will be created if applicable.
WIND.INP		Contains information regarding wind shear stress calculated in advance using WINDSHEAR.FOR and wind data (from file WIND.DAT).
*.IWX	yes	Stores the total number of runs applied to a specific problem.
*.TEMP		Created in during the simulation of thermally stratified flow and contains temperature data required for graphic presentations.
*.SAL		Contains output of salinity computations.
*.VEL	yes	Contains general output information to be used in vector and contour plotting programs.
BOUND.DAT		Contains water surface elevation data prescribed at the open boundaries.
*.RES.		Stores Eulerian residual velocity arrays.

Note that * denotes a user defined name that will be selected by the program to match the input data file name.

Files not created in all HYDRO3D runs are created only for specialized simulations. For a detailed explanation of these files the reader is referred to Section 5.6 of this manual.

SECTION 4

CASE STUDIES

In this section, several applications of the model are presented for the purpose of illustrating the utility of the program and the feasibility of its use in several diverse settings. Although limited field data are available for direct comparison with model results, much can be learned about the model performance by analyzing the general and specific results from site specific simulations. The sites chosen for these case studies include, Suisun Bay of San Francisco Bay, Charlotte Harbor in Florida, Green Bay of Lake Michigan, Prince William Sound, and Mississippi Sound. In addition, the case studies begin with a comparison with a simple analytical solution that illustrates the general validity of the program. Appendix D is a related type of case study that is used to illustrates the structure and format of the input and output data sets. The study described in Appendix D is a simulation of wind driven currents in an hypothetical enclosed basin.

The specific objectives of this Section are to:

- Illustrate the feasibility of using the program in several important types of water bodies,
- Describe the results that may be obtained from screening-level studies,
- Demonstrate the options available,
- Document the validity of the program, and
- Show how the model has been calibrated in at least one study.

To illustrate the feasibility of using this model in diverse bodies of water we have selected studies from Prince William Sound, Alaska (site of the March 24, 1989 Oil Spill), Suisun Bay of the San Francisco Bay, Mississippi Sound and adjacent deep waters of the Gulf of Mexico, the partially mixed Charlotte Harbor on the west coast of Florida, and Green Bay off of Lake Michigan. Prince William Sound is relatively deep, though not as deep as the waters of the Gulf of Mexico off the Mississippi Sound. Tide ranges in Prince William Sound are typically 3 to 5 m (12 to 15 feet). Use of the model in a screening mode for the emergency response to the EXXON Valdez spill was a primary consideration in the selection of Prince William Sound as a case study. The complex bathymetry and the unique influence of San Francisco Bay on many aspects of the American economy and culture are the appealing attributes of the study in Suisun Bay. Charlotte Harbor is a partially mixed, shallow estuary of a classical type (see Ambrose and Martin 1990). The Harbor is significantly influenced by freshwater flow and has moderate tides of a few feet. Both San Francisco Bay and eastern estuaries like Charlotte Harbor (i.e., Tampa Bay and Sarasota Bay) are expected to be important in the U.S. EPA National Estuaries Studies. The Green Bay study explores the effects of

wind and river flow on circulation in a seriously contaminated part of the U.S.-Canadian Great Lakes where a number of studies are underway.

In addition to the case studies selected, there are a number of other studies that demonstrate the adaptability of the model to many different sites, including other critically important sites. These include recent work by Smith and Cheng (1989) in San Pablo Bay adjacent to Suisun Bay. Johnson et al. (1989) used a significantly modified z-grid model in Chesapeake Bay. Sheng et al. (1978) made a realistic application of an early version the model to Lake Erie that produced very satisfactory agreement with measured data.

Curvilinear versions of the model have also been applied to the James River Estuary (Sheng et al. 1989a), in Lake Okeechobee (1989c) where a version of this σ-stretched model is also being implemented for a comprehensive test, and other sites by the Corps of Engineers (Los Angeles-Long Beach Harbor and Humboltd Bay in California).

The validity of the code is supported by the comparison with a simple analytical solution in Section 4.1, as well as the other case studies where various options have been explored. In addition, Appendix D illustrates that reasonable results are possible for shallow water conditions. However, these are not the primary studies by which the validity of the code has been assessed. Other comparisons with analytical solutions and laboratory data are presented in Sheng and Lick (1980) and Sheng (1983).

Studies by Smith and Cheng (1989), including others to be reported in the summer of 1990; studies reported by Zakikhani et al. (1989); and studies by the Corps of Engineers (e.g., see Johnson et al. 1989), are also noteworthy. These studies, although influenced by the primary architect of the model, indicate that the code is sound and useful enough for other investigators to implement. It is hoped that this documentation will accelerate the use of the program and others like it by other investigators who need to understand effects of circulation in water-quality studies.

There are several case studies included in this section that are not complete calibrations of the program. The study in Prince William Sound was purposely designed as a feasibility investigation and it is reported as such. The study of Green Bay is in an early stage of calibration where the model has been calibrated and checked out with historic data, as recommended earlier in this manual. The studies of Suisun Bay and Charlotte Harbor were selected to demonstrate the use of several option and the general implementation of the program. These studies were examples from a workshop found in Sheng et al. (1986) and the reviewers point out, as do the written sections, that these studies do not provide definitive conclusions about the circulation in Suisun Bay and Charlotte Harbor. The same can be said of the feasibility study in Prince William Sound and the preliminary calibration in Green Bay. However, the case study for Mississippi Sound does represent an adequate calibration of the model and is useful for that reason. Both project mangers and applications experts should benefit for the brief review given for the Mississippi Sound calibration and applications experts may wish to examine the

details of the application. Review of the case study in this section should provide an adequate idea of the data requirements and the intensity of the calculations.

4.1 COMPARISON WITH A ONE-DIMENSIONAL ANALYTICAL SOLUTION

In this section a comparison was made between the applications of HYDRO3D and a one-dimensional analytical solution for standing waves in rectangular basins. A square basin with sides of 50 km in length and a depth of 10 meters deep, and with one open boundary along y-axis was used. The open boundary was subjected to a sinusoidally oscillating wave forcing with an amplitude of ζ_o = 10 cm and a wave frequency $\omega = 2\pi/12$.

The linearized governing equation for a one dimensional standing wave in a rectangular basin, assuming that the flow is incompressible and inviscid, and the water depth is shallow compared to wave amplitude, is given as (Lynch and Gray, 1978):

$$\frac{\partial \zeta}{\partial t} + h \frac{\partial u}{\partial x} = 0$$
$$\frac{\partial u}{\partial t} + g \frac{\partial \zeta}{\partial x} = 0 \qquad (63)$$

The boundary conditions are:

and $$\zeta\ (x=L,\ t) = \zeta_o \sin\Omega t \qquad (64)$$

$$U\ (x=0,\ t) = 0 \qquad (65)$$

The variables were defined in Section 2 and Appendix A.

A steady-state solution these equations may be obtained using the method of separation of variables as:

$$\zeta(x,t) = \zeta_o \frac{\mathrm{Cos}(kx)}{\mathrm{Cos}(kl)} \sin wt \qquad (66)$$

$$u(x,t) = -\zeta_o \frac{gk}{\omega} \frac{\sin(kx)}{\mathrm{Cos}(kl)} \mathrm{Cos}(wt) \qquad (67)$$

where h is the water depth, and the wave number $k = \frac{\omega}{(gh)^{1/2}}$ is the wave number.

To obtain a numerical solution, the flow domain was divided with 5 grid lines in each lateral directions resulting in 25 grid cell s of size of 10 x 10 km. Other parameters are assigned as h = 10 m, g = 980 cm^2/sec, and L = 50 km. The initial conditions for the numerical model simulation were selected to be the at-rest conditions. The results of water surface elevation and velocities for two locations are plotted in Figures 12 and 13.

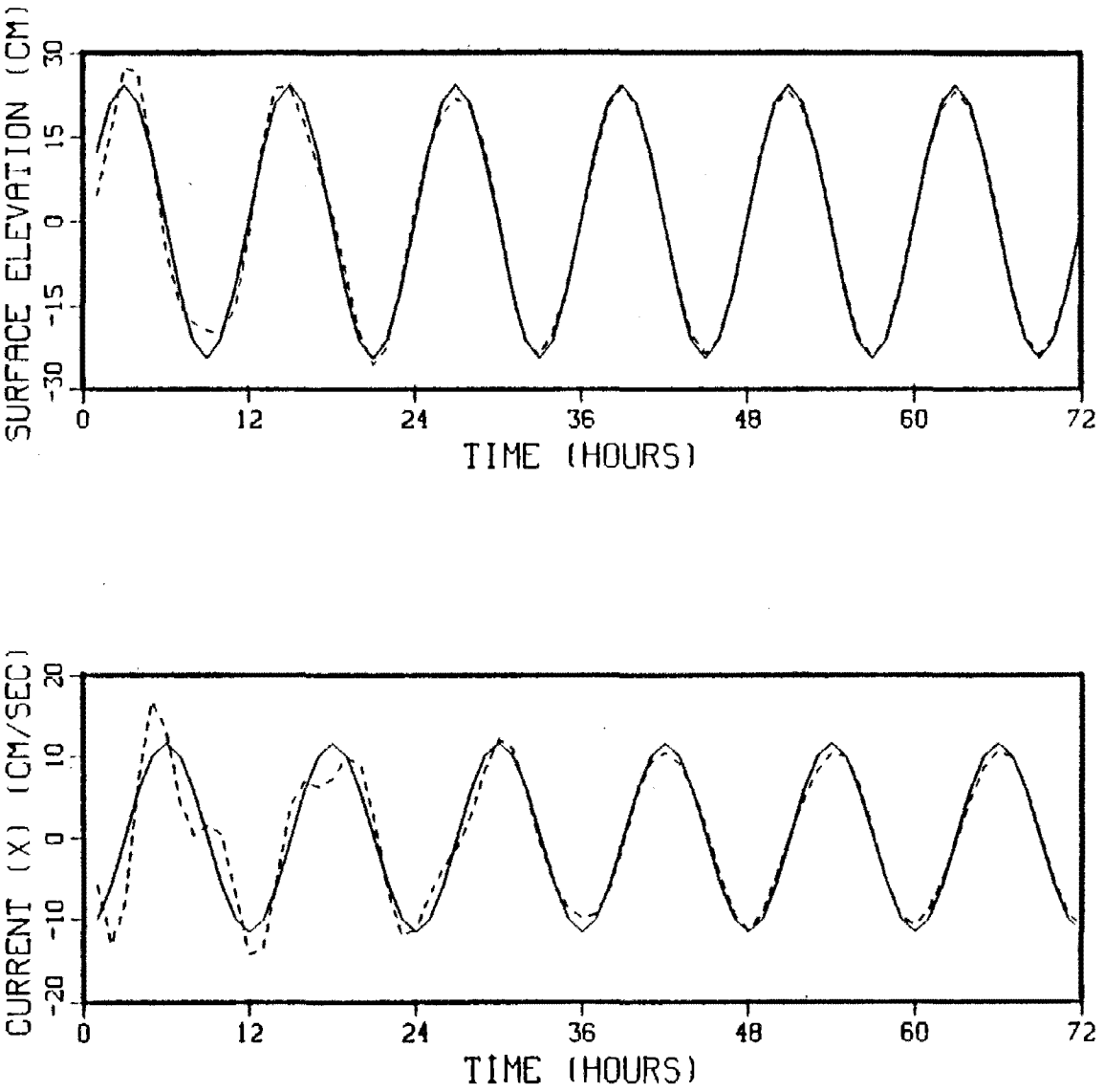

Figure 12. Water Surface elevation and current velocity at x = 5 km (solid lines represent the analytical solution and dashed lines represent the numerical solution).

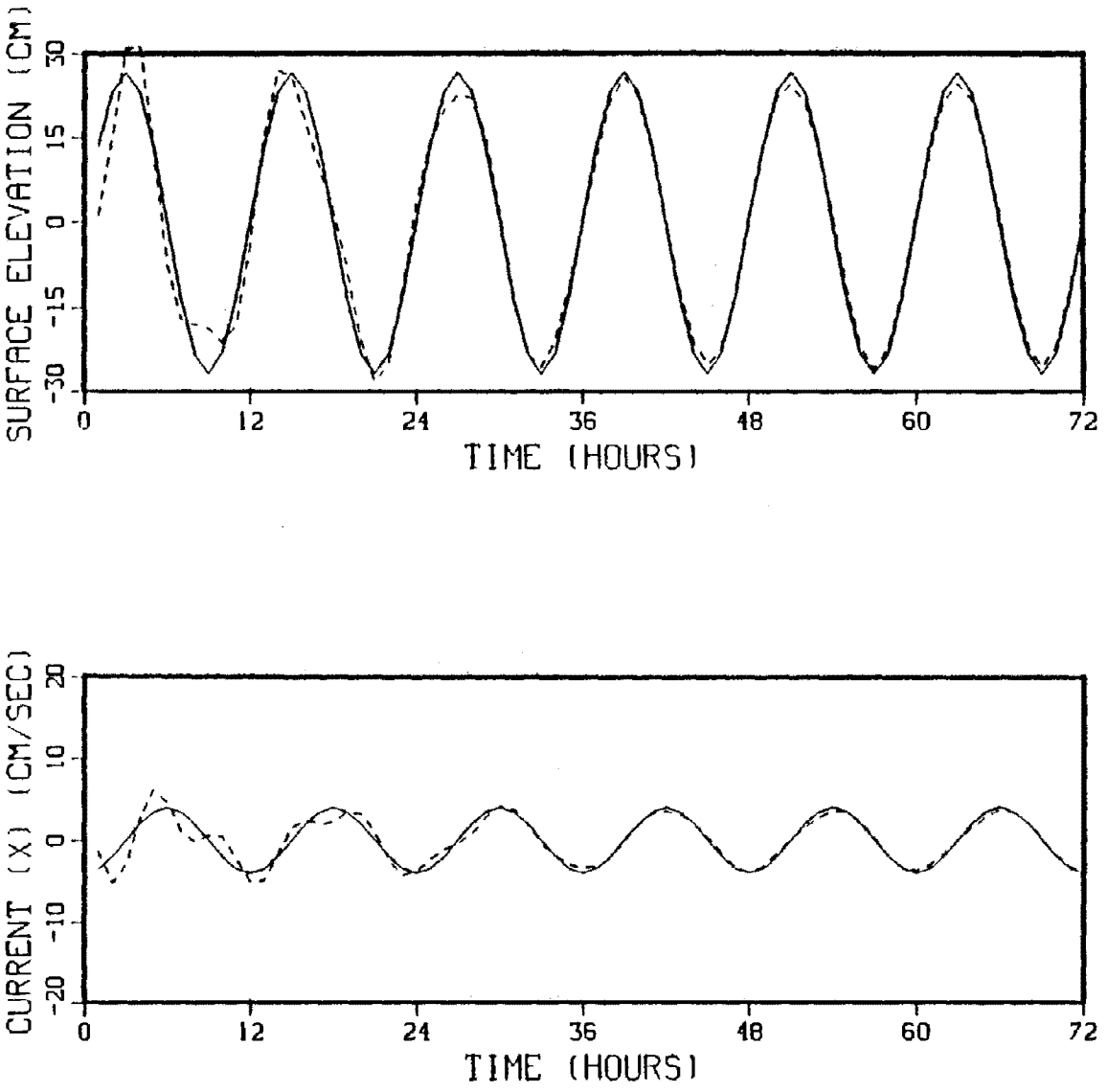

Figure 13. Water surface elevation and current velocity at x = 25 km (solid lines represent the analytical solution and dashed lines represent the numerical solution).

The analytical solutions are given as solid lines and the numerical solutions as dashed lines. As can be noted, there is good agreement between the numerical (HYDRO3D) and analytical solutions. The initial differences between the results are due to the selection of the at-rest initial condition for the numerical solution. After the initial transient response lasting approximately 4 to 5 cycles, the model results closely mimics the steady state analytical solution. The relative maximum differences between the model results and the analytical solution, after 5 cycles, is less than 5 percent. Other factors which contribute to the difference between the numerical and analytical results may be due to the assumptions used to linearize the one-dimensional wave equations used to derived the analytical solution.

4.2 SUISUN BAY, CALIFORNIA

A previous study of Suisun Bay (Sheng et al. 1986) was chosen to illustrate the feasibility of applying this model in areas of San Francisco Bay. The model has not been calibrated or validated, but enough work has been done to establish that the model is potentially useful. The follow-up study by Smith and Cheng (1989) in the adjoining San Pablo Bay, is an additional indication of the feasibility of this model for estuary studies in San Francisco Bay.

This case study is based on simulations done prior to 1986 with the EHSM3D code. That code is essentially the same as the code being documented in this report (see Preface), but there are a few changes and modifications that have been made since that time. However, none of the changes invalidate the use of these results to show feasibility of the present code.

One advantage of this study is that it provides a brief review of the process involved in initially setting up a study. In fact, it has been used for that purpose in a training workshop (Sheng et al. 1986). Briefly reviewed in this illustrative example are:

- Investigation of pertinent data and previous studies,
- Investigation of the processes that may influence circulation,
- Initial model setup, including selection of boundary conditions, initial condition options, and model parameters, and
- Interpretation of preliminary results.

Although the study was not carried to the calibration stage, the process of implementing the model in a feasibility study is well illustrated.

Another advantage in selection this study for illustrative purposes, is that it may be possible to do additional work to calibrate and validate the model. Studies have continued in San Francisco Bay that may provide data to evaluate these initial results.

4.2.1 Physical Setting

Suisun Bay is part of the San Francisco Bay and Delta system in

California, which is one of the world's largest and most complex estuarine systems (Figure 14). The central bay (mean depth 10.7m) is connected to the Pacific Ocean at Golden Gate (depth of 110m). To the north and northeast, the system extends to the extremely shallow San Pablo Bay (more than 50% of the Bay has a depth less than 2m), through the Carquinez Strait (mean depth 8.8m) to Suisun Bay (mean depth 4.3m) and finally into the Delta (See Figures 15 and 16). Each of the embayments of the system usually consist of a deep navigation channel (depth > 9m) surrounded by shallow shoals. In spite of their similarity, the various embayments exhibit very distinctive features.

Suisun Bay (Figure 15) is quite complex. It consists of several deep navigation channels surrounding numerous shoals and islands (see Simmons, Chips, Van Sickle, Sherman, and other minor islands), and includes two very shallow sub-embayments, Grizzly and Honker Bays (mean depth <2m). Suisun Bay has an area of 94 km^2 and a mean depth of 4.3m. The main navigation channel depth is between 9 and 14m and it connects Carquinez Strait and the Delta. The Delta, which provides 90% of the freshwater in the San Francisco Bay system has a volumetric outflow rate between 50 and 150 m^3/sec in summer and 8,000 and 12,000 m^3/sec in winter.

4.2.2 Circulation Patterns

Observations and analysis indicate that circulation in Suisun Bay is affected by four major factors: (1) tides, (2) salinity gradients, (3) meteorological forcing and (4) bathymetry and geometry. These factors are explored in this section to indicate what phenomena the model should simulate.

Ocean tides enter the Bay System at Golden Gate and travel a significant distance through Suisun Bay into the north by northeast end of the Bay system. Extensive field studies on tidal circulation in the Bay system have been performed by the U.S. Geological Survey and others (e.g., Conomos and others 1978; Patchen and Cheng 1979; Cheng and Conomos 1980; Smith, 1980; Cheng and Gartner 1984). The recent report by Cheng and Gartner (1984) provides the most comprehensive database on tides, tidal currents, and residual currents in the San Francisco Bay system. Water levels were measured at several stations, and currents were measured at several current meter located within Suisun Bay as shown in Figure 15. Salinity intrusion within the navigation channels of San Francisco Bay and in particular, the Delta system, was investigated by a U.S. Army Corps of Engineers contractor Kinnetics Laboratories, Inc., (1981).

A tidal harmonic analysis of Suisun Bay data indicate that the major constituents are the M_2 and the K_1 tides. Figure 17 graphically illustrates the spatial distribution of properties of M_2 and K_1 tides, at Stations C26, C27, C28, C30, C239, and at the east boundary of Suisun Bay. At Station 5103, the M_2 and K_1 amplitudes are 52.4 cm and 30 cm, respectively. Values of the same parameters are 43 cm and 25.4 cm at Station 5112. There is a net phase shift of approximately 33 degrees between the two stations.

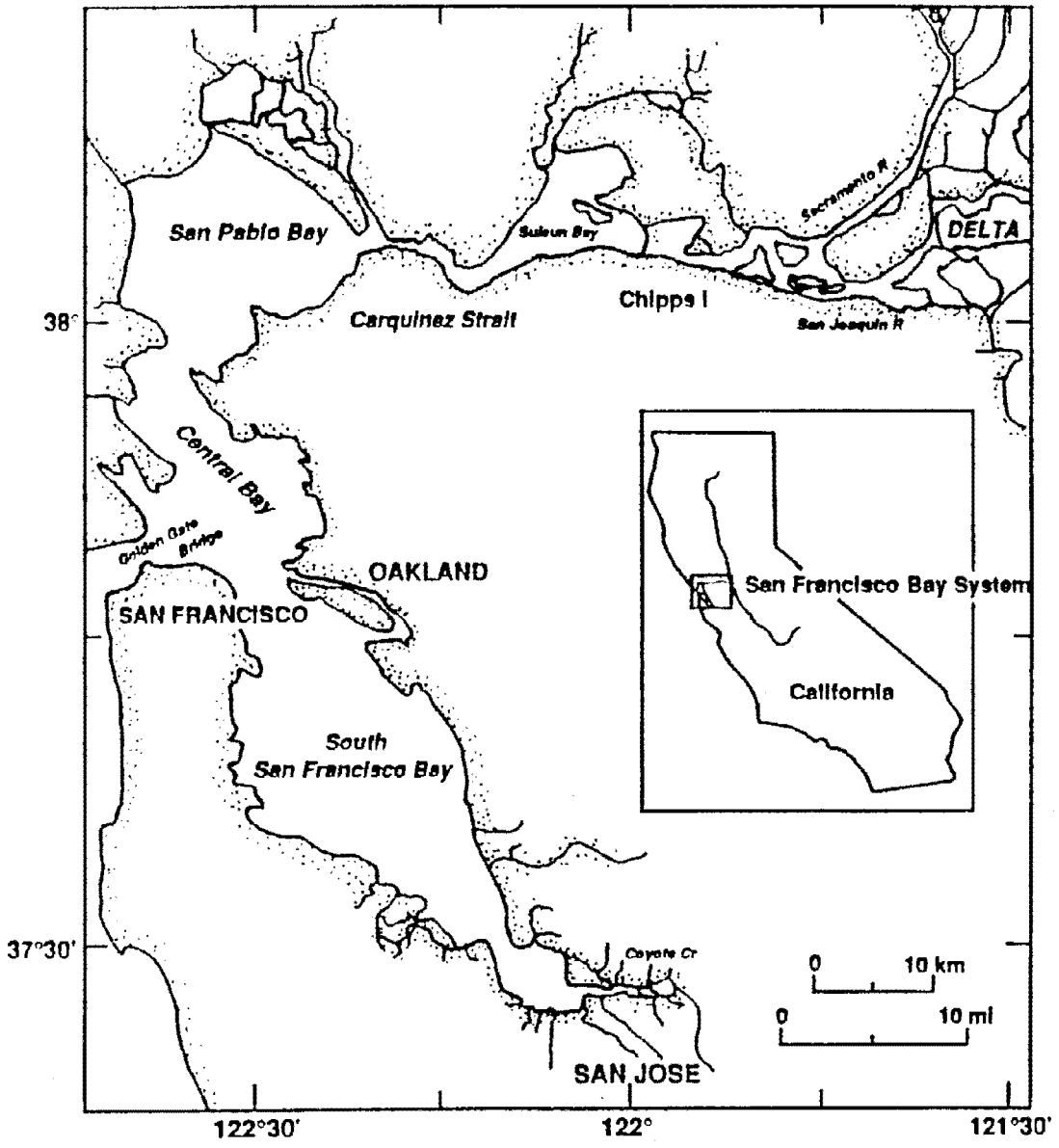

Figure 14. Map of San Francisco Bay estuarine system.

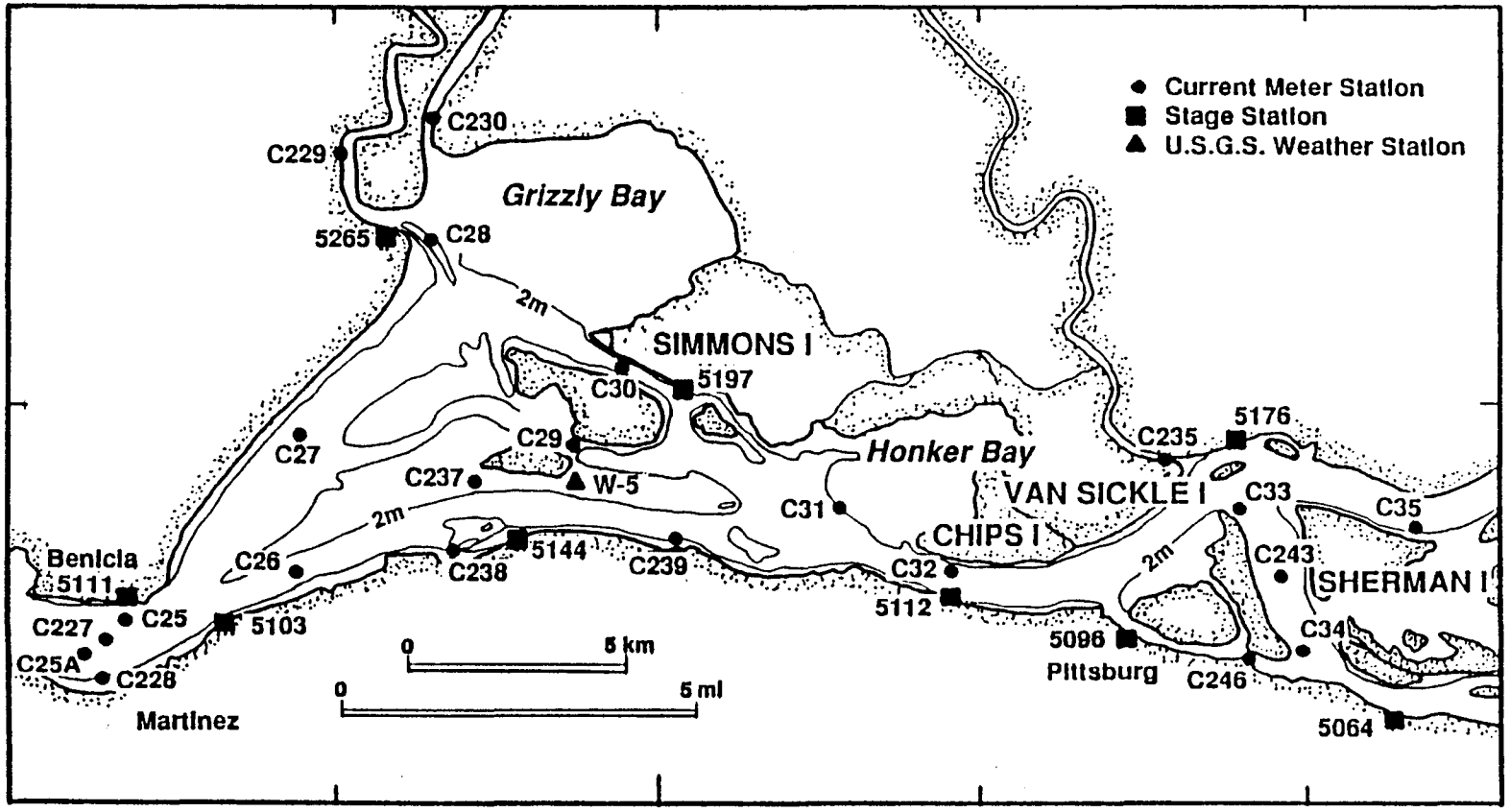

Figure 15. Map of the Suisun Bay region and the location of current-meter moorings, tide stations, and a USGS weather station.

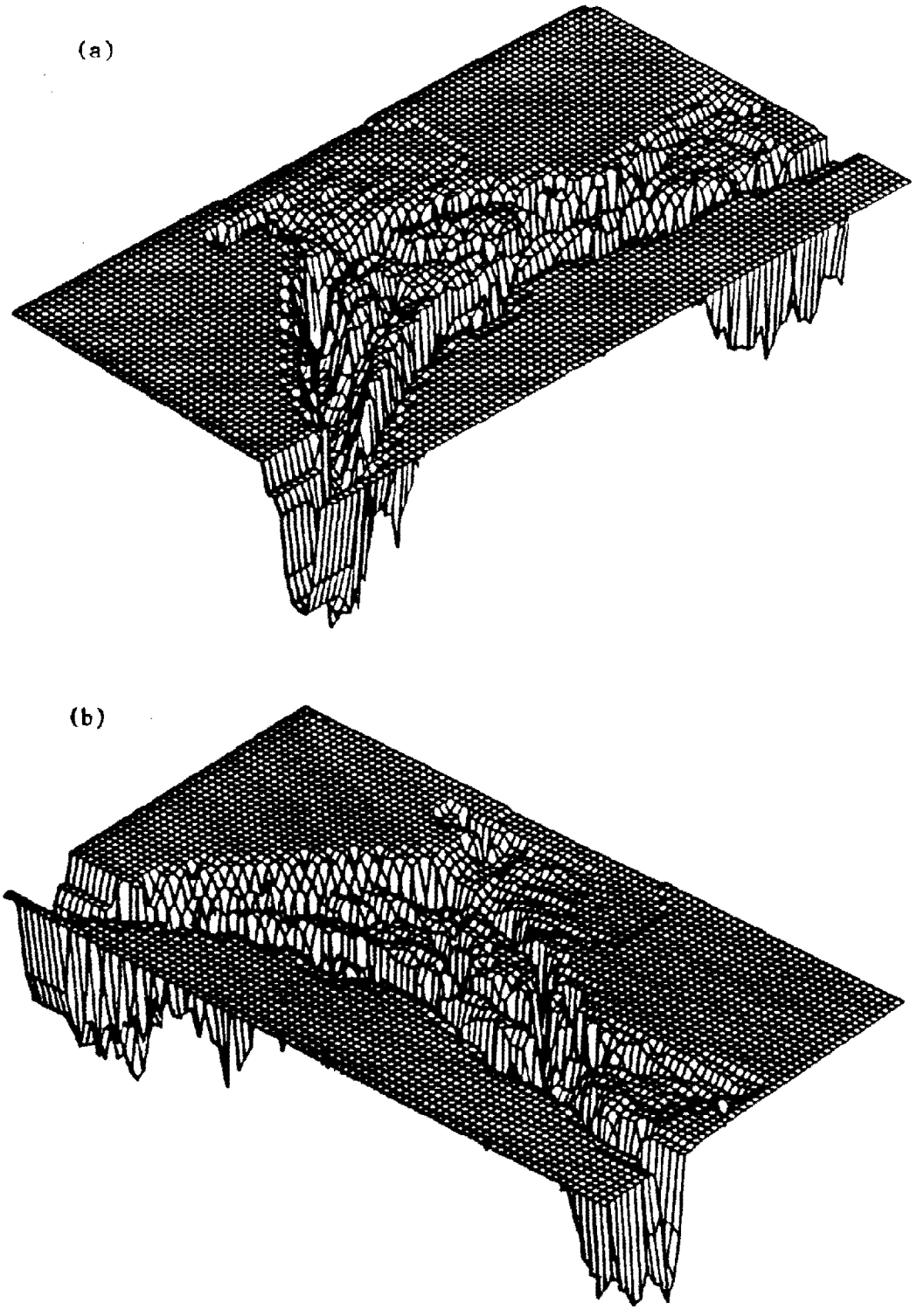

Figure 16. Three-dimensional plot of the Suisun Bay bathymetry when viewed from (a) the southwest and (b) the southeast.

Tidal currents within Suisun Bay were analyzed to determine the O_1, K_1, N_2, M_2, S_2 and M_4 tides. Harmonic constants were given along the major and minor axes of the tidal current ellipses. A strong bi-directional tendency was observed at most stations and the basin bathymetry was found to significantly affect the principal current direction also see Cheng and Gartner 1984). In addition, it was noted that the tidal current speed can vary up to a factor of two between spring and neap tides.

Salinity varies from the ocean value of approximately 30 ppt at Golden Gate to the freshwater value of approximately 0 ppt upestuary at the Delta. The location of the salinity front and the detailed salinity distribution within the northern reach of the Bay system is significantly influenced by the Delta outflow. During the low flow summer months, the salinity front may reach into the confluence of the Sacramento and San Joaquin Rivers (see Figure 14). During winter, the salinity front may retreat into San Pablo Bay. Salinity within Suisun Bay varies between 10 to 15 ppt at the western end to between 0 to 10 ppt at the eastern end. Salinity data also exhibit significant daily and temporal variations. From this it seems clear that the salinity distribution may have a significant effect on the currents within Suisun Bay and must be taken into account to properly simulate circulation.

The bathymetry of Suisun Bay is another element that influences circulation, and it is relatively complex as described above. To illustrate the complexity, Figure 16 shows 3-D plots of the bathymetry viewed from the southwest and southeast. In addition and perhaps most important is the findings of a tidal analysis by Cheng and Gartner (1984) that indicates a strong influence of bathymetry.

In the initial report, Sheng et al. (1986) does not review any direct influence of meteorological forcing. It is clear from the initial discussion above, however, that indirect affects on fresh water inflows are at least an important seasonal effect on the location of the salt water wedge. In addition, it is likely that the open shallow Grizzly Bay and Honkers Bay are subject to some wind-driven circulation. Since a decision was made to ignore short-term episodic events in the initial study (Sheng et al. 1986), consideration of meteorological forcing is of lessened importance for this case study.

4.2.3 Modeling 3-D Circulation in Suisun Bay

For illustrative modeling in Suisun Bay, a grid was defined, initial conditions were specified, selected data were used to provide a reasonable representation of the tide and salinity boundary conditions, model parameters were initially selected, and the resulting simulations were investigated. Major features and trends of the circulation became the focus of the initial study. Short-term events episodic were ignored.

The model grid was setup to simulate five vertical layers. Each layer was divided by grid line spacings of 1/2 km. The resulting network had a total of 46 x 26 x 5 grid points. The bathymetry arrays were smoothed by the option provided to eliminate sharp bottom slopes.

(a) (b)

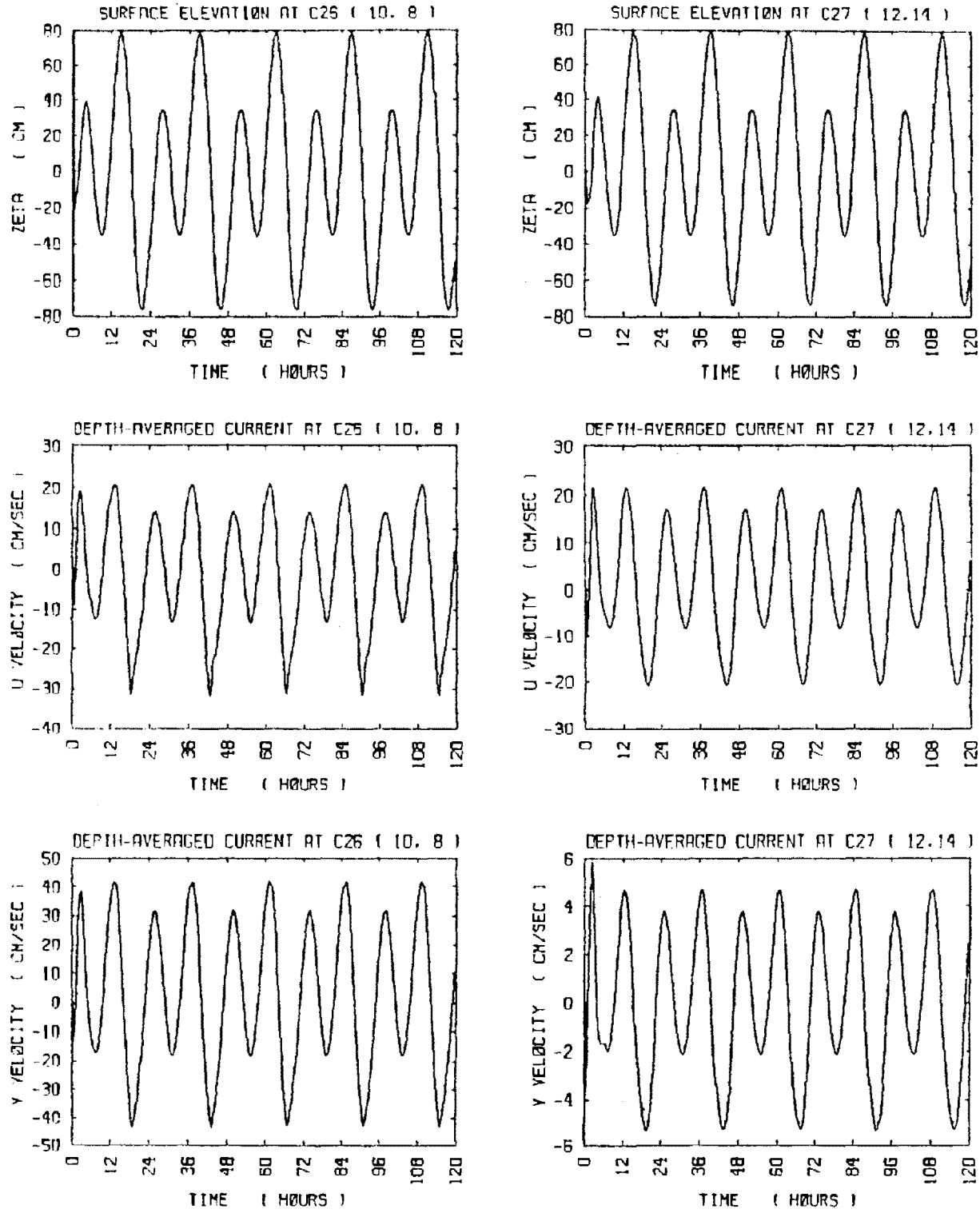

Figure 17. Time histories of simulated surface elevation and depth-averaged velocity components at (a) C26, (b) C27, (c) C28, (d) C30, (e) C239 and (f) the west boundary during a 5-day model simulation of tidal circulation in Suisun Bay.

(c) (d)

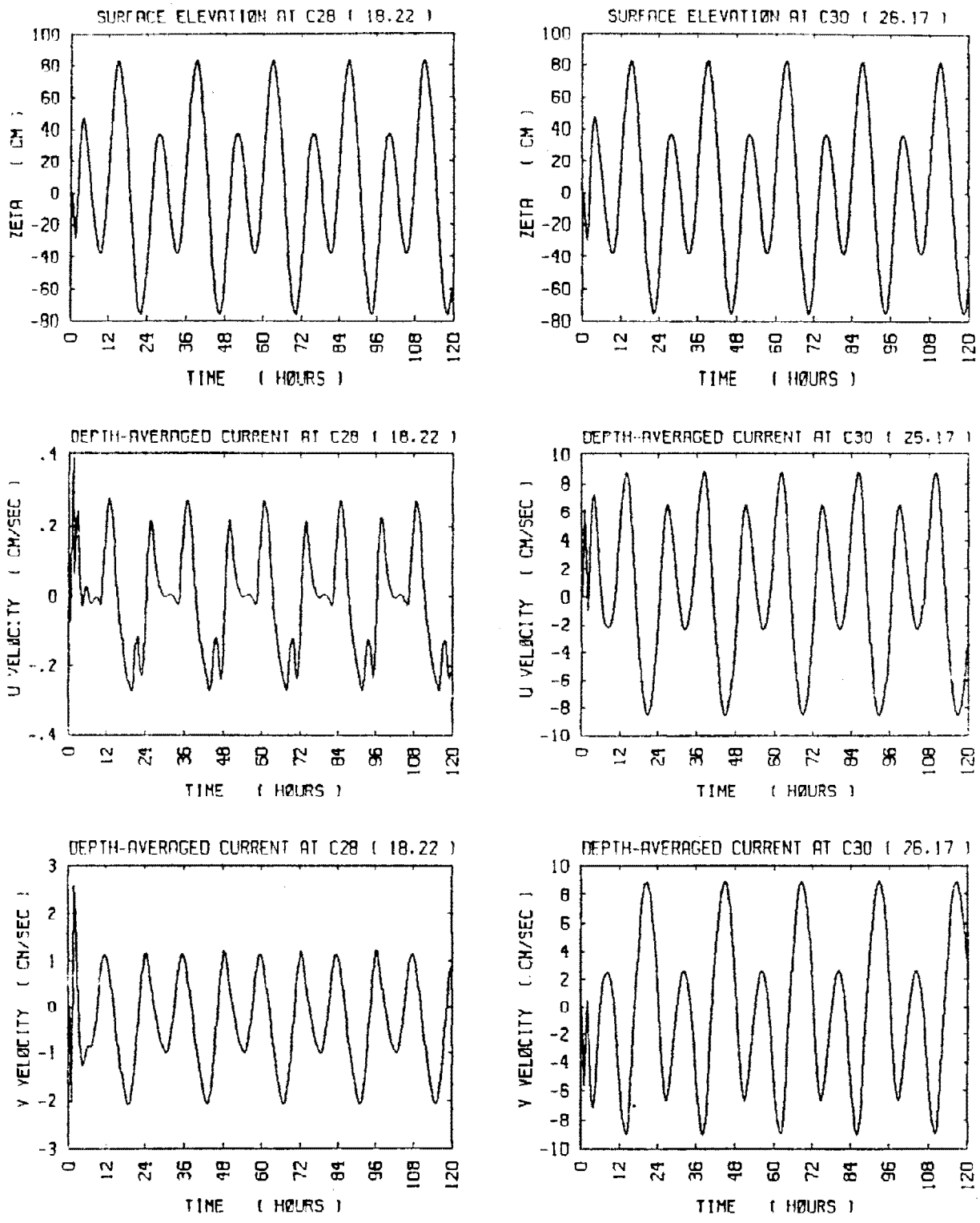

Figure 17. Time histories of simulated surface elevation and depth-averaged velocity components at (a) C26, (b) C27, (c) C28, (d) C30, (e) C239 and (f) the west boundary during a 5-day model simulation of tidal circulation in Suisun Bay.

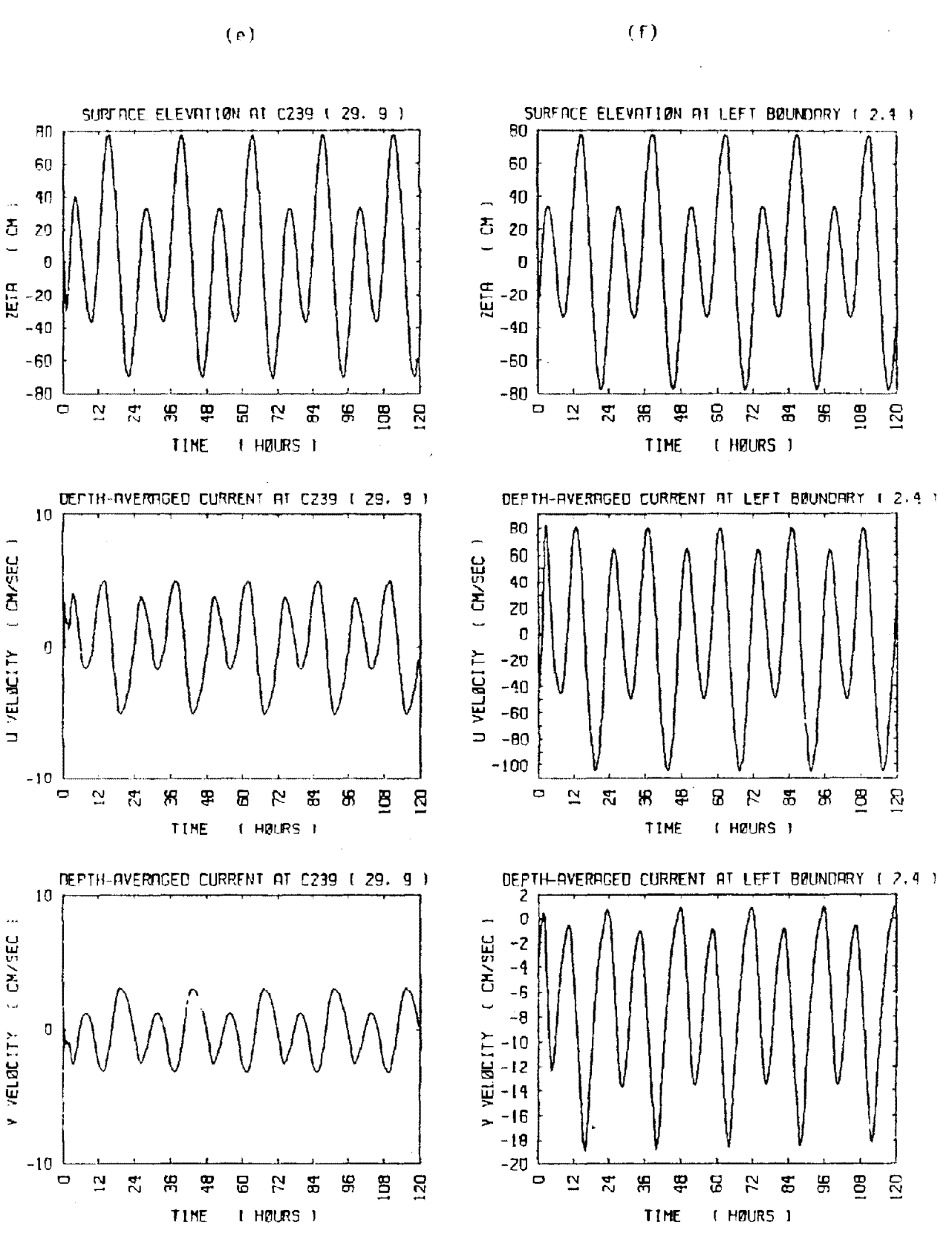

Figure 17. Time histories of simulated surface elevation and depth-averaged velocity components at (a) C26, (b) C27, (c) C28, (d) C30, (e) C239 and (f) the west boundary during a 5-day model simulation of tidal circulation in Suisun Bay.

Turbulence and friction losses were simulated in straight forward manner. The simplified second order turbulence closure option was select to represent vertical mixing. A horizontal eddy viscosity of 100 m^2/sec was selected. The related bottom roughness height of 0.4 cm was chosen.

Tidal boundary conditions were developed from a synthetic tide based on the previous analysis. A synthetic tide composed of the M_2 and K_1 constituents only, was applied to the west and east boundaries. Along the west boundary, the M_2 and K_1 tides were assigned amplitudes 55 cm and 31 cm, respectively, and a phase angle of 90 degrees. Along the east boundary, amplitudes were assigned as 43 cm and 23 cm, respectively. A phase shift of 38 degrees between the west and east boundaries for both the M_2 and K_1 tide constituents, was selected. This was necessary because the west boundary of the computational domain was established westward of the Benicia tide station (see Figure 15).

Salinity boundary conditions were selected to provide reasonable representations of observed vertical salinity gradients at the west and east boundaries, and of the horizontal gradient across the computational domain. At the west boundary, top layer values of 18 ppt and bottom layer values of 20 ppt were specified. At the east boundary, a top to bottom variation of 14 ppt was specified.

Boundary fluxes were described with an advection calculation for outflow and a constant concentration inflow. This was necessary because the EHSM3D model only allows for outflow-inflow open boundary conditions. When outflows occurred, the flux was calculated from the one-dimensional advection equation. Inflows were computed assuming that the flow originated from a constant concentration "reservoir" (i.e., inflows were assumed to have a constant concentration regardless of the history of the outflows).

Simplified initial conditions were selected for circulation and salinity. The at-rest option as selected to represent a quiescent flow conditions in the beginning of the simulations. A linear salinity gradient was assumed to describe salinity across the computational domain.

4.2.4 Results

Simulation of 120 hours (5 days) provided a number of notable results. Time history results for simulated water level and depth averaged velocity, illustrated in Figures 18 to 24 for stations C25, C26, C28, C30, C239, and at the west boundary, show some of the same features noted in the tidal measurements. These include:

- That simulated ebb currents are stronger that simulated flood currents at many stations, and
- That bi-directionality is also apparent in the depth-averaged simulations of currents.

Simulated current speeds are comparable to observed neap tide

measurements in Cheng and Gartner (1984), but spring tide simulations of current speed are generally smaller than observations. This is probably due to the idealized synthetic tidal boundary condition, and the simplified salinity boundary conditions. In addition, there are concerns that the salinity boundary conditions selected for this simulation do not necessarily allow the complete internal propagation of baroclinic perturbations at the boundaries.

Although the water level and currents appeared to reach a dynamic steady-state in relatively short time periods, salinity values at various stations were still very slowly changing at the end of 120 hours of simulation. This is illustrated in Figure 18 that shows the salinity at three vertical levels (near-bottom, mid-depth, and near-surface) gradually increasing at each of the stations except at the west boundary that is constrained as shown. The vertical structure of the velocity fields at 96, 108 and 120 hours shown in Figures 19, 20 and 21, respectively, indicated that a dynamic steady-state may have been achieved in the simulations. Other notable occurrences include flow reversals at some locations and near-surface currents well in excess of 1 m/sec at 108 hours. The lest satisfactory simulations involved the vertical salinity structure. The simulated salinity fields at 96, 108, and 120 hours are shown in Figures 22, 23, and 24, respectively. Figure 18 shows the simulated vertical structure of the salinity field at six stations over the full course of the simulation. The simulated vertical stratification is not very pronounced and there are indications that greater degrees of stratification actually exist (Peter Smith, in review).

The simulation of limited stratification is cause for further investigation and indicates that present results can only be used for illustrative purposes until additional calibration is possible. In this case, it does not seem possible to reach into preliminary conclusions about the flow and salinity distributions. When calibration is undertaken, the specifications for the open boundaries, initial conditions, and the coarse five-layer grid spacing should be examined. Ten or more layers are likely to improve vertical resolution and a nonuniform Cartesian grid could be used to better resolve the steep topography between the navigation channel and the shallow areas. Comparison with additional calibration data is also likely to point out other input data should be investigate, however, the results for simulated circulation in Suisun Bay and the test of the model in the adjacent San Pablo (Smith and Cheng 1989) indicate there seem to be no insurmountable problems that would prevent calibration.

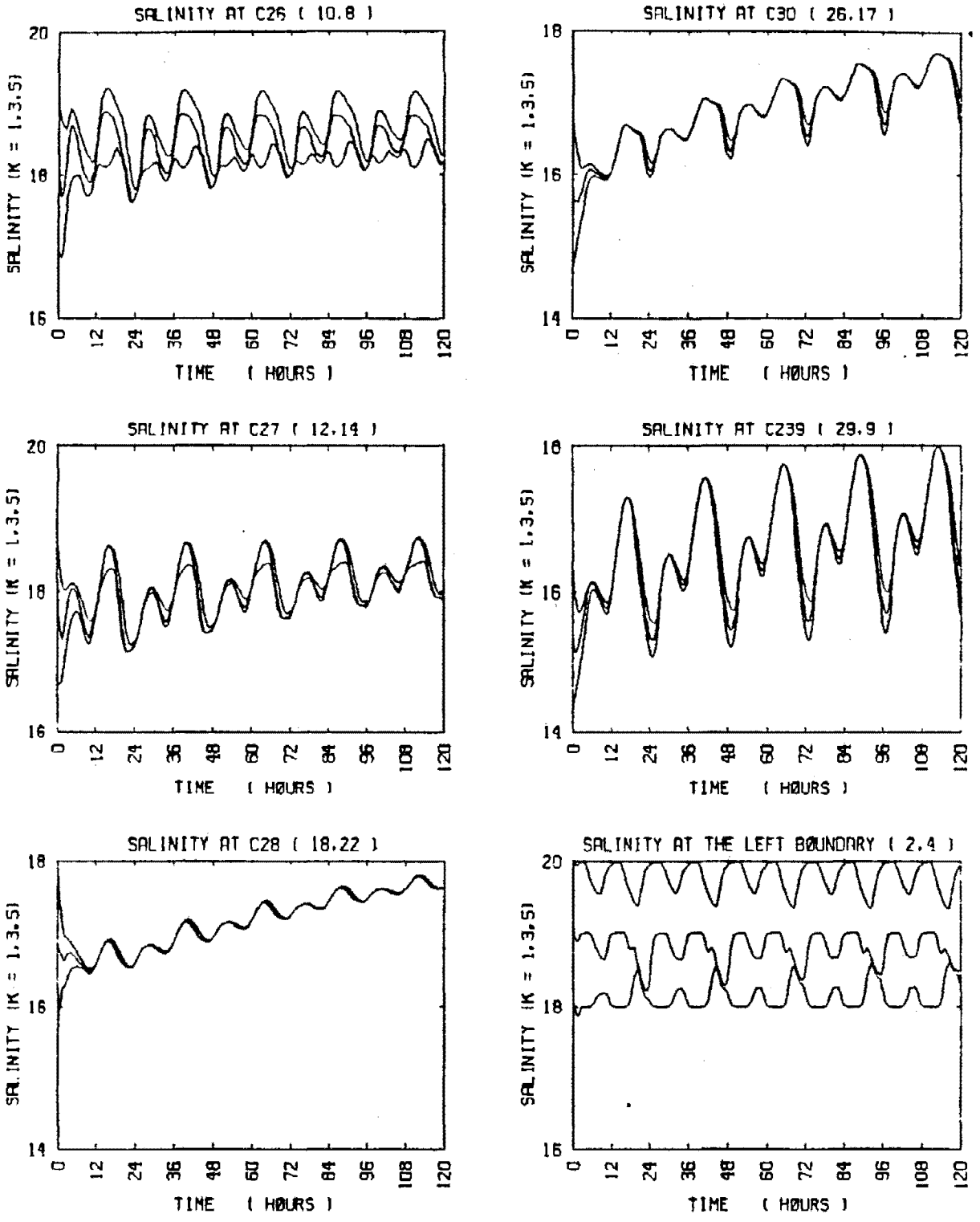

Figure 18. Time histories of simulated salinity at 3 vertical levels near-bottom, mid-depth and near-surface during a 5-day model simulation of tidal circulation in Suisun Bay.

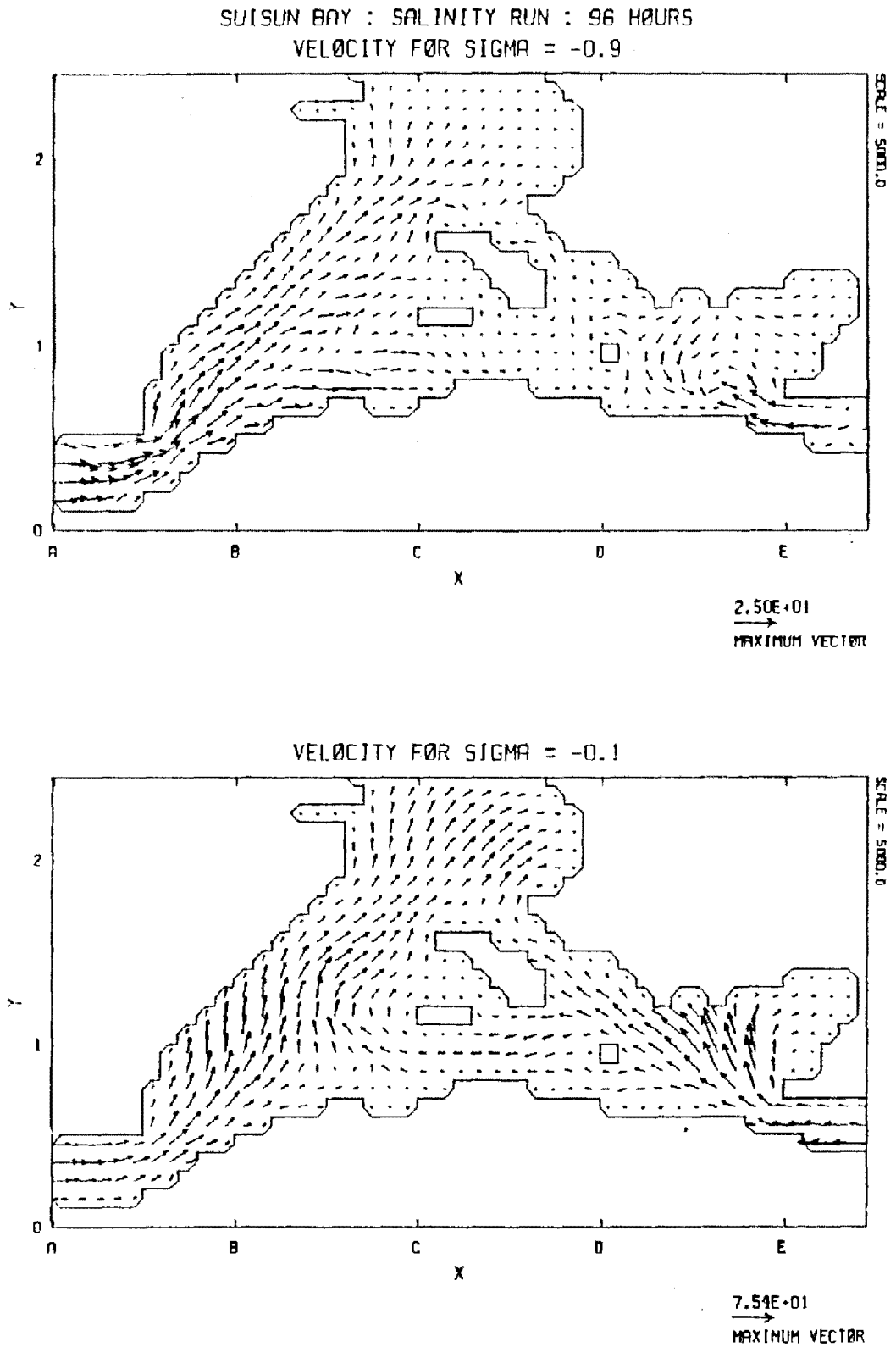

Figure 19. Simulated Tide- and salinity-driven currents in Suisun Bay near the bottom (σ = -0.9) and near the surface (σ = -0.1) at 96 hours.

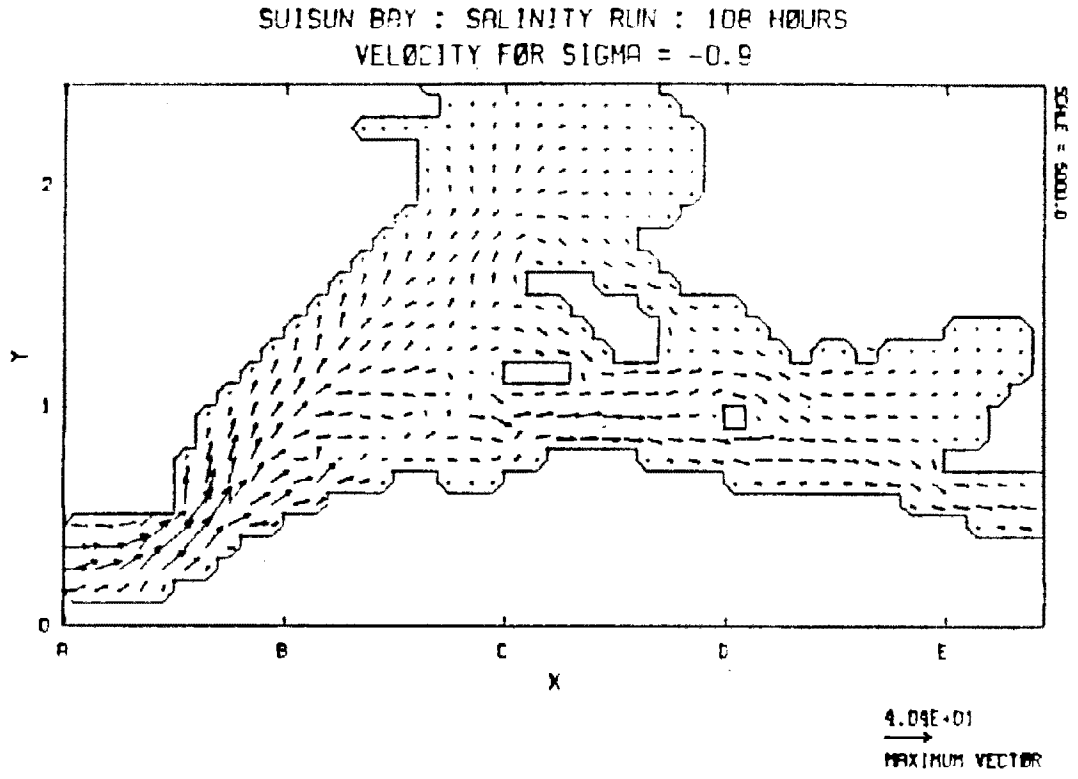

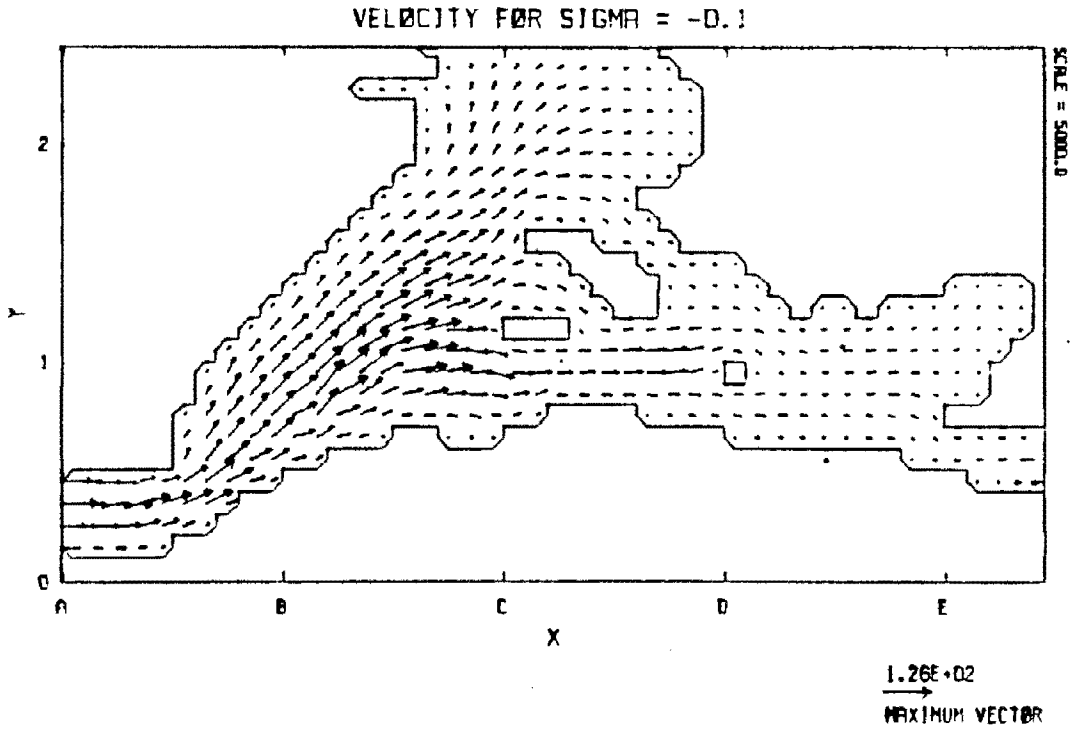

Figure 20. Simulated Tide- and salinity-driven currents in Suisun Bay near the bottom (σ = -0.1) and near the surface (σ = -0.1) at 108 hours.

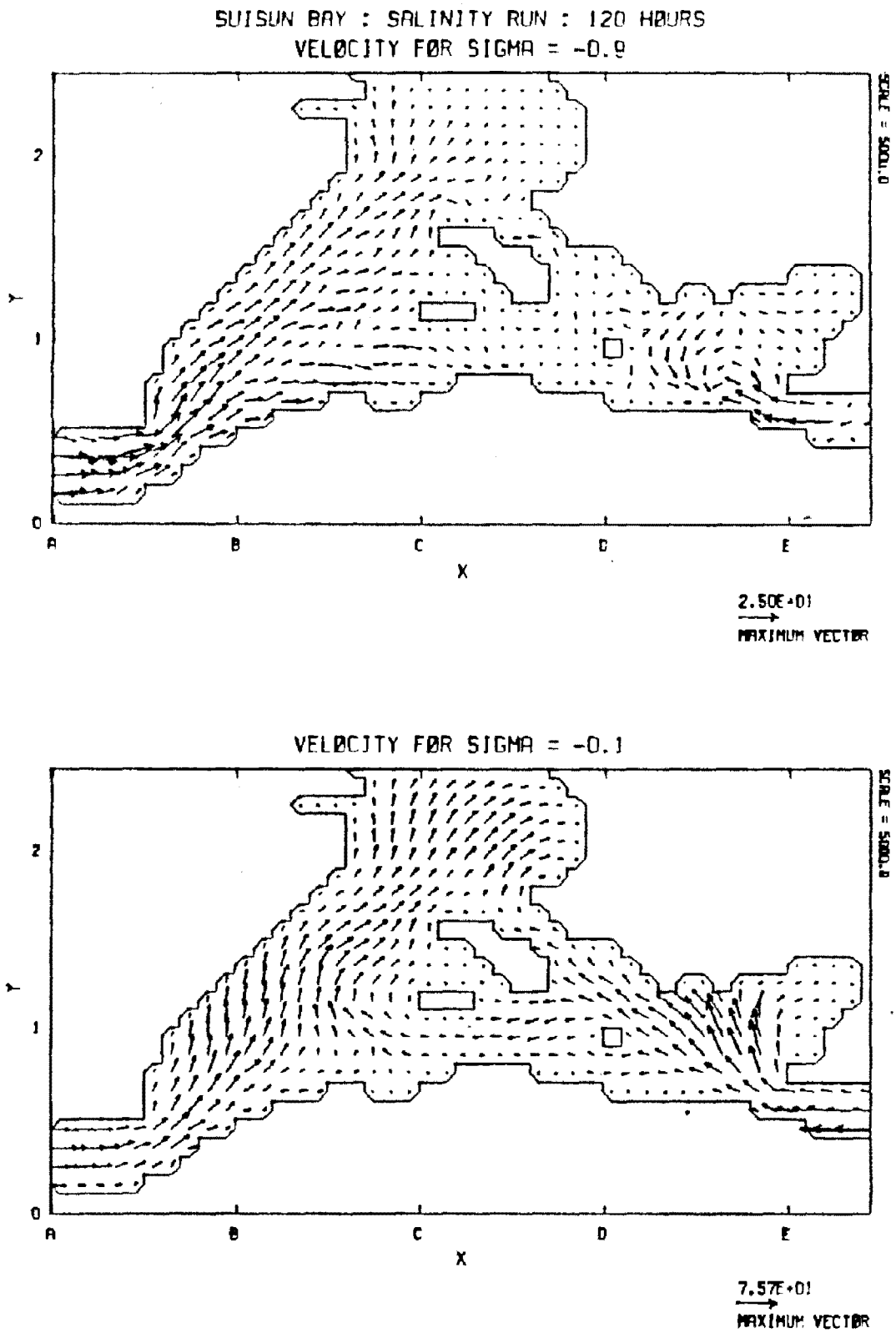

Figure 21. Simulated Tide- and salinity-driven currents in the Suisun Bay near the bottom (σ = 0.9) and near the surface (σ = -0.1) at 120 hours.

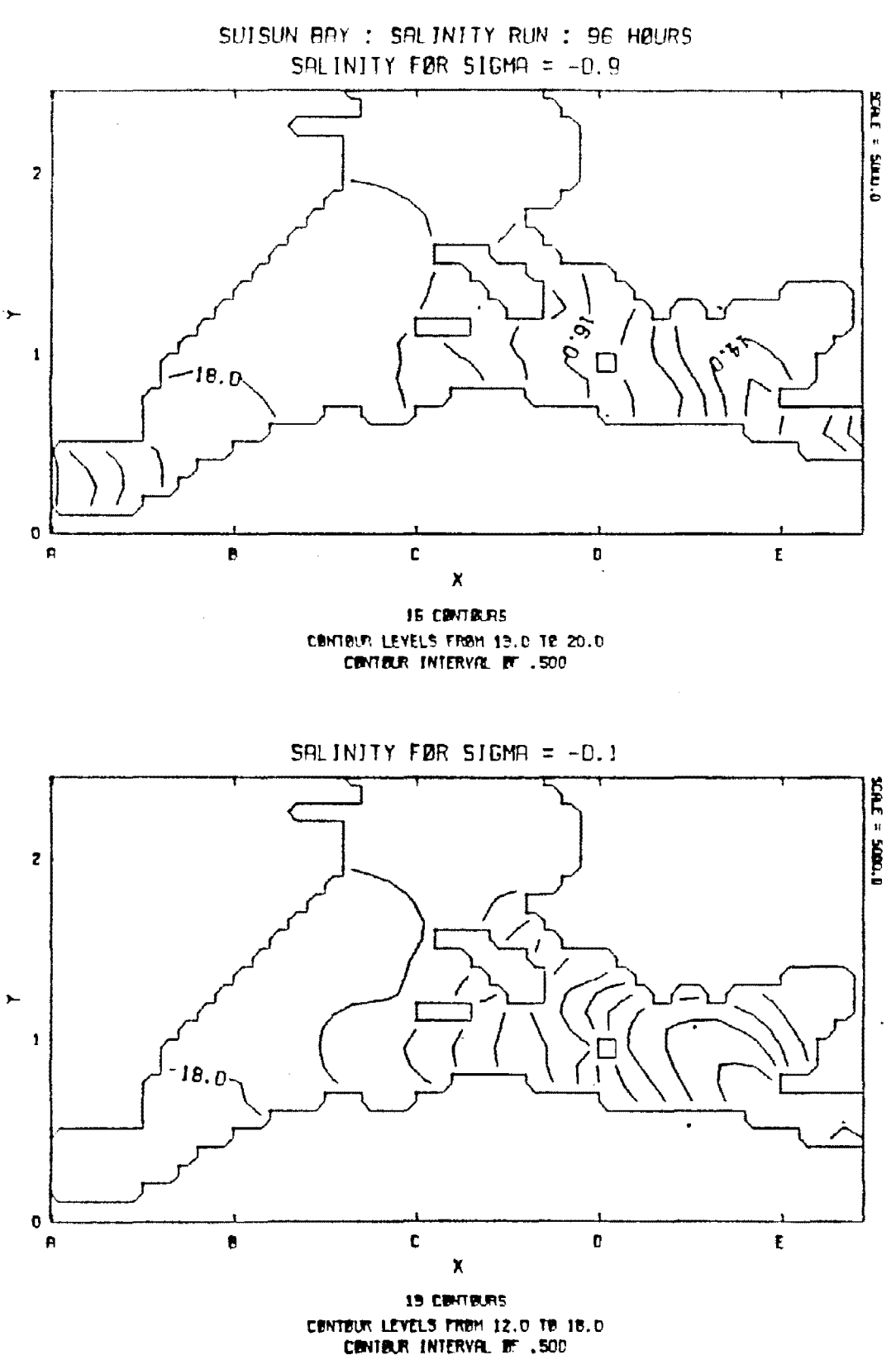

Figure 22. Simulated salinity distribution in Suisun Bay near the bottom (σ = -0.9) and near the surface (σ = -0.1) at 96 hours.

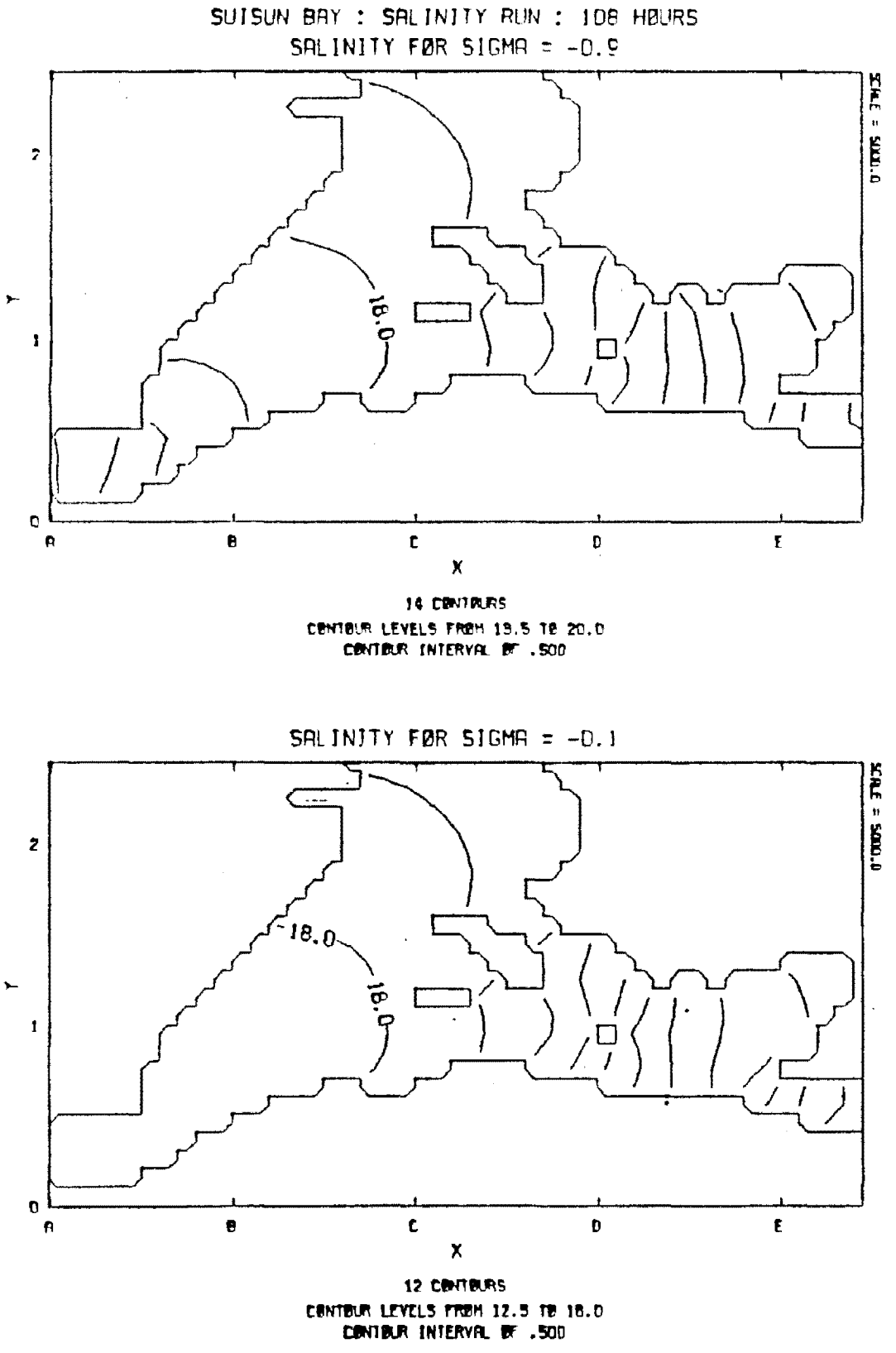

Figure 23. Simulated salinity distribution in Suisun Bay near the bottom (σ = -0.9) and near the surface (σ = -0.1) at 108 hours.

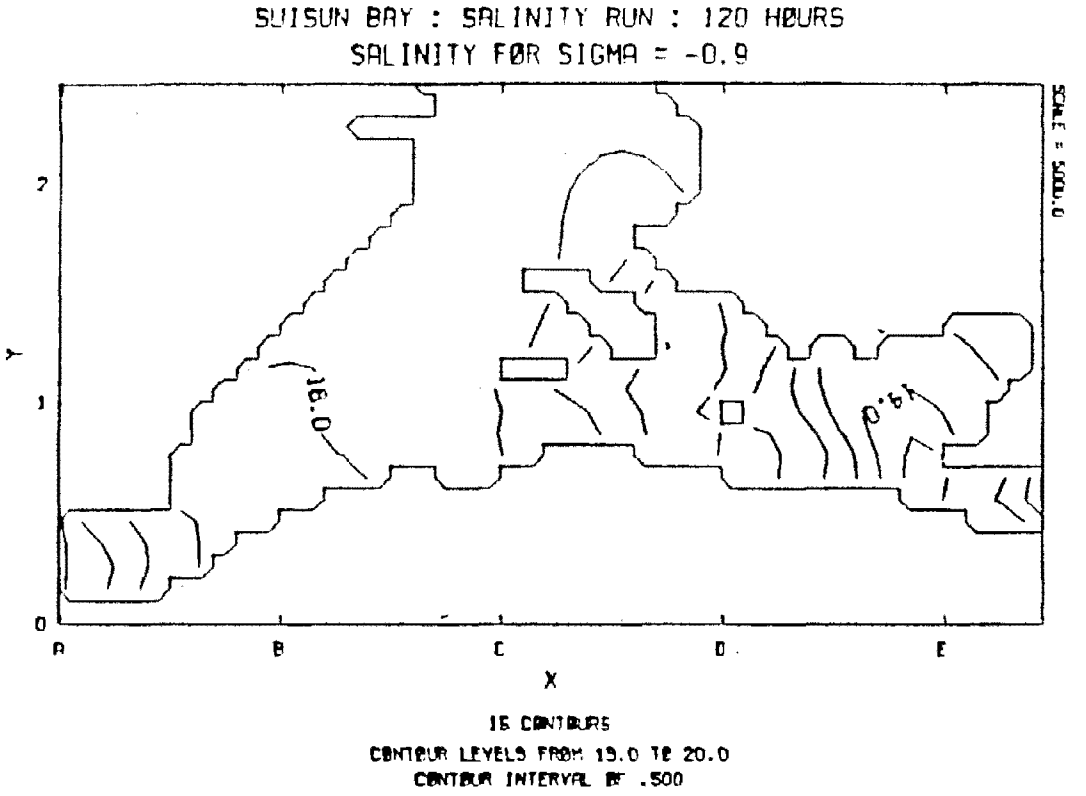

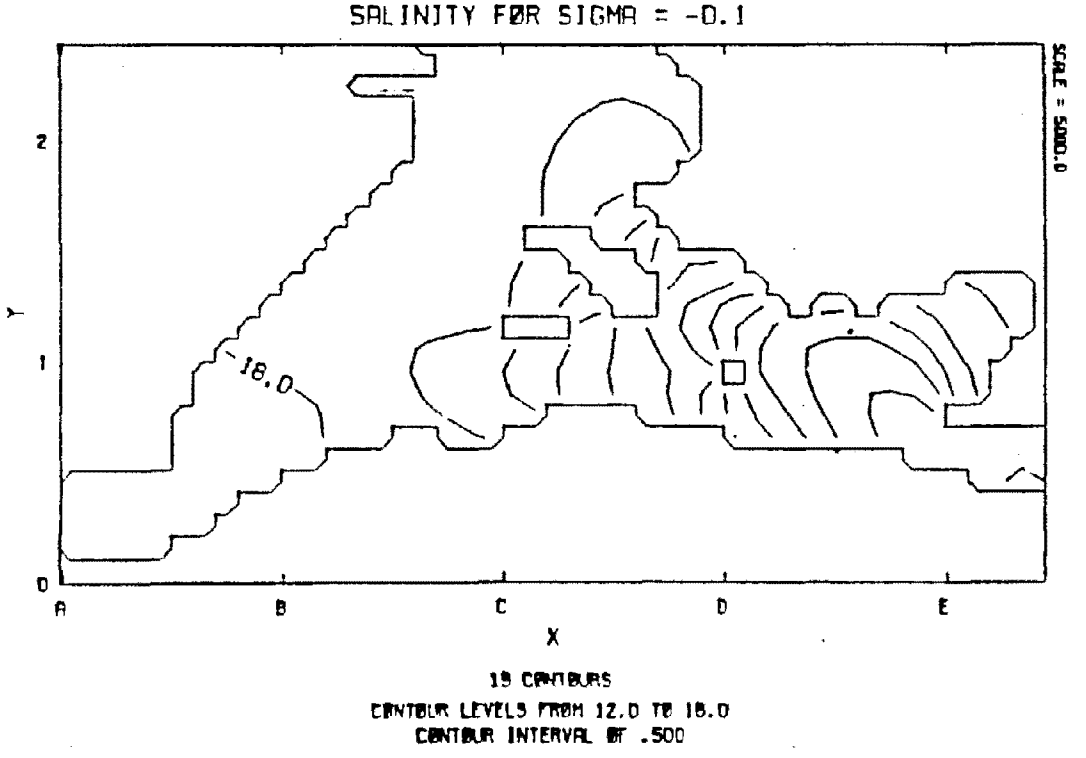

Figure 24. Simulated salinity distribution in Suisun Bay near the bottom (σ = -0.9) and near the surface (σ = -0.1) at 120 hours.

4.3 Charlotte Harbor, Florida

A previous study of Charlotte Harbor (Sheng et al. 1986) was also chosen to illustrate the feasibility of applying this model, as was done with the case study for Suisun Bay. The model has also not been calibrated or validated for Charlotte Harbor, but enough work has been done to establish that the model is potentially useful in partially mixed U.S. Gulf Coast estuaries.

The simulations for this case study were also performed prior to 1986 with the EHSM3D code. As noted before (see Preface), that code is essentially the same as the code being documented in this report. There are a few changes and modifications that have been made since that time, but none invalidate the use of these results to demonstrate the feasibility of using the present code.

This case study also provides a brief review of the process involved in initially setting up a study. It has also been used in a training workshop (Sheng et al. 1986) for that purpose. In addition, this study includes other illustrative investigations of interest. Briefly reviewed in this illustrative example are:

- Investigation of pertinent data and previous studies,
- Processes that may influence circulation,
- Initial model setup, including selection of boundary conditions, initial condition options, and model parameters,
- Investigation of pronounced freshwater effects,
- Analysis of affects of the grid scale,
- A study of the affects of initialization, and
- Interpretation of preliminary results.

Although the study was not carried to the calibration stage, the process of implementing the model in a feasibility study is well illustrated. The study focussed on investigation of general trends and behavior, and the sensitivity of the results to various model options and approaches. Short-term episodic events, including the affects of tropical storms, have not been considered.

4.3.1 Physical Setting

The Charlotte Harbor area of southwest Florida is a shallow water body with complex boundaries and flow patterns. The estuary (Figure 25) receives discharges from the drainage of 16 percent of the State of Florida through the Peace, Myakka and Caloosahatchee Rivers. The estuarine system is connected with the Gulf of Mexico through various inlets between the barrier islands on the west of the system. The northern area of Charlotte Harbor (Figure 26), which has a maximum water depth of approximately 7m, is of particular importance because of the rapid development of adjacent land areas. The Pine Island Sound to the south of Charlotte Harbor is extremely shallow (maximum depth 2 m). The hydrodynamics of the system are complicated by islands, shoals, and multiple openings to the Gulf of Mexico.

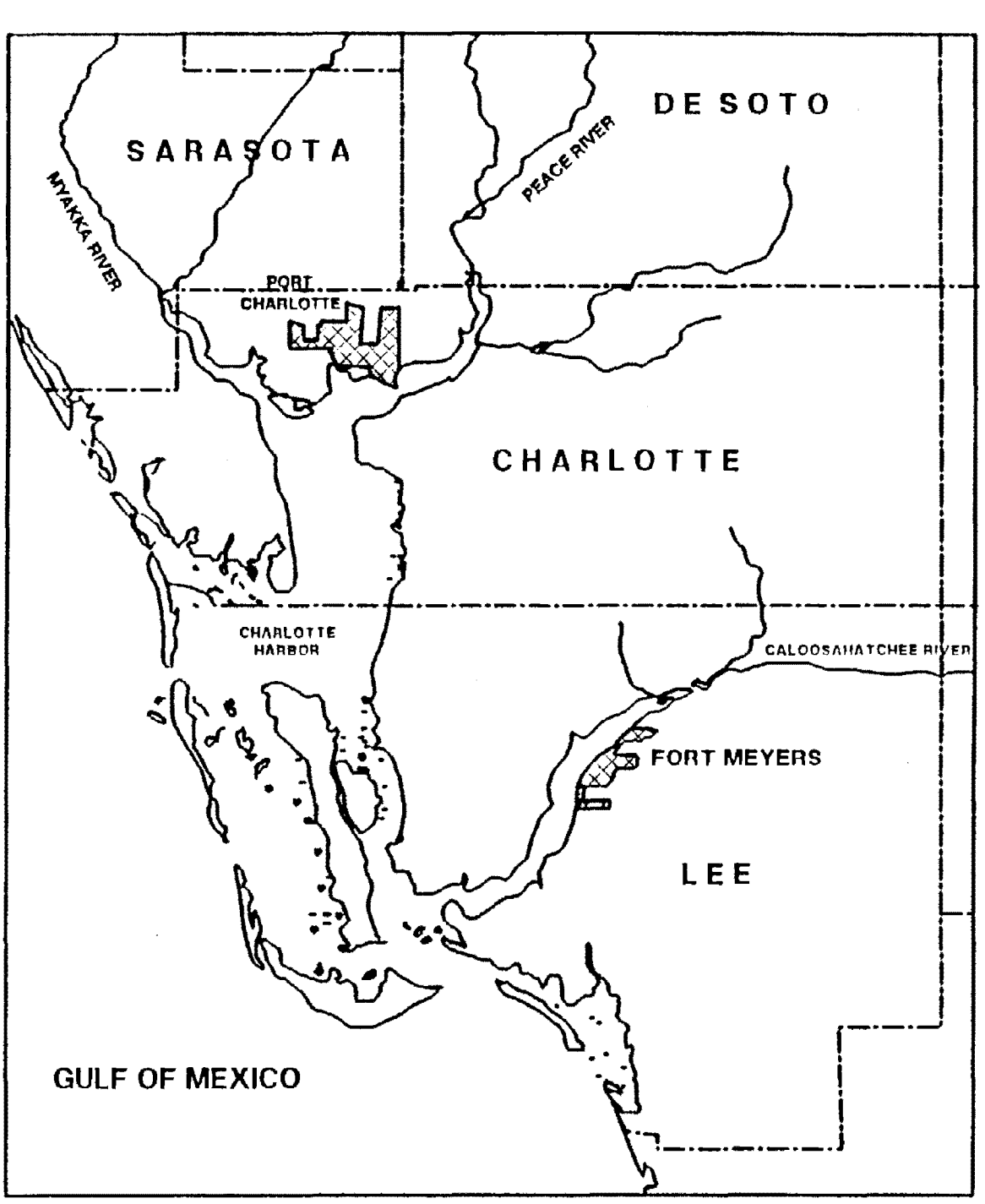

Figure 25. Map of Charlotte Harbor Estuarine System.

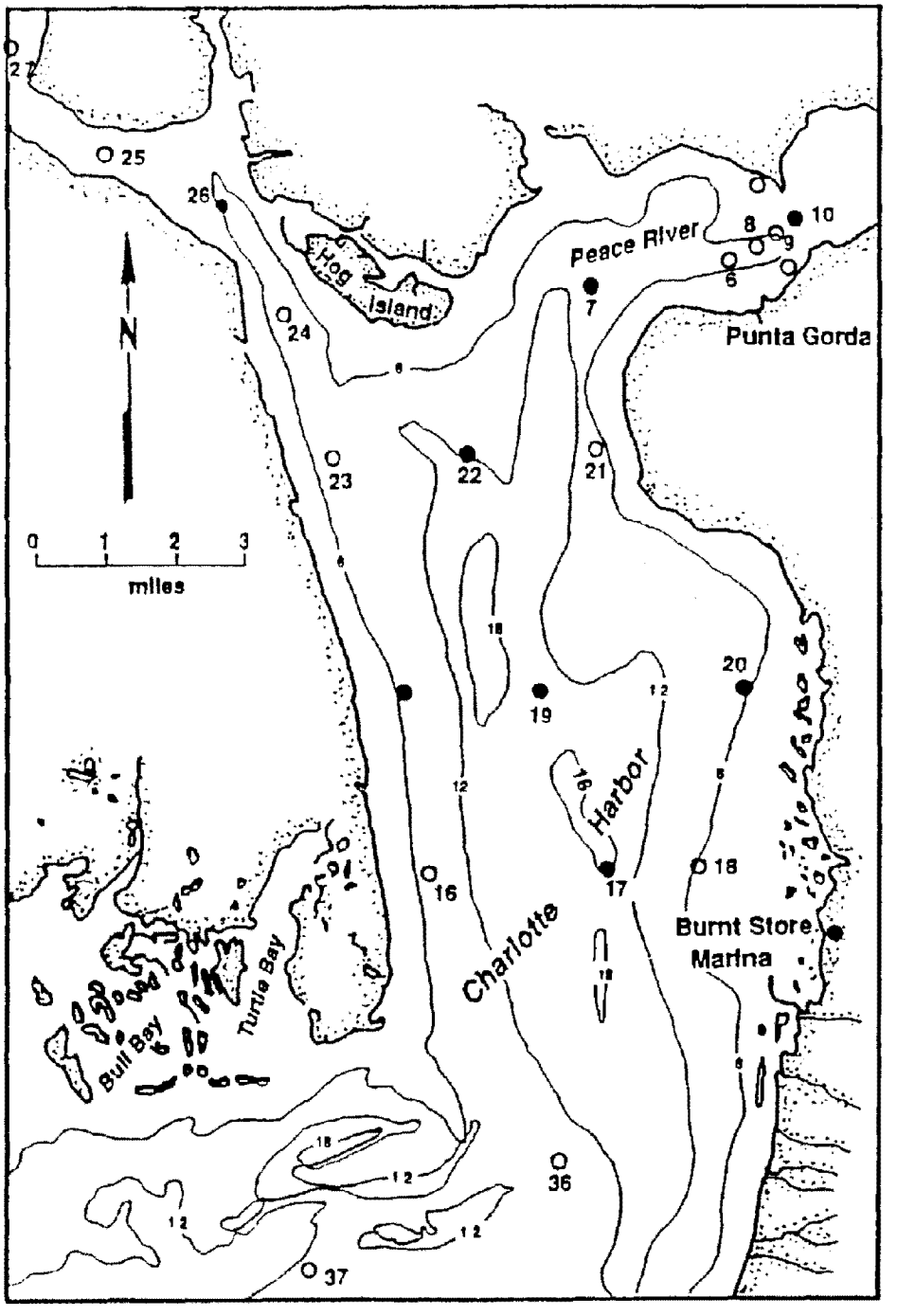

Figure 26. Map of northern Charlotte Harbor with locations of water quality/current meter stations during the June and July 1982 study.

4.3.2 Circulation in Charlotte Harbor

Like that in most partially mixed estuaries, circulation in Charlotte Harbor is affected by ocean tides propagating through the Harbor entrances, salinity gradients caused by freshwater inflows, meteorological forcing, and Harbor bathymetry and geometry. Tidal records indicate a primary diurnal tide with some semi-diurnal influence. Measurements of water surface elevations on which the analysis of the tides were based, were made at the Harbor entrance, Brunt Store Marina, and north and south of Pine Island. Figure 27 shows the tidal elevations measured during July 20 and 21, 1982 at Brunt Store Marina.

Water quality and current meter data were collected at a number of stations shown in Figure 26. The data of interest were collected during June and July 1982.

The freshwater inflow from the Peace River strongly influences the circulation within Charlotte Harbor. The volumetric flow rate can vary from less than 2,000 cubic feet per second (cfs) to 18,000 cfs within a week (Figure 28). This kind of flow variation can significantly affect the location of the salinity intrusion front. Potentially the tides can propagate upstream into the Peace River.

Due to the shallowness of the estuarine system, tropical storms from the Gulf of Mexico can significantly affect the tides and circulation within Charlotte Harbor. In this study, however, these extreme events have not been investigated. Other meteorological effects and the effects of bathymetry and geometry were also not investigated in detail in the initial phases of this study (Sheng et al. 1986).

4.3.3 Modeling 3-D Circulation in Charlotte Harbor

For illustrative modeling, a grid was defined, initial conditions were specified, selected data were used to provide a reasonable representation of the tide and salinity boundary conditions, model parameters were initially selected, and the resulting simulations were investigated. Select sensitivity analyses of grid resolution and other options were performed.

The model grid consisted of nine vertical layers and horizontal grid line spacings of 1 km. The computational domain was extended from the northern part of the Harbor to between stations 17 and 19 shown in Figure 26. The domain extended about 1 km into the Peace River beyond station 10 shown in Figure 26. This resulted in a domain of 11 x 11 x 9 grid points.

The tidal boundary condition at the southern end of the computational domain was based on water elevation data collected during June 25 to 27, 1982 at the Harbor entrance. From these data, the water elevations (ζ) for the boundary condition were determined to be:

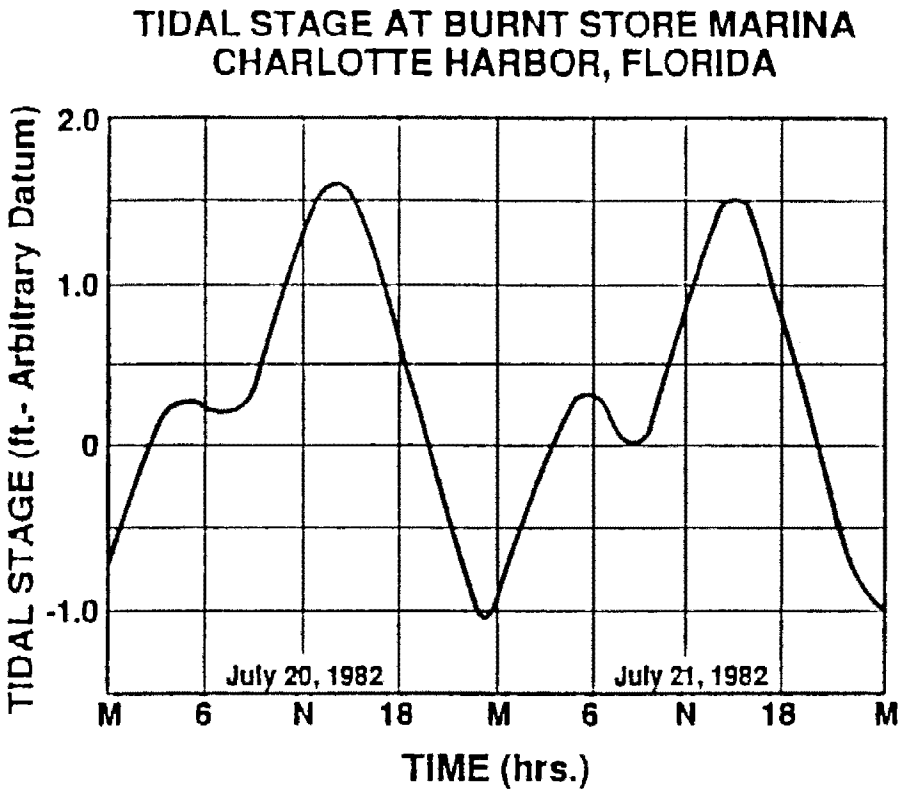

Figure 27. Tidal stage at Burnt Store Marina during July 20 and July 21, 1982.

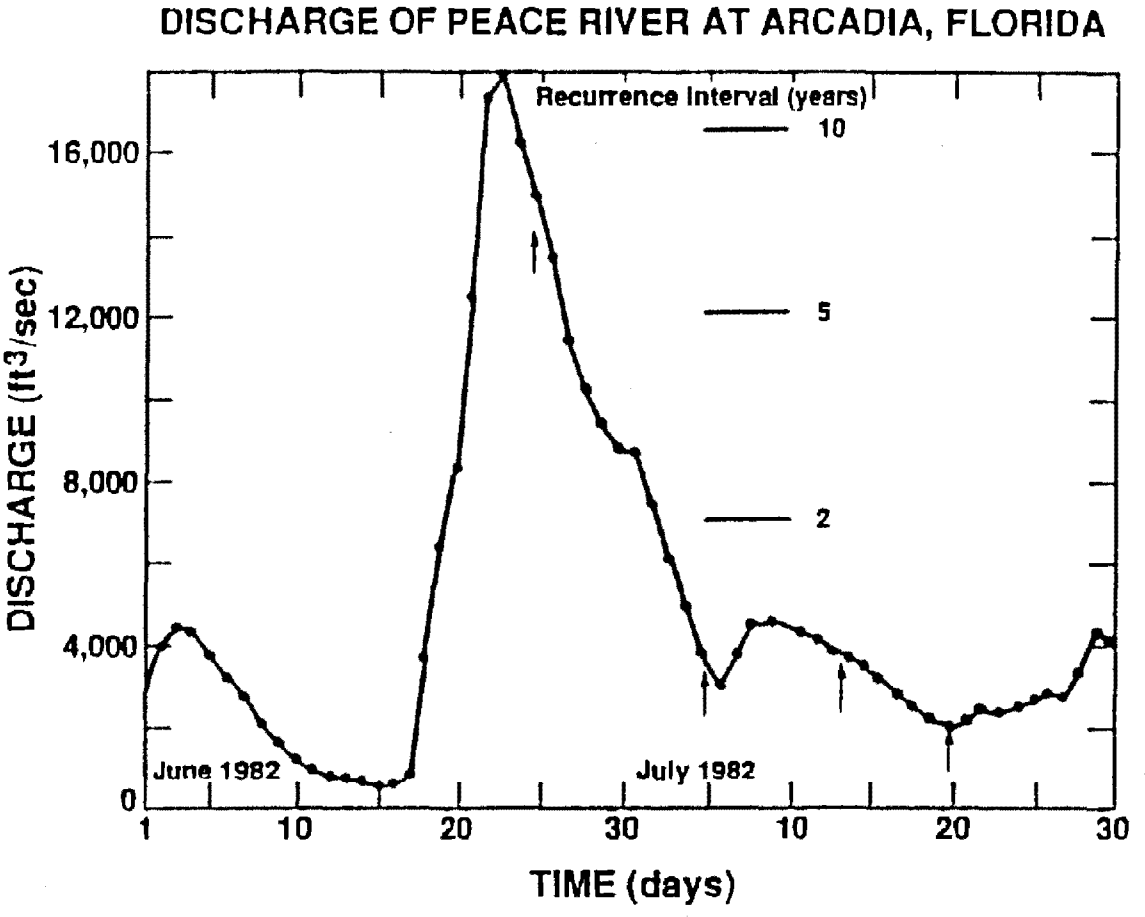

Figure 28. Discharge of Peace River during June 1 to July 30, 1982.

$$\zeta = A \sin (2\pi t/T) + C \quad (62)$$

where A is 33 cm, T is 24 hours, and C is 11 cm.

It was suspected a priori that the inflow from the Peace River should be influenced by tides and stratification. As a result, the boundary condition was selected to modify the boundary velocities accordingly. It was assumed for illustrative purposes that the inflow velocity at the surface was 2.5 times the average velocity known from measurements upstream. The bottom velocity was assumed to be -1.5 times the average velocity, where the negative sign denotes that the bottom waters are assumed to move upstream and out of the domain at the boundary, partially in compensation for the increased surface inflow rates. Inflow rates of freshwater were specified as follows:

- Peace River: 15,000 cfs, and
- Myakka River: 1000 cfs.

The salinity boundary conditions were approximately represented for the southern boundary and assumed to be constant at the Peace River boundary. Salinity along the open southern boundary is computed from the one-dimensional advection equation with a prescribed valued obtained from measurements at station 17 (see Figure 26) located outside the model domain. No tidal variation in salinity was specified for the river inflow and outflows.

Specification of initial conditions involved several steps, including preliminary simulations to set up the final simulations. Initially the simulations were begun with a quiescent flow field (at-rest conditions) and no salinity stratification. A simulation was conducted for 24 hours and this new condition used to establish the initial velocity field for the next series of simulations. The simulated currents after 24 hours are shown in Figure 29. These are idealized presentations that are difficult to interpret, but the strong surface currents from the Peace River are simulated as expected.

The salinity initial conditions for the next series of simulations was obtained by quadratic interpolation from the measurements at seven stations in northern Charlotte Harbor over the 2-day period between June 25 and 27, 1982. These interpolated salinity fields are shown in Figure 30, where bottom salinities of up to 21 ppt were derived in the bottom layer of the southeastern section of the domain. The interpolations indicated that the surface waters were relatively fresh.

The effects of finer grid resolution were explored by switching to a 1/2 km grid line spacing in the lateral and horizontal directions. This led to differences in the model domain and the open boundary condition at the southern end of the Harbor. In testing the finer grid, the domain was extended to station 17 (Figure 26) in the southern part of the Harbor and extended further past station 10 into the Peace River.

A better representation of the southern tidal boundary condition was employed. Two tidal constituents were used to approximate tidal forcing. Vertical salinity profiles were estimated from the data collected at stations

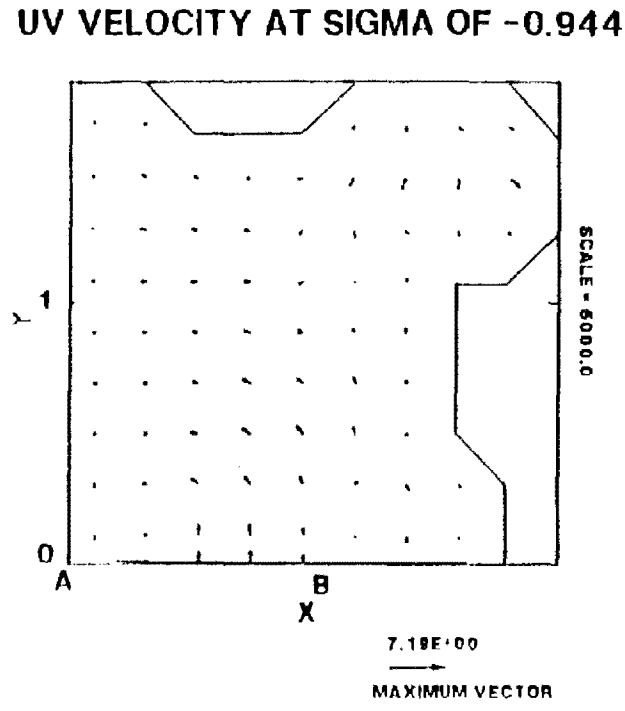

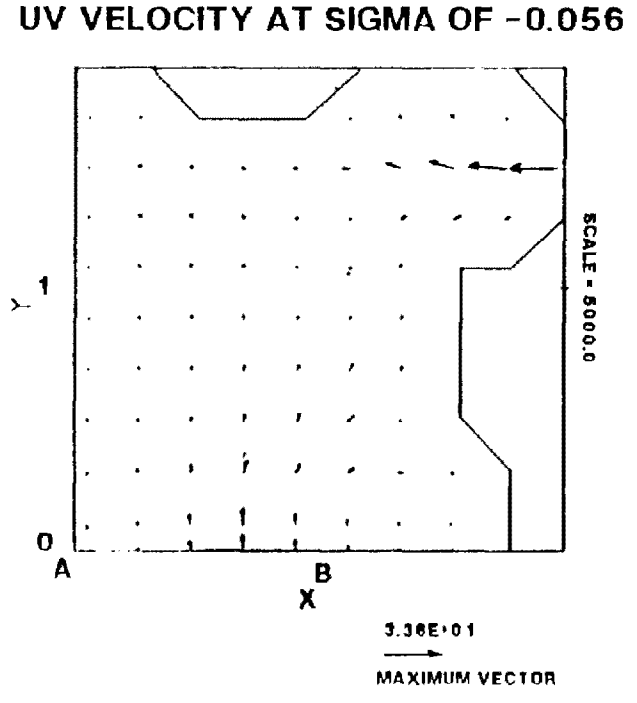

Figure 29. Initial 3-D velocity field in Charlotte Harbor for a model simulation from June 25 to June 27, 1982.

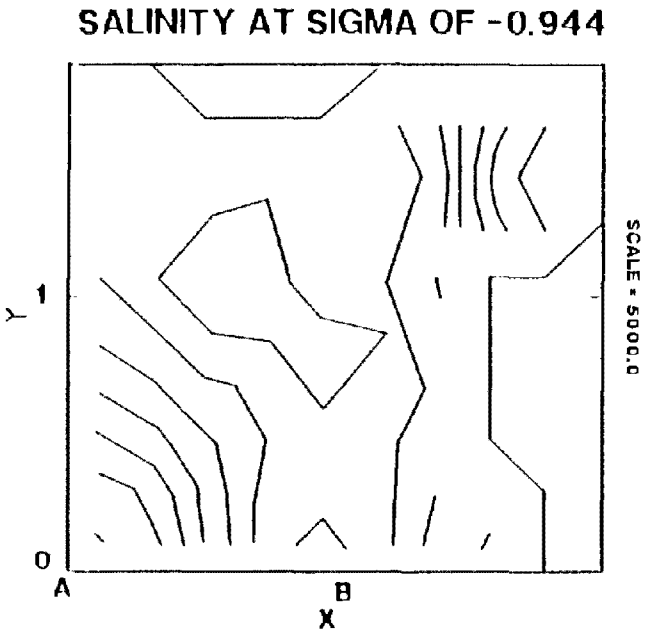

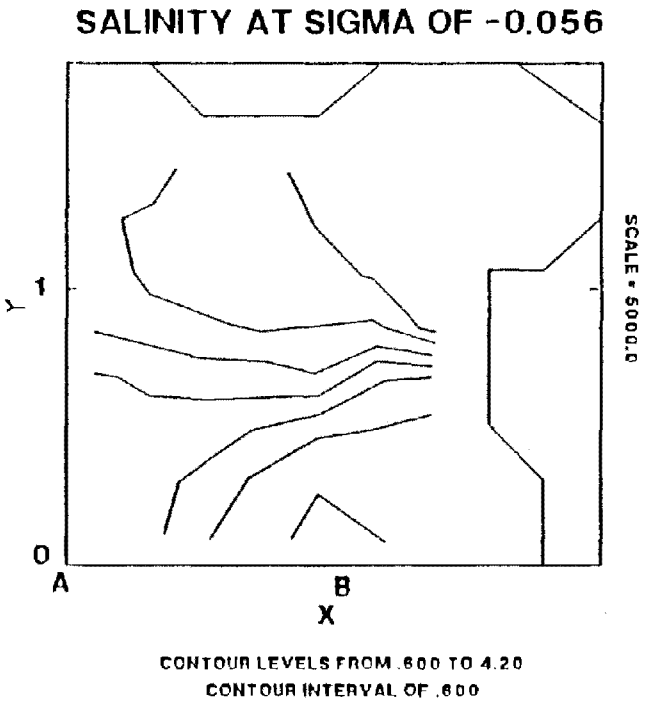

Figure 30. Initial salinity field in Charlotte Harbor for June 25, 1982.

Vertical salinity profiles were estimated from the data collected at stations 15, 19, 20, and 17 and employed in the simulations. Consequently, stratification is weaker along the southern boundary in the fine grid simulation. Initial conditions were selected in the same manner as for the coarser grid.

4.3.4 Results

A series of records for velocity and salinity distributions were produced during the model simulation of 72 hours. Surface and bottom, velocity and salinity distributions are presented in Figures 31 through 34 for stations 10, 7, 22, and 19. From these results there are several observations worth noting. First, a dynamic steady state was obtained. Second, the Peace River flow is a dominate influence. The relatively strong currents at stations 10, 7, and 22, and the initial reduction in the high salinities at the bottom locations of stations 7 and 22, are related to the freshwater inflow.

The velocity and salinity fields are shown in Figures 35 and 36, respectively. In these illustrations, the surface currents are distinctly different from the bottom currents and significant stratification exists, as would be expected in a partially mixed estuary. Conditions are similar at the end of the 72-hour simulation period as shown in Figures 37 and 38. Dimensionless depth profiles of salinity shown in Figure 39 illustrate the stratification simulated by the model. These results are for stations 7, 22, 15, and 19 at the end of the 72-hour simulation.

The 48-hour simulations were performed after the initial 24-hour simulation, using the finer grid and the boundary conditions described above. These results were not interpreted (Sheng et al. 1986), but are presented for the reader to investigate here. The resulting circulation pattern at the end of the 48-hour simulation is shown by the surface and bottom currents in Figure 40. The salinity distributions at the same time are shown in Figure 41. The time variations of surface elevation, surface currents, bottom current, surface salinity, and bottom salinity at a number of stations are shown in Figures 42 through 45.

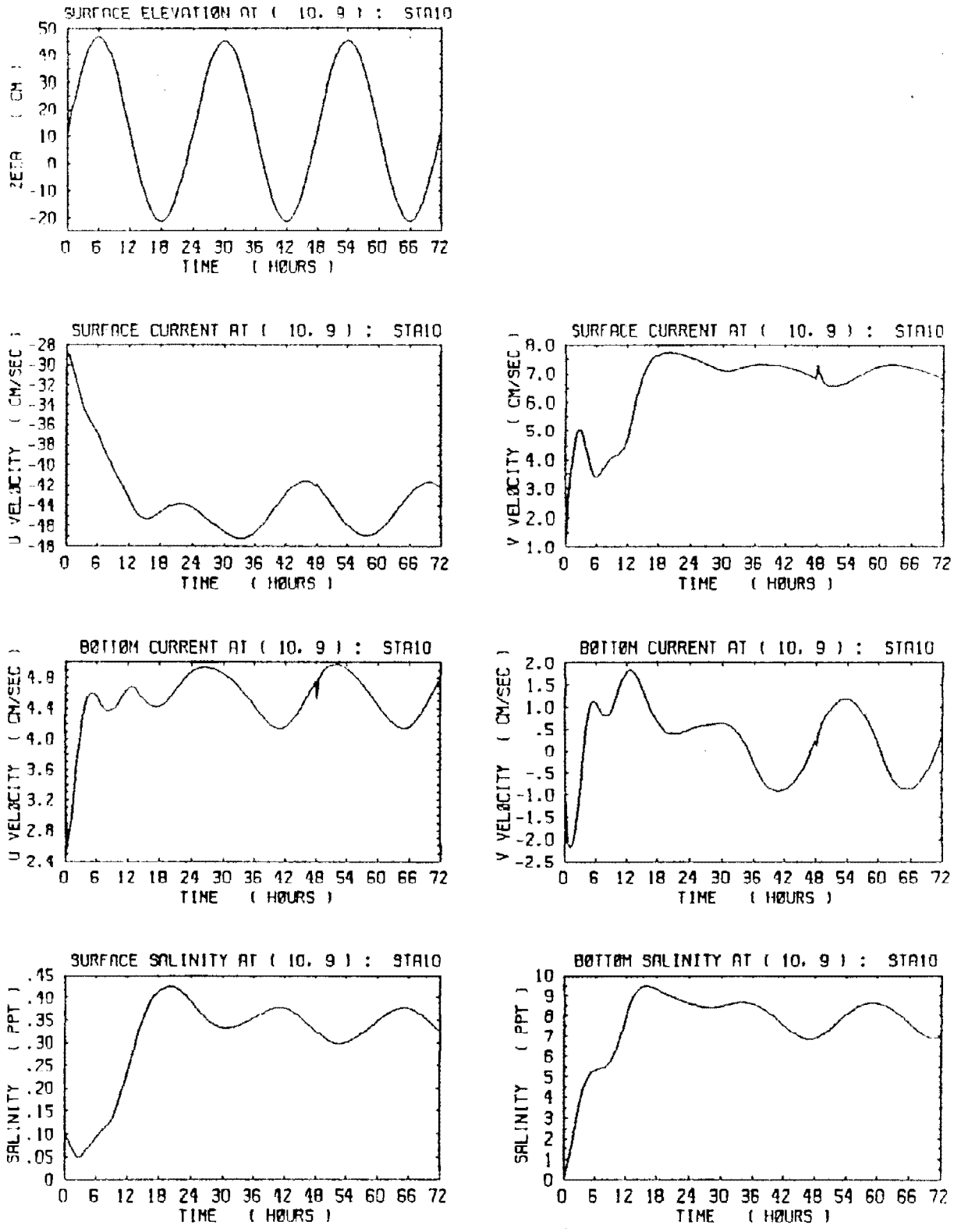

Figure 31. Time Histories of water level, surface currents, bottom currents, surface salinity and bottom salinity at Station 10 during the 3-day model simulation period.

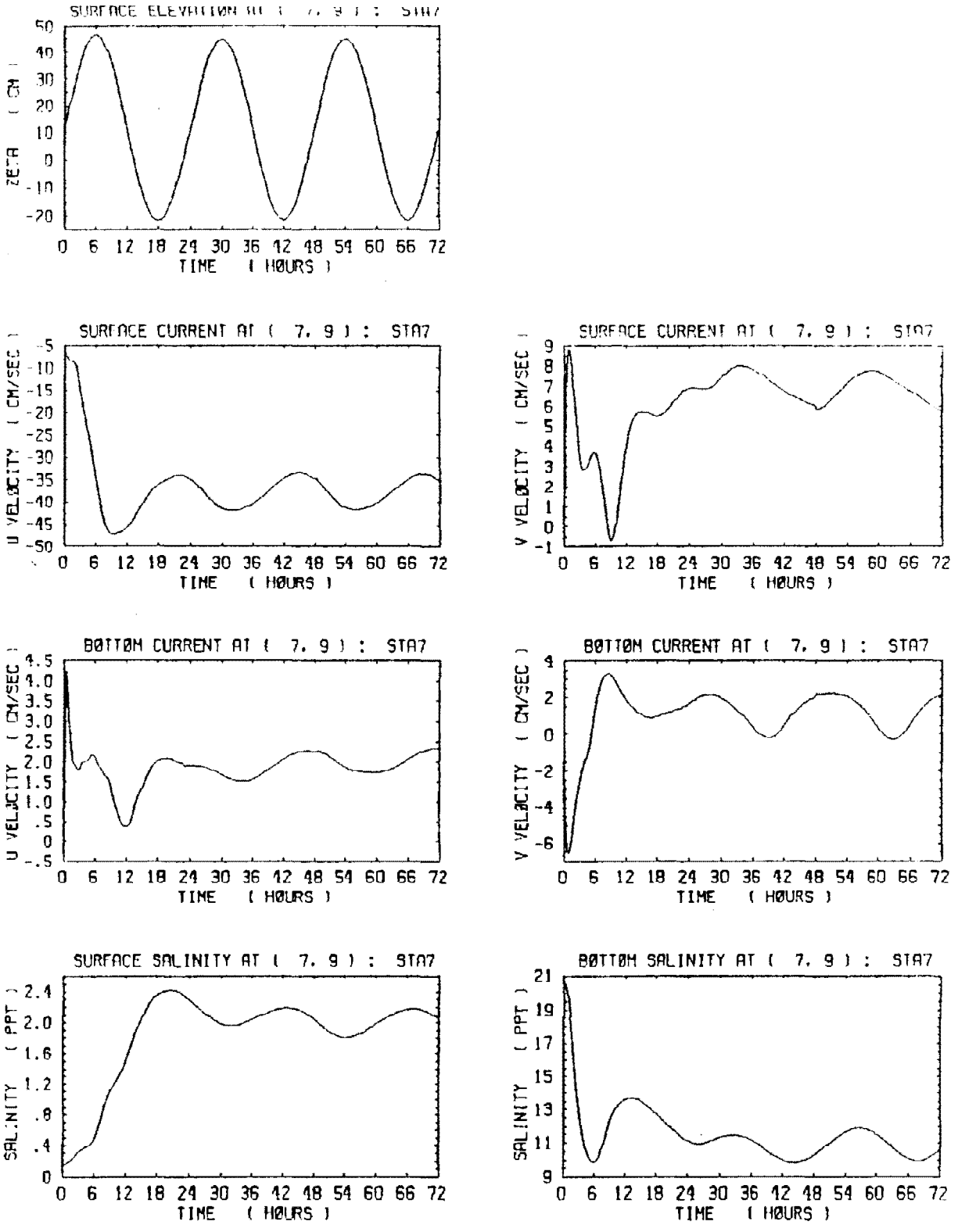

Figure 32. Time histories of water level, surface currents, bottom currents, surface salinity and bottom salinity at Staion 7 during the 3-day model simulation period.

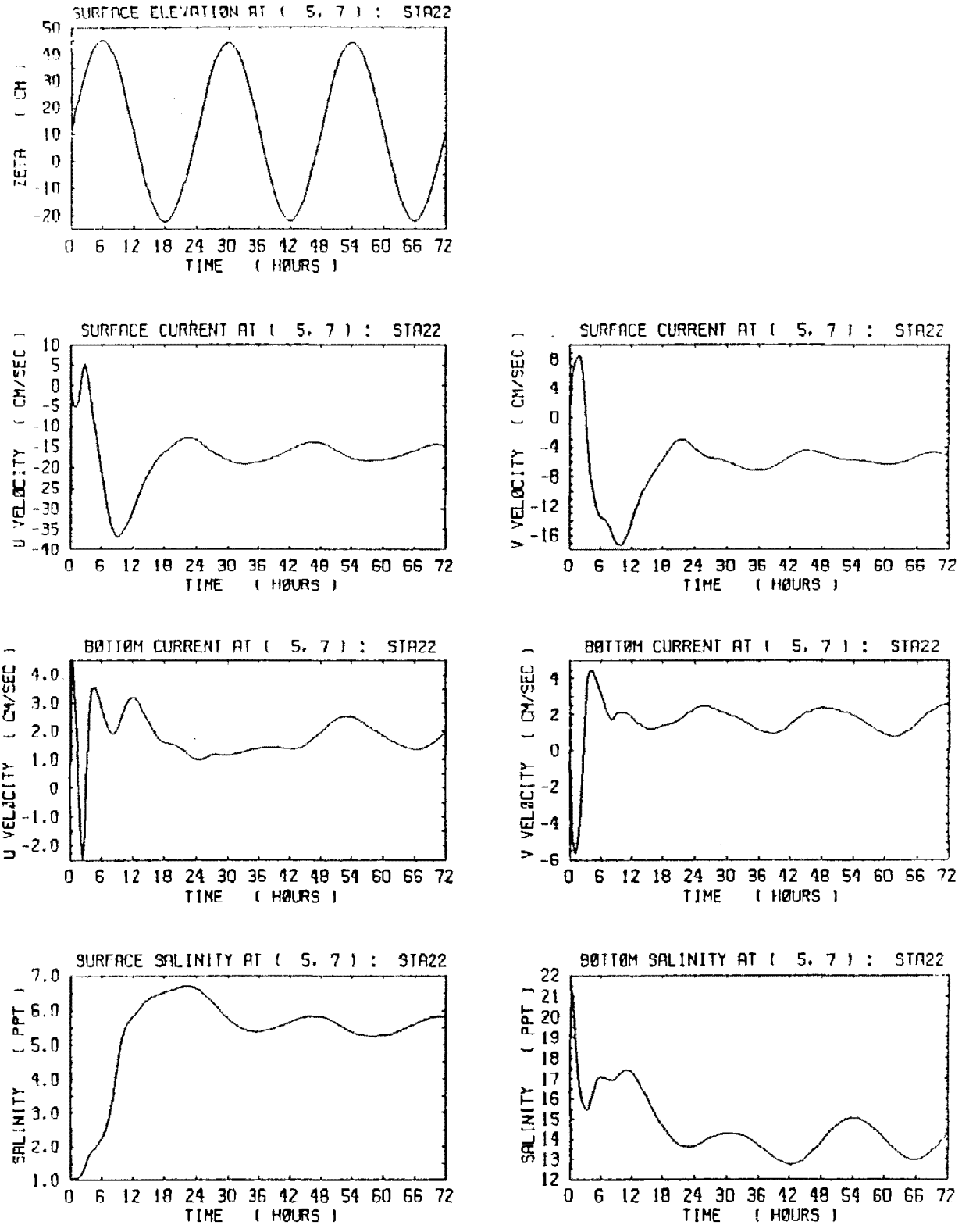

Figure 33. Time histories of water level, surface currents, bottom currents, surface salinity and bottom salinity at Station 22 during the 3-day model simulation period.

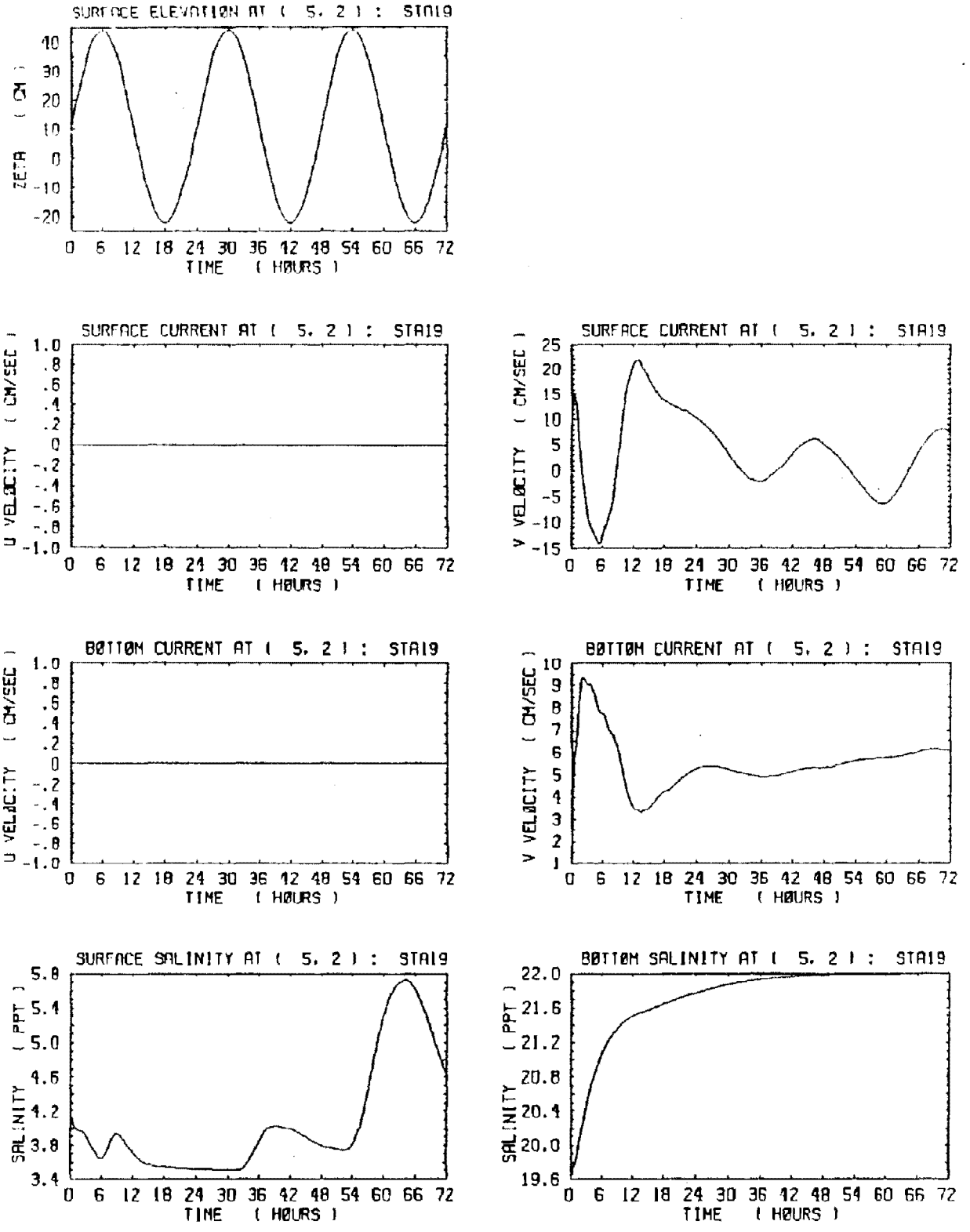

Figure 34. Time histories of water level, surface currents, bottom currents, surface salinity and bottom salinity at Station 19 during the 3-day model simulation period.

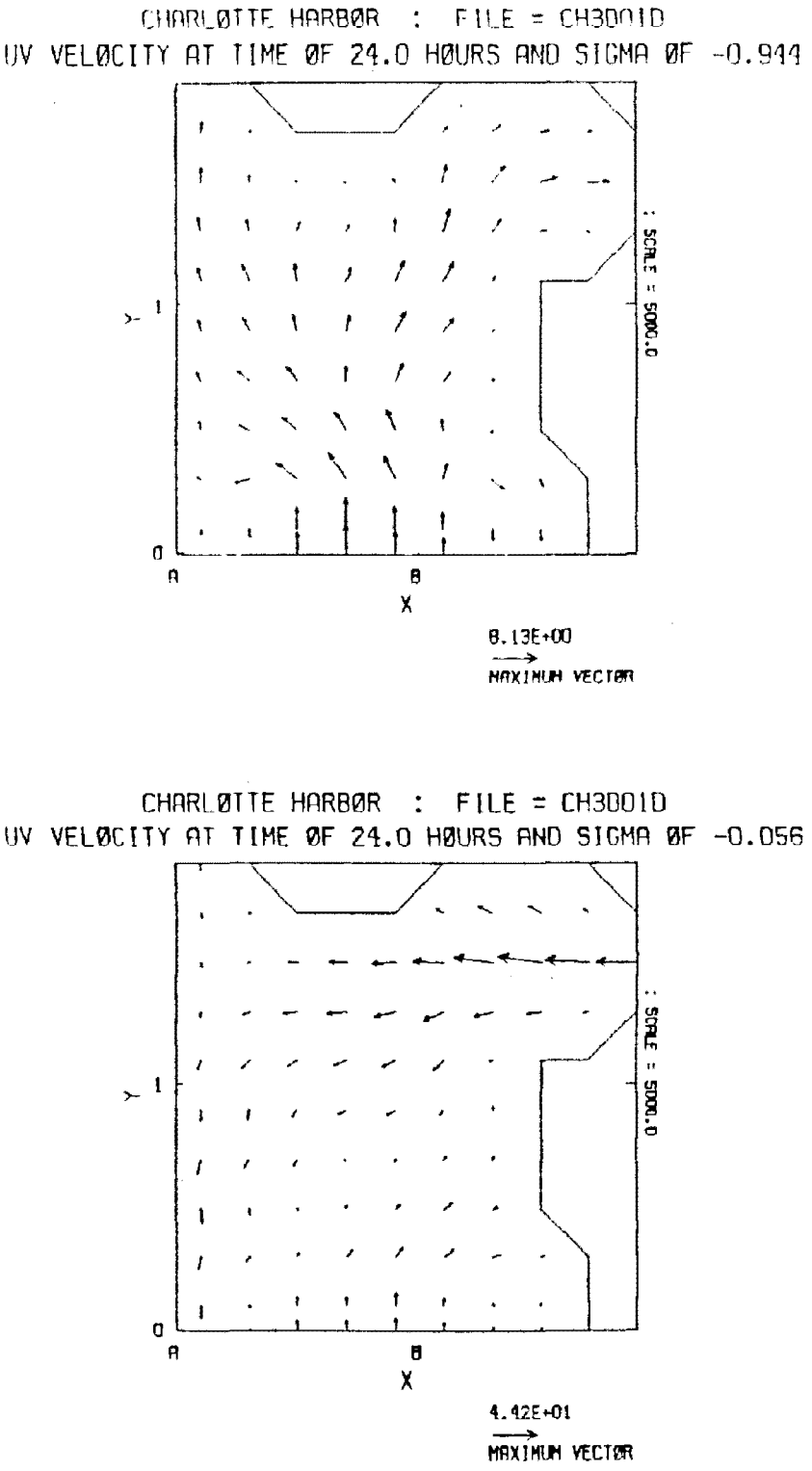

Figure 35. Computed 3-D velocity field in Charlotte Harbor after 24 hours of simulation.

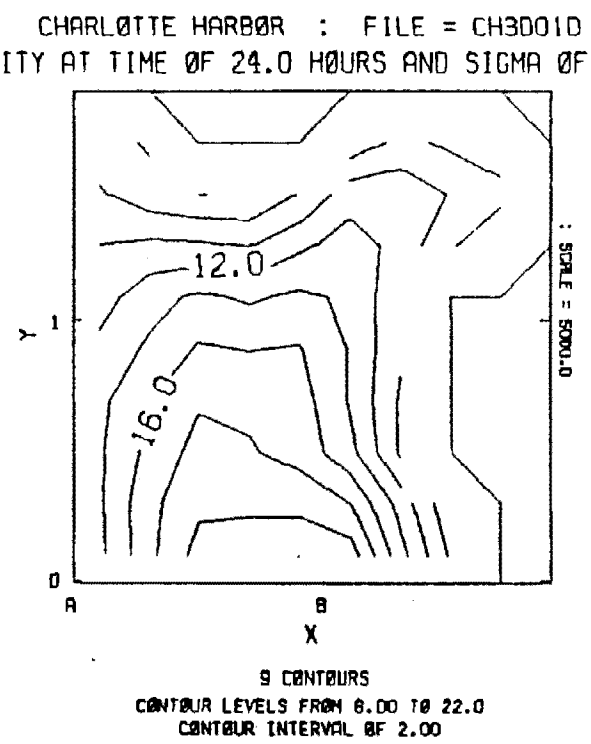

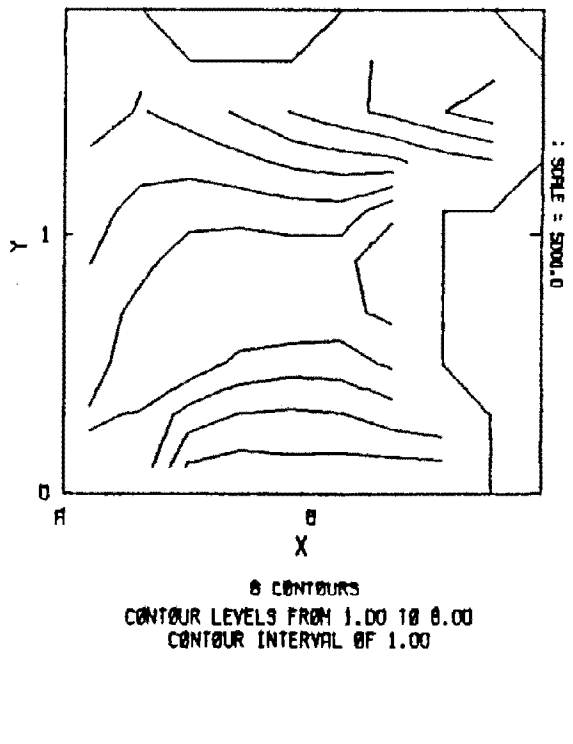

Figure 36. Computed salinity field in Charlotte Harbor after 24 hours of simulation.

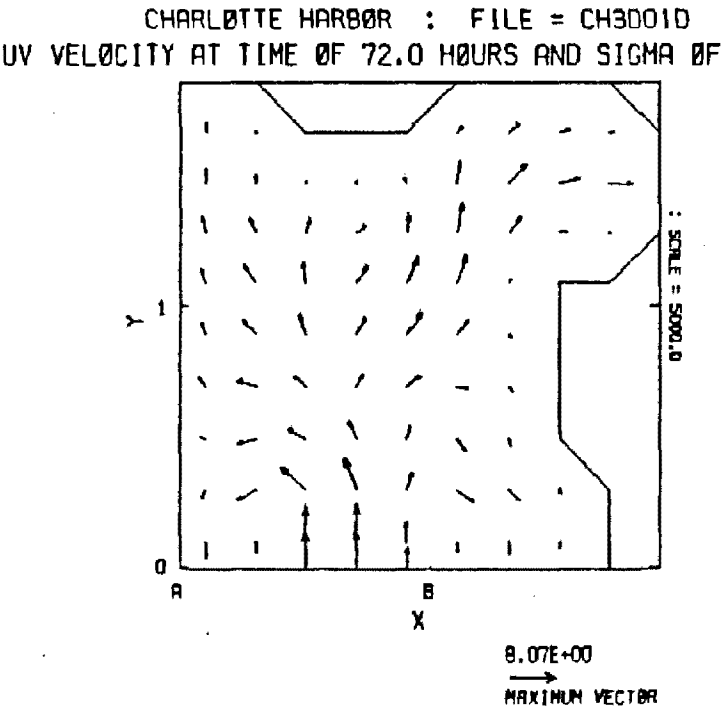

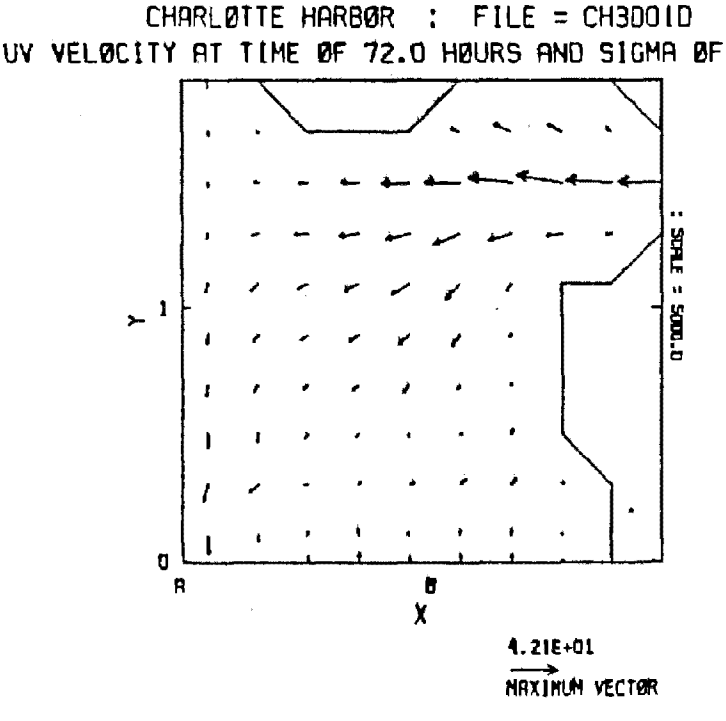

Figure 37. Computed 3-D velocity field in Charlotte Harbor after 72 hours of simulation.

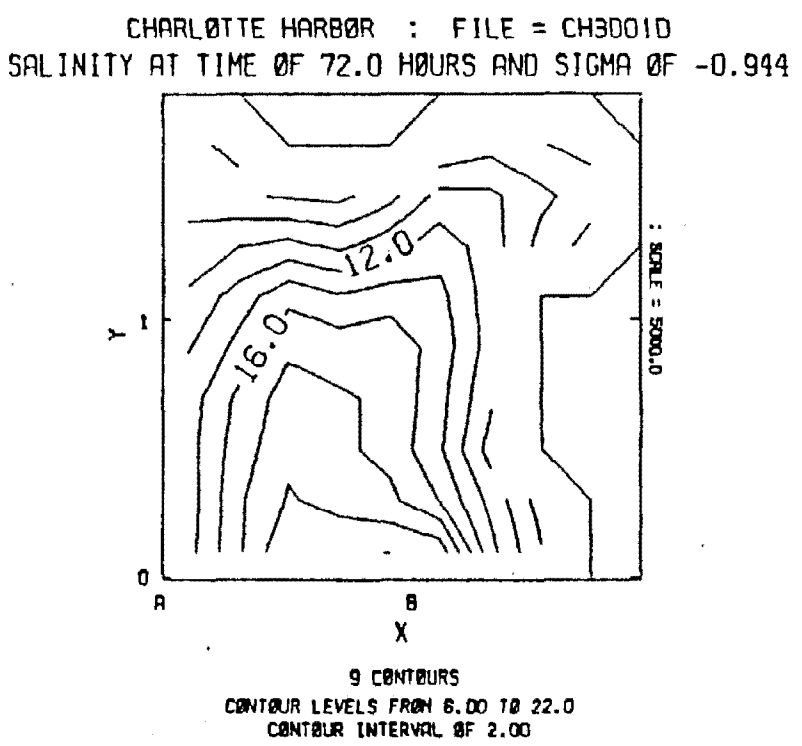

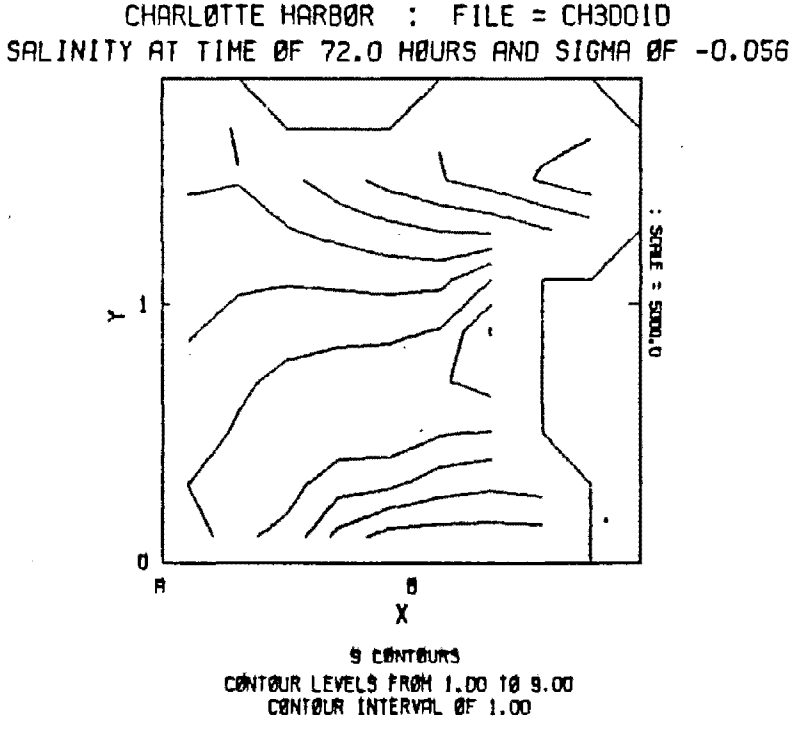

Figure 38. Computed salinity field in Charlotte Harbor after 72 hours of simulation.

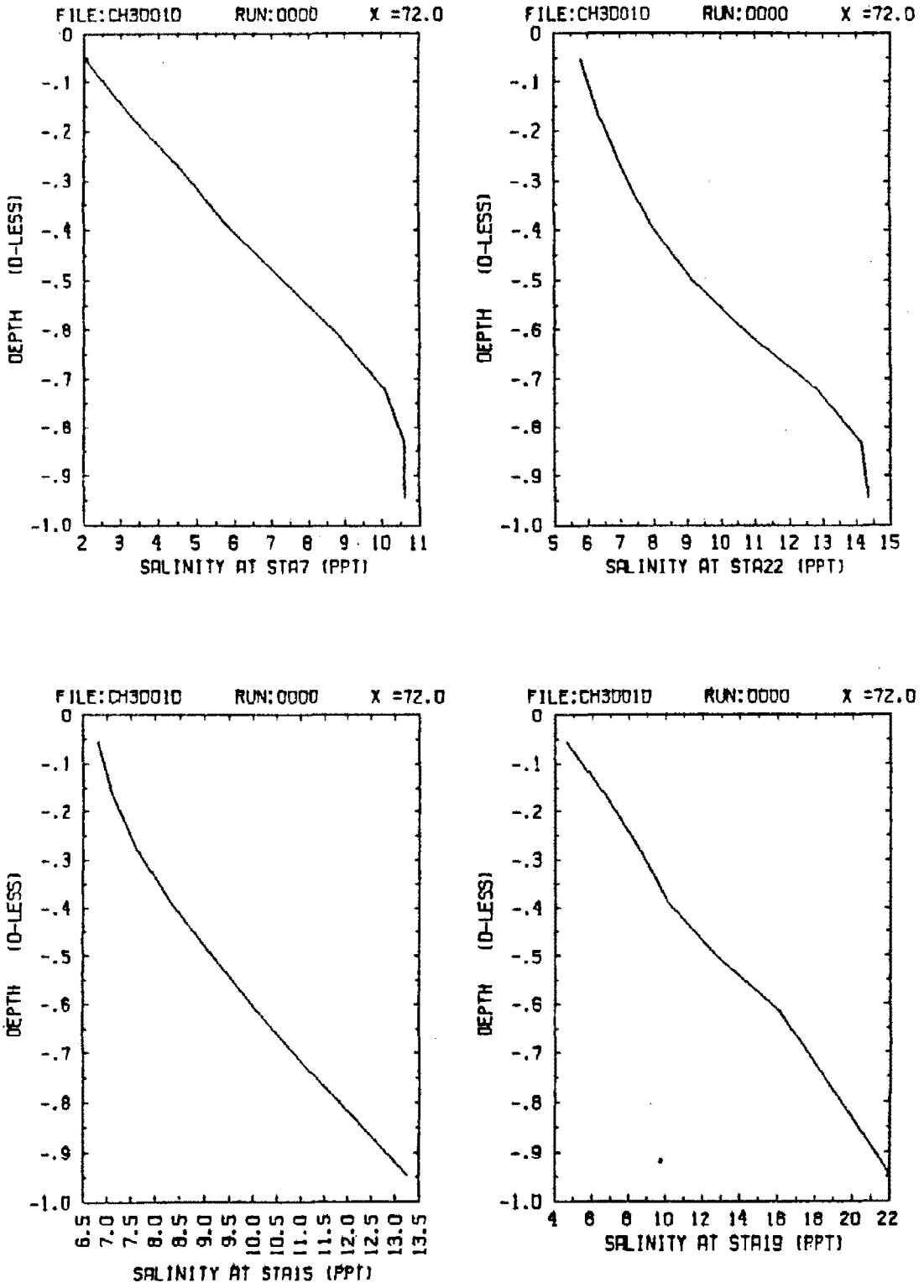

Figure 39. Vertical salinity profiles at Stations 7, 22, 15 and 19 in Charlotte Harbor after 72 hours.

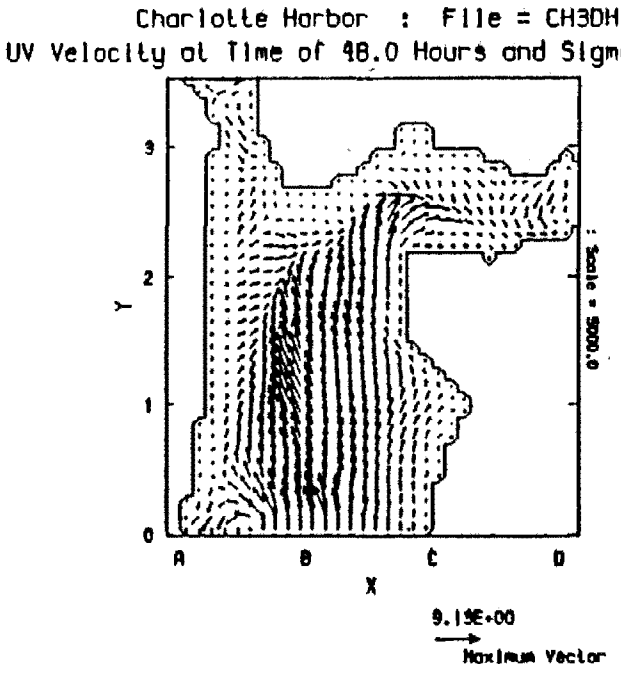

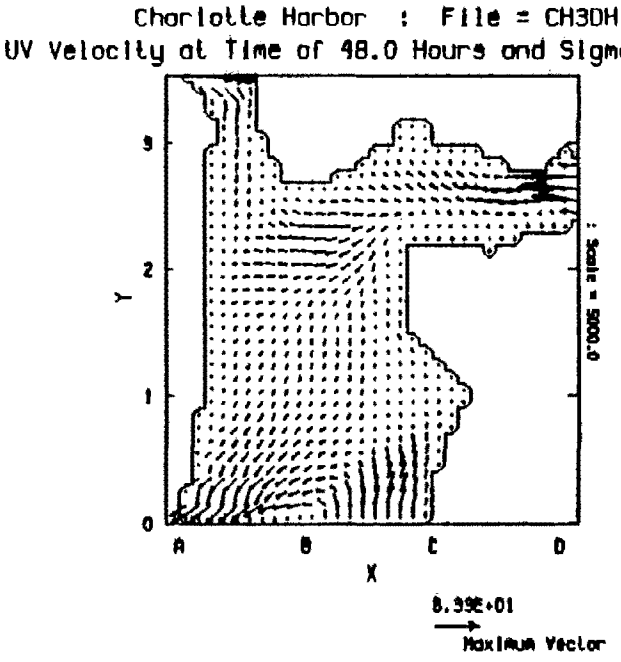

Figure 40. Computed 3-D velocity field in Charlotte Harbor after 48 hours of simulation with a 1/2-km grid.

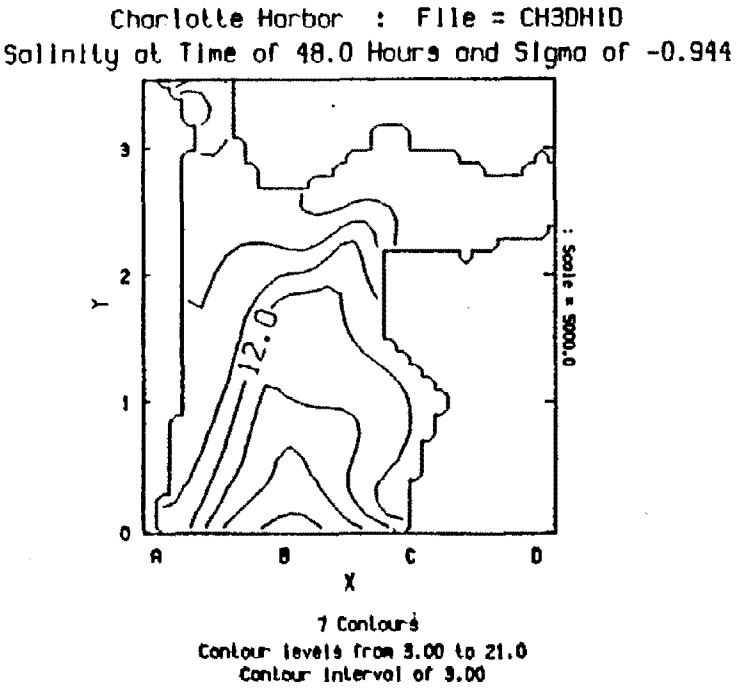

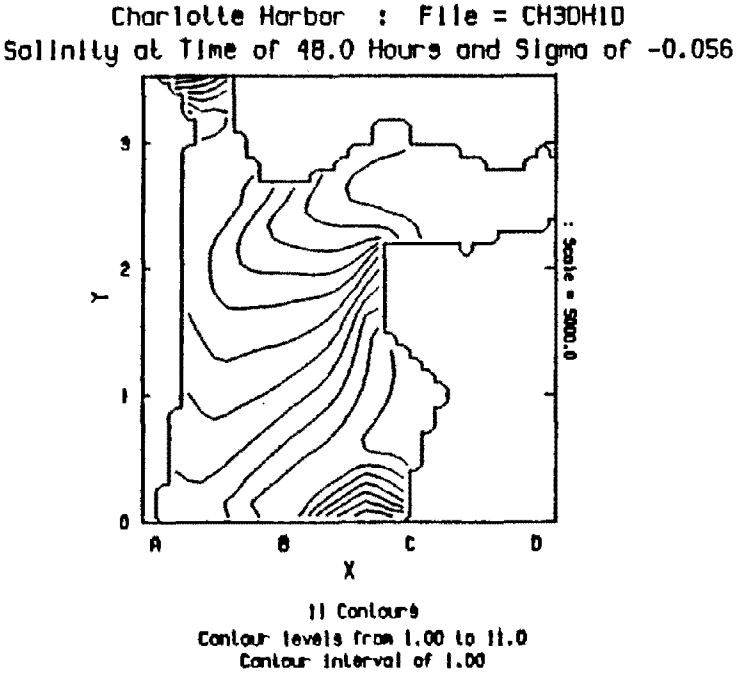

Figure 41. Computed salinity field in Charlotte Harbor after 48 hours of simulation with a 1/2-km grid.

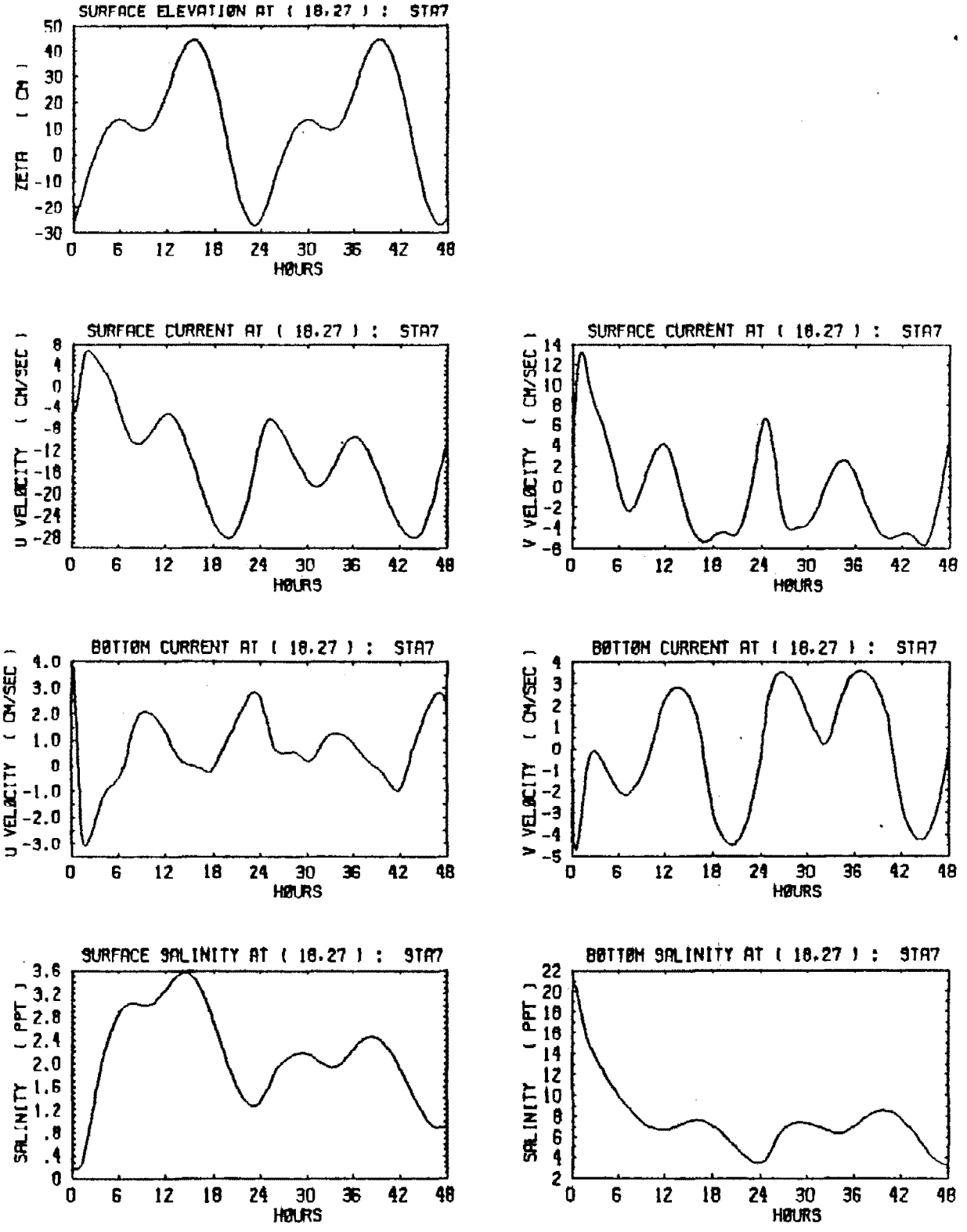

Figure 42. Simulated time histories of water level, surface currents, bottom currents, surface salinity and bottom salinity at Station 7 during the 2-day simulation period.

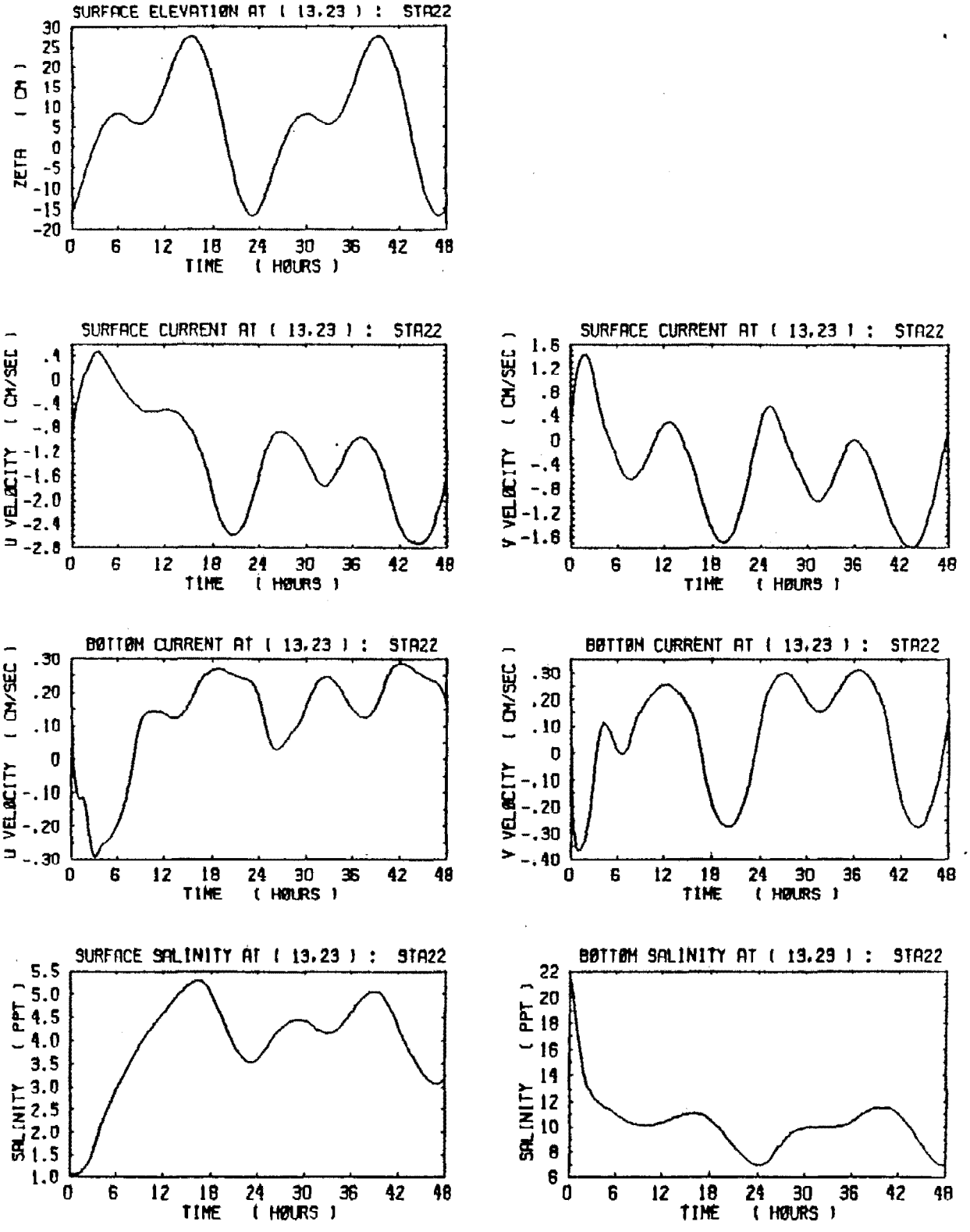

Figure 43. Simulated time histories of water level, surface currents, bottom currents, surface salinity and bottom salinity at Station 22 during the 2-day period.

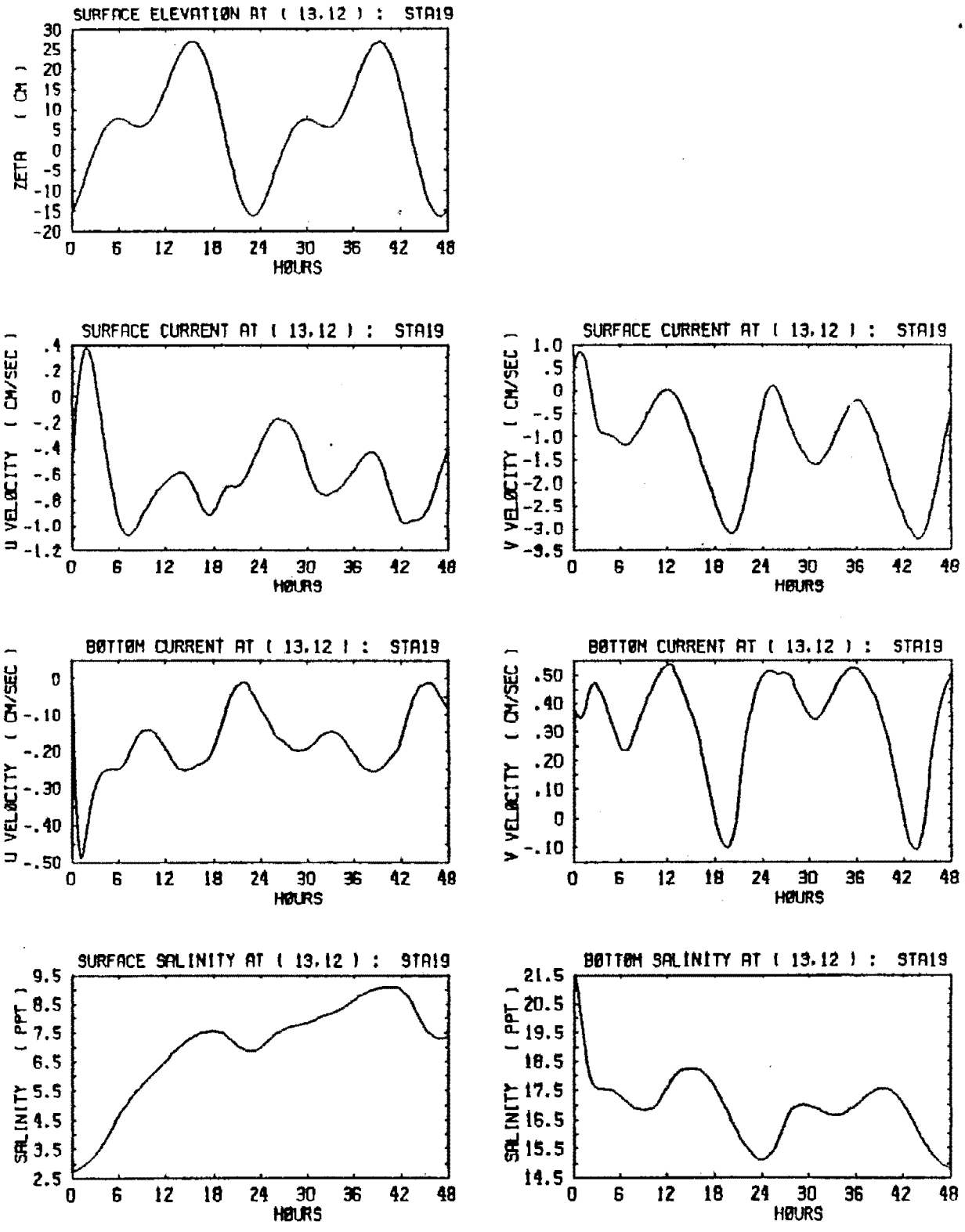

Figure 44. Simulated time histories of water level, surface currents, bottom currents, surface salinity and bottom salinity at Station 19 during the 2-day model simulation period

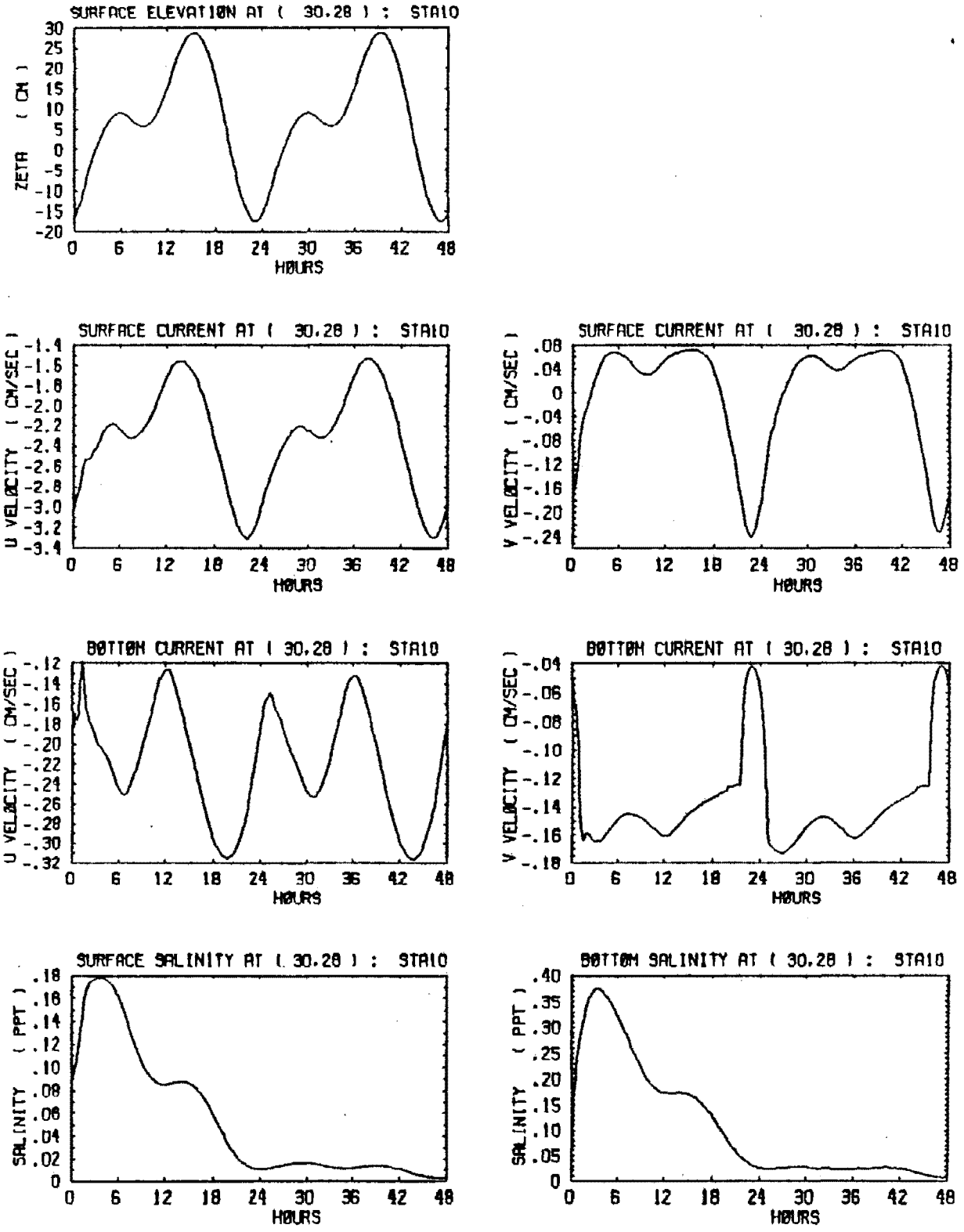

Figure 45. Simulated time histories of water level, surface currents, bottom currents, surface salinity and bottom salinity at Station 10 during the 2-day model simulation period.

4.4 GREEN BAY, LAKE MICHIGAN

In this case study HYDRO3D is applied as a part of a comprehensive study of the effects of PCB's in Green Bay sediments. Historically, the Fox River in Wisconsin has contributed a significant amount of PCB,s to the environment and it is suspected that much of this contaminant has migrated into Green Bay. The Fox River has one of the largest concentrations of pulp and paper mills in the world, from which PCB's are suspected to have been discharged. Most of the fisheries are presently closed because of the PCB levels in fish.

The study involves a preliminary calibration of the hydrodynamics model and a sediment model with the historic data available. Following the preliminary calibration, both hydrodynamics and sediment transport models will be calibrated with data being processed from the 1989 field season. If the study is fully successful, it will involve the linkage of hydrodynamics, sediment transport, and large scale water-quality models of the box type (Ambrose et al. 1987). Presently, large scale box modeling suffers from an inability to simulate and predict the effects of complex stratified flows on transport. An important test will be calibrating the model with historic data and checking the calibrated parameters with data collected in the summer of 1989 to see if the simulations are predictively valid.

In this case study, results from the preliminary calibration are reported to illustrate the use of the model in a large lake setting with complex wind driven circulation. The dynamic nature of Green Bay (Miller and Saylor, 1985) indicates the need for unsteady state two- and three-dimensional simulations. HYDRO3D, which is capable of treating stratification and lake-bay interactions, is used to model the flow and transport processes in the Bay. In this case study the model is applied to simulate 2-D and 3-D circulation patterns and these results are found to be similar to general and specific observations of the Bay.

4.4.1 Physical Setting

Green Bay is a long and relatively shallow water body in northern Lake Michigan. The Bay is separated from Lake Michigan by the Door Peninsula and connected to the lake by four main channels near its northern end. These channels are Martin Island Passage, Rock Island Passage, Porte des Morts Passage, and Poverty Island Passage (see Figure 46). The Bay is approximately 40 km wide and 190 km long and its main axis is oriented from the north by 38 degrees to the east. More than a dozen streams drain the area around and in the vicinity, and discharge into the Bay. Major tributaries that contribute water and sediment to the Bay include the Fox, Oconto, Peshtigo, Menominee, and Escanaba rivers. The upper part of Green Bay is generally deeper than 20 m, with a maximum depth of 48 m west of Washington Island. The lower half of the Bay, south of Chambers Island, is 30 m deep near the island, but very shallow (few meters deep) at the southern end (see Figure 47). Several small islands exist in the Bay. However for these simulations, only the effects of Chambers Island will be simulated. Chambers Island has an area of 12 km^2 and is located midway between the mouth of the Bay and Green Bay city.

The flow and circulation are controlled by wind, Lake Michigan water

levels (also wind dominated), and river inflows. As the historic data to be presented in the following sections indicate, seiche is an important phenomenon in the Bay. In addition, winds significantly control local circulation. There is a counterclockwise gyre northeast and a clockwise gyre southwest of Chambers Island in Green Bay that typically describe the general circulation patterns. These general trends must be simulated for the hydrodynamics model to achieve general usefulness in this study.

4.4.2 Two-Dimensional Simulation of Flow

The HYDRO3D model is tested in the 2-D mode using historical data from Green Bay given by Heaps et al. (1982). The main objective of these tests are to show the response of the Bay to wind forcing and Lake Michigan water level changes. The limited data available for a 2-D simulation consist of:

a) Water level observations at the mouth of the Bay (St. Martin Island, and Plum Island) and at two other stations: Menominee and Green Bay cities.

b) Hourly wind observations at the airport in Green Bay city. No current data are available due to the malfunction of current meters.

These data are used to specify the boundary conditions at the passages into Lake Michigan and the wind shear on the Bay. The simulations of water movements in the Bay are performed for two periods when data were collected. These periods are September 17-20 and October 8-12, 1969. The simulation for each period was started from the at-rest condition to define the initial velocity field for the simulations.

Hourly wind data taken at the airport (a short distance from the south end of the Bay), are used to calculate the time-varying wind stresses acting over the entire water surface of the Bay. Winds were variable during the two simulation periods. During the September period, the wind directions were mostly northward for the first day of simulation (September 17), northeasterly during September 18, easterly during September 19, and southwesterly during September 20. The maximum wind speed during this period was about 8.5 m/sec and occurred on September 8. Wind speeds during the October period were stronger than those for the September period. The maximum wind speed during the October period was about 12 m/sec and occurred on October 9. The wind directions during this period were westerly during October 8, southerly during October 9, southwesterly during October 10, northerly during October 11, and northeasterly during October 12.

Two dimensional simulations of water surface elevations and depth-averaged velocities are performed on a 2 km x 2 km horizontal grid network. This network has a total of 21 x 96 grid cells, as shown in Figure 48.

The water surface elevation data measured at the mouth of the Bay and near Green Bay city for the September and October periods are given in Figures 49 and 50, respectively. These data are used as input for the model. As shown, the variation of the water surface at the mouth ranges from 5 to 10 cm for each period of the data set. The major force that distinguished the October results from the September results is the wind force. The wind direction also plays a major role on the general circulation in the Bay. Figures 51 and 52 show these

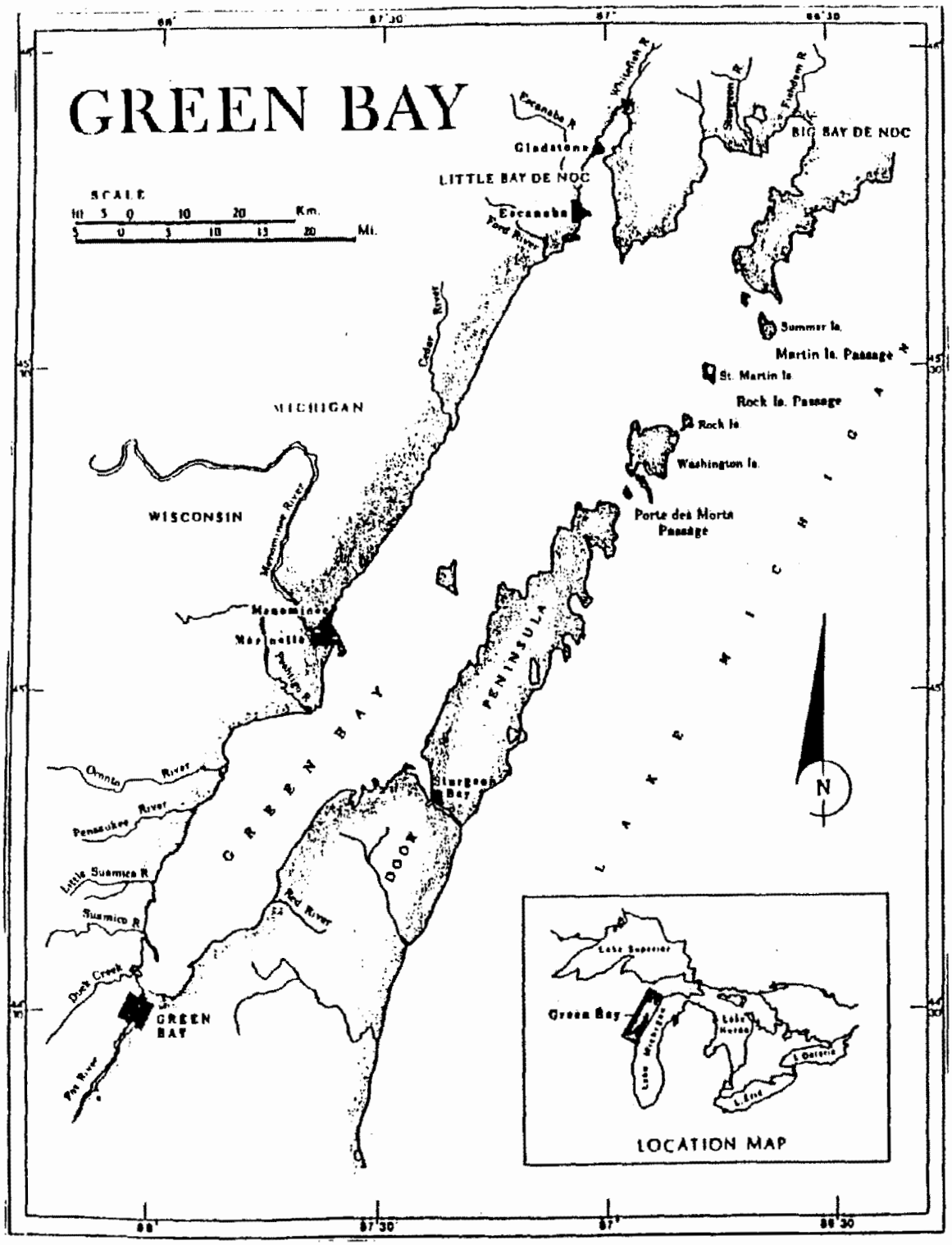

Figure 46. Map of Green Bay showing relation to Lake Michigan and other Great Lakes

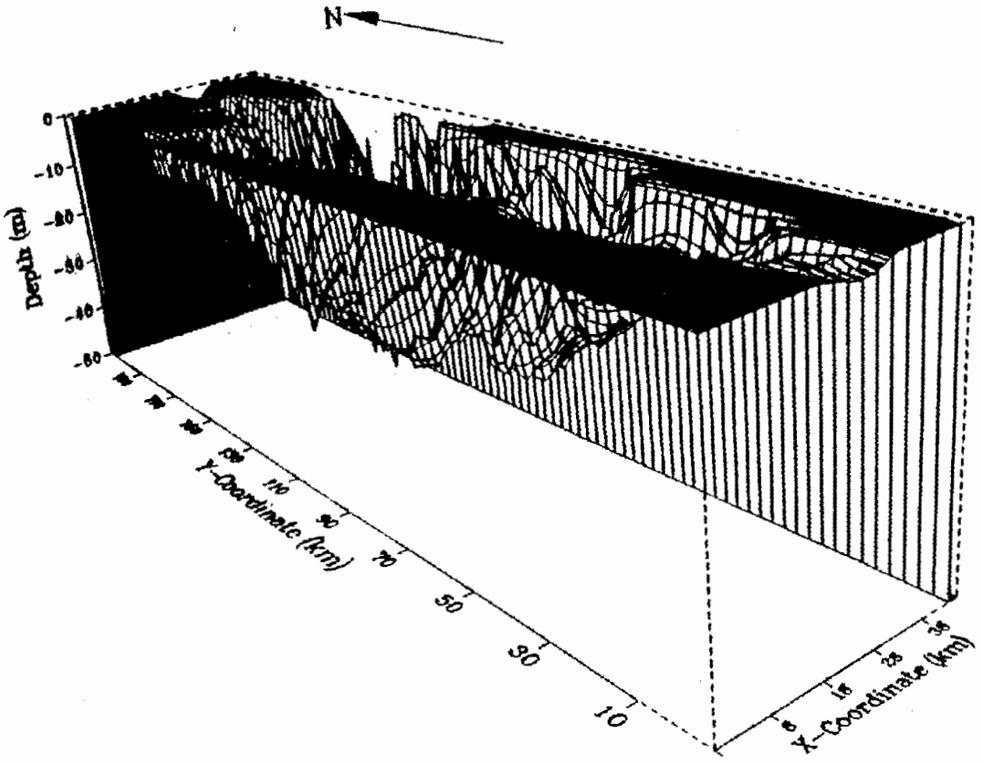

Figure 47. Three-dimensional plot of Green Bay bathymetry

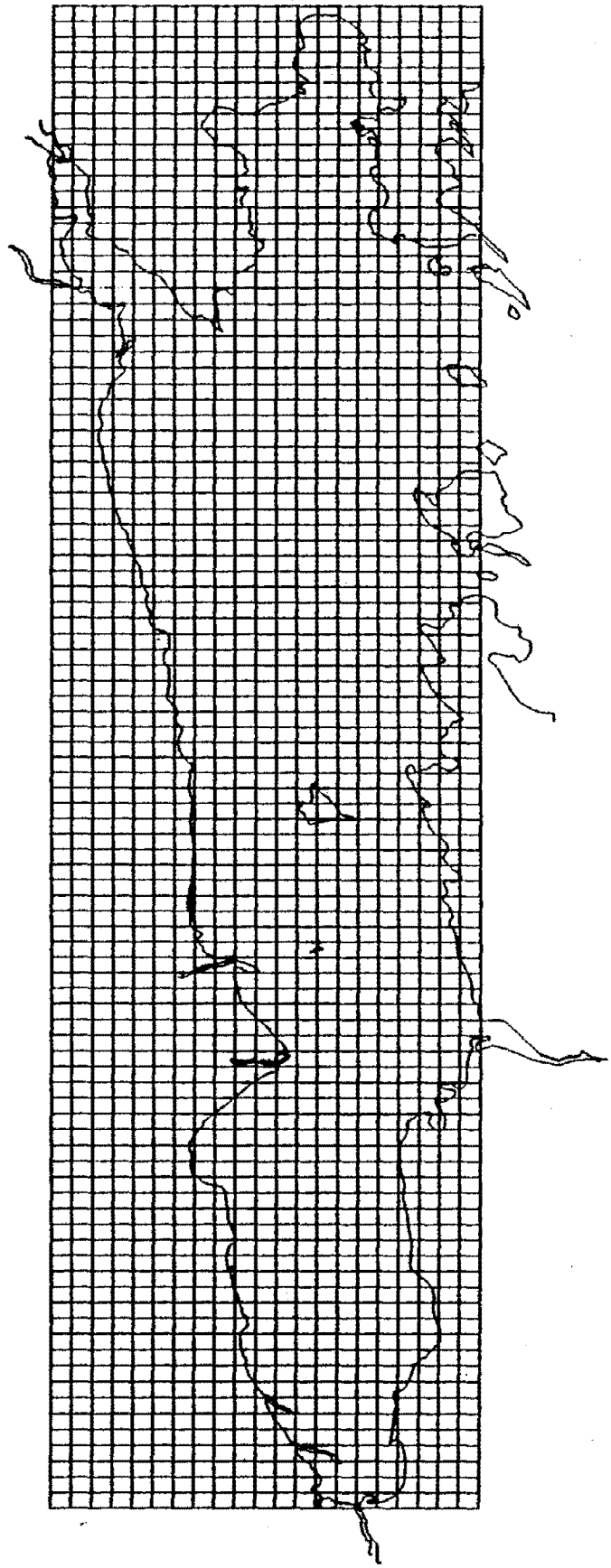

Figure 48. Grid network of Green Bay

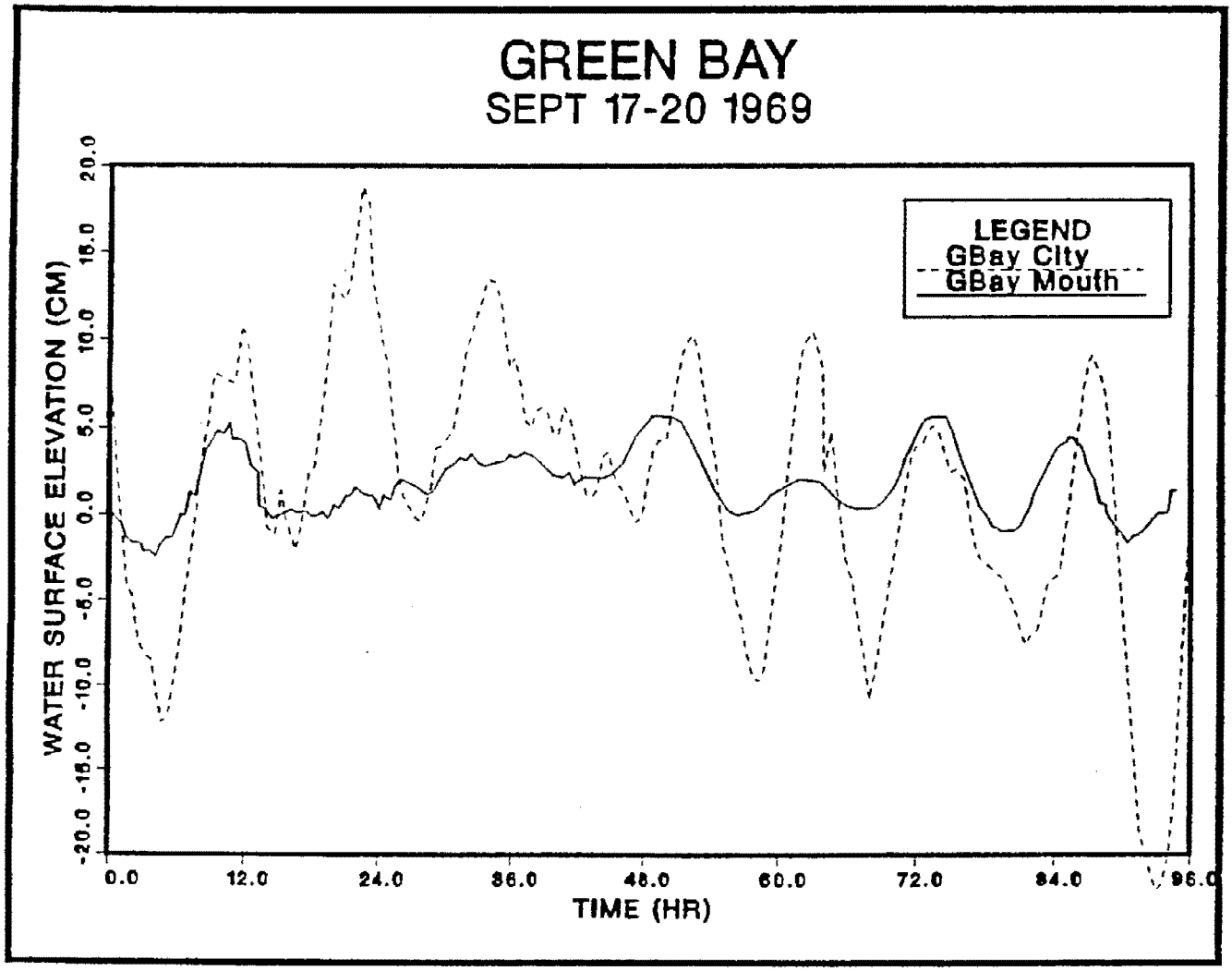

Figure 49 . Measured water surface elevation at the mouth of Fox River near Green Bay city during September, 1969

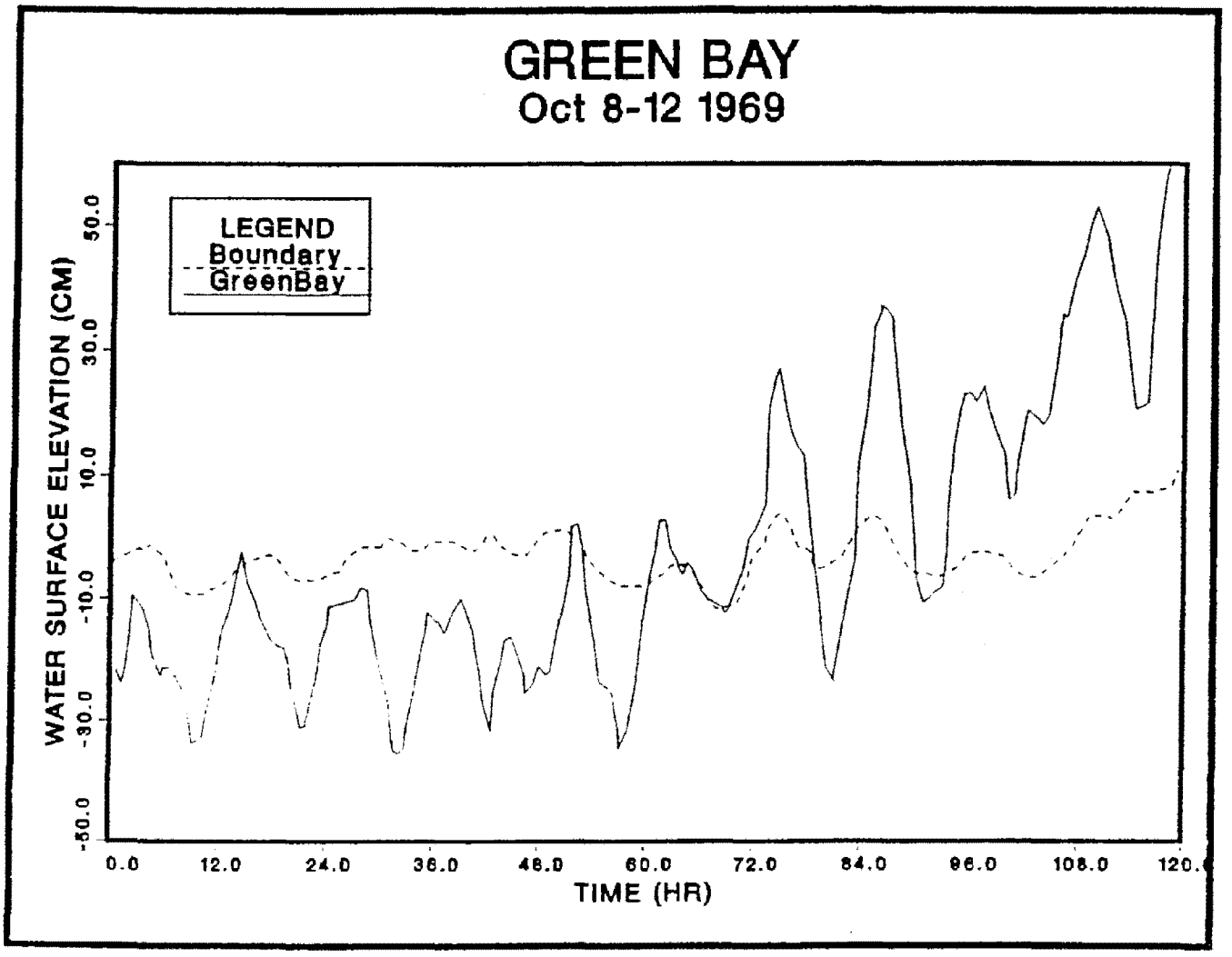

Figure 50. Measured water surface elevation at the mouth of Green Bay and at Green Bay city during October, 1969

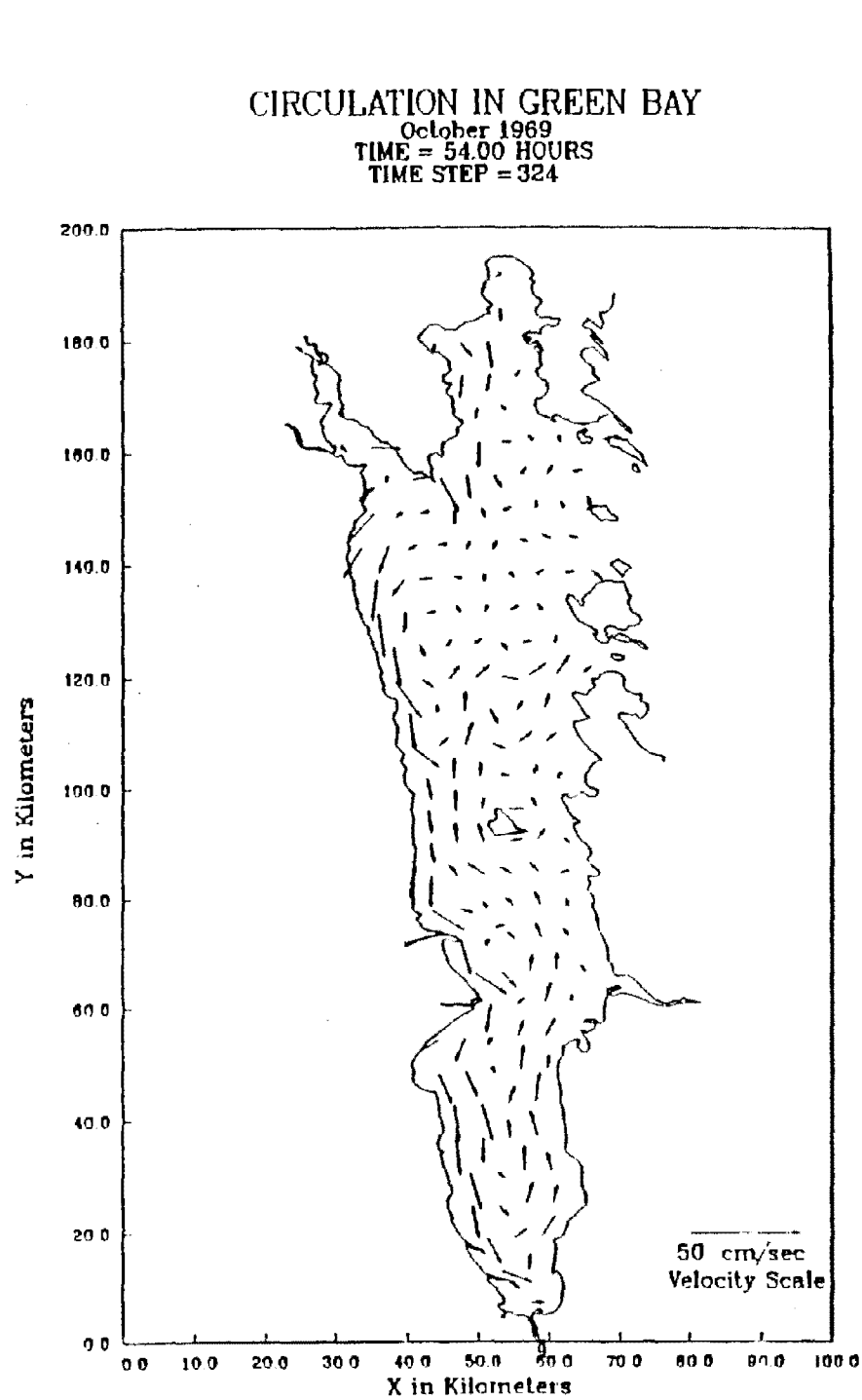

Figure 51. Simulated circulation in Green Bay using October 1969 data (54 hours from at the at-rest)

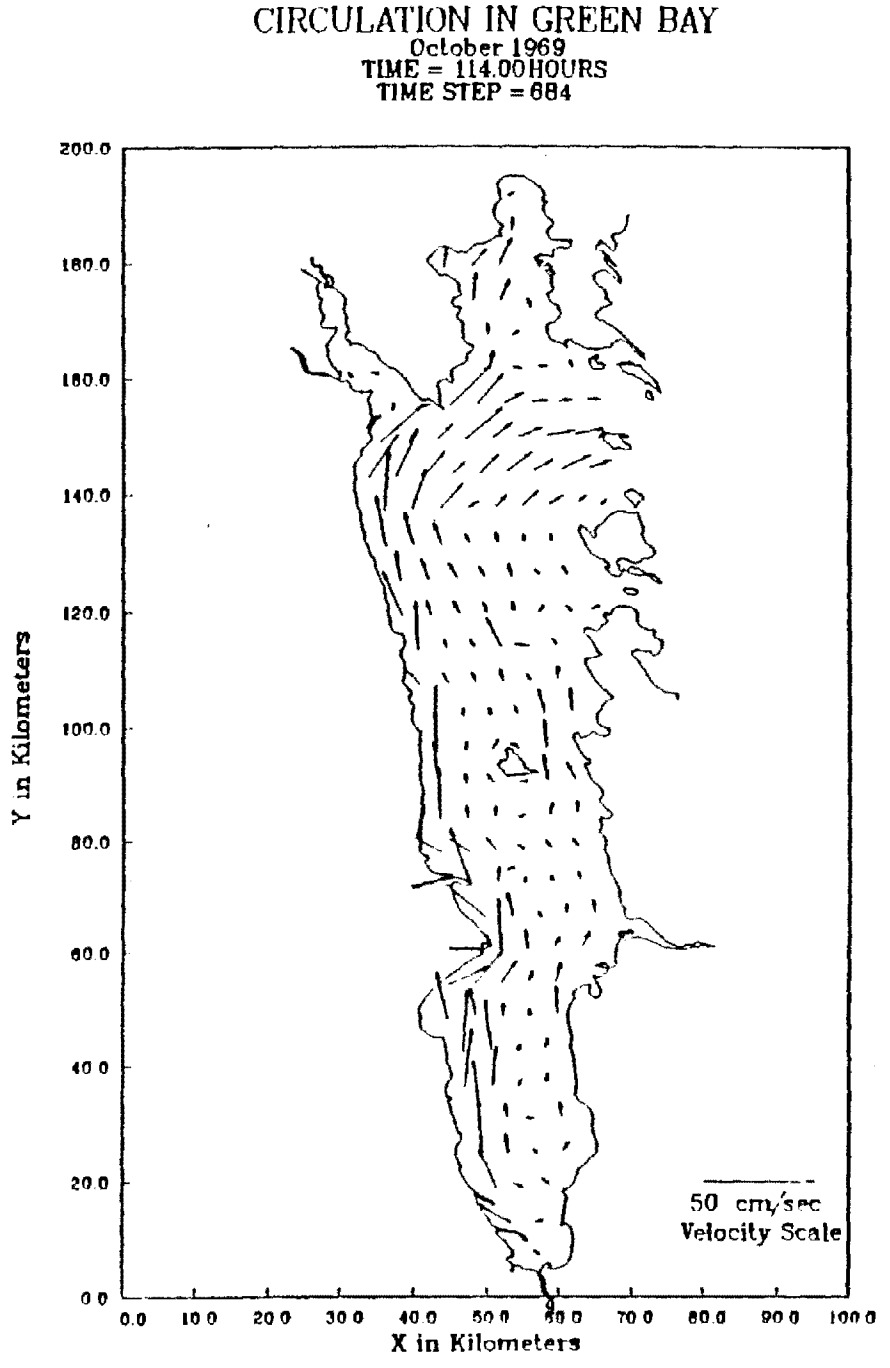

Figure 52. Simulated circulation in Green Bay using October 1969 data (114 hours from the at-rest)

effects for southwesterly and northeasterly winds during the October period. During certain times in October, a counterclockwise circulation was calculated due to southwesterly wind. These two-dimensional results, however, should not be compared with the general pattern of circulation in the Bay which was reported by Miller and Saylor (1985) and Modlin and Beeten (1970). This counterclockwise circulation is shown in Figure 51 where, along the western shore of the Bay flow is southward, along eastern side flow is northward in respect to long axis of the Bay, and near Green Bay city the flow is from left to right parallel to the x-axis of the grid. With the forcing of northeasterly wind, the currents run along both shores, producing counterclockwise flow along Chambers Island in the northern part of the Bay (Figure 52).

Figure 53 shows the computed and measured water surface elevations versus time at a station near the City of Green Bay for September 17-20, 1969. During the first day of the simulation a lag was observed between the measured and computed water surface elevations. Because zero initial values for dependent variables such as water surface elevation and velocities were used, it was concluded that this lag is due to stabilization time, or the time that a column of water will take to absorb the inertia of a suddenly applied wind stress. Differences between the measured and computed water surface elevations during the last day of simulation may be attributed to the use of the over-land wind data measured at the Green Bay airport for over-water wind data in the Bay.

For the October simulation shown in (Figure 54) substantial differences are apparent between the measured and computed water surface elevation during the first two days and last day of the simulation. Nevertheless, there is good agreement between the observed and computed oscillatory patterns. Again as mentioned by Heaps, et al. (1982), the large differences between the simulated and measured water level elevations may be due to some forces that affected the observed values and were not included in the computations. But in general, the model responded fairly well considering the inadequacy of available data used in the simulation.

4.4.3 3-D Simulation of Flow

Since circulation in Green Bay seems to be three dimensional, the application of the 3-D mode is expected to provide improved simulations. This is investigated in this case study by applying the model in the 3-D mode.

Heaps et al. (1982) studied water motion in Green Bay by analyzing the measured field data for September and October 1969. These investigators pointed out that the main external forcing mechanisms to the Bay water included the wind, the semidiurnal tide, and the first free longitudinal mode of oscillation of the Lake Michigan, with the latter two forcing components acting at the Bay mouth. Using a vertically averaged 2-D numerical model, Heaps et al. was able to simulate the water surface and the vertically integrated currents due to specific external forces. With the currents and temperature measured at different depths and locations within the Bay, Miller and Saylor (1985) analyzed the data and found strong variations of water motion and temperature in both the horizontal directions and in the water column.

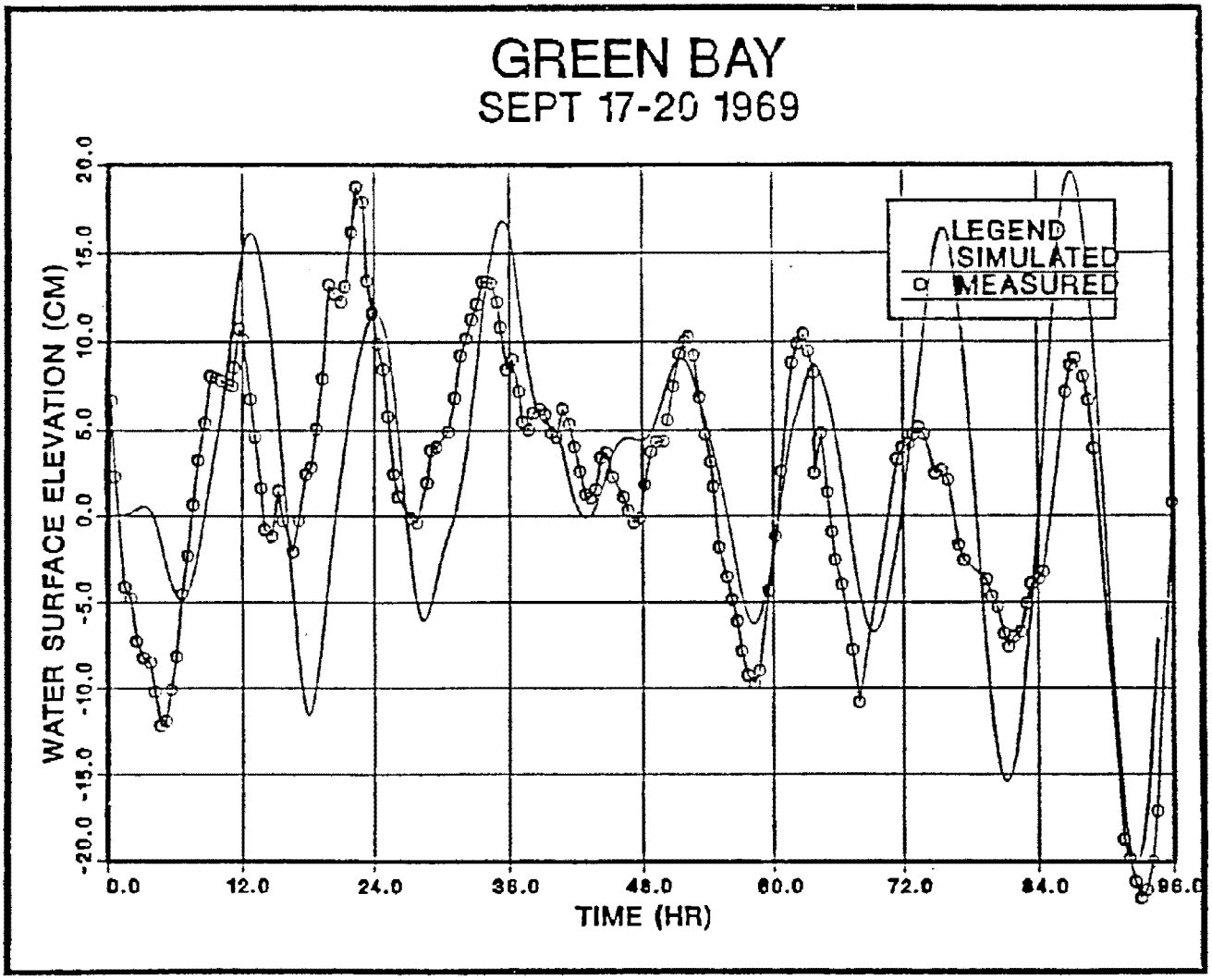

Figure 53. Measured and calculated water surface elevation at Green Bay mouth near Green Bay city during September 17-20, 1969

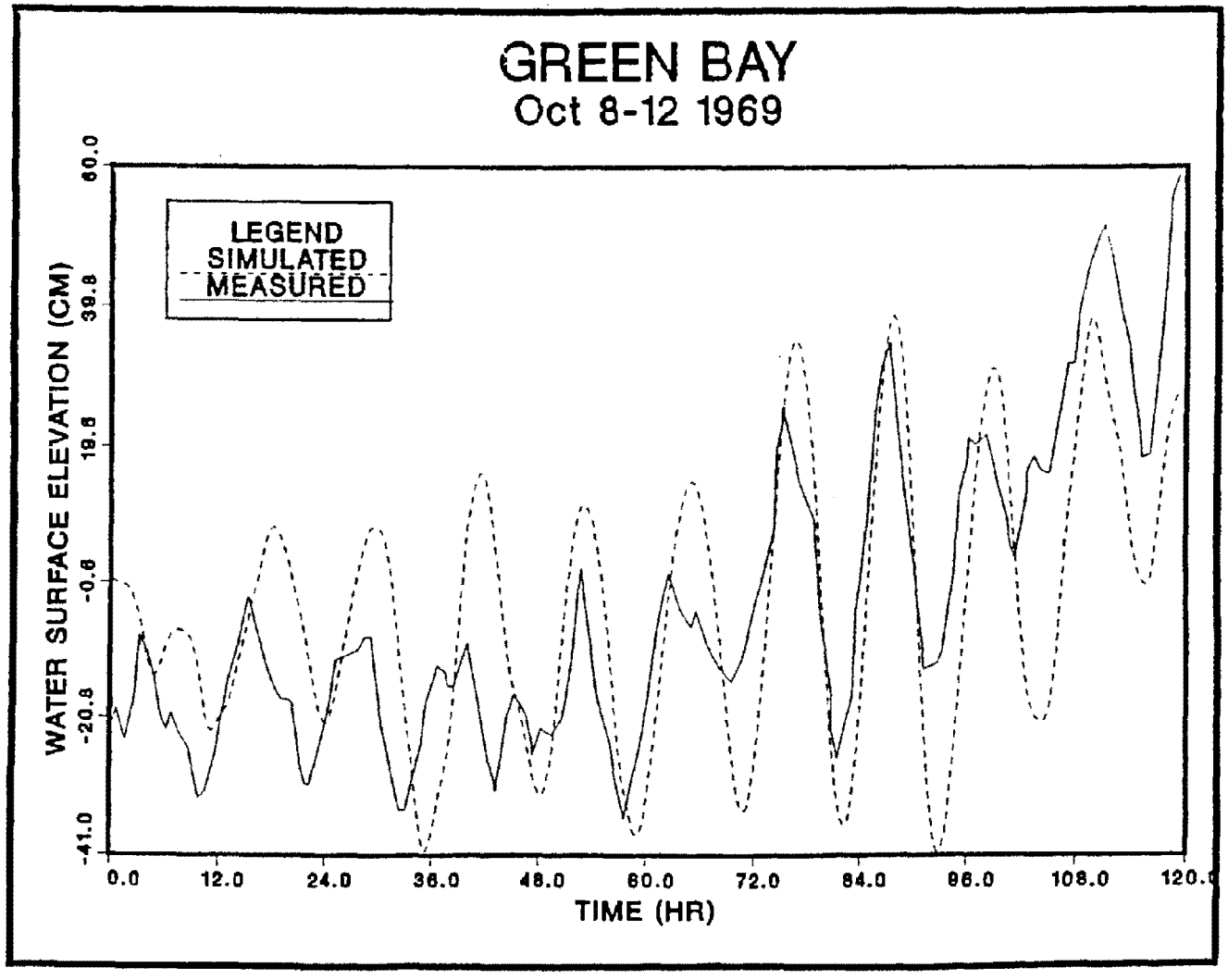

Figure 54. Measured and calculated water surface elevation at Green Bay mouth near Green Bay city during October 8-12, 1969

Due to the 3-D characteristics of water motions within the Bay, both Heaps et al. (1982) and Miller and Saylor (1985) pointed out that a 3-D numerical hydrodynamic model is essential to accurately simulate the circulations in the Bay. The HYDRO3D model was used to simulate the 3-D currents within the Bay; in which the domain was divided into 21 grid points in x-direction and 96 grid points in y-direction, and 5 vertical layers resulting 21 x 96 x 5 square cells.

An experiment using the model, was conducted to determine the responses of water motion in Green Bay under the action of a uniform wind field. Starting from a zero initial condition, we applied a uniform wind of 8 m/sec to the Bay and held it constant throughout the simulation period. The wind was primarily directed along the main axis of the Bay (negative x-axis), 38° clockwise from the north toward the City of Green Bay. For the sake of simplicity and the unavailability of boundary conditions at the mouth, the Bay was assumed to be an enclosed domain.

With the above assumptions and grid configurations, a 3-D simulation was performed for a duration of 40 hours. Figure 55 shows the water surface elevations in Green Bay after 40 hours. Due to the direction of the wind, a positive water surface profile is maintained toward the City of Green Bay. The profile decreases to zero somewhere in the middle of the main axis and then to negative values in the two northern gulfs. Figure 56 shows the 3-D, vertically averaged currents in the Bay at the same time. The currents along the shallow shore regions are driven by the wind. Currents against the wind in deeper central regions are driven by the pressure gradient associated with the positive surface setup as was shown in Figure 55. This phenomenon is often seen in the studies of estuarine and lake hydrodynamics.

Several small gyres are distributed in the Bay. These gyres are associated with the bathymetry and geometry of the Bay. Comparing Figures 55 and 56 with the Heaps's 2-D model results, we find that the agreement between surface elevations from both models is remarkably good. The (maximum) surface setup at the City of Green Bay is 11.7 cm from HYDRO3D and 11 cm from Heaps' model. The general patterns of 2-D circulation in Figure 56 are very similar to those of Heaps' model except in regions near the mouth. In Figure 56, from the mouth to the northern shore, there exists two types of circulation. One is counterclockwise near the mouth and the other clockwise near the northern shore. In Heaps' results, these two gyres are merged into one large counterclockwise gyre extending from the mouth to the northern shore. This difference of local circulation may be attributed to the fact that in Heaps' model, the mouth is not a boundary; rather, it is continuously connected to the lake. An open boundary is assumed to exist in the central region of the lake, which is far away from the mouth and hence the Bay. In the present model, however, we assume rigid, closed boundaries along the mouth. Figure 57 shows the currents in the near-surface layer and Figure 58 shows those in the near-bottom layer.

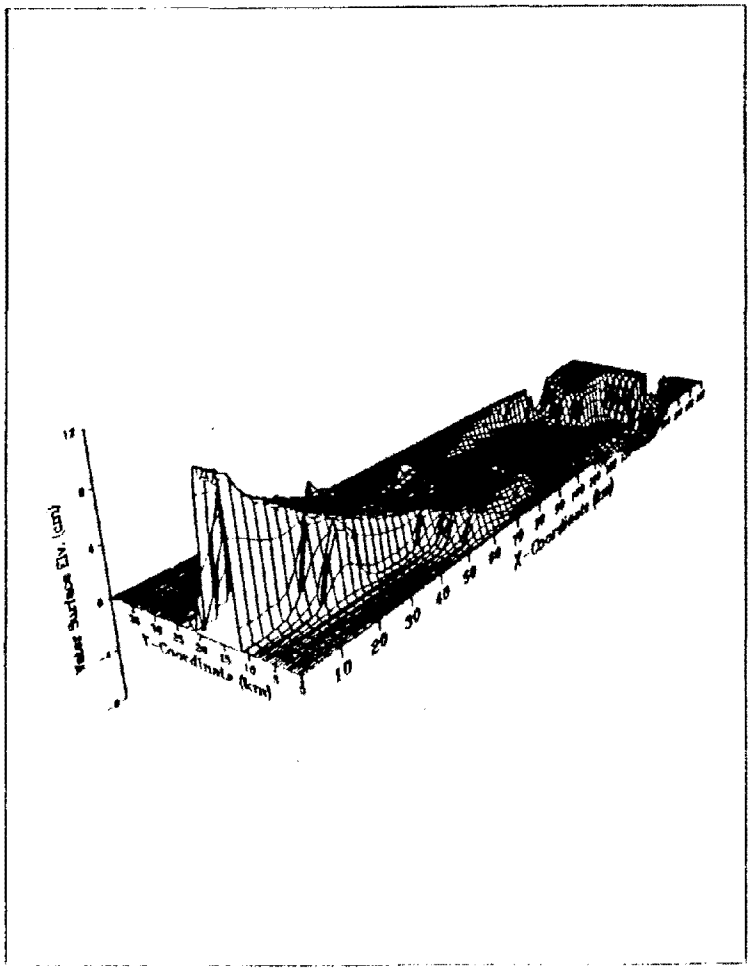

Figure 55. Water surface elevation in Green Bay after 40 hours

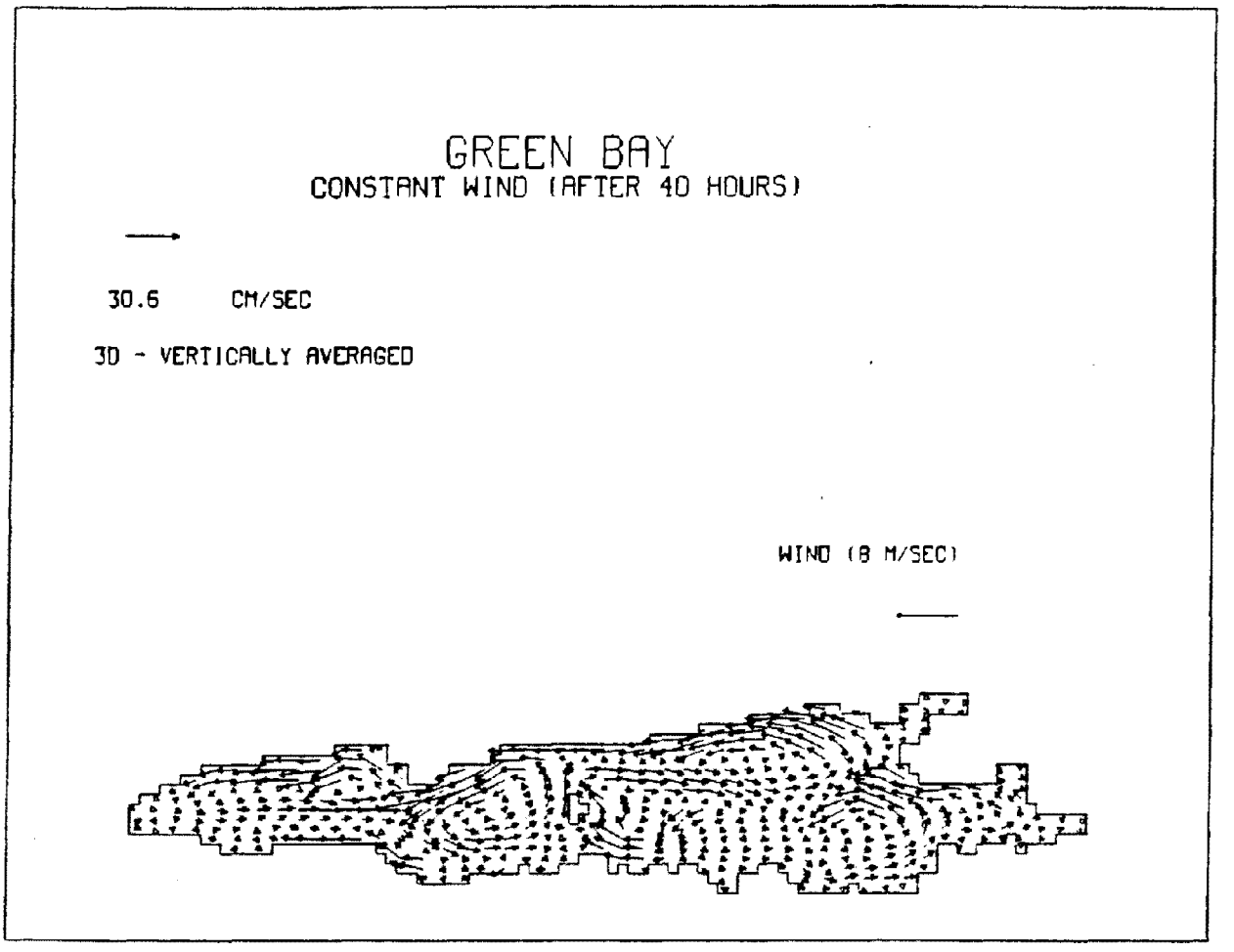

Figure 56. 3-D vertically averaged currents in Green Bay after 40 hours

Similar to the wind-driven currents along the shallow shore regions, the near-surface currents also are driven by the wind and hence follow the direction of the wind. These unidirectional surface currents cause a gradient of water surface elevation along the wind direction. To balance the pressure gradients caused by the water surface setup, the currents return in the lower layers (near the bottom), in particular, the deeper regions, as shown in Figures 57 and 58.

4.5 Prince William Sound, Alaska

To further test the capability of HYDRO3D under a different situation it was applied to Prince William Sound in Alaska, to simulate water circulation during the recent oil spill from the EXXON Valdez that began on March 24, 1989.

4.5.1 Physical Setting

Prince William Sound (Figure 59) lies on the southern coast of Alaska. The sound covers an area of approximately 8000 square kilometers (3090 square miles) and includes many islands of various sizes. Most of the islands are concentrated in the western half of the sound, leaving a large open area of approximately 1800 square kilometers (700 square miles) in the eastern half. The terrain in the area is very rough, creating numerous bays and causing the shoreline of the sound and islands to be quite irregular.

The sound is separated from the Gulf of Alaska by Montague and Hinchinbrook Islands, which form the south-eastern boundary, and has two major connections to the Gulf of Alaska. The Hinchinbrook Entrance is 11.4 kilometers (7.1 miles) wide and opens directly to the gulf between Hinchinbrook and Montague Islands, at about the middle of the eastern side of the sound. At the southern end of Montague Island and of the sound, Montague Strait forms an 8.4 kilometer (5.2 miles) wide passage parallel to the main shoreline. The average depth in the Hinchinbrook Entrance and Montague Strait is 300 meters (980 feet) and 195 meters (630 feet), respectively.

A navigation channel extends from the port of Valdez in a bay at the northern end of the sound, across the previously mentioned open stretch of water, and out through the Hinchinbrook Entrance. Depths along this channel are primarily in the range of 275 to 460 meters (900 to 1500 feet). These depths are typical of the more open, western half of the sound. In the eastern half, a scattering of islands separates the sound into a network of passages of widely varying widths and depths. The two major passages lie on either side of the largest interior island, Knight Island. The passage between Montague and Knight Islands averages about 6.3 kilometers (3.9 miles) wide and 180 meters (600 feet) deep; the narrower passage between Knights Island and the main shoreline averages about 10.1 kilometers (6.3 miles) wide and 400 meters (1300 feet) deep. The maximum depth in the sound is approximately 870 meters (2860 feet) and occurs in the western half of the sound, off the northern end of Knight Island.

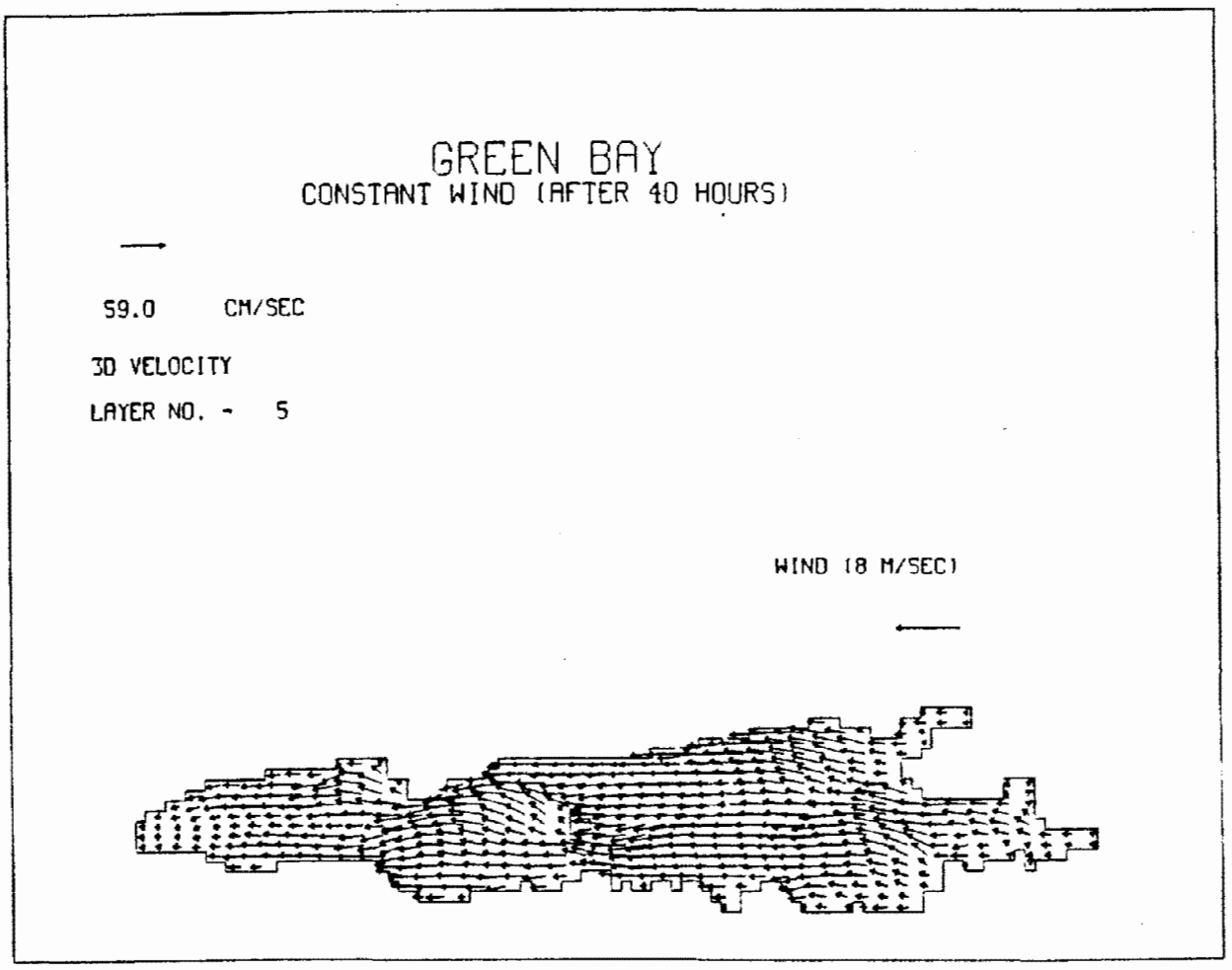

Figure 57. 3-D simulation of currents in Green Bay (near the surface layer).

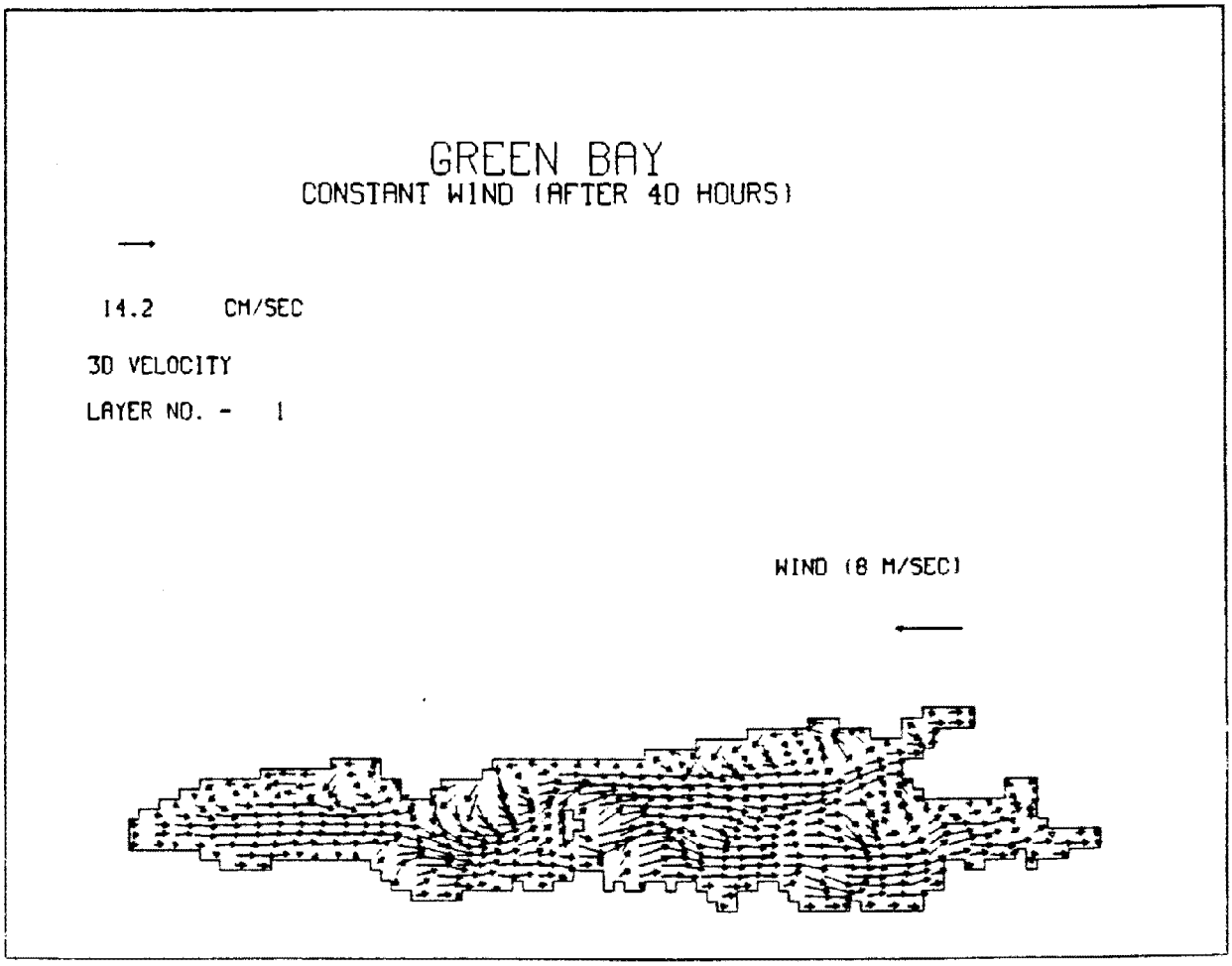

Figure 58. 3-D simulation of currents in Green Bay (near the bottom layer).

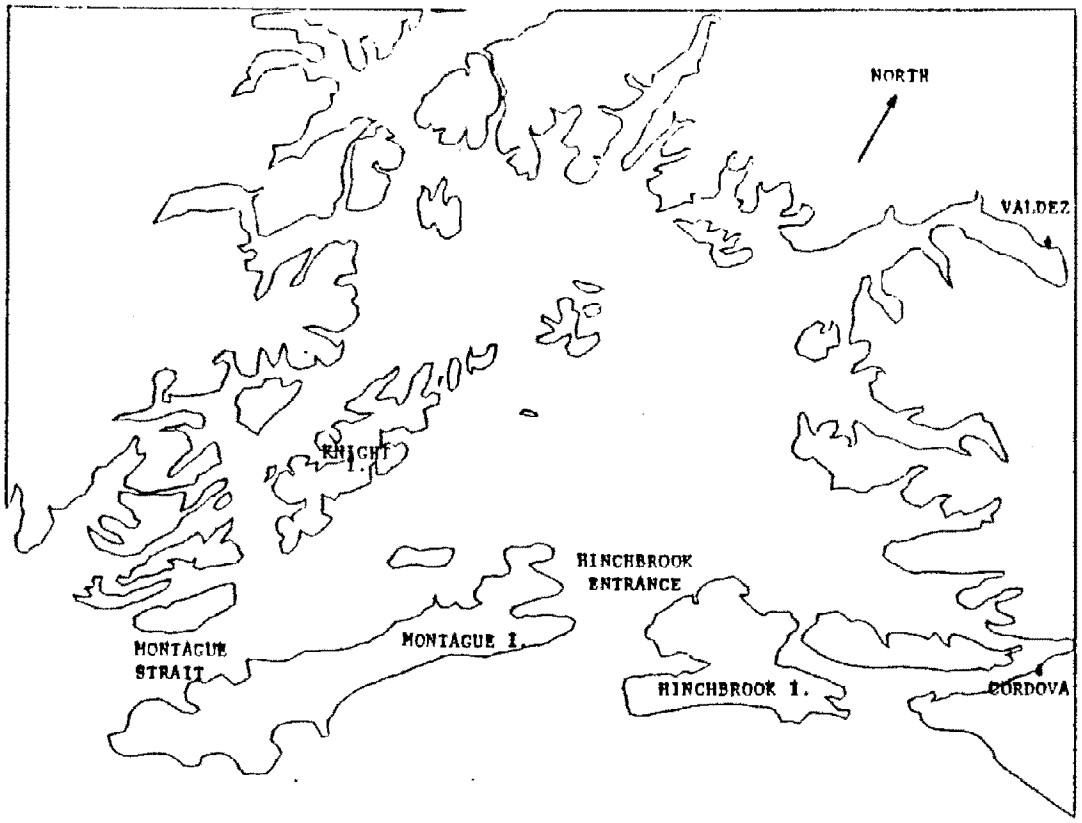

Figure 59. Map of Prince William Sound, Alaska.

4.5.2. Modeling Parameters

Two finite difference grid networks were used to describe the Prince William Sound area. Initially a coarse uniform grid network (Figure 60) of 35 x 28 square blocks was used to minimize data processing and computation time. In this grid system the area of each grid block was 25.8 square kilometers (10.0 square miles). This relatively coarse grid failed to represent the highly irregular nature of the shoreline, omitting many small islands, passages, and bays. The second grid was (Figure 61) four times as fine as the first, consisting of 70 x 56 square blocks where the area of each grid block was 6.5 square kilometers (2.5 square miles). This finer grid was much more successful in representing the features missed by the coarser grid.

Both circumscribing grids had an open boundary on their western and southern sides (approximately corresponding to the south and east of the map). On the western side, the open boundary extended from blocks 2 to 10 for thecoarse grid and blocks 2 to 21 for the fine grid. On the eastern side, the open boundary extended from blocks 2 to 29 for the coarse grid and blocks 2 to 63 for the fine grid.

Three simulation runs were performed to calculate the flow field in the sound. One run for each grid was completed in the 2-D mode in addition to a 3-D run (with three layers) using the coarse grid. For simplicity in these comparative test runs, a tidal amplitude of 3.0 meters (9.8 feet) with no phase angle was assumed along the open boundaries. All other factors, such as wind stresses and river inflows, were neglected. A time step of 1.0 and 1.5 minutes was used for the coarse grid and fine grid runs, respectively. These runs were used to compare the results from a 2-D and 3-D analysis and from a coarse and fine grid analysis (2-D only).

4.5.3 Results

Scale vector plots of the calculated velocity field were obtained at hourly intervals for each run. These plots are shown in Figures 62 to 64. The scale of the velocity vector is given in terms of its horizontal, and vertical components one inch equals 0.77 meters per second (2.5 feet per second). An arrow with no stem indicates that the velocity is too small to be revealed at this scale. The map scale is 1 inch equals 23.4 kilometers (14.6 miles).

Several velocity vectors in the lower right corner were unexpectedly large. At one point in particular, the velocity was so great that, for several plots, this vector was truncated at the boundary of the plot. Extensive mud flats exist here, causing some of this area to be declared as land (the blank area) and others to be very shallow. The isolated large velocities in this corner may be attributed to this shallowness combined with the boundary effects.

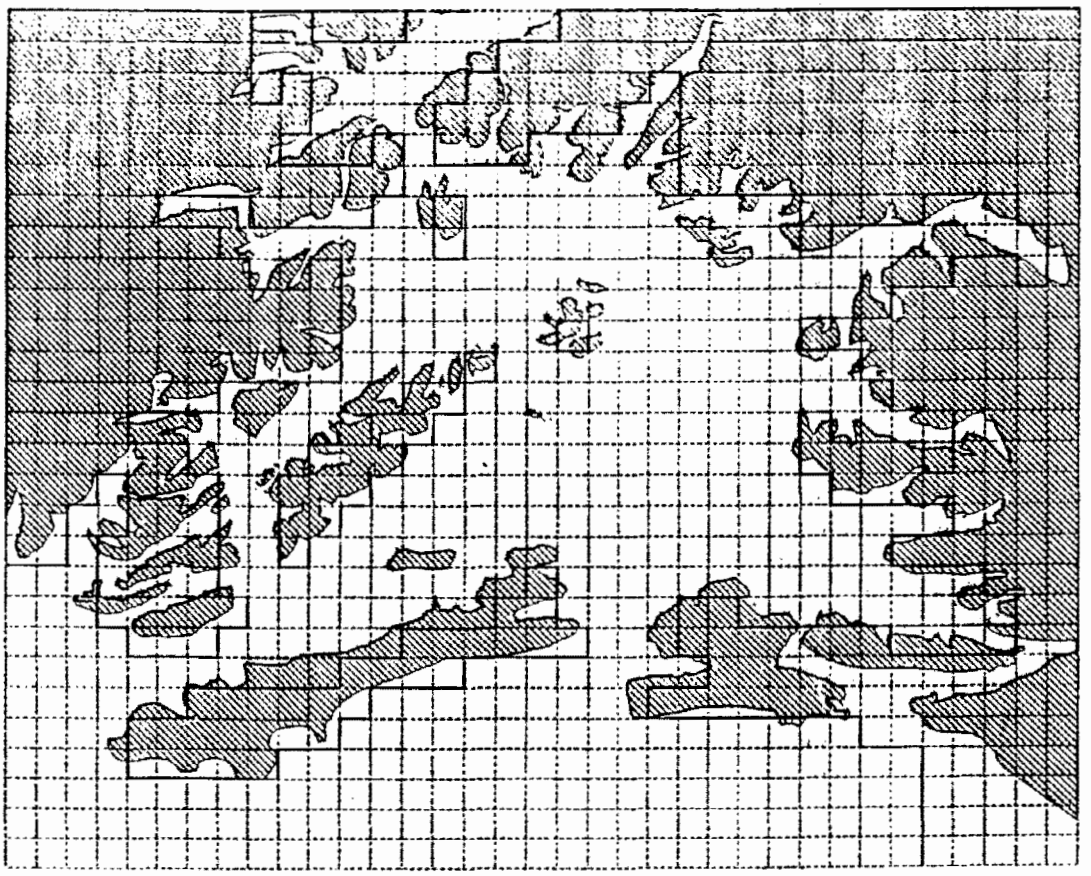

Figure 60. Coarse grid of Prince William Sound, Alaska.

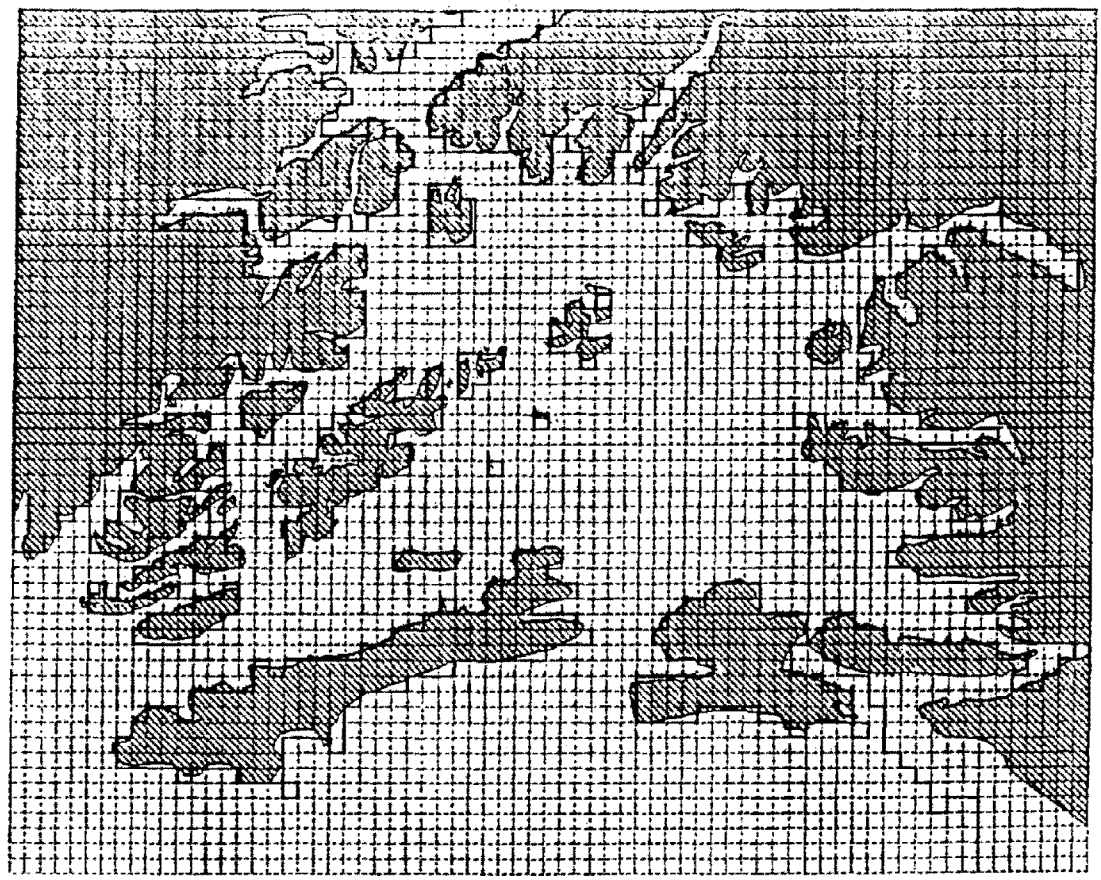

Figure 61. Fine grid of Prince William Sound, Alaska.

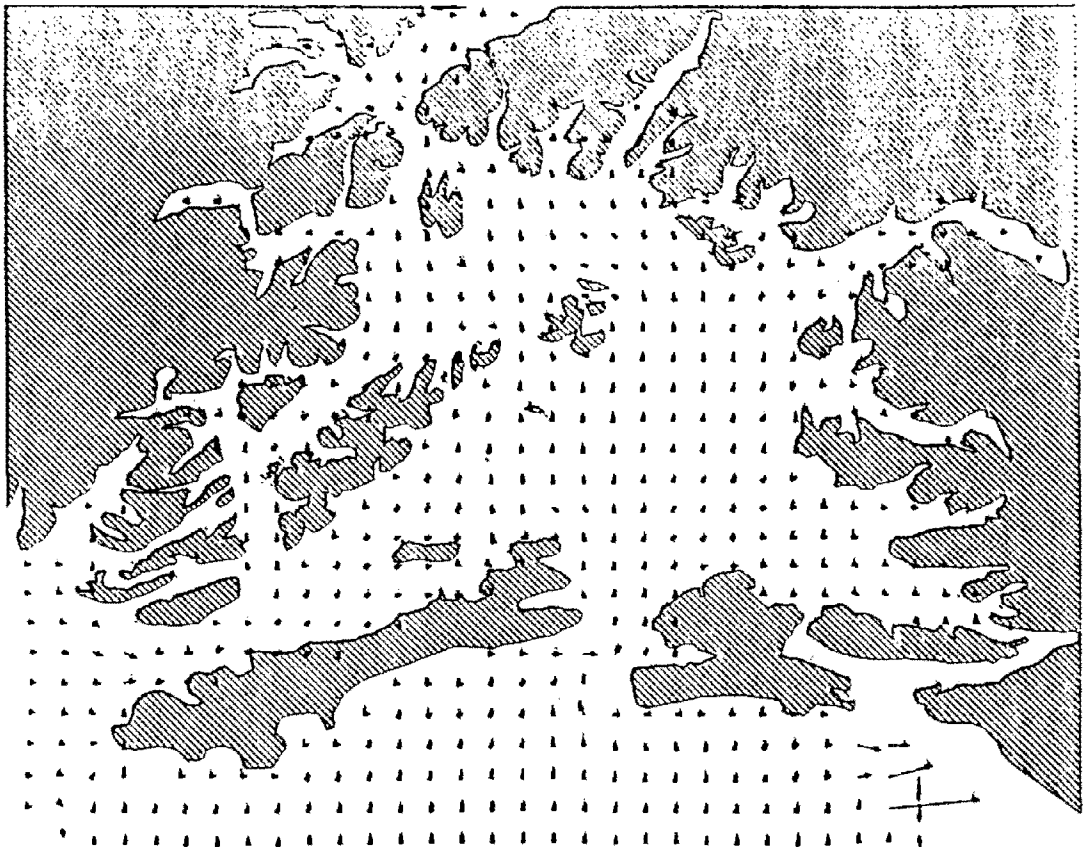

Figure 62. 2-D vertically averaged of currents in Prince William Sound using coarse grid (1 hour after simulation).

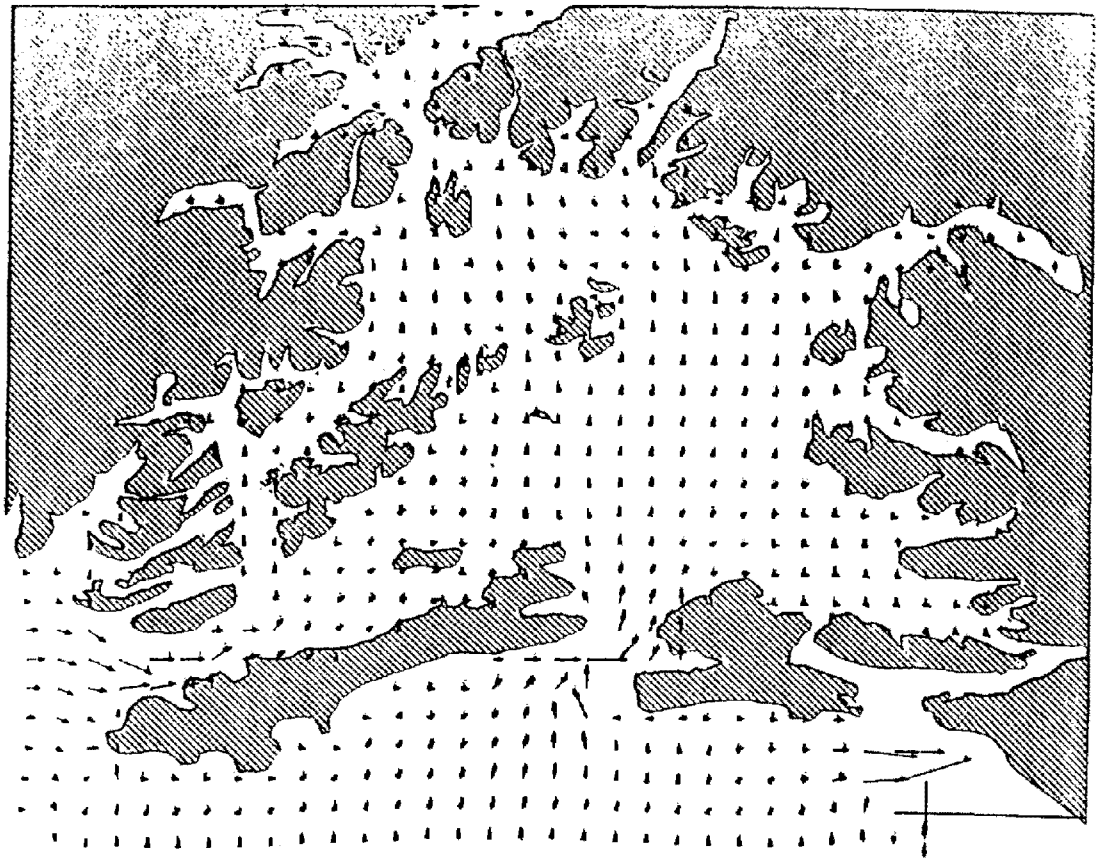

Figure 63. 2-D vertically averaged of currents in Prince William Sound using coarse grid (2 hours after simulation).

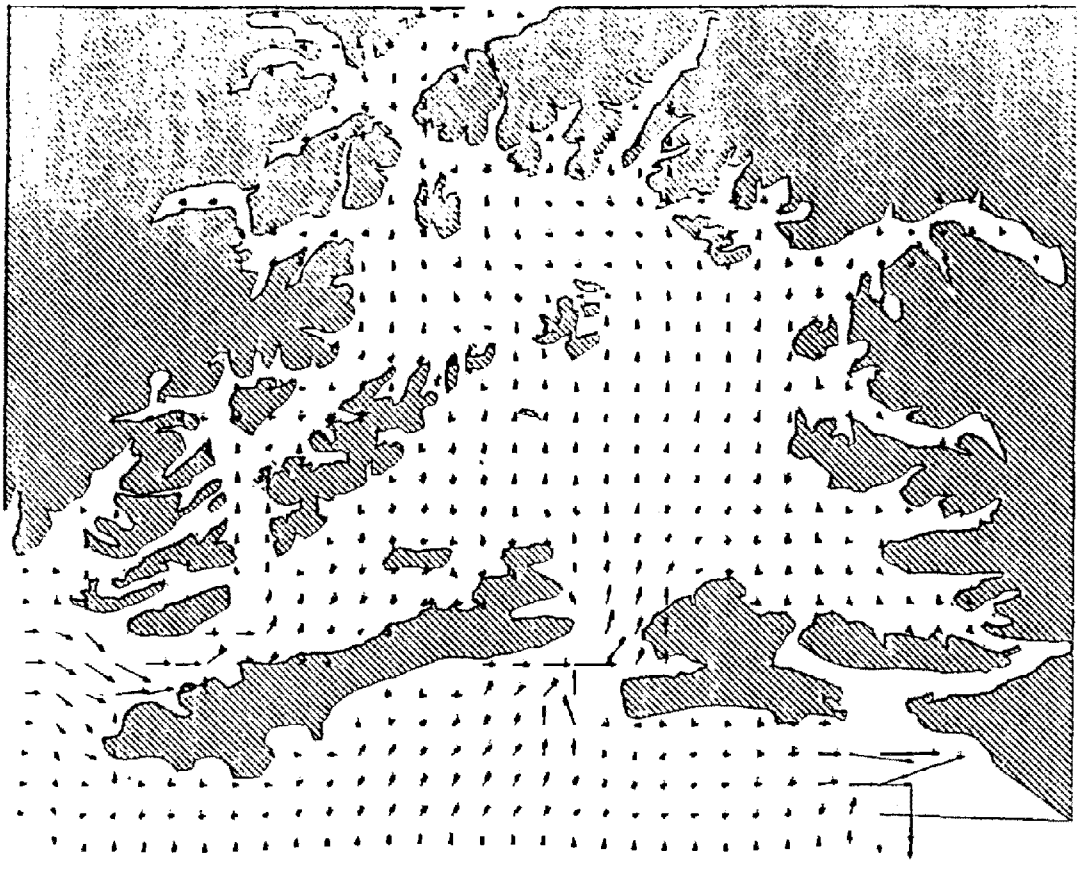

Figure 64. 2-D vertically averaged of currents in Prince William Sound using coarse grid (3 hours after simulation).

Some velocity vectors are plotted over land. This is due to the discretization process. Attempting to represent the shoreline with a fixed grid resulted in some blocks containing both land and water. Velocity vectors are plotted at the center of the block, occasionally resulting in the vector being plotted on land. This phenomenon occurs most often in the coarse grid due to its poorer representation of the actual shoreline. (This grid has also been slightly rotated from its original position in order to match the alignment of the fine grid.)

4.5.4. Discussion

In comparing the results from the 2-D and 3-D runs utilizing the coarse grid (Figures 64-66), we note two factors. First, the flow direction varied with time and space in a similar manner for each run. Thus, at any given point in time, the current pattern for the sound was the same for the 2-D and 3-D runs. Second, the magnitude of the flow velocities at any given point in time and space varied little for these runs. Only at the third hour (Figures 64 and 67) can any detectable difference be discerned. At this time, the velocities at the two main entrances to the sound are slightly greater for the 2-D run. Thus, it appears that the 2-D and 3-D options differ most in the calculated magnitudes of the flow field with little or no impact on the directionality.

A comparison of the 2-D coarse grid and fine grid results (Figures 64-69) yields a similar conclusion. Due to the longer time step and better resolution of the fine grid, it took slightly longer for the flow field to stabilize so no comparison could be made in the first hour. At subsequent hours, however, it was again seen that the flow direction varied with time and space in a similar manner for each run, resulting in similar current patterns. Also, some difference was noted in the magnitude of the flow velocities at any given point in time and space. One must compare the velocities with care as the greater density of the vectors in the fine grid plots tends to exaggerate any differences in magnitude. By examining individual, corresponding velocity vectors in each run, it may be seen that within the two main entrances to the sound, only a small difference occurs whereas, on either side of the entrances, the differences are greater. At a given time for the fine grid run, the flow gains speed more rapidly approaching the entrances, reaches a slightly greater maximum velocity within the entrance, and loses speed more slowly on the other side. The fine grid, as would be expected, provided a much more detailed visualization of the flow field, including the representation of flows through several smaller entrances that parallel Montague Strait. Thus, it appears that the velocity magnitude is affected by the degree of resolution of the finite difference grid while the directionality remains unchanged.

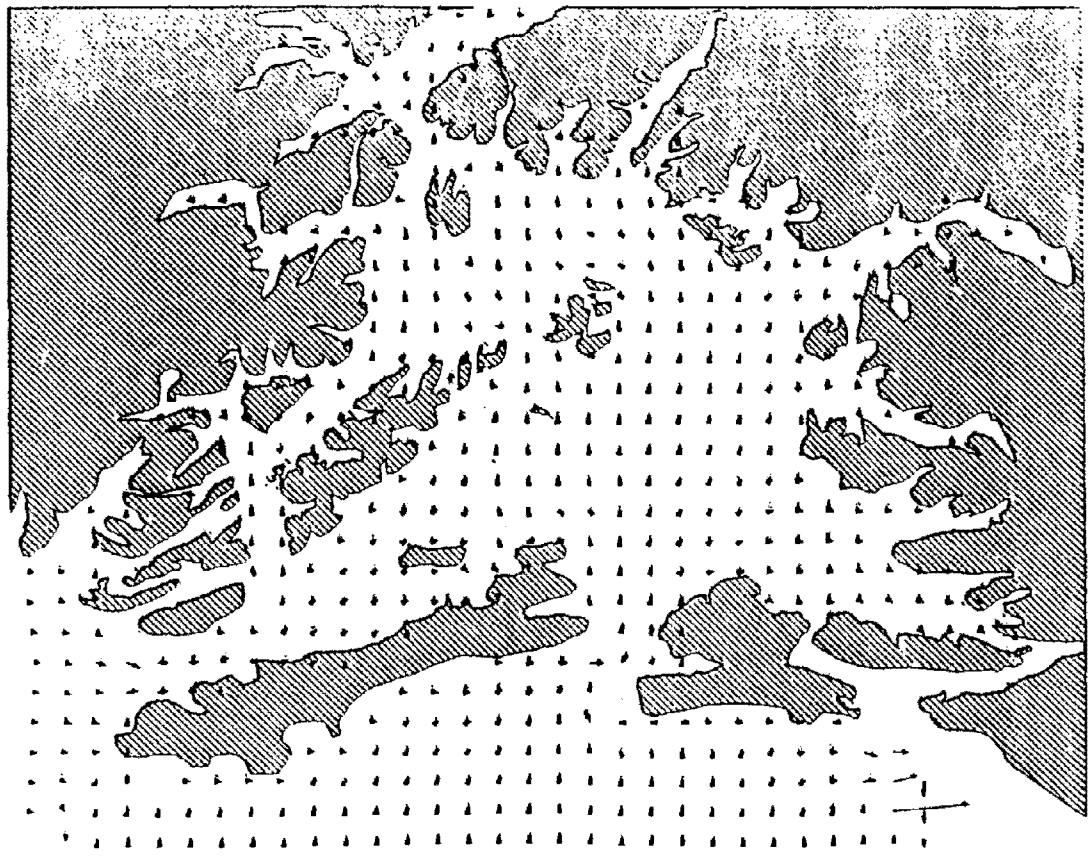

Figure 65. 3-D simulation of currents in Prince William Sound using coarse grid (1 hour after simulation).

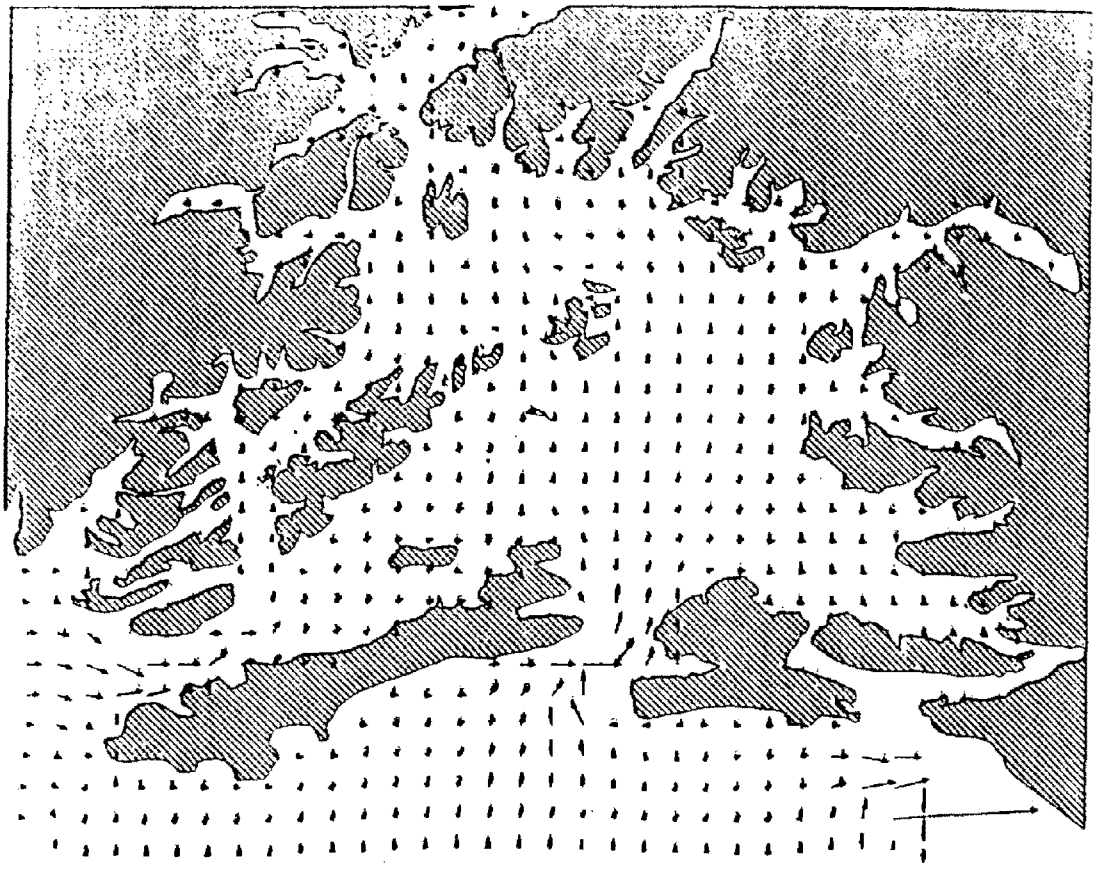

Figure 66. 3-D simulation of currents in Prince William Sound using coarse grid (2 hours after simulation).

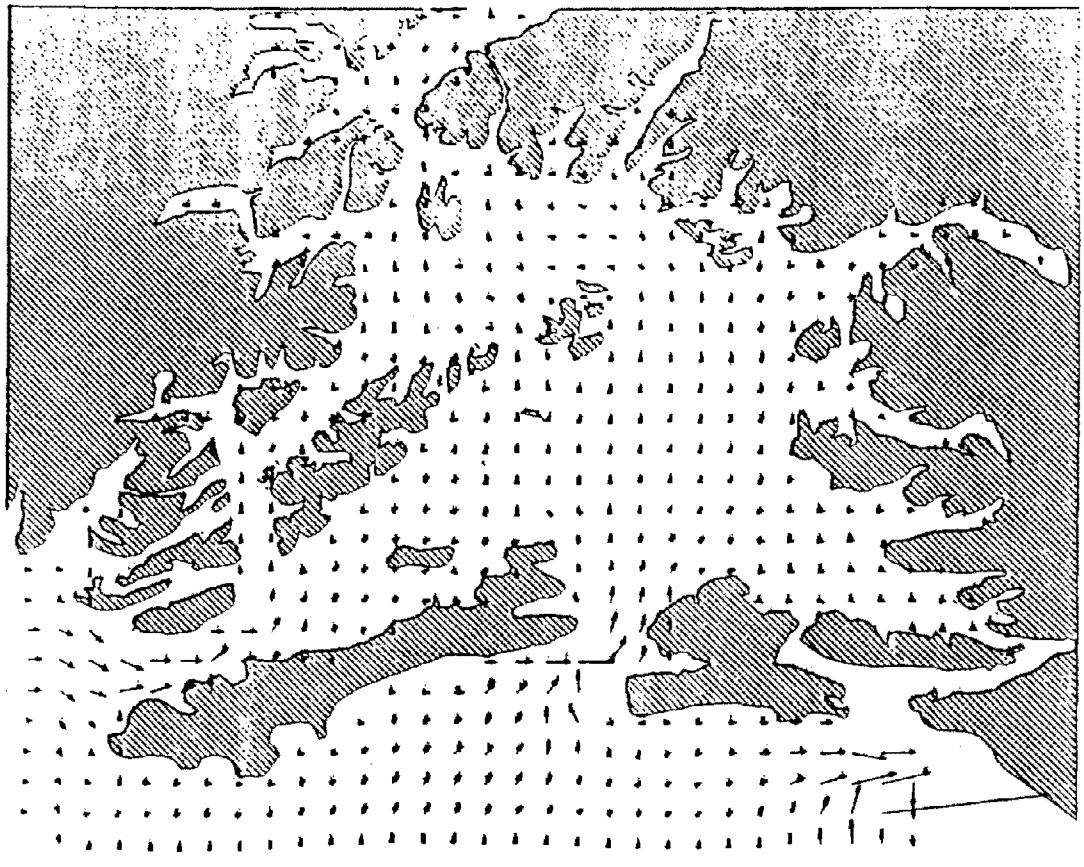

Figure 67. 3-D simulation of currents in Prince William Sound using coarse grid (3 hours after simulation).

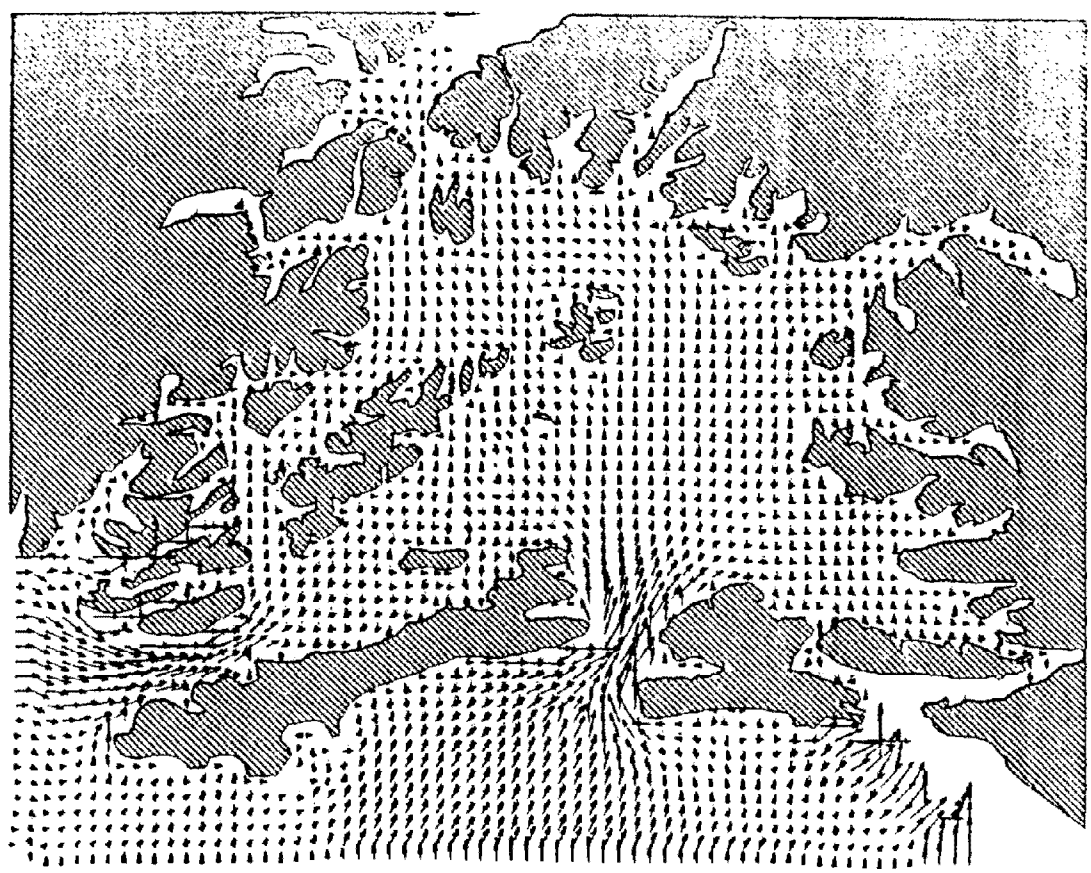

Figure 68. 2-D vertically averaged of currents in Prince William Sound using fine grid (2 hours after simulation).

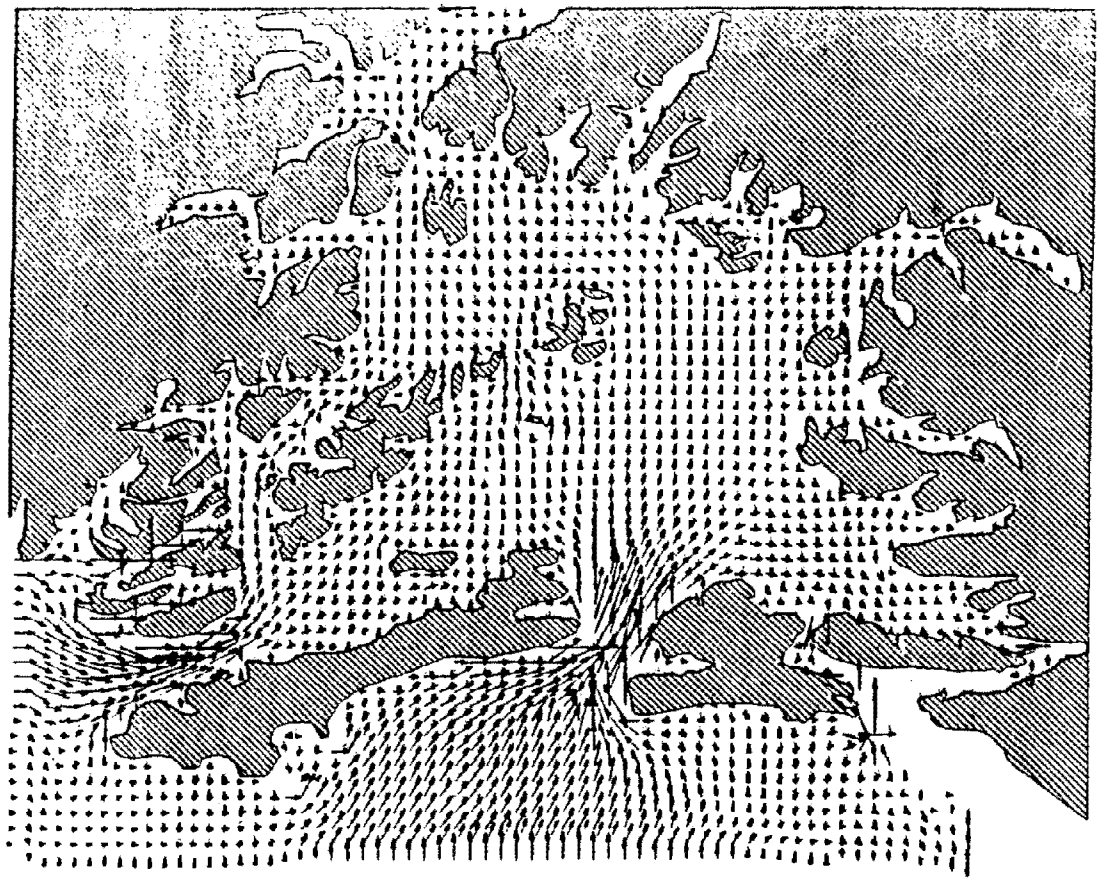

Figure 69. 2-D vertically averaged of currents in Prince William Sound using fine grid (3 hours after simulation).

4.6 Currents in Mississippi Sound

In this application, an earlier version of the model has been applied to simulate the tide- and wind-driven currents in Mississippi Sound and adjacent continental shelf waters of the Gulf of Mexico (Sheng, 1983).

4.6.1 Physical Setting

Mississippi Sound and adjacent areas (Figure 70) is a region that has received greater attention due to increasing utilization of its resources, including the dredging of shipping channels and the disposal of dredged materials. The Mississippi River is located at the Western end of the sound and it dominates flow and sediment transport in area. Other major tributaries which discharge into the sound include the Pearl, Pascagoula, and Mobile Rivers.

4.6.2 Circulation in Mississippi Sound

The circulation in Mississippi Sound is affected by (1) ocean tides propagating from the Gulf of Mexico through the sound entrance, (2) meteorological forcing, and (3) bathymetry and geometry.

Gulf tides in the area consist of the diurnal components K1, O1, and P1 collectively over the semi-diurnal components M2 and S2, except along the Western Florida Coast. Platzman (1972) and Hansen (1974) found that the period of the lowest mode of long gravity waves in the Gulf might be quite close to the diurnal tide period, hence suggesting a quasi-resonant condition. Reid and Whitaker (1981) developed a numerical tide model for the Gulf based on the vertically-integrated linearized, Laplace tidal equations in spherical coordinates to portray the barotropic response of the Gulf to tidal forcing. Their study on the Gulf tides may provide a useful option to supply seaward boundary conditions for this application.

The water level response for a given tidal constituent is usually expressed in the following form (Shureman, 1941) in terms of the surface displacement ζ:

$$\zeta = F(t)\, A(\lambda,\phi) \cos [\, \omega t + x - G(\lambda,\phi)] \qquad (68)$$

where λ is the longitude, ϕ is the latitude, A is the mean amplitude over 18.6 years and G the Greenwich phase or epoch at given position (λ,ϕ), is tidal frequency, χ is the astronomical argument, while F is the nodal factor (a slowly varying function of time). Tides at particular stations are characterized by A and G for individual constituents. In Sheng's study (1983), A's and G's for 5 constituents (O1, K1, P1, S2 and M2) along the open boundaries of our grid are supplied from Reid and Whitaker's model. Surface displacements at the open boundary stations are determined from a linear combination of those due to the five tidal constituents.

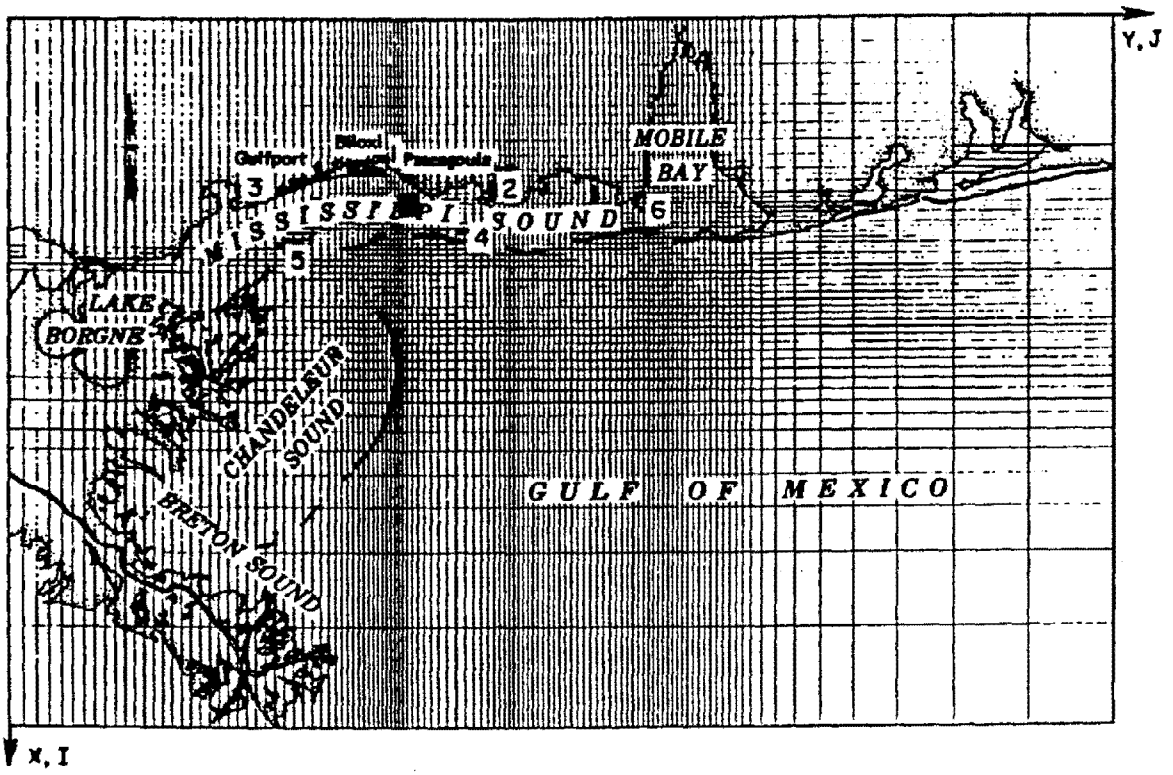

Figure 70. Lateral Numerical Grid Used for Dynamic Simulation of Coastal Currents within the Mississippi Coastal Waters.

4.6.3 Results

Simulations were performed for tide and wind-driven current during September 20 to September 25, 1980 and briefly are described below.

4.6.3.1 Tidal Simulation

In this example, the model was run using water surface displacement (Equation 68) as the boundary conditions. The model-simulated water surface displacements at four stations (see Figure 70 for locations) within the Mississippi Sound are compared with measured data in Figure 71. The measured data shown on those figures have been filtered such that variations due to short period oscillations on the order of a few hours or less are not included. Over the simulation period, diurnal tides dominate over the semi-diurnal tides. Towards the end of the five-day period, the diurnal tides become somewhat less predominant while the semi-diurnal tides became gradually more apparent. Good agreement is found at all stations.

Surface displacement over the coastal area at the end of the third day of simulation is shown in Figure 72. The results exhibit variation in surface displacement from nearly zero along the open boundary to -7 cm within the Mississippi Sound, indicating the phase difference in tide.

In this simulation, a relatively large time step of 12 minutes was used for both the external and the internal modes. Seven grid points were used in the vertical direction. A relatively smooth bottom with a roughness length, Z_o, of 0.1 cm was assumed. A parabolic length scale, Λ, no more than 25% of the local depth, was assumed in the vertical direction. River inflows from six rivers were considered: Pearl, Jourdon-Wolf, Biloxi, W. Pascagoula, Pascagoula, and Mobile.

The tide-driven horizontal currents at mid-depth are shown in Figure 73 for two stations in the Mississippi Sound. Currents on the order of 1 ft/sec (30 cm/sec) exists at both stations. Again, reasonable agreement is found between data and model results.

The horizontal velocity field at 1 m depth, after 3 days of simulation, is shown in Figure 74. Relatively large currents exist at the various tidal inlets and in the area between Ship Island and Chandeleur Island. Except in these areas, at this instant of time, bottom shear stress generated by the tidal currents are generally less than 0.3 dyne/cm^2.

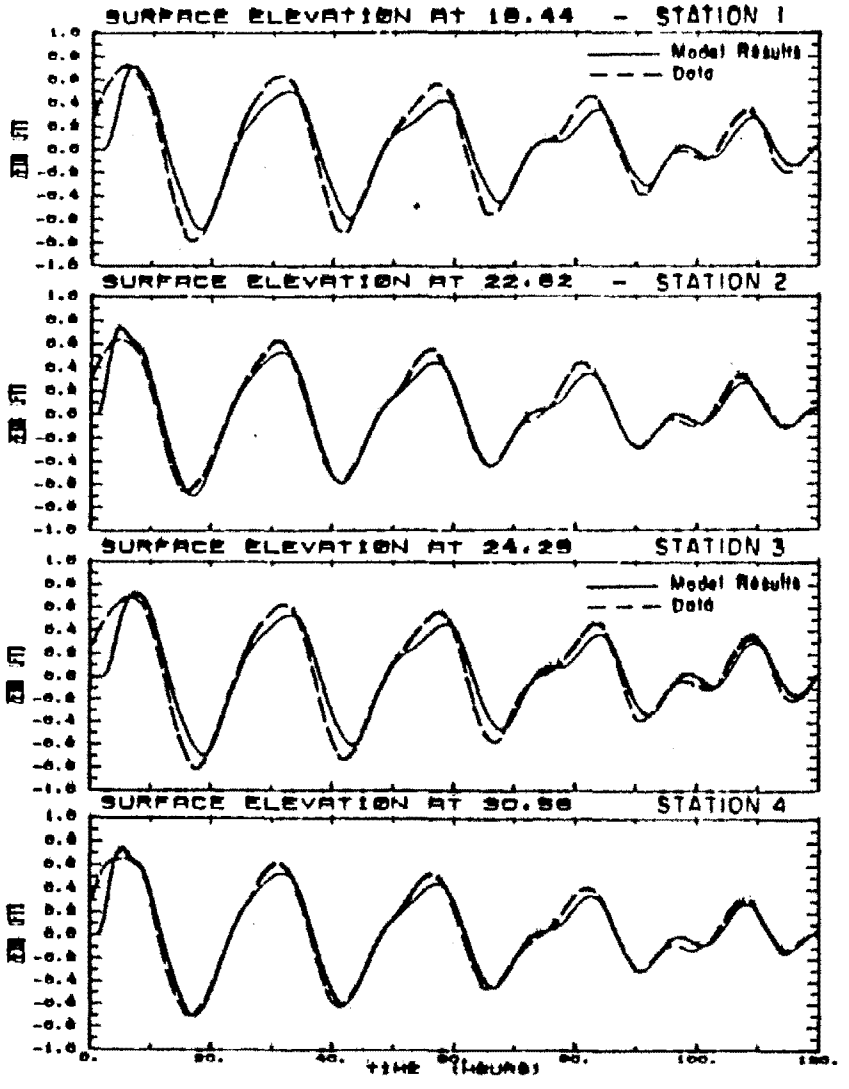

Figure 71. Transient Variation of Surface Displacements at Four Stations Within the Mississippi Sound from 9/20/80 to 9/25/80.

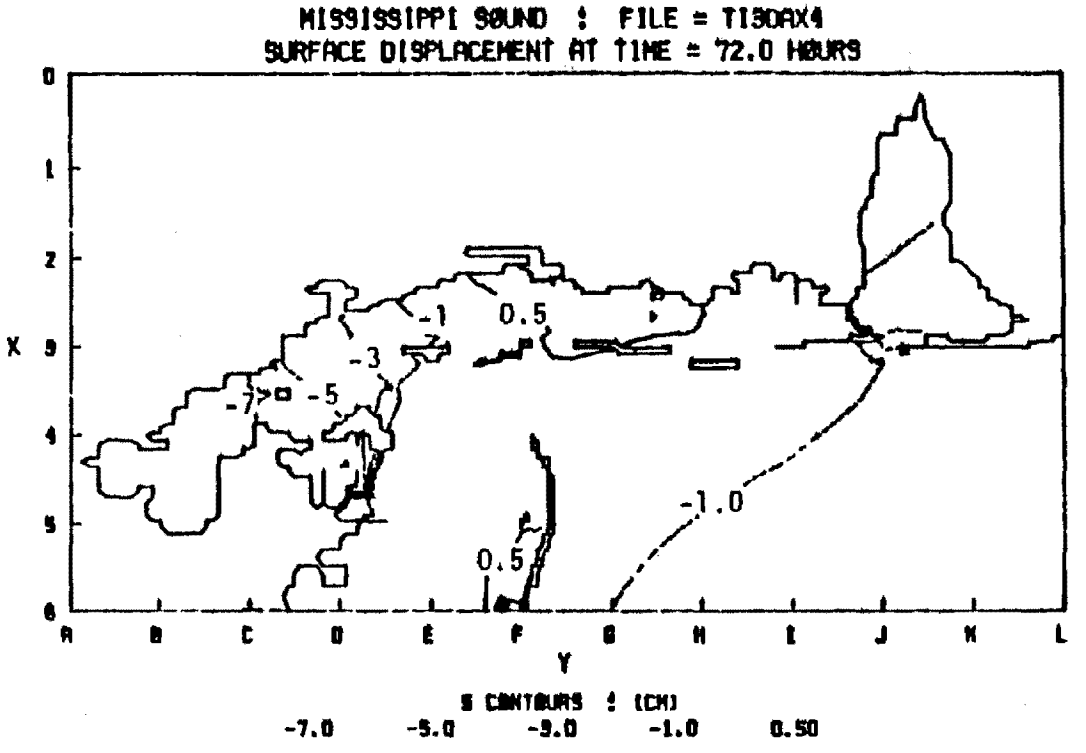

Figure 72. Surface Displacement Contours Within the Mississippi Coastal Waters at 0 Hr., 9/23/80.

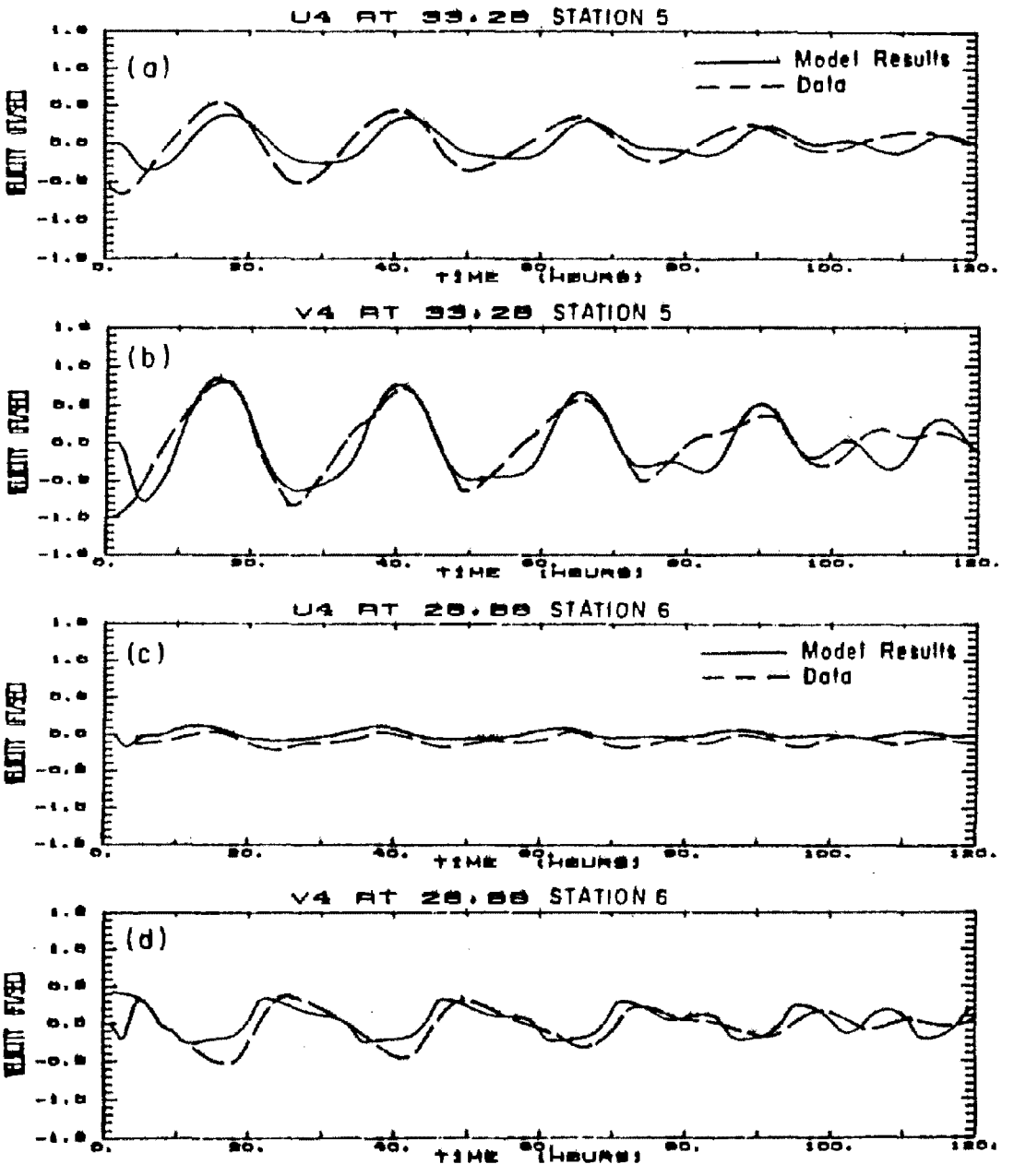

FIGURE 73. Transient Variation of Mid-Depth Velocities at Two Stations Within the Mississippi from 9/20/80 to 9/25/80.

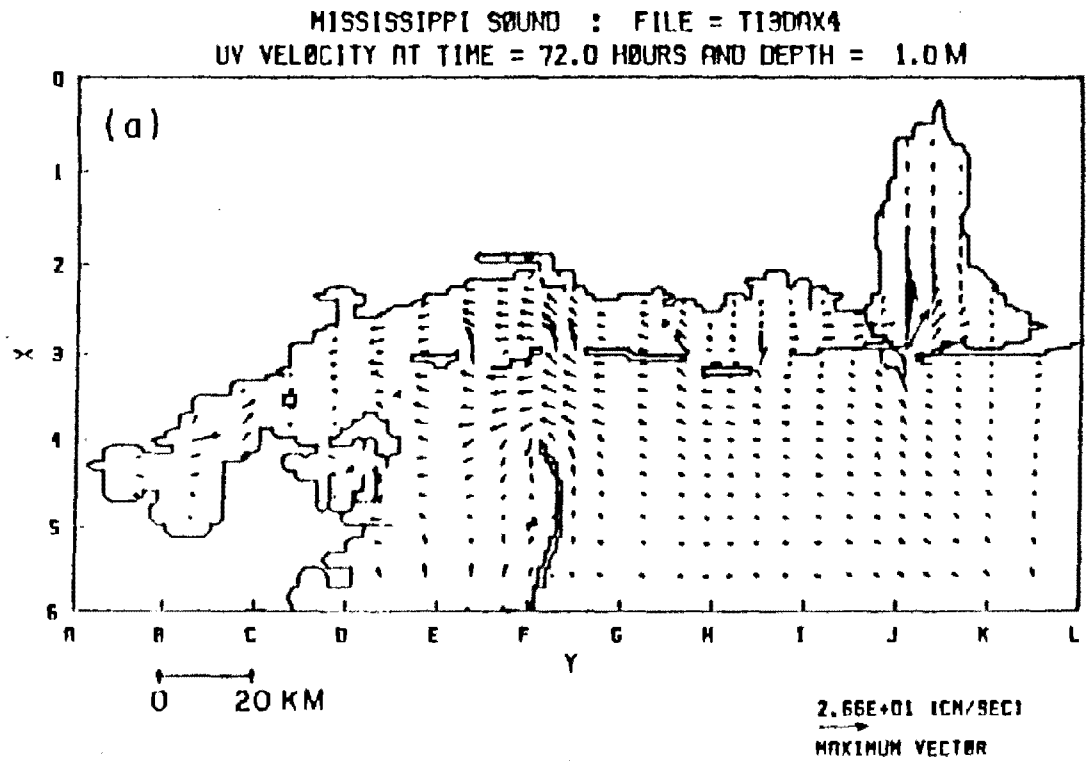

FIGURE 74. Horizontal Velocity Field at 0 hour and 1 m depth, 9/23/80.

4.6.3.2 Wind-effect on Tidal-Driven Currents

The results presented above did not contain any wind-driven effect. During this study, wind data were collected at several meteorological stations surrounding the Mississippi Sound. The wind during the 5-day period between September 20 and September 25, 1980, was generally quite mild (~ 10 mph) blowing from the southeast. To examine the effect of wind on the currents, Sheng (1983) carried out a three-day simulation from September 20 using a uniform wind stress of 1 dyne/cm^2 from the southeast. As shown in Figure 75, the southeasterly wind caused water to pile up within the Mississippi Sound at (I,J)=(22,62), outside Pascagoula Harbor along the northern shore. The wind resulted in a set-up of 0.4 ft. The wind set-up at (I,J)=(30,56), however, is only 0.2 ft. due to the shielding effect of the Horn Island.

The influence of wind on the current also depends on the location. Figure 76 shows the along-shore velocity at 2 locations over the 3-day period. At (I,J) = (33,28), off Cat Island, the presence of the wind did not have an appreciable effect on the tidal current. At (I,J) = (26,88), within the pass between the Mississippi Sound and the Mobile Bay, the wind caused significant flow from the Mobile Bay into the Sound. This resulted in a significantly larger bottom shear stress, which leads to the reduction in the amplitude of the tide-driven currents. For detailed information on this application, the reader is referred to Sheng (1983).

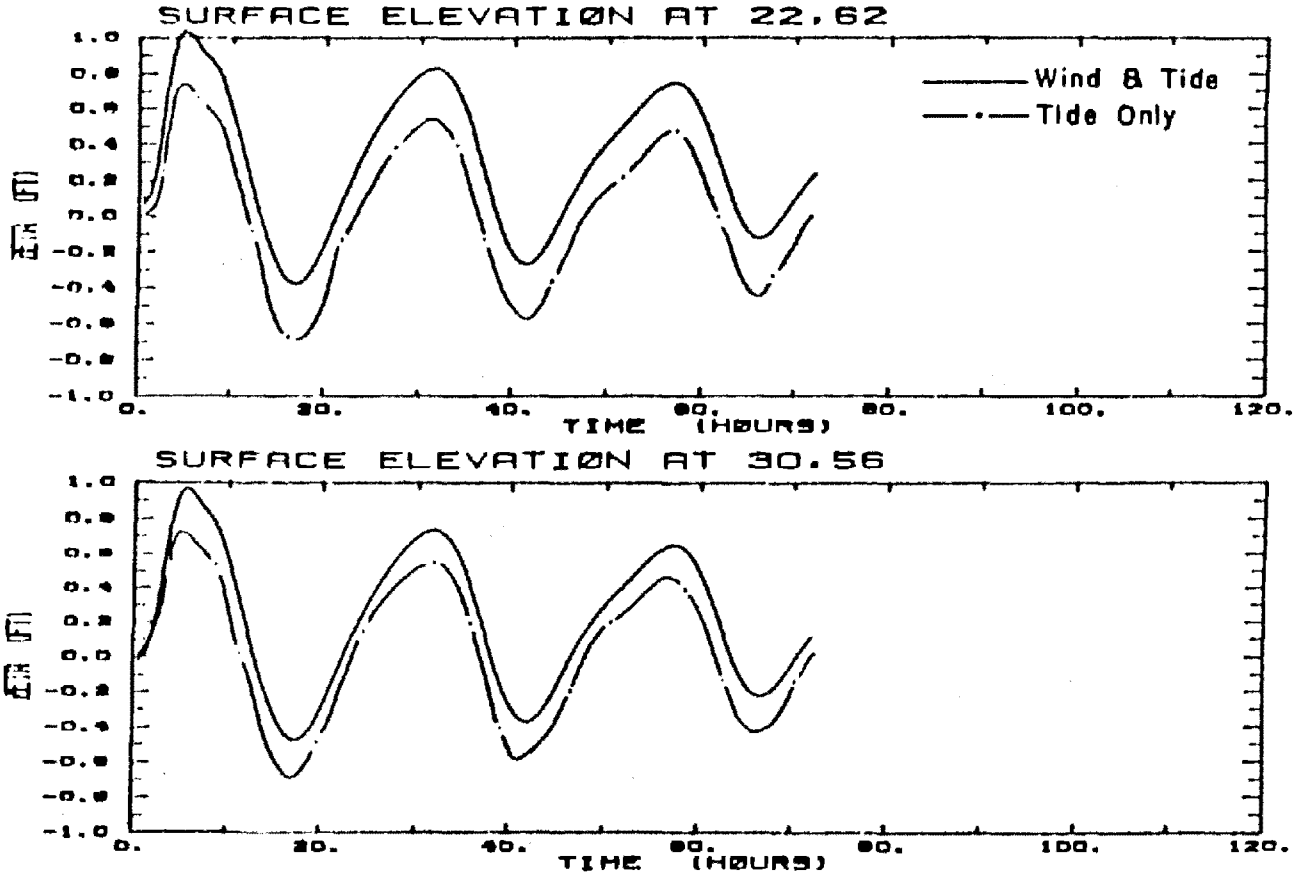

FIGURE 75. Influence of Wind on Surface Displacements at Two Stations from 9/20/80 to 9/24/80.

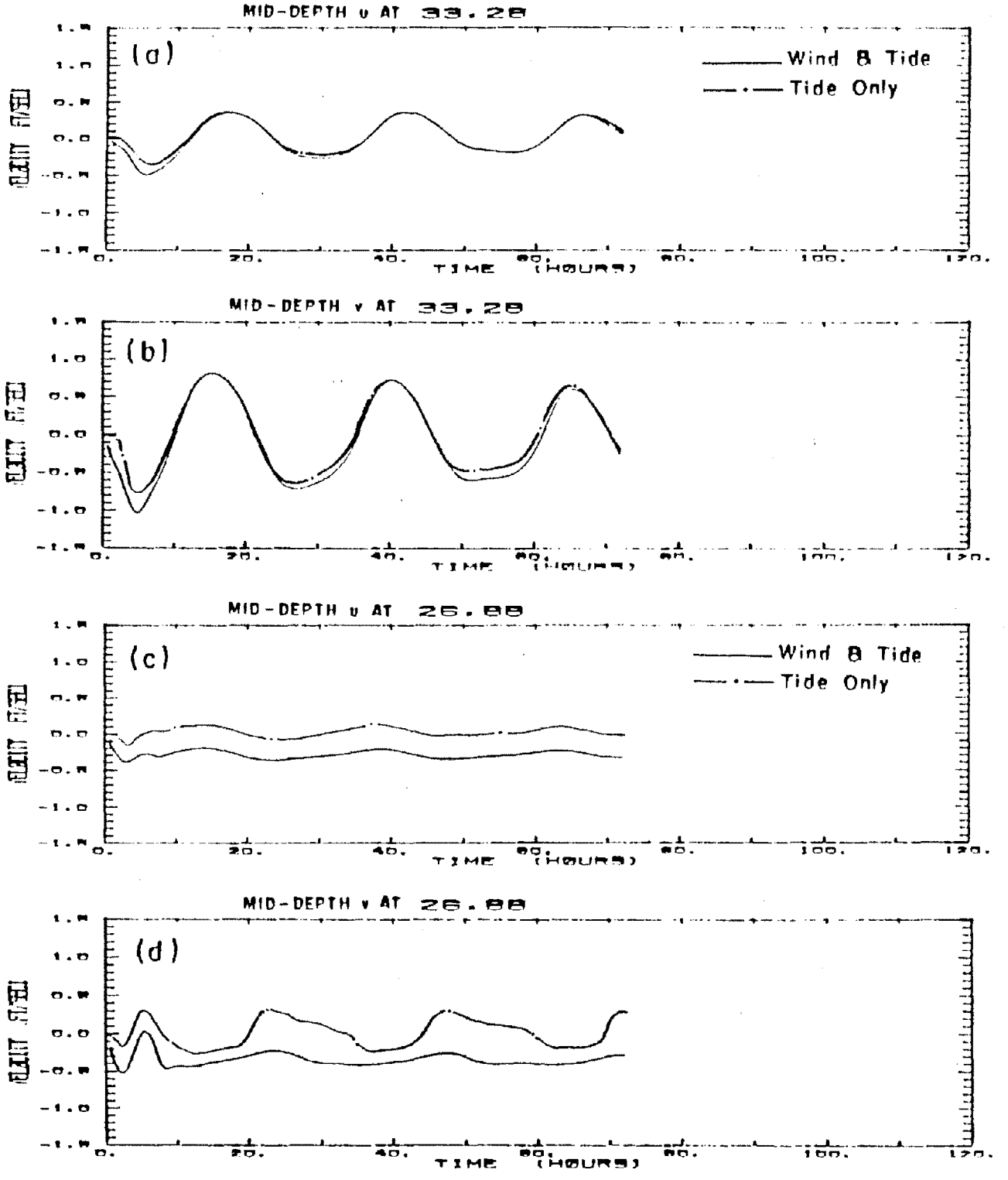

Figure 76. Influence of Wind on Mid-depth Horizontal Velocities at Two Stations from 9/20/80 to 9/24/80.

SECTION 5

HYDRO3D PROGRAMMER'S GUIDE

5.1 OVERVIEW

This section of the manual provides information for the operation of the program on a computer system such as the Digitial Equipment Corporation VAX. This section will also explain the various subroutines in the model which should facilitate modification of the program for specific application and design of a specialized input/output by adding new modules. A description of to the programming aspects of the code will also help users in linking the hydrodynamic program to water quality modeling packages.

5.2 HARDWARE AND SOFTWARE REQUIREMENTS

At this time, the model is operational only on the DEC VAX computer systems. The program modifications and test runs have been done on the VAX and therefore the model operations on the VAX system are described here. The program code is written in VAX FORTRAN 77 and requires about 3000 blocks of hard disk storage, which increases proportionately with the 2-D or 3-D mode of operation and the length of simulation time. For output in the graphic forms the CA-DISSPLA graphic software package is used.

5.3 INSTALLATION AND IMPLEMENTATION

Although the program is designed for operation on a VAX computer system, it can be run with some modifications on other computer systems that support the VAX FORTRAN programming language. For VAX operation, the supplied program on tape must be installed on the computer system according to the instructions in the README file accompanying the program codes. The executable code should then be tested with the sample input file supplied with the model and the output compared with the sample output file to ensure that the program is installed properly on the computer system. If it is desired to modify the program or add extra subroutines to perform specialized calculations, then the source code must be re-compiled after the modification and linked before it can be used in performing hydrodynamic simulations.

5.4 DESCRIPTION OF THE COMPUTER PROGRAM

The model consists of 64 subroutines which enable the code to perform various tasks in a structured fashion. These subroutines facilitate

the input of data to the program, perform the mathematical calculations, and output the simulation results in either numerical or graphical form. The main routine supervises the overall model operation. It opens input files, calls subroutines, closes input files and opens output files. For graphical presentation of the simulation results the software package DISSPLA is used. The graphical outputs are the basin topography, temporal and spatial variation of velocities, elevations, temperature, and salinity. Figure 77 illustrates the functional relationships among the different modules of the program.

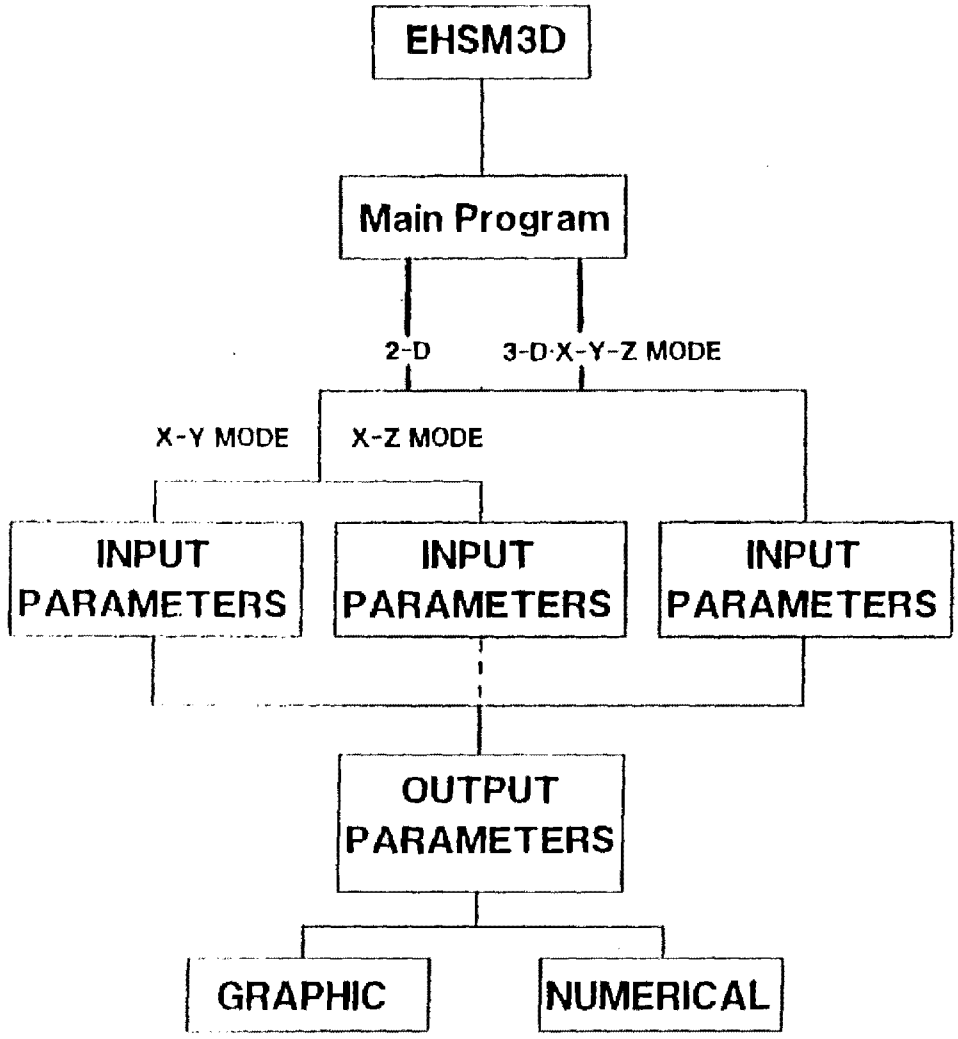

Figure 77. Operational Chart of the EHSM3D model.

5.5 SUBROUTINE DESCRIPTIONS

This section describes the characteristics of each individual subroutine of the HYDRO3D code.

EHSM3D : Main program that supervises the overall model simulation, as shown in the flowchart in the previous section.

EHSMAI : Sets the lateral turbulent eddy viscosities on the computational star used to compute the lateral diffusion terms of the horizontal (u) velocity in subroutine EHSMD4 (2-D runs only).

EHSMAJ : Sets the lateral turbulent eddy viscosities on the computational star used to compute the lateral diffusion terms of the horizontal (v) velocity in subroutine EHSMD4 (2-D runs only).

EHSMAS : Sets the lateral turbulent eddy diffusivities on the computational star used to compute the lateral diffusion terms of the water quality parameters in subroutine EHSMC4.

EHSMAU : Sets the lateral turbulent eddy viscosities on the computational star used to compute the lateral diffusion terms of the horizontal u velocity in subroutine EHSMB4(3-D runs only).

EHSMAV : Sets the lateral turbulent eddy viscosities on the computational star used to compute the lateral diffusion terms of the horizontal (v) velocity in subroutine EHSMB4(3-D runs only).

EHSMB3 : Advances the 3-D velocity fields. Using a vertically implicit scheme, the horizontal perturbation velocities (u',v') and computes. These are then combined with the horizontal vertically integrated velocities (U,V) to obtain the horizontal velocities (u,v). The continuity equation then is used to compute the vertical velocity on both the vertically stretched grid and the original grid.

EHSMB4 : Computes the explicit advection and horizontal diffusion terms of the momentum and vertically integrated momentum equations. These are then saved for use by EHSMB3 and EHSMFF for advancing the velocity fields (3-D runs only).

EHSMC4 : Computes the explicit advection and horizontal diffusion terms of the concentration, salinity or temperature equation. These are then saved for use by EHSMCN, EHSMSA or EHSMTE for advancing the fields (3-D runs only).

EHSMCN : Advances the concentration field using a vertically implicit scheme and the explicit terms computed by EHSMC4.

EHSMCS : Sets the field values on the computational star used to compute the explicit terms of the water quality parameters in subroutine EHSMC4.

EHSMCU : Computes the coefficients and inverts the matrix for advancing the water quality parameters.

EHSMD4 : Computes the explicit advection and horizontal diffusion terms of the vertically integrated momentum equations. These are then saved for use by EHSMFF for advancing the vertically averaged velocity fields (2-D runs only).

EHSMDE : Computes the water density field and the baroclinic pressure gradient terms for the horizontal momentum equations.

EHSMDP : Dumps step number information to a disk file (DUMP.TMP)when

switch-1 is sent while the program is running.

EHSMDT : Computes the individual parts of horizontal diffusion terms for EHSMB4, EHSMC4 and EHSMD4. Entry point EHSMDO computes the basic diffusion term. Entry point EHSMDF computes the higher order terms.

EHSMED : Computes the lateral turbulent eddy viscosity and diffusivity fields. This routine also computes the Richardson number, square-root of the turbulent energy and turbulent scale fields.

EHSMEX : Advances the external variables (surface elevation and vertically integrated velocities). The river flows, tidal conditions and wind stresses are first set. Then using a horizontally implicit scheme (implicit in the x direction only) the surface elevation is partially advanced. From this the vertically integrated u velocity is advanced. Then using a similar horizontally implicit scheme (implicit in the y direction) the advance of the surface elevation is completed. From this the vertically integrated v velocity is advanced.

EHSMEZ : Computes the lateral turbulent eddy viscosity or diffusivity for a given water column (called by EHSMED).

EHSSFF : Computes the explicit terms for the x- and y-sweeps of the surface elevation equation (called by EHSMEX).

EHSMPN : A subroutine composed of functions CONCEN and DIFFUS, which provide values of concentration and diffusion coefficient at grid points according to grid indices MS and NS.

EHSMGA : Tridiagonal matrix inversion routine called by EHSMCU and EHSMZS.

EHSMGR : Generates a printer plot of 2-D or 3-D field.

EHSMHC : Supervises the computation of the hydrodynamic variables(surface elevation, vertically integrated velocities, velocities, salinity and temperature).

EHSMHR : Reads the hydrodynamic variables (surface elevation,vertically integrated velocities, velocities, salinity and temperature) from disk. Used to compute concentration fields from a previously made run.

EHSMIF : Provides the initial 2-D and 3-D fields at the beginning of a run.

EHSMIH : Initializes the bottom topography fields at the beginning of a run.

EHSMII : Initializes the index fields at the beginning of a run.

EHSMIN : Supervises the input and initialization of the fields.

EHSMIR : Reads the input parameters.

EHSMIS : Initialize the salinity field based on quadratic interpolation of salinity data at up to 10 stations.

EHSMPT : To initialized temperature field based on quadratic interpolation.

EHSMIT : Computes individual advection terms for subroutines EHSMB4, EHSMC4 and EHSMD4.

EHSMIW : Outputs input parameters and initial fields.

EHSMMI : Matrix inversion routine for momentum equations (called by EHSMB3).

EHSMND : Computes nondimensional parameters and normalizes initial fields.

EHSMOT : Output routine. This routine supervises the output and checks for

run termination. If variable time steps are used this routine computes the maximum change of the controlling variables and the maximum Courant number and adjusts the time step accordingly.

EHSMRF : Reads the 2-D and 3-D fields from disk then restarting a run.

EHSMRI : Computes the river flows and advances velocity and salinity fields at river points (called by EHSMEX).

EHSMRS : Computes velocity and bottom stress residuals in the output routine.

EHSMSA : Advances the salinity field using a vertically implicit scheme and the explicit terms computed by EHSMC4.

EHSMSB : Computes salinity value at the open boundaries using a linear time interpolation.

EHSMSC : Controls the smoothing of fields. This routine may be called by EHSMED to smooth the lateral turbulent eddy viscosities and diffusivities (KSMALL. NE. 0) or by ENSMOT to smooth the velocity fields (ISPAC(8). NE. 0) and/or the water quality parameters (ISPAC(2). NE. 0).

EHSMBT: Computes temperature values at the open boundaries using a linear time interpolation.

EHSMSE : Sets the surface elevations and depths for all computational stars. This routine is called by most routines that need the surface elevation or depth when ISMALL = 1.

EHSMSM : 1-D spatial smoother routine (called by EHSMSC).

EHSMSS : Routine called by EHSMOT to check for steady state.

EHSMTB : Computes the bottom stress (called by EHSMFF).

EHSMTD : Computes the tidal surface elevations and advances the surface elevation field on tidal points (called by EHSMEX).

EHSMTE : Advances the temperature field using a vertically implicit scheme and the explicit terms computed by EHSMC4.

EHSMTP : Generates test output (ITEST flag).

EHSMU4 : Computes u velocity at v points (contains EHSMV4 to compute v velocities at u points, and EHSMW4 to compute v velocities at w points).

EHSMVI : Sets the velocities on the computational star used to compute the advection and lateral diffusion terms of the horizontal u velocity in subroutine EHSMD4 (2-D runs only).

EHSMVJ : Sets the velocities on the computational star used to compute the advection and lateral diffusion terms of the horizontal v velocity in subroutine EHSMD4 (2-D runs only).

EHSMVS : Sets the velocities on the computational star used to compute the advection terms of the water quality parameters in subroutine EHSNC4.

EHSMVU : Sets the velocities on the computational star used to compute the advection and lateral diffusion terms or the horizontal u velocity in subroutine EHSMB4 (3-D runs only).

EHSMVV : Sets the velocities on the computational star used to compute the advection and lateral diffusion terms of the horizontal v velocity in subroutine EHSMB4 (3-D runs only).

EHSMW3 : Generates numerical printout of 3-D fields.

EHSMWR : Generates numerical printout of 2-D fields.

EHSMWS : Reads surface wind stress from disk and interpolates the

surface wind stress field (called by EHSMEX).

EHSMWW : Computes the vertical velocity field from the continuity equation (called by EHSMB3).

EHSMXX : This is the external routine name called to set surface elevations and depths. If ISMALL = 0 then EHSMXX is EHSMZE else it is EHSMSE.

EHSMXY : Computes x and y grids if not read from disk.

EHSMZE : Sets the depths for all computational stars. This routine is called by most routines that need the depths when ISMALL = 0.

EHSMZS : Computes the matrix coefficients for the surface elevation equation, inverts the matrix, sets new surface elevation and computes new vertically integrated velocity field (called by EHSMEX). In addition to the above subroutines of the HYDRO3D code, the following programs are used to generate the depth arrays and the various grid indices:

DEPTH_FILE_CREATE : This program reads the depths at the corner points of the grid lines and creates the 3 depth arrays for the U, V and ζ points.

INDEX_FILE_CREATE : This program reads the depth file created by DEPTH_FILE_CREATE and produces the grid indices NS, MS, JU1, JU2, JV1, JV2, IU1, IU2, IV1, and IV2.

5.6 INPUT/OUTPUT UNITS

Unit 4 - This is the main input file providing the essential input information via formatted card images that are described in detail in Section 2.

Unit 6 - This is the file containing the major printouts.

Unit 8 - This is a formatted sequential input/output file which stores the surface displacements, vertically-integrated velocities and three-dimensional velocities at selected stations and time intervals. It is created in EHSMOT by:

```
    WRITE(8,911) TIME,IT
911 FORMAT (1PE13.6, 0PI13)
    WRITE(8,912) (S(JST(I),IST(I)), I=1,NSTA)
    WRITE(8,912) (UI(JST(I),IST(I), I=1,NSTA)
    WRITE(8,912) (VI(JST(I),IST(I), I=1,NSTA)
912 FORMAT (1P10E13.6)
    DO 10120 KZ=1,KM
    WRITE(8,912) (U(KZ,JST(I),IST(I)),I=1,NSTA)
    10120 CONTINUE
    DO 10130 KZ=1,KM
    WRITE(8,912) (V(KZ,JST(I),IST(I)),I=1,NSTA)
    10130 CONTINUE
```

Unit 11 - This input file contains the variable bottom topography provided by the user. It is an unformatted sequential file containing HU, HV, and HS each dimensioned as (JM, IM). It is read in EHSMIR by:

```
READ (11) HU,HV,HS.
```

This unit is required if IBTM=3 (IBTM is used in input file).

Unit 12 - This is an unformatted sequential output file containing the grid parameters NS, MS, JU1, JU2, JV1, JV2, IU1, IU2, IV1, and IV2. It is read in EHSMII by:

```
READ(12) NS,MS
READ(12) JU1,JU2,JV1,JV2
READ(12) IU1,IU2,IV1,IV2
```

Unit 13 - This is an unformatted sequential file that stores the major species concentration data at desired time instants. It is created in EHSMDT by:

```
WRITE(ICONC)TIME,IT,FNAME(5),FNAME(6),IM,JM,KM,XREF,
ZREF,UREF,COR
WRITE(ICONC) XS,XU,YS,YV,HU,HV,HS
WRITE(ICONC) C
```

Unit 14 - This file contains user-generated non-uniform grid when IGRID=1. It is created by

```
WRITE(14) XU
WRITE(14)YV
```

Unit 16 - This is a formatted sequential file that contains the run number and two indices needed for restarting a run:

Unit 18 - This is a formatted sequential file that stores the salinity at selected stations and time intervals. It is created in EHSMOT by:

```
WRITE(18,911) TIME,IT
DO 10140 KZ = 1,KM
WRITE(18,912) (SA(KZ,JST(I),IST(I)), I=1,NSTA)
10140 CONTINUE
```

Unit 20 - This is the sequential file that contains the river inflow data at selected time instants. It is read in EHSMRI by:

```
DO N = 1,NRIVER
READ(20,*) IDAY,IHOUR,URIVER(N),VRIVER(N)
END DO
```

Unit IRD - This is an unformatted sequential file that contains all the necessary information when initiating or restarting the run. The structure of this file can be found in subroutine EHSMRF.

Unit IW - This is an unformatted sequential file that stores the major flow output data at desired time instants. The structure of this file is similar to that of unit IRD file and is created in subroutine EHSMOT by:

```
WRITE(IW)TIME,IT,FNAME(3),FNAME(4),IM,JM,KM,
XREF,ZREF,UREF,COR,AVO
WRITE(IW) XS, XU, YS, YV, HU, HS, FMU, FMV, FMS, FMSV
WRITE(IW) U, V, W, WW
WRITE(IW) UI, VI
WRITE(IW) S
WRITE(IW) T
WRITE(IW) SA
WRITE(IW) GA,GB
WRITE(IW) TBX,TBY
WRITE(IW) QQQ, SL
```

Unit IWS - This is the output file for storing residual flow data and contains the same variable groups as the unit IRD and IRW files.

Unit IR4 - This is the sequential file that contains the wind stress field at selected time instants.

SECTION 6

CONCLUSIONS AND RECOMMENDATIONS

This report documents existing and developing programmatic needs in the U.S. EPA for a stratified flow model to simulate complex flows in lakes, estuaries, harbors, and coastal waters. This model is needed to assist in ecological assessments, risk assessments, and exposure predictions for dissolved and sediment-bound contaminants. The model is needed for estuary studies to support the National Estuary Studies and wasteload allocations. There is a need to assist in the clean up of contaminated sediments in the Great Lakes and other lakes. A number of research programs ranging from oil spill initiatives to investigation of the effect of global climate change could benefit from a simulation tool designed to determine circulation and transport in lakes, estuaries, and near coastal marine waters.

To meet these well defined needs, the U.S. EPA Environmental Research Laboratory located at Athens, Georgia, has worked cooperatively with others to document the hydrodynamics model, HYDRO3D. This model is a dynamic three dimensional circulation model. The model simulates water circulation, dissolved solids or salinity, water temperature, and a dissolved species concentration. The model will also be used with the SED3D sediment resuspension and dispersion model due to be completed in FY 1991 (see Preface).

HYDRO3D has been tested in a number of estuaries and lakes. In this documentation, the model is used to simulate diverse water bodies that include Prince William Sound in Alaska, Suisun Bay of the San Francisco Bay, Charlotte Harbor in Florida, Green Bay of Lake Michigan, and the Mississippi Sound in the Gulf of Mexico. In addition, these illustrative examples and other hypothetical cases are reviewed to demonstrate the validity of the code and the flexibility of the program to simulate different conditions.

This documentation provides other important elements to aid the user as well as establishing the validity and flexibility of the program. This report reviews the data required, and the form that the data must be transformed into. It reviews the structure of the program and provides information about the derivation of the governing equations that form the basis of the model. From all of this, one can conclude that a useful and necessary tool is available to support U.S. EPA studies and other environmental investigations.

It should be noted, however, that this is a complex model that may require assistance beyond that available in the manual. It is recommended that potential users, including program managers and applications experts, consult the Introduction (Section 1) and introduction to the major sections for guidance on how best interpret and use this document. For further assistance, contact the Center for Exposure Assessment Modeling (CEAM). CEAM

can assist in the design of studies involving stratified flows, aid in the development of data collection programs, and provide expert assistance in implementing and interpreting the results for Superfund investigations and a number of other different types of studies.

REFERENCES

Ambrose, R.A., T.A. Wool, J.P. Connolly, R. W. Schanz, 1988. WASP4, A Hydrodynamic and Water Quality Model--Model Theory, User's Manual, and Programmer's Guide, EPA/600/3-87/039, U.S. Environmental Protection Agency, Athens, Georgia.

Ambrose, R.A., Jr., and J.L., Martin, 1990. Techmical Guidance Manual for Performing Waste Load Allocations, Book III: Estuaries, Part 1, Estuaries and Waste Load Allocation Models, U.S. EPA, Office of Water, Washington, D.C.

Ambrose, R.A., Jr., Martin, J.L., and McCutcheon, S.C., 1990, Technical Guidance Manual for Performing Waste Load Allocations, Book III: Estuaries, Part 2, Application of Estuarine Waste Load Allocation Models, U.S. EPA, Office of Water, Washington, D.C.

ASCE Task Committee on Turbulence Models in Hydraulics Computations, 1988. Turbulence modeling of surface water flow and transport: Parts I to V, *Journal of Hydraulics Engineering*, American Society of Civil Engineers, 114(9), 970-1073.

Bird, R.B., R.C. Armstrong, and O. Hassager, 1977. *Dynamics of Polymeric Liquids, Vol. 1, Fluid Mechanics*, Wiley, New York.

Blumberg, A. F. 1975. A Numerical Investigation into the Dynamics of Estuarine Circulation. Chesapeake Bay Institute Report No. 91, Baltimore MD.

Blumberg, A.F., 1986. Turbulent Mixing Processes in Lakes, Reservoirs, and Impoundments, in *Physics-Based Modeling of Lakes, Reservoirs, and Impoundments*, W.G. Grey, ed., American Society of Civil Engineers, New York.

Bowden, K. F. and P. Hamilton. 1975. Some Experiments with a Numerical Model of Circulation and Mixing in a Tidal Estuary. *Est. Coastal Mar. Sci.*, 3, 281.

Bowie, G.L, W.B. Mills, D.B. Porcella, C.L. Campbell, J.R. Pagenkopf, G.L. Rupp, K.M. Johnson, P.W.H. Chan, and S.A. Gherini, 1985. Rates, Constants, and Kinetics Formulations in Surface Water Quality Modeling, 2nd Edition, EPA/600/3-85-040, U.S. Environmental Protection Agency, Athens, Georgia.

Butler, H. L. 1978. Coastal Flood Simulation in Stretched Coordinates. Proc. 16th Coastal Engineering Conference, ASCE, Hamburg, Germany.

Chapra, S.C., and K.H. Reckhow, 1983. *Engineering Approaches for Lake Management, Volume 2: Mechanistic Modeling*, Butterworth Publishers, Boston.

Cheng, R. T., and T. J. Conomos, 1980. Studies of San Francisco Bay by the U.S. Geological Survey, *Institute of Environmental Sciences Proceedings*, 299-303.

Cheng, R. T., and J. W. Gartner, 1984. Tides, Tidal and Residual Currents in San Francisco Bay, California - Results of Measurements, 1979-1980. 5-Part Report, U. S. Geological Survey Water Resources Investigation Report 84-4339.

Cheng, R.T., T.M. Powell and T.M. Dillon, 1976. Numerical Models of Wind-Driven Circulation in Lakes, *Appl. Math. Modeling* 1, 141-159.

Conomos, T. J. and others. 1978. Field and Modeling Studies of San Francisco Bay. Coastal Zone '78 Proceedings, ASCE.

Cox, R. A. and others. 1967. The Electrical Conductivity/Chlorinity Relationship in Natural Seal Water. *Deep-Sea Research*, 14, 203-220.

Csanady, G.T., 1975. Hydrodynamics of Large Lakes, *Ann. Rev. Fluid Mech.*, 7, 357-386.

Doneker, R.L., and G.H. Jirka, 1988. CORMIX1: An Expert System for Mixing Zone Analysis of Convential and Toxic Single Port Discharges, U.S. EPA Report EPA/600/3-88/013, Athens, Georgia.

Ekeart, C., 1958. Properties of Water, Part II. The Equation of State of Water and Sea Water at Low Temperature and Pressure, *American Journal of Science*, 256, 225-240.

Fischer, H.B., List, E.J., Koh, R.C.Y., Imberger, J., and Brooks, N.H., 1979. Mixing In Inland and Coastal Waters, Academic Press, New York.

Goldstein, S., 1960. *Lectures on Fluid Mechanics*, Interscience London.

Grey, W.G., ed., 1986. *Physics-Based Modeling of Lakes, Reservoirs, and Impoundments*, American Society of Civil Engineers, New York.

Hansen, K.W., 1974. Calculation of Normal Modes for the American Mediterranean Seas, Technical Report No. 26, University of Chicago.

Heaps, N.S., C.H. Mortimer, and E.J. Fee, 1982. Numerical Models and Observations of Water Motion in Green Bay, Lake Michigan. *Phil. Trans. Royal Society of London*, Series A, 306, 371-398.

Henderson-Sellers, B., 1982. A simple formula for vertical eddy diffusion coefficients under conditions of non-neutral stability, *Journal of Geophysical Research*, American Geophysical Union, 87(C8), 5860-5864.

Henderson-Sellers, B., 1984. *Engineering Limnology*, Pitman, London.

Hinze, J.O., 1959. *Turbulence*, 2nd Ed., McGraw-Hill , New York.

Jirka, G.H., 1982. Multiport Diffusers for Heat Disposal - A Summary, *American Society of Civil Engineers Journal of the Hydraulics Division*, Vol. 108.

Johnson, B., Y.P. Sheng, K. Kim, and R. Heath, 1989. Development of a Three Dimensional Hydrodynamic Model of Chesapeake Bay, Proceedings of the American Society of Civil Engineers Conference on Estuarine and Coastal Modeling, M.L. Spaudling and J.C. Swanson, Eds., American Society of Civil Engineers, In Press.

Kent, R. E., and D. W. Pritchard, 1959. A Test of Mixing Length Theories in a Coastal Plain Estuary, *J. Mar. Res.*,18, 62-72.

Kinnetics Laboratories, Inc., 1981. In-Site Field Data Gathering Stations San Francisco-Delta Salinity Intrusion With Navigation Channels. KLI-81-1, Final Report to San Francisco District, U. S. Army Corps of Engineers.

Lai, C., Flows of Homogeneous Density in Tidal Reaches; Solution by Method of Characteristics, U.S. Geological Survey Open File Report, 1965.

Leendertse, J.J., and S.-K. Liu, 1975. A Three-Dimensional Model for Estuaries and Coastal Seas: Volume II, Aspects of Computation, Rand Corp., Report R-1764-OWRT, prepared for the Office of Water Research and Technology, U.S. Department of Interior, Santa Monica, California.

Lynch, D. R. and W.G., Gray, 1978. "Analytic Solutions for Computer Flow Model Testing" *Journal of the Hydraulics Division*, American Society of Civil Engineers, 1409-1428.

Lynch, D.R., 1986, Basic Hydrodynamic Equations for Lakes, in *Physics-Based Modeling of Lakes, Reservoirs, and Impoundments*, W.G. Grey, ed., American Society of Civil Engineers, New York.

McCormick, M.J., and Scavia, D., Calculation of vertical profiles of lake-averaged temperature and diffusivity in Lakes Ontario and Washington, *Water Resources Research*, 17(2), 305-310.

McCutcheon, S.C., 1983. Vertical mixing in models of stratified flow, in *Frontiers in Hydraulic Engineering*, Proceedings of the Hydraulics Specialty Conf., American Society of Civil Engineers, Cambridge, Mass. 15-20.

McCutcheon, S.C., 1989. *Water Quality Modeling, Volume I Transport and Surface Exchange in Rivers*, CRC Press, Inc., Boca Raton, Florida.

McCutcheon, S.C., D.-W. Zhu, Bird, S., 1990. Chapter 5 Model Calibration, Validation and Use, Technical Guidance Manual for Performing Waste Load Allocations, Book III: Estuaries, Part 2: Application of Estuarine Waste Load Allocation Models, Ambrose, R.A., Jr., Martin, J.L. and McCutcheon, S.C., Eds., U.S. Environmental Protection Agency. Office of Water, Washington, D.C.

Miller, G.S., and J.H. Saylor, 1985. Currents and Temperature in Green Bay, Lake Michigan, *J. of Great Lakes Res.*, 11(2), 97-109

Moldin, R., and A.M. Beeton, 1970. Dispersal of Fox River Water in Green Bay, Lake Michigan, Proceedings of Thirteenth Conference on Great Lakes Resources, International Assoc. Great Lakes Res., 468-476

Monin, A.S., and A.M. Yaglom, 1971. *Statistical Fluid Mechanics: Mechanics of Turbulence, Vol. I*, The MIT Press, Cambridge.

Munk, W. H. and E. P. Anderson. 1948. Notes on the Theory of the Thermocline, *J. Mar. Res.*, 1, 276-295.

Prandtl, L. 1925. Bericht uber untersuchungen zuraus-gebildete turbulenz, Zs, Angew. Math. Mech., 5(2), 136-139.

Patchen, R. C., and R. T. Cheng. 1979. Current Survey of San Francisco Bay by NOS/USGS, *EOS*, American Geophysical Union, 60, p. 843.

Platzman, G.W., 1972. Two-Dimensional Free Oscillations in Natural Basins, *J. Phys. Oceanography*, 2(2), pp. 117-130.

Reid, R.O., and R.E. Whitaker, 1981. Numerical Model for Astronomical Tides in the Gulf of Mexico, Vol. I: Theory and Application, Dept. Oceanography, Texas A & M University, College Station, TX.

Reynolds, A.J., 1974. *Turbulent Flows in Engineering*, A Wiley, London, New York.

Richardson, L.F., The supply of energy to and from atmospheric eddies, *Proceedings of the Royal Society*, Series A, 97, 354-373.

Roberts, P.J.W., 1979. Line Plume and Ocean Outfall Dispersion, *American Society of Civil Engineers Journal of the Hydraulics Division*, Vol. 105.

Rodi, W., 1980. *Turbulence Models and Their Application in Hydraulics*, International Association for Hydraulic Research, Delft, The Netherlands.

Rodi, W., 1984. Examples of turbulence model applications, in Simulation of Turbulence Models and Their Applications, Vol. 2, Collection de la Direction des Estudes et Recherches, Electricite de France, editions Eyrolles, Paris, France.

Schlichting, H., 1979, Boundary-Layer Theory, McGraw-Hill, New York.

Sheng, Y.P., 1975. Wind-driven Currents in Contaminant Dispersion in The Nearshore of Large Lakes, Ph.D. Dissertation, CASE Western Reserve University, Cleveland, OH.

Sheng, Y.P., 1980. Modeling Sediment Transport in Shallow Waters, *Estuarine and Wetland Processes with Emphasis on Modeling*, P. Hamilton and K.B. Mocdonald, Ed.s, Plenum Press, 299-337.

Sheng, Y.P., 1981. Modeling the Hydrodynamics and Dispersion of Sediments in the Mississippi Sound, Technical Report No. 455, Aeronautical Research Associates of Princeton, Princeton, NJ.

Sheng, Y.P., 1982. Hydraulic Applications of a Second-Order Closure Model of Turbulent Transport, in *Applying Research to Hydraulic Practice*, P. Smith, Ed., American Society of Civil Engineers, New York, 106-119.

Sheng, Y.P., 1982. A Review on LA-LB Harbor Study, Technical Memo No. 82-11, Aeronautical Research Associates of Princeton, Princeton, NJ.

Sheng, Y.P., 1983. Mathematical Modeling of Three-Dimensional Coastal Currents and Sediment Dispersion: Model Development and Application, Technical Report CERC-83-2, U.S. Army Corps of Engineers Waterways Experiment Station, Vicksburg, MS.

Sheng, Y.P., 1984. A Turbulent Transport Model of Coastal Processes, Proceedings 19th International Conference on Coastal Engineering, American Society of Civil Engineers, 2380-2396.

Sheng, Y.P., 1986a. A Three-Dimensional Hydrodynamic Model in Generalized Curvilinear Coordinates, Technical Report 587, Aeronautical Research Associates of Princeton, Princeton, NJ.

Sheng, Y.P., 1986b. Finite Difference Models for Hydrodynamic Lakes and Shallow Seas, in *Physics-Based Modeling of Lakes, Reservoirs, and Impoundments*, W.G. Grey, ed., American Society of Civil Engineers, New York.

Sheng, Y. P., 1987. On Modeling Three-Dimensional Estuarine and Marine Hydrodynamics, in *Three-Dimensional Models of Marine and Estuarine Dynamics*, J. C. J. Nihoul and B. M. Jamart, Eds., Elsevier, 35-54.

Sheng, Y.P. and W. Lick, 1979. The Transport and Resuspension of Sediment in a Shallow Lake, *Journal of Geophysical Research*, Vol. 84, pp. 1809-1826.

Sheng, Y. P. and W. Lick. 1980. A Two-Node Free-Surface Numerical Model for the Three-Dimensional Time Dependent Current in Large Lakes, U.S. Environmental Protection Agency, Duluth MN., EPA-600/3-80-047, 62.

Sheng, Y. P., W. Lick, R. T. Gedney, and F. B. Molls. 1978. Numerical Computation of Three-Dimensional Circulation in Lake Erie; A comparison of a Free-Surface Model and a Rigid-Lid Model, *J. Phys. Oceanography*, 8, 713-27.

Sheng, Y. P., and H. Butler, 1982. Modeling Coastal Currents and Sediment Transport, Proc. 18th Coastal Engineering Conference, American Society of Civil Engineers Capetown, South Africa, pp. 1127-1148.

Sheng, Y.P. and S.S. Chin, 1986. Tropical Cyclone Generated Currents, Proc. of the 20th International Conference on Coastal Engineering, American Society of Civil Engineers, 737-751.

Sheng, Y. P., S.F. Parker and D.S. Henn. 1986. A Three-Dimensional Estuarine Hydrodynamic Software Model (EHSM3D), Aeronautical Research Associates of Princeton, Inc. Princeton, NJ 08543-2229.

Sheng, Y.P., J.K. Chou and A.Y. Kuo, 1989a, Three Dimensional Numerical Modeling of Tidal Circulation and Salinity Transport in James River Estuary, Proceedings of the American Society of Civil Engineers Conference on Estuarine and Coastal Modeling, M.L. Spaudling and J.C. Swanson, Eds., American Society of Civil Engineers, In Press.

Sheng, Y.P., H.K. Lee and K.H. Wang, 1989b. On Numerical Strategies of Estuarine and Coastal Modeling, Proceedings of the American Society of Civil Engineers Conference on Estuarine and Coastal Modeling (M.L. Spaudling and J.C. Swanson, Eds.), American Society of Civil Engineers, In Press.

Sheng, Y.P., V. Cook, S. Peene, D. Eliason, P.F. Wang and S. Schofield, 1989c, A Field and Modeling Study of Fine Sediment Transport in Shallow Waters, Proceedings of the American Society of Civil Engineers Conference on Estuarine and Coastal Modeling, M.L. Spaudling and J.C. Swanson, Eds., American Society of Civil Engineers, In Press.

Shureman, P., 1941. Manual of Harmonic Analysis and Prediction of Tides. U.S. Department of Commerce, Coast and Geodetic Survey, Special Pub. No. 98.

Smith, P.E. and R.T. Cheng, 1989. Recent Progress on Hydrodynamic Modeling of San Francisco Bay, Proceedings of the American Society of Civil Engineers Conference on Estuarine and Coastal Modeling, M.L. Spaudling and J.C. Swanson, Eds., American Society of Civil Engineers, In Press.

Smith, R. A., 1980. Golden Gate Tidal Measurements, 1854-1978. *ASCE J. of Waterways, Port, Coast and Ocean Division*, 106, WW3, pp. 401-410.

Tennekes, H. and J.L. Lumley, 1972. *A First Course in Turbulence*, The MIT Press, Cambridge. Mass.

Turner, J.S., 1973. *Buoyancy Effects in Fluids*, Cambridge University Press.

U.S. EPA, 1985. Technical Support Document for Water Quality-based Toxics Control, Office of Water, Washington, D.C.

White, F.M., 1974. *Viscous Fluid Flow*, McGraw-Hill, New York.

Wright, S.J., 1977. Mean Behavior of Buoyant Jets in a Crossflow, *American Society of Civil Engineers Journal of the Hydraulics Division*, Vol. 103.

Zakikhani, M., S. L. Bird, and S. C. McCutcheon, 1989. Hydrodynamic and Sediment Transport Modeling of Green Bay, Lake Michigan. Presented at 32nd Conference of International Association for Great Lakes Research, Madison, Wisconsin.

APPENDIX A

LIST OF SYMBOLS AND MAJOR VARIABLES

Symbol	FORTRAN label	Array Size	Definition
ζ	S	JM, IM	Surface Displacement
U	UI	JM, IM	Vertically-integrated velocity
V	VI	JM, IM	Vertically-integrated velocity
ρ	R, RU	KM, JM, IM	Density
A_v, K_v, D_v	GA, GB	KM, JM, IM	Vertical eddy coefficients
A_H, K_H, D_H	AH	JM, IM	Lateral eddy coefficients
u	U	KM, JM, IM	Velocity in x direction
v	V	KM, JM, IM	Velocity in y direction
ω	W	KM, JM, IM	Vertical velocity in ζ direction
w	WW	KM, JM, IM	Vertical velocity in Z direction
T	T	KM, JM, IM	Temperature
S	SA	KM, JM, IM	Salinity
C	C	KM, JM, IM	Species Concentration
h	HU,HV,HS	JM, IM	Depths
τ_{sx}, τ_{sy}	TX, TY	JM, IM	Wind Stresses
τ_{bx}, τ_{sy}	TBX, TBY	JM, IM	Bottom Stresses
x	XS, XU	IM	X Position of ζ and u points
y	YS, YV	JM	Y Position of ζ and v points
σ	Z, SG	KM	Z Position of u and w points
μ_x	FMS, FMU	IM	X-stretching coefficients at ζ and u points
μ_y	FMSV, FMV	JM	Y-stretching coefficients at ζ and v points

APPENDIX B

DERIVATION OF THE GOVERNING EQUATIONS FOR A σ-STRETCHED COORDINATE SYSTEM

The governing equations for hydrodynamics can be expressed in terms of the σ-stretched coordinates. The following is an illustration of the derivation for the continuity equation.

The continuity equation in σ stretched coordinates can be derived from the continuity equation in Cartesian coordinates (x,y,z), a definition of the σ coordinate system, and the chain rule of differentiation. The continuity equation in Cartesian coordinates (x,y,z) is:

$$\frac{\partial u}{\partial x} + \frac{\partial v}{\partial y} + \frac{\partial w}{\partial z} = 0 \tag{A-1}$$

The σ-stretched coordinate system is defined as follows:

$$\sigma(x,y,x;t) = \frac{z-\zeta(x,y;t)}{H(x,y;t)} \tag{A-2}$$

where $H(x,y;t) = h(x,y) + \zeta(x,y;t)$ is the total instantaneous water depth. The chain rule is:

$$\frac{\partial}{\partial y} = \frac{\partial}{\partial y} + \frac{\partial \sigma}{\partial y} \frac{\partial}{\partial \sigma} \tag{A-3}$$

$$\frac{\partial}{\partial y} = \frac{\partial}{\partial y} + \frac{\partial \zeta}{\partial y} \frac{\partial}{\partial \zeta} \tag{A-4}$$

$$w = \frac{dz}{dt}$$

$$w = \frac{d}{dt} \left(\zeta(x,y;t) + \sigma(x,y,z;t)\, H(x,y;t)\right)$$

$$w = H\omega + (1+\sigma)\frac{d\zeta}{dt} + \sigma\left(u\frac{\sigma h}{\sigma x} + \sigma\frac{\sigma h}{\sigma y}\right) \tag{A-5}$$

where

$$\omega = \frac{d\sigma}{dt} \tag{A-6}$$

Substituting Equations 2 through 6 into Equation 1, we obtain the continuity equation in the new coordinate system (x,y,ζ)

$$\frac{\partial \zeta}{\partial t} + \frac{\partial}{\partial x}(Hu) + \frac{\partial}{\partial y}(Hv) + \frac{H\partial \omega}{\partial \sigma} = 0 \tag{A-7}$$

Non-dimensionalization is based on the definition of the following nondimensional variables:

$$\begin{aligned} (x^*,y^*) &= (x,y)/x_r) \\ (u^*,v^*) &= (u,v)/u_r) \\ \omega^* &= \omega x_r/u_r \\ \zeta^* &= g\zeta/fu_r x_r \\ t^* &= tf \\ \beta &= \frac{gz_r}{f^2 x_r^2} \end{aligned} \tag{A-8}$$

Substituting Equation (A-8) into (A-7) yeilds the continuity equation in the non-dimensional form:

$$\frac{\partial \zeta}{\partial t} + \beta \frac{\partial Hu}{\partial x} + \beta \frac{\partial Hv}{\partial y} + \beta H \frac{\partial \omega}{\partial \zeta} = 0 \tag{A-9}$$

The Equation A-9 is the same as Equation 13 in Section 2.2.6 with $\mu_x = \mu_y = 1$. Following a similar approach, may obtain the non-dimensional forms of the momentum equations in the (x,y,σ) coordinates as given in Equations 14 to 17 in Section 2.2.6.

APPENDIX C

CHARACTERISTIC TIME SCALES OF VARIOUS PHYSICAL PROCESSES IN ESTUARIES

Physical Process	Time Scale	Order of Magnitude
Periodic Forcing	t_f	$1/w$
Convection	t_c	X_r/U_r
Inertia Oscillation	t_i	$1/f$
Vertical Turbulent Diffusion	t_{vdm}, t_{vdh}, t_{vds}	$Z_r^2, A_{vr}, Z_r^2/K_{vr}, Z_r^2/D_{vr}$
Lateral Turbulent Diffusion	$t_{\ell dm}$, $t_{\ell dh}$, $t_{\ell ds}$	$X_r^2/A_{Hr}, X_r^2/K_{Hr}, X_r^2/D_{Hr}$
Gravity Wave	t_{ge}	X_r/gZ_r
Internal Gravity Wave	t_{gi}	$X_r/\Delta\rho/\rho_o gZ_r$
Ekman Layer Diffusion	t_e	$Z_r/2f$

APPENDIX D

SAMPLE INPUT AND OUTPUT FOR THE SIMULATION OF WIND-DRIVEN CURRENTS IN AN ENCLOSED BASIN

In this appendix a sample input/output is described to be used to examine the code. This test example solves a wind-driven currents in an enclosed basin of 50 km x 50 km. The depths at the north and south are 3 meters and vary linearly to 10 meters at the central region of the basin. A uniform wind with speed of 9m/sec (1 dyne/cm^2) is blowing from east to west (toward the negative x-axis) 1 dyne/cm^2 starts blowing from a zero initial condition. The simulation stops after 24 hours. The domain is divided into 10 x 10 uniform grid cells in the horizontal plane. The local depth is divided into 5 layers with equal length. The vertical eddy viscosity is assumed to be constant and $5C_m^2$/sec. The boundary conditions at the lateral boundaries and bottom are assumed to be 'no slip' condition. Starting with the action of the east wind, the surface elevation reaches steady state within 24 hours (Figure 12). In this run the Coriolis effect is not considered and since the basin geometry is symmetrical, the responses of currents and surface elevation also exhibit symmetrical characteristics.

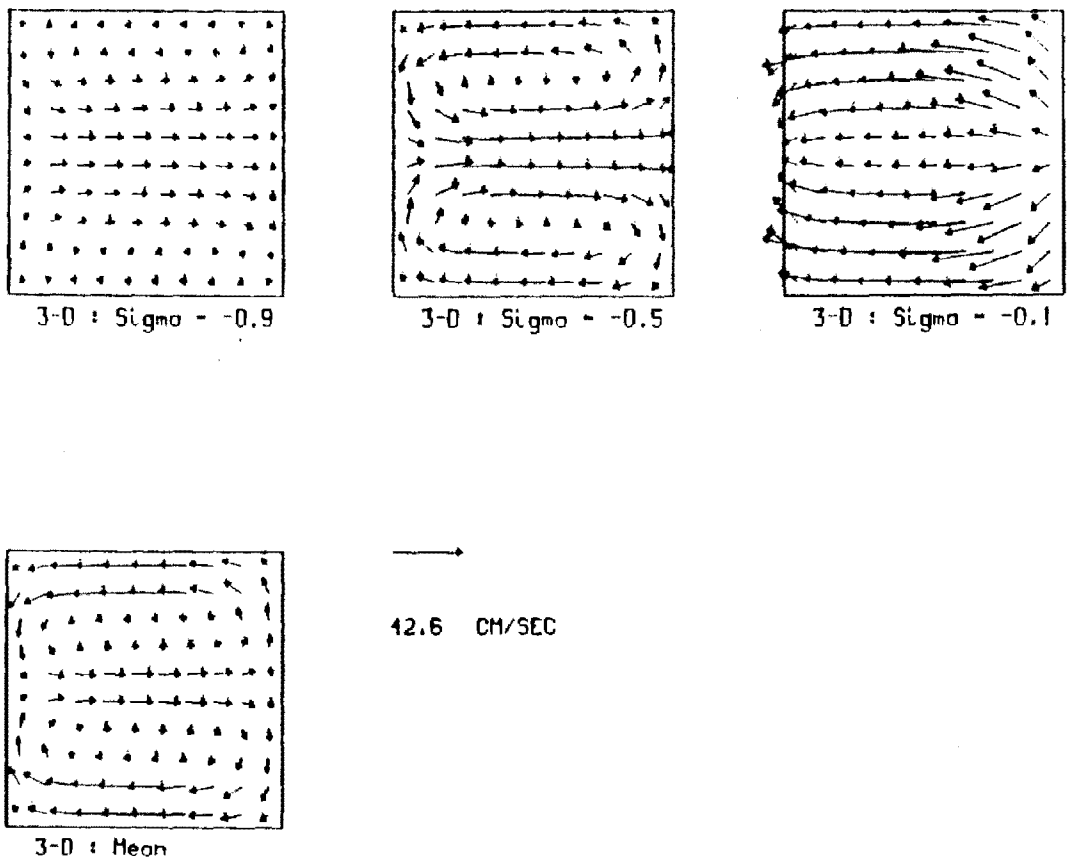

Figure 78. Steady-state Wide-driven currents in an enclosed square basin of 50 km on each side; linearly varying bottom from 3 m (South and North) to 10 m (at center)

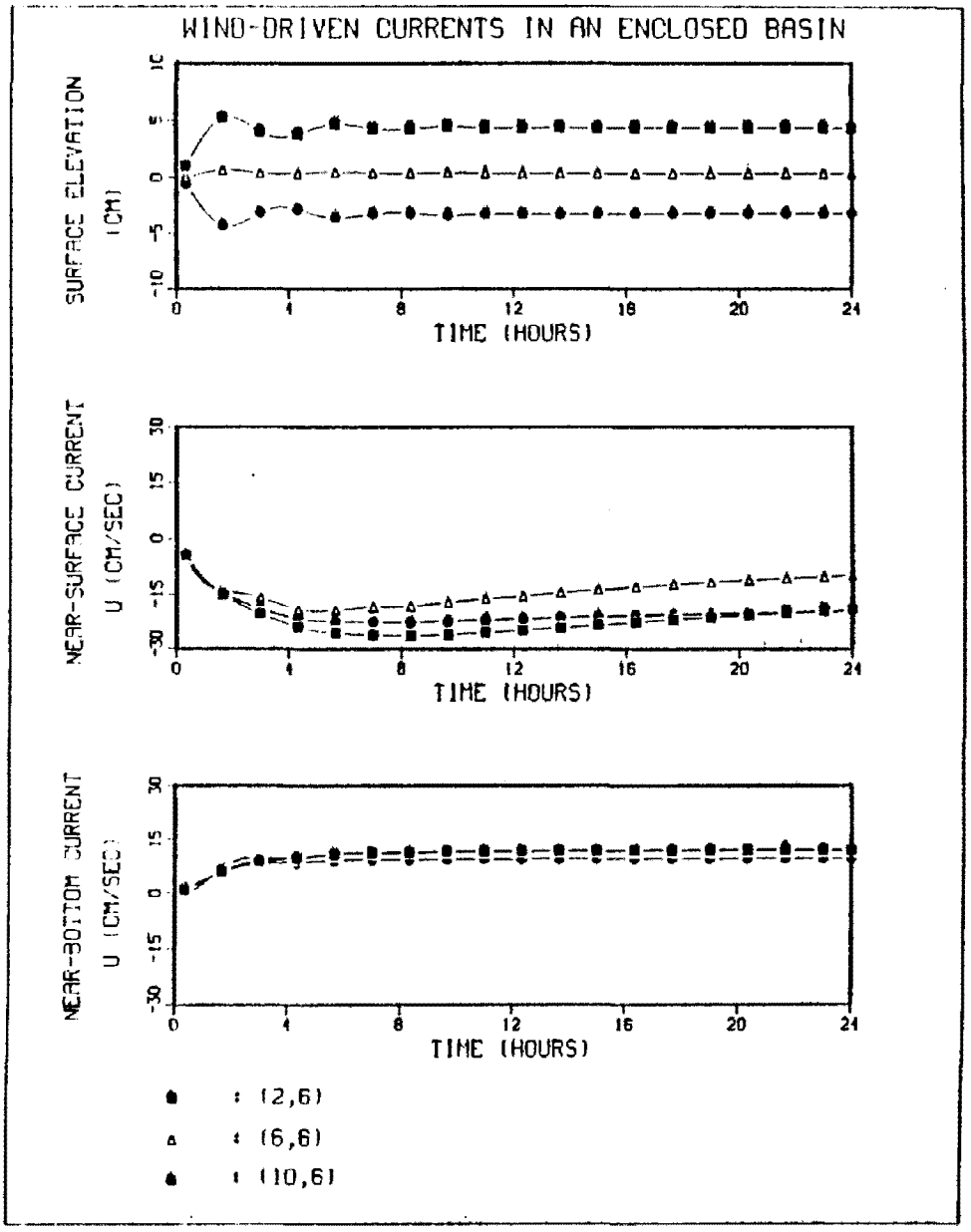

Figure 79. Three-dimensional simulation of wind-driven currents in an enclosed basin; results are for three grid points of (2,6), (6,6) and (10,6)

EXAMPLE INPUT DATA FILE

FOR AN ENCLOSED BASIN

```
#1 ISTART(I4),TITLE(A64)  ***TITLE CARD***
   0  3-D RUN FOR SAMPLE RUN WITH WIND=-1 DYNE/CM**2 (1 DAY)
#2   XREF       ZREF   UREF      COR      GR      RO0     ROR     T0   TR
*PHYSICAL CONSTANTS*
  1000000.    500.  10.    .00009  981.    1.  1.001    0.  20.
#3 IVLCY IFI IFA IFB IFC IFD ICC1(icon) ICC2(isal) ICC3(itemp)
ICC4(isedi)
     1    1   0   0   0   1   0           0           0
0
#4: BVR   S1    S2    PR   PRV   TWE    TWH   FKB   TQ0 **TEMPERATURE
PARAMETERS
     1.  0.    0.    1.    1.    0.    0.    5.    0.
#5:   IVER   ICON   IUBO   IBL   IBR   JBM   JBP   CREF   CMAX   C0
IC1IC2JC1JC2ID1ID2JD1JD2*CONCEN. PARAMETERS*
      2    4    0   1   26  1   29  1. 10000. 1. 0  0  0  0  0  0
0  0
#6: IEXP  IAV   AVR   AV1   AV2   AVM     AHR         ***TURBULENCE
PARAMETERS***
      0   0   5.   0.   0.   1.   10000.
#6A:  FM1   FM2   ZTOP   SLMIN  QQMIN

     -.5   -1.5   -.05     1.     .01

#6B: QCUT  ICUT  GAMAX  GBMAX  FZS  KSMALL

     .15      1   300.   300.  .10    0
#7: IWIND  TAUX  TAUY    ***WIND PARAMETERS***

      0     -1.   0.
#8:ISMALL IBTM ITB  HADD  HMIN  ZREFBN CTB   BZ1   H1   H2 **VERT
B.C.
      1     2   5    0.   1.    5.  .004   .4    .25   .75

#8A:ZREFTN TZ1 SSS0  ** MORE VERT B.C.**

       5.   .4  .0

#9: ITIDE IOPEN JWIND  IJLINE   ***LATERAL B.C. FLAGS***

       0   0000    0        0
#10: IJGAGE IJDIR IJROW IJSTRT IJEND ***IF(IJLINE.GT.0), FOR EACH
IJLINE***
#11   (1)   (2)   (3)   (4)   (5)   (6)   (7)   (8)   (9)   (10)
***ISPAC(I),I=1,10***
      0    0    0    -1   0    0    0    0    0     0
#12   (1)   (2)   (3)   (4)   (5)   (6)   (7)   (8)   (9)   (10)
***JSPAC(I),I=1,10***
      0    1   -1    0    0    0   0    1    0     0
#13   (1)   (2)   (3)    (4)    (5) (6)   (7)   (8)   (9)   (10)
***RSPAC(I),I=1,10***
     .020  .1  .00001 -.0001  0. .0   100.  1.  .25    4.

#14: ISTEP IT1 IT2 ITS DELT DELTMIN DELTMAX EPSILON BUFAC WTS WTU
WTV*TIMESTEP*
```

```
      0    1  144  1  600.    1.     900.   .075    10.    1.  1.
1.
#15: ITEST IP1 IP2 IP3 IPU IPW IPA IPB ID JPA JPB JD KPA KPB
KD**PRINTOUT INFO**
      3    72  72  72  1   1   1   11  1  1  11  1   1   5   4
#16: IGI IGH IGT IGS IGU IGW IGC IGQ IGL IGR IGRI IGTB**PRINTOUT
FORMAT FLAGS***
     1   1   1   1   1   1   1  -1   -1  -1   -1   -1
#17: IRD IW IWR ICI IWC ICO   ISED IWS IREAD IR4   ***DISCFILE
INFO***
     9  9  1   0   0    0   14   1    0    15

#18:    FNAME(6A4)                                        ***3    DISCFILE
NAMES(FLOWIN,FLOWOUT,CONCENTRATION)***
6_6_sal 6_6_sal 6_6_sal
#19:(1)    (2)    (3)    (4)    (5)    (6)    (7)    (8)    (9)    (10)
***TBRK(I),TIMEBREAKS***
    240.  -480. -480. -480. -480. -480. -480. -480. -480. -480.
#20: NSTA NRANGE NFREQ    ***TIMEFILE GAGE STATIONS***

      5     0       2
#21+:IST(K)    JST(K)    KST(K)    STATID(K)(3I4,A48)
***IF(NSTA.GT.0),STATION INFO***
   2   6   1
   4   6   1
   6   6   1
   8   6   1
  10   6   1
#22: NRIVER   ***NUMBER OF RIVERS***

  0
#22A:     IRIVER(K)  JRIVER(K)  LRIVER(K)  URIVER(K)  VRIVER(K)
***IF(NRIVER.GT.0)***
#23: (SAB(K),K=1,KM)**VERTICAL SALINITY PROFILE ALONG W,S,E,N (IF
ISALT.NE.0)**
#23A: NISS  **NUMBER OF STATIONS WITH INITIAL SALINITY DATA
#23B:(ISS(N),JSS(N),NDEPTH(N),TDEPTH(N),N=1,NISS)**I,J,NO.   OF
PTS,TOTAL DEPTH
#23C: (CONT'D) /  DEPTH  /  SALINITY  /
#24:  (TB(K),K=1,KM)     ***VERTICAL  TEMPERATURE  PROFILE  (IF
ITEMP.NE.0)***
#24A: NITT  **NUMBER OF STATIONS WITH INITIAL TEMPERATURE DATA
#24B:(ISST(N),JSST(N),NDEPTT(N),TDEPTT(N),N=1,NITT)*I,J,NO.OF
PTS,TOTAL DEPTH
#24C: (CONT'D) /  DEPTH  /  TEMPERATURE  /
#25:  (CB(K),K=1,KM)   ***VERTICAL  CONCENTRATION  PROFILE  (IF
ICC.NE.0)***
#25A: NISSS  **NUMBER OF STATIONS WITH INITIAL  CONC. DATA
#25B:(ISSS(N),JSSS(N),NDEPTHS(N),TDEPTHS(N),N=1,NISSS)*I,J,NO.OF
PTS,TOTAL DEPTH
#25C: (CONT'D) /  DEPTH  /  Dissolved CONC.  /
#26:    NCG    NCONST    XYR    XMONTH    XDAY    XHR    XMIN*TIDAL
PARAMETERS(ITIDE.NE.1 SKIP 27THRU30)
      0    1     82     7   20   14   5
```

```
#26A:   (NCST(I),I=1,NCONST)          ***INDEX   NUMBER   OF   TIDAL
CONSTITUENTS***
#26B: KNGAGE(J)    H0(J)    XLONG(J)(*)   ***IF NCG>0,READ 28,29,30
FOR J=1,NCG***
#27: (AMP(I,KNGAGE(J)),I=1,NCONST)   ***TIDAL AMPLITUDES***

#28: (XKAPPA(I,KNGAGE(J)),I=1,NCONST)   ***TIDAL PHASES***

#29 : (TP(I),I=1,NCONST)        ***TABULAR TIDE DATA***

#30: J NC AMPW(J,NC) PHW(J,NC) CAW(J,NC) AMPE(J,NC) PHE(J,NC)
CAE(J,NC)
#31: I NC AMPS(I,NC) PHS(I,NC) CAS(I,NC) AMPN(I,NC) PHN(I,NC)
CAN(I,NC)
#32: NBAR  ***NUMBER OF THIN-WALL BARRIERS***

      0

#32A: IJBDIR(I),IJBROW(I),IJBSTR(I),IJBEND(I) ***IF NBAR.GT.0, FOR
EACH NBAR**
#33: IGRID    XMAP    ALREF    ALYREF  ***LATERAL GRID MAPPING***

       0       1.    5000000.  5000000.
#34:  NRG ALPHA1   ***VARIABLE GRID MAPPING IN X DIR***

#34A: LPR   A   B   C   ***FOR EACH NRG, READ VARIABLE GRID MAPPING
IN X DIR***
#35:  NRG ALPHA1   ***VARIABLE GRID MAPPING IN Y DIR***

#36: LPR   A   B   C   ***FOR EACH NRG, READ VARIABLE GRID MAPPING
IN Y DIR***
#37:   IF(IBTM.EQ.2)   READ   ((HS(J,I),I=2,IM),J=2,JM)   (12F6.1)
***BATHYMETRY***
   300.   300.   300.   300.   300.   300.   300.   300.   300.
300.
   450.   450.   450.   450.   450.   450.   450.   450.   450.
450.
   700.   700.   700.   700.   700.   700.   700.   700.   700.
700.
   850.   850.   850.   850.   850.   850.   850.   850.   850.
850.
  1000.  1000.  1000.  1000.  1000.  1000.  1000.  1000.  1000.
1000.
  1000.  1000.  1000.  1000.  1000.  1000.  1000.  1000.  1000.
1000.
   850.   850.   850.   850.   850.   850.   850.   850.   850.
850.
   700.   700.   700.   700.   700.   700.   700.   700.   700.
700.
   450.   450.   450.   450.   450.   450.   450.   450.   450.
450.
   300.   300.   300.   300.   300.   300.   300.   300.   300.
300.
```

EXAMPLE OUTPUT DATA FILE

FOR AN ENCLOSED BASIN

```
***THREE-DIMENSIONAL MODEL OF:     3-D RUN FOR SAMPLE RUN WITH
WIND=-1 DYNE/CM**2 (1 DAY)            RUN:  135 DATE: 12-APR-90


  *THERMALLY HOMOGENEOUS  *NO   SALINITY *NO   SEDIMENT *NO
RIVER *NO   TIDE *NO   WIND *     OPEN BDRY*(IM,JM,KM)= 11 11  5


      ***** PHYSICAL CONSTANTS AND REFERENCE LENGTHS(IN CGS
UNITS):
        XREF          ZREF          UREF          COR           GR
   RO0           ROR           T0            TR
     1.0000E+06  5.0000E+02  1.0000E+01  9.0000E-05  9.8100E+02
1.0000E+00  1.0010E+00  0.0000E+00  2.0000E+01

      ***** FLAGS GOVERNING HYDRODYNAMIC EQUATIONS :
        IVLCY         ITEMP         ISALT         IFI           IFA
   IFB           IFC           IFD
          1             0             0             1             0
    0             0             1
       ICC(1)        ICC(2)        ICC(3)        ICC(4)
          0             0             0             0

      ***** TEMPERATURE PARAMETERS :
          BVR           S1            S2            PR            PRV
   TWE           TWH           FKB           TQ0
     1.0000E+00  0.0000E+00  0.0000E+00  1.0000E+00  1.0000E+00
0.0000E+00  0.0000E+00  5.0000E+00  0.0000E+00

      ***** CONCENTRATION PARAMETERS :
        IVER          ICON          IUBO          IBL           IBR
   JBM           JBP           CREF          CMAX          C0
          2             4             0             1             26
    1             29          1.0000E+00  1.0000E+04  1.0000E+00
        IC1           IC2           JC1           JC2           ID1
   ID2           JD1           JD2
          0             0             0             0             0
    0             0             0

      ***** TURBULENCE PARAMETERS :
        IEXP          IAV           AVR           AV1           AV2
   AVM           AHR
          0             0          5.0000E+00  0.0000E+00  0.0000E+00
1.0000E+00  1.0000E+04
         FM1           FM2           ZTOP          SLMIN         QQMIN
     -5.0000E-01 -1.5000E+00 -5.0000E-02  2.0000E-03  1.0000E-03

        QCUT          ICUT          GAMAX         GBMAX         FZS
 KSMALL
     1.5000E-01     1             3.0000E+02  3.0000E+02  1.0000E-01
  0

      ***** WIND PARAMETERS :
```

```
        IWIND        TAUX         TAUY
          0       -1.0000E+00  0.0000E+00

      ***** VERTICAL BOUNDARY CONDITION PARAMETERS :
       ISMALL        ISF         ISIE         IBTM          ITB
          1           0           0            2            5
       HADD         HMIN        ZREFBN        BZ1          H1
   H2          ZREFTN         TZ1         SSS0
      0.0000E+00  2.0000E-03  5.0000E+00  4.0000E-01  2.5000E-01
7.5000E-01  5.0000E+00  4.0000E-01  0.0000E+00

      ***** LATERAL BOUNDARY CONDITION PARAMETERS :
        IOPEN        ITIDE        JWIND       IJLINE
          0            0            0            0

      ***** LATERAL BOUNDARY INFO :
          J         IJGAGE        IJDIR        IJROW       IJSTRT
  IJEND


      ***** ISPAC(I),I=1,10 :
          0            0            0           -1            0
    0           0           0           0           0

      ***** JSPAC(I),I=1,10 :
          0            1           -1           0            0
    0           0           1           0           0

      ***** KSPAC(I),I=1,10 :
          0            0            0           0            0
    0           0           0           0           0

      ***** RSPAC(I),I=1,10 :
      2.0000E-02  1.0000E-01  1.0000E-05 -1.0000E-04  0.0000E+00
0.0000E+00  1.0000E+02  1.0000E+00  2.5000E-01  4.0000E+00

      ***** DERIVED D-LESS PARAMETERS:
         RB           EV           EH           FR           FRD
   DX          DY          DZ          DT          DTI
      1.1111E-01  2.2222E-01  1.1111E-04  1.4278E-02  4.5151E-01
5.0000E-01  5.0000E-01  2.0000E-01  5.4000E-02  5.4000E-02

      ***** DERIVED REFERENCE QUANTITIES:
        WREF         SREF         TAUR
      5.0000E-03  9.1743E-01  4.5000E-01

      ***** TIMESTEP INFORMATION :
        ISTEP         IT1          IT2          ITS          DELT
DELTMIN     DELTMAX
          0           1          144            1       6.0000E+02
1.0000E+00  9.0000E+02
       EPSILON        BUFAC         WTS          WTU          WTV
      7.5000E-02  1.0000E+01  1.0000E+00  1.0000E+00  1.0000E+00
```

```
      ***** PRINTOUT INFORMATION :
         IP1           IP2           IP3           IPU           IPW
  ITEST
         72            72            72             1             1
    3
         IPA           IPB           ID            JPA           JPB
   JD           KPA           KPB           KD
          1            11             1             1            11
    1             1             5             4
         IGI           IGH           IGT           IGS           IGU
   IGW
          1             1             1             1             1
    1
         IGC           IGQ           IGL           IGR           IGRI
   IGTB
          1            -1            -1            -1            -1
   -1

      ***** DISCFILE INFORMATION :
         IRD           IW            IWR           ICI           IWC
  ICO           ISED          IWS           IREAD         IR4
          9             9             1             0             0
    0            14             1             0            15

      ***** MAJOR DISCFILE NAME :
       UVINPUT       UVOUTPUT       SEDIMENT
      6_6_sal       6_6_sal        6_6_sal

      ***** TIMEBREAKS FOR MAJOR OUTPUT TO DISC :
        TBRK1         TBRK2         TBRK3         TBRK4         TBRK5
  TBRK6         TBRK7         TBRK8         TBRK9         TBRK10
      2.4000E+02 -4.8000E+02 -4.8000E+02 -4.8000E+02 -4.8000E+02
-4.8000E+02 -4.8000E+02 -4.8000E+02 -4.8000E+02 -4.8000E+02

      ***** TIMEFILE GAGE STATIONS : (NSTA,NRANGE,NFREQ) =    5
0   2
      STATION         IST           JST           KST    STATIONID
          1            2             6             1

          2            4             6             1

          3            6             6             1

          4            8             6             1

          5           10             6             1

      ***** HORIZONTAL DISTANCES AND SLOPES
            XMAP =            1.   ALREF =     5000000.   ALYREF
=     5000000.

      ***** X-DIRECTION
          CELL
```

```
          NUMBER                                                XS
XU        FMS        FMU
                    FACE          NOT USED IN COMPUTATION
               1   CENTER         NOT USED IN COMPUTATION
                    FACE      1
0.0000000                 1.00000
               2   CENTER                                  0.2500000
      1.00000
                    FACE
0.5000000                 1.00000
               3   CENTER                                  0.7500000
      1.00000
                    FACE
1.0000000                 1.00000
               4   CENTER                                  1.2500000
      1.00000
                    FACE
1.5000000                 1.00000
               5   CENTER                                  1.7500000
      1.00000
                    FACE
2.0000000                 1.00000
               6   CENTER                                  2.2500000
      1.00000
                    FACE
2.5000000                 1.00000
               7   CENTER                                  2.7500000
      1.00000
                    FACE
3.0000000                 1.00000
               8   CENTER                                  3.2500000
      1.00000
                    FACE
3.5000000                 1.00000
               9   CENTER                                  3.7500000
      1.00000
                    FACE
4.0000000                 1.00000
              10   CENTER                                  4.2500000
      1.00000
                    FACE
4.5000000                 1.00000
              11   CENTER                                  4.7500000
      1.00000
                    FACE
5.0000000                 1.00000
      ***** Y-DIRECTION:
          CELL
          NUMBER                                              YS
YV        FMSV       FMV
                    FACE          NOT USED IN COMPUTATION
               1   CENTER         NOT USED IN COMPUTATION
                    FACE      1
0.0000000                 1.00000
```

```
            2   CENTER                                  0.2500000
      1.00000
                 FACE
0.5000000                 1.00000
            3   CENTER                                  0.7500000
      1.00000
                 FACE
1.0000000                 1.00000
            4   CENTER                                  1.2500000
      1.00000
                 FACE
1.5000000                 1.00000
            5   CENTER                                  1.7500000
      1.00000
                 FACE
2.0000000                 1.00000
            6   CENTER                                  2.2500000
      1.00000
                 FACE
2.5000000                 1.00000
            7   CENTER                                  2.7500000
      1.00000
                 FACE
3.0000000                 1.00000
            8   CENTER                                  3.2500000
      1.00000
                 FACE
3.5000000                 1.00000
            9   CENTER                                  3.7500000
      1.00000
                 FACE
4.0000000                 1.00000
           10   CENTER                                  4.2500000
      1.00000
                 FACE
4.5000000                 1.00000
           11   CENTER                                  4.7500000
      1.00000
                 FACE
5.0000000                 1.00000

      ***** Z-DIRECTION:
               K          Z              DZZ            SG
               5     0.0000E+00     2.0000E-01    -1.0000E-01
               4    -2.0000E-01     2.0000E-01    -3.0000E-01
               3    -4.0000E-01     2.0000E-01    -5.0000E-01
               2    -6.0000E-01     2.0000E-01    -7.0000E-01
               1    -8.0000E-01     2.0000E-01    -9.0000E-01

         ***** DEPTHS AT CELL CENTERS (HS)
      MAXIMUM MODULUS:  2.0000E+00          PLOT INCREMENT :
1.3333E-01

                          **************************
```

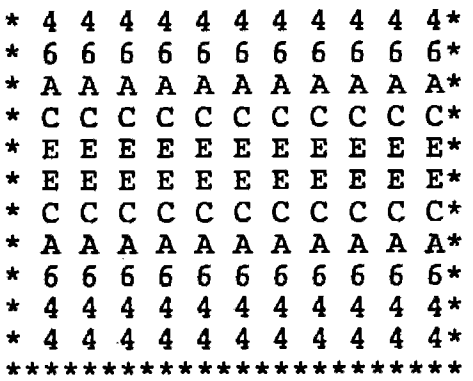

***** DEPTHS AT U CELL FACES (HU)
MAXIMUM MODULUS: 2.0000E+00 PLOT INCREMENT : 1.3333E-01

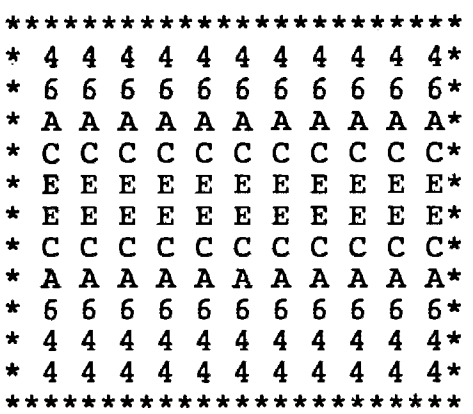

***** DEPTHS AT V CELL FACES (HV)
MAXIMUM MODULUS: 2.0000E+00 PLOT INCREMENT : 1.3333E-01

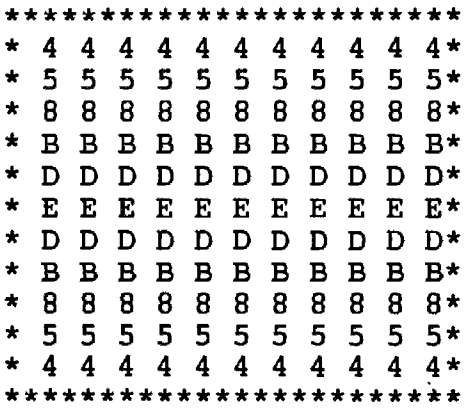

***** SLOPES IN THE X-DIRECTION (AT U PTS)
MAXIMUM MODULUS: 0.0000E+00 PLOT INCREMENT : 0.0000E+00

EMPTY FIELD - NO PLOT GENERATED

***** CURVATURES IN THE X-DIRECTION (U)
MAXIMUM MODULUS: 0.0000E+00 PLOT INCREMENT : 0.0000E+00

EMPTY FIELD - NO PLOT GENERATED

***** SLOPES IN THE Y-DIRECTION (AT V PTS)
MAXIMUM MODULUS: 1.0000E+00 PLOT INCREMENT : 6.6667E-02

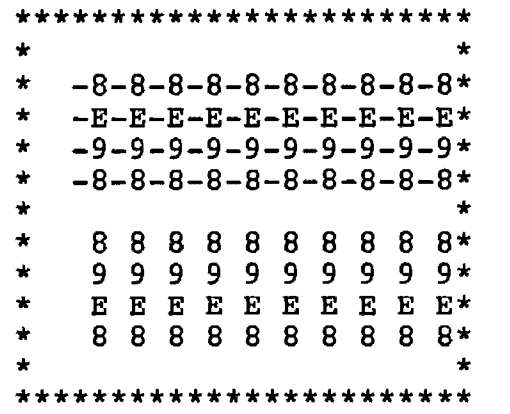

***** CURVATURES IN THE Y-DIRECTION (V)
MAXIMUM MODULUS: 1.2000E+00 PLOT INCREMENT : 8.0000E-02

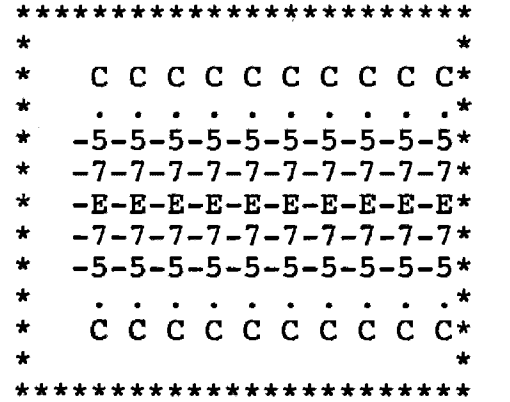

***** MOD DEPTHS AT CELL CENTERS (HS)
MAXIMUM MODULUS: 2.0000E+00 PLOT INCREMENT : 1.3333E-01

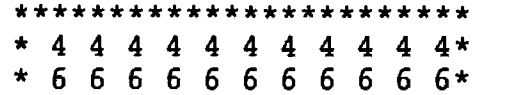

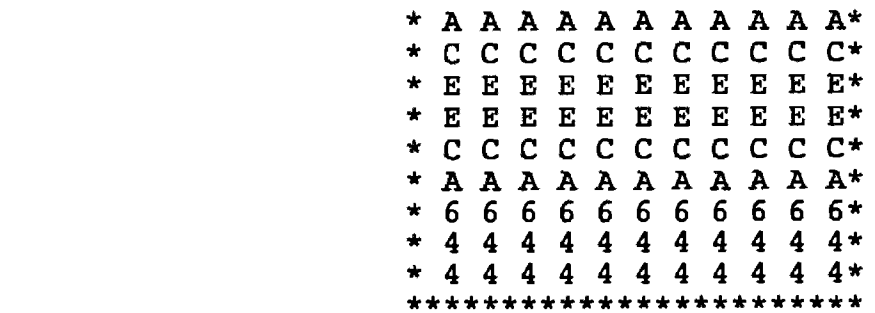

***** MOD DEPTHS AT U CELL FACES (HU)
MAXIMUM MODULUS: 2.0000E+00 PLOT INCREMENT :
1.3333E-01

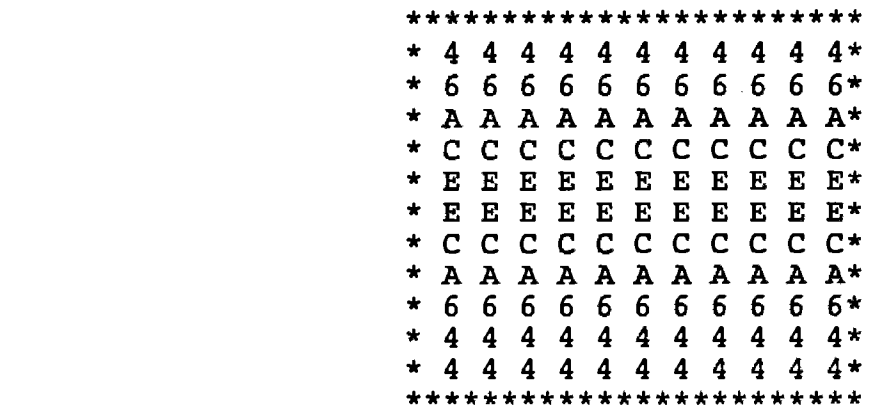

***** MOD DEPTHS AT V CELL FACES (HV)
MAXIMUM MODULUS: 2.0000E+00 PLOT INCREMENT :
1.3333E-01

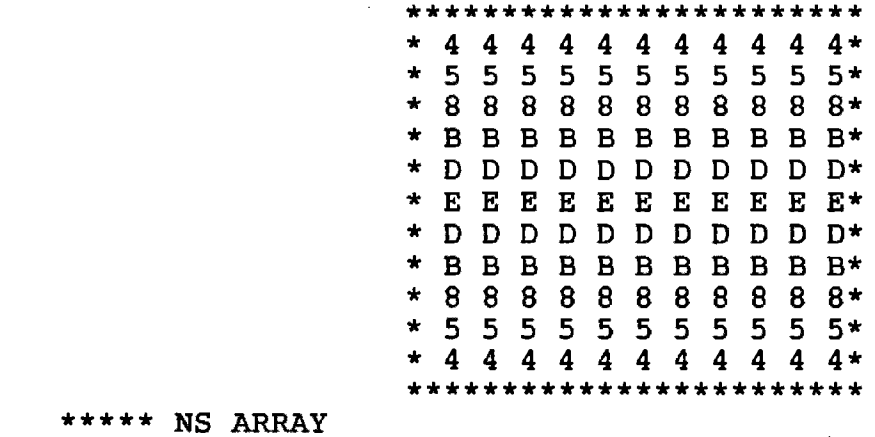

***** NS ARRAY

```
12345678901234567890123456789012345678901234567890123456789012345
678901234567890

   11      02111111115
   10      02111111115
```

```
    9      02111111115
    8      02111111115
    7      02111111115
    6      02111111115
    5      02111111115
    4      02111111115
    3      02111111115
    2      02111111115
    1      00000000000
          ***** MS ARRAY


12345678901234567890123456789012345678901234567890123456789012345
678901234567890

   11      05555555555
   10      01111111111
    9      01111111111
    8      01111111111
    7      01111111111
    6      01111111111
    5      01111111111
    4      01111111111
    3      01111111111
    2      02222222222
    1      00000000000

 JU1  JU2  JV1  JV2   I

  1   11    2   10    1
  1   11    2   10    2
  1   11    2   10    3
  1   11    2   10    4
  1   11    2   10    5
  1   11    2   10    6
  1   11    2   10    7
  1   11    2   10    8
  1   11    2   10    9
  1   11    2   10   10
  1   11    2   10   11

 IU1  IU2  IV1  IV2   J

  2   10    1   11   11
  2   10    1   11   10
  2   10    1   11    9
  2   10    1   11    8
  2   10    1   11    7
  2   10    1   11    6
  2   10    1   11    5
  2   10    1   11    4
  2   10    1   11    3
  2   10    1   11    2
  2   10    1   11    1
```

TX

MAXIMUM MODULUS: 2.2222E+00 PLOT INCREMENT : 1.4815E-01

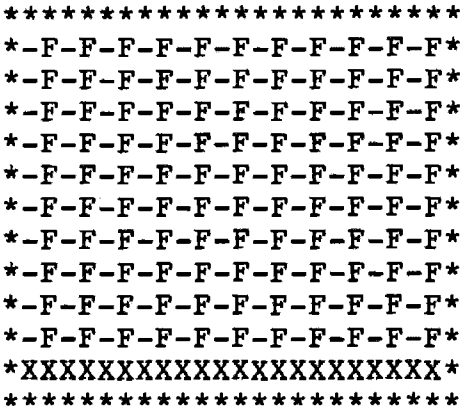

TY

MAXIMUM MODULUS: 1.2340E-07 PLOT INCREMENT : 8.2267E-09

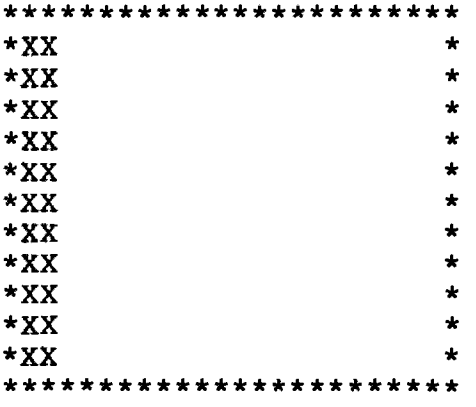

HU AT (1,2):0.6000E+00

BZ0

MAXIMUM MODULUS: 4.0000E-01 PLOT INCREMENT : 2.6667E-02

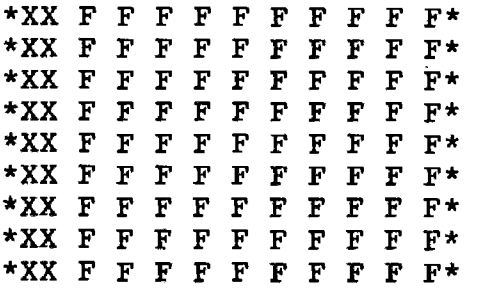

```
                          *XX F F F F F F F F F*
                          *XX F F F F F F F F F*
                          ************************

     BZOU
      MAXIMUM MODULUS:  4.0000E-01          PLOT INCREMENT :
2.6667E-02

                          ************************
                          * F F F F F F F F F F*
                          * F F F F F F F F F F*
                          * F F F F F F F F F F*
                          * F F F F F F F F F F*
                          * F F F F F F F F F F*
                          * F F F F F F F F F F*
                          * F F F F F F F F F F*
                          * F F F F F F F F F F*
                          * F F F F F F F F F F*
                          * F F F F F F F F F F*
                          *XXXXXXXXXXXXXXXXXXXXX*
                          ************************

** TIME INDEX =   72        ** TIME =   12.0000  HOURS

 SSUM =       2.58684158E-05  :  SASUM =       0.00000000E+00

SURFACE ELEVATION

      MAXIMUM MODULUS:  5.8933E+00          PLOT INCREMENT :
3.9289E-01

                          ************************
                          *XX F A 6 3 1-1-4-6-9-D*
                          *XX D 9 6 3 1-1-4-6-9-C*
                          *XX C 9 6 3 1-1-4-6-9-B*
                          *XX C 8 6 3 1-1-4-6-9-A*
                          *XX B 8 6 3 1-1-4-6-8-A*
                          *XX B 8 6 3 1-1-4-6-8-A*
                          *XX C 8 6 3 1-1-4-6-9-A*
                          *XX C 9 6 3 1-1-4-6-9-B*
                          *XX D 9 6 3 1-1-4-6-9-C*
                          *XX E A 6 3 1-1-4-6-9-D*
                          *XXXXXXXXXXXXXXXXXXXXX*
                          ************************

 X MASS FLUX (UI)

      MAXIMUM MODULUS:  2.2921E+00          PLOT INCREMENT :
1.5280E-01

                          ************************
                          *  -5-7-8-8-8-8-8-7-5  *
                          *  -5-8-9-A-A-9-8-7-4  *
```

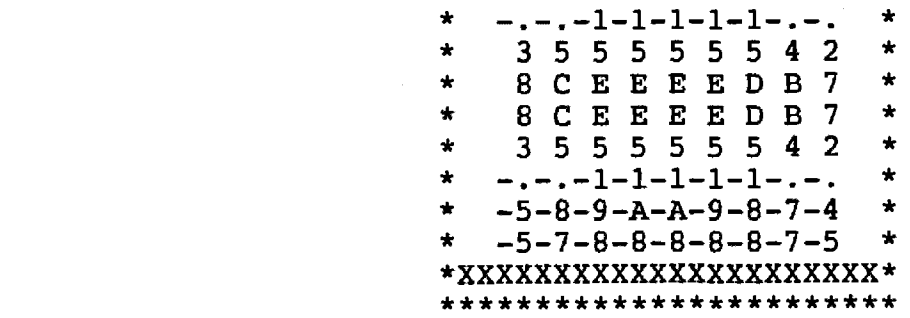

Y MASS FLUX (VI)

MAXIMUM MODULUS: 1.8115E+00 PLOT INCREMENT : 1.2077E-01

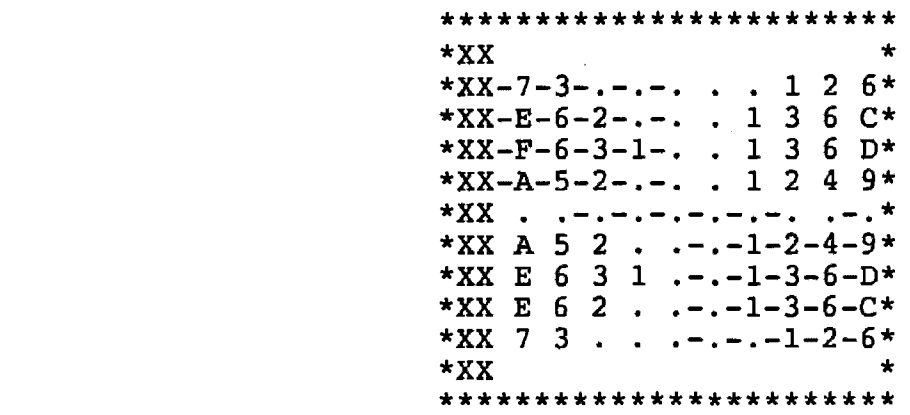

U-VELOCITY IS

K = 1

MAXIMUM MODULUS: 1.1710E+00 PLOT INCREMENT : 7.8066E-02

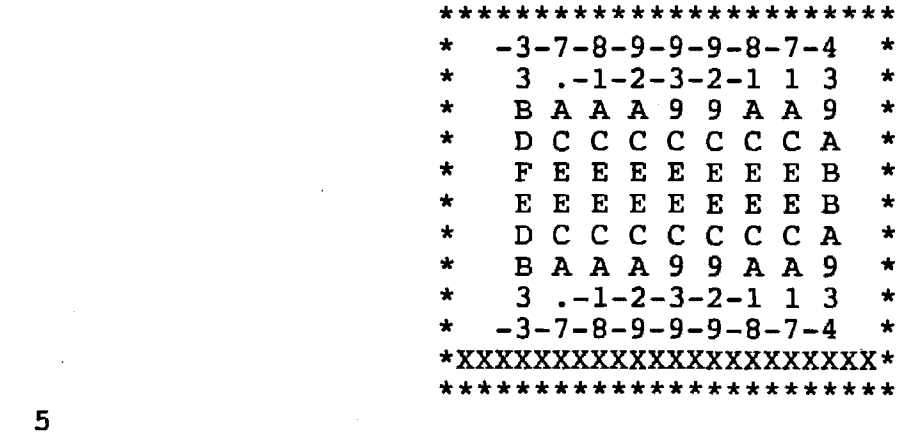

K = 5

MAXIMUM MODULUS: 4.1082E+00 PLOT INCREMENT : 2.7388E-01

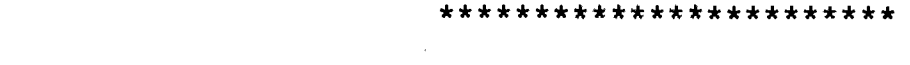

```
*  -A-D-E-E-E-E-E-D-A  *
*  -B-D-D-E-E-D-D-B-9  *
*  -9-9-9-9-9-9-9-9-8  *
*  -9-7-7-7-7-7-7-8-8  *
*  -9-6-5-5-5-5-6-7-7  *
*  -9-6-5-5-5-5-6-7-7  *
*  -9-7-7-7-7-7-7-8-8  *
*  -9-9-9-9-9-9-9-9-8  *
*  -B-D-D-E-E-D-D-B-9  *
*  -A-D-E-E-F-E-E-D-A  *
*XXXXXXXXXXXXXXXXXXXXX*
************************
```

V-VELOCITY

K = 1
MAXIMUM MODULUS: 7.0147E-01 PLOT INCREMENT : 4.6765E-02

```
************************
*XX                     *
*XX-D-7-2-.-. . . 2 6 C*
*XX-E-7-3-1-. . 1 3 5 D*
*XX-B-4-2-.-. . . 1 3 A*
*XX-6-2-1-.-. . . 1 2 6*
*XX-. .-.-.-.-. .-. .-.*
*XX 6 2 1 . .-.-.-1-2-6*
*XX B 4 2 . .-.-.-1-3-A*
*XX E 7 3 1 .-.-1-3-5-D*
*XX D 7 2 . .-.-.-2-6-C*
*XX                     *
************************
```

K = 5
MAXIMUM MODULUS: 1.9781E+00 PLOT INCREMENT : 1.3188E-01

```
************************
*XX                     *
*XX-A-4-1-.-. . . 1 4 B*
*XX-E-5-2-. . . 1 3 7 E*
*XX-B-4-2-. . . 1 3 6 A*
*XX-6-2-1-. . . 1 2 4 6*
*XX . .-.-.-.-.-.-. .-.*
*XX 6 2 1 .-.-.-1-2-4-6*
*XX B 4 2 .-.-.-1-3-6-A*
*XX F 5 2 .-.-.-1-3-7-E*
*XX A 4 1 . .-.-.-1-4-B*
*XX                     *
************************
```

W-VELOCITY IS

K = 1
MAXIMUM MODULUS: 3.6162E-01 PLOT INCREMENT :

2.4108E-02

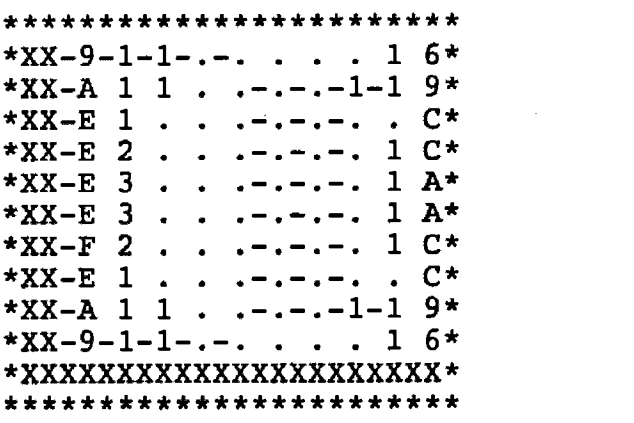

K = 5

MAXIMUM MODULUS: 1.2340E-07 PLOT INCREMENT : 8.2267E-09

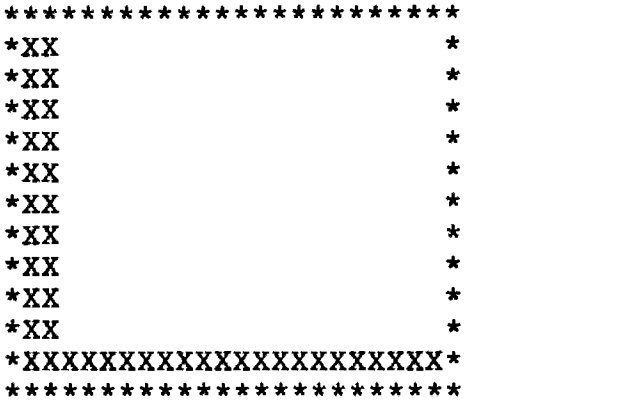

** TIME INDEX = 144 ** TIME = 24.0000 HOURS

SSUM = 7.93933868E-05 : SASUM = 0.00000000E+00

SURFACE ELEVATION

MAXIMUM MODULUS: 5.9791E+00 PLOT INCREMENT : 3.9861E-01

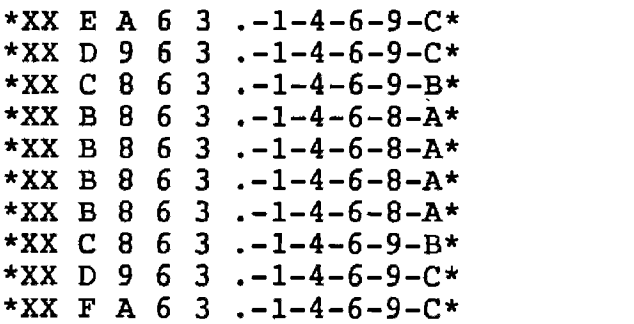

```
                        *XXXXXXXXXXXXXXXXXXXXXX*
                        ************************
```

X MASS FLUX (UI)

```
      MAXIMUM MODULUS:  3.0327E+00          PLOT INCREMENT :
2.0218E-01

                        ************************
                        *  -4-5-6-6-6-6-6-6-4  *
                        *  -6-8-9-9-9-9-8-6-4  *
                        *  -1-2-2-2-2-2-2-1-1  *
                        *   3 4 4 4 4 4 3 3 1  *
                        *   9 D E E E E D B 7  *
                        *   9 D E F E E D B 7  *
                        *   3 4 4 4 4 4 3 3 1  *
                        *  -1-2-2-2-2-2-2-1-1  *
                        *  -6-8-9-9-9-9-8-6-4  *
                        *  -4-5-6-6-6-6-6-6-4  *
                        *XXXXXXXXXXXXXXXXXXXXXX*
                        ************************
```

Y MASS FLUX (VI)

```
      MAXIMUM MODULUS:  2.5646E+00          PLOT INCREMENT :
1.7098E-01

                        ************************
                        *XX                    *
                        *XX-4-2-.-.-. . . . 2 5*
                        *XX-C-4-1-. . . 1 2 5 9*
                        *XX-F-5-2-. . . 1 3 6 B*
                        *XX-B-4-1-. . . 1 2 4 8*
                        *XX-. .-.-. .-. .-. . .*
                        *XX B 4 1 .-.-.-1-2-4-8*
                        *XX E 5 2 .-.-.-1-3-6-B*
                        *XX C 4 1 .-.-.-1-2-5-9*
                        *XX 4 2 . . .-.-.-.-2-5*
                        *XX                    *
                        ************************
```

U-VELOCITY IS

```
 K =  1
      MAXIMUM MODULUS:  1.2088E+00          PLOT INCREMENT :
8.0586E-02

                        ************************
                        *  -2-7-8-8-9-9-8-8-4  *
                        *   1-3-5-5-5-5-4-1 2  *
                        *   A 9 9 9 9 9 9 9 8  *
                        *   C C C C C C C B A  *
                        *   E E E E E E E E B  *
                        *   E E E E E E E E B  *
```

```
*   C C C C C C C B A  *
*   A 9 9 9 9 9 9 9 8  *
*    1-3-5-5-5-5-4-1 2  *
*  -2-7-8-8-9-9-8-8-4   *
*XXXXXXXXXXXXXXXXXXXXXX*
************************
```

K = 5
MAXIMUM MODULUS: 4.5494E+00 PLOT INCREMENT : 3.0329E-01

```
************************
*  -9-C-D-D-D-D-D-C-9   *
*  -C-E-E-E-E-E-D-B-9   *
*  -9-9-9-A-9-9-9-9-8   *
*  -8-6-6-6-6-6-7-7-7   *
*  -6-3-3-3-3-3-4-5-6   *
*  -6-3-3-3-3-3-4-5-6   *
*  -8-6-6-6-6-6-7-7-7   *
*  -9-9-9-A-9-9-9-9-8   *
*  -C-E-E-E-E-E-D-B-9   *
*  -9-C-D-D-D-D-D-C-9   *
*XXXXXXXXXXXXXXXXXXXXXX*
************************
```

V-VELOCITY

K = 1
MAXIMUM MODULUS: 8.1753E-01 PLOT INCREMENT : 5.4502E-02

```
************************
*XX                     *
*XX-B-6-2-.-. . . 1 5 B*
*XX-E-7-3-1-. . 1 3 6 B*
*XX-C-4-1-.-. . . 1 3 9*
*XX-7-2-.-.-. . . 1 2 7*
*XX-. . . . .-. .-.-. .*
*XX 7 2 . . .-.-.-1-2-7*
*XX C 4 1 . .-.-.-1-3-9*
*XX F 7 3 1 .-.-1-3-6-B*
*XX B 6 2 . .-.-.-1-5-B*
*XX                     *
************************
```

K = 5
MAXIMUM MODULUS: 2.4508E+00 PLOT INCREMENT : 1.6339E-01

```
************************
*XX                     *
*XX-8-3-1-.-. . . 1 4 9*
*XX-E-4-1-. . . 1 3 7 C*
*XX-C-3-1-. . . 1 3 6 A*
*XX-7-2-.-. . . 1 2 4 7*
*XX . .-.-. .-. .-. .-.*
```

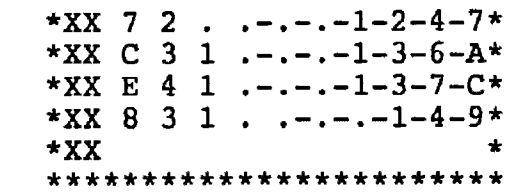

W-VELOCITY IS

K = 1
MAXIMUM MODULUS: 3.5428E-01 PLOT INCREMENT : 2.3619E-02

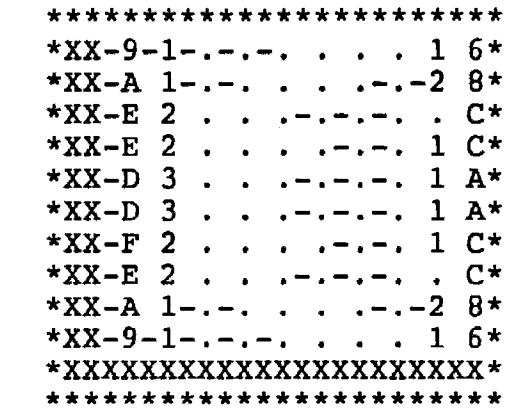

K = 5
MAXIMUM MODULUS: 1.2340E-07 PLOT INCREMENT : 8.2267E-09

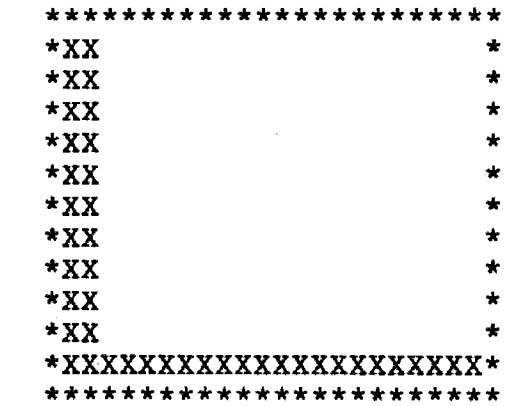

***** MAXIMUM STEP REACHED : IT = 144

NERL-ATH-1285

TECHNICAL REPORT DATA
(Please read Instructions on the reverse before completing)

1. REPORT NO. 600/R-99/049	2.	3. RECIPIENT'S ACCESSION NO.
4. TITLE AND SUBTITLE Three Dimensional Hydrodynamic Model for Stratified Flows in Lakes and Estuaries (HYDRO3D)		5. REPORT DATE June 1999 6. PERFORMING ORGANIZATION CODE
7. AUTHOR(S) Y. Peter Sheng, Mansour Zakikhani, Steven C. McCutcheon, E.Z. Hosseinipour, Pei-Fang Wang, Donald Eliason, D.S. Henn, and S.F. Parker.E. Hayter.P.Kohl		8. PERFORMING ORGANIZATION REPORT NO.
9. PERFORMING ORGANIZATION NAME AND ADDRESS University of FLorida Gainesville, FL		10. PROGRAM ELEMENT NO. 11. CONTRACT/GRANT NO.
12. SPONSORING AGENCY NAME AND ADDRESS Ecosystems Research Division - Athens, GA Office of Research and Development U.S. Environmental Protection Agency Athens, GA 30605-2700		13. TYPE OF REPORT AND PERIOD COVERED Research 14. SPONSORING AGENCY CODE EPA/600/01
15. SUPPLEMENTARY NOTES		

16. ABSTRACT

Increasing demands for maintaining the quality of stratified surface waters at reasonable levels have required the development of three-dimensional hydrodynamic models. To meet these needs, the HYDRO3D program has been documented to aid in the simulation of lakes, harbors, coastal areas, and estuaries.

HYDRO3D is a dynamic modeling system that can be used to simulate currents in water bodies as they respond to tides, winds, density gradients, river flows, and basin geometry and bathymetry. The code is a three-dimensional, time-dependent, σ-stretched coordinate, free surface model that can be run in fully three-dimensional (3-D) mode, two-dimensional vertically-averaged (x-y), and two-dimensional laterally-averaged x-z mode.

The applications provided here demonstrated that the model is capable of realistic simulation of flow and salinity transport in complex and dynamic water bodies. These applications include simulations of tidal circulation and salinity transport in Suisun Bay, California and Charlotte Harbor, Florida and wind-forced circulation in Green Bay, Lake Michigan. Tidal circulation in Prince William Sound, Alaska was investigated to determine the feasibility of applying the model under emergency conditions. Finally, the calibration of the model for the Mississippi Sound is illustrated.

17. KEY WORDS AND DOCUMENT ANALYSIS

a. DESCRIPTORS	b. IDENTIFIERS/OPEN ENDED TERMS	c. COSATI Field/Group
Water Quality HYDRO3D Modeling Estuaries Lakes		

18. DISTRIBUTION STATEMENT RELEASE TO PUBLIC	19. SECURITY CLASS *(This Report)* UNCLASSIFIED	21. NO. OF PAGES 223
	20. SECURITY CLASS *(This page)* UNCLASSIFIED	22. PRICE

EPA Form 2220-1 (Rev. 4-77) PREVIOUS EDITION IS OBSOLETE